Universidade do Minho
Escola de Medicina

Vanessa Alexandra Morais Sardinha

The influence of gliotransmission on higher cognitive functions

setembro de 2017

UMinho | 2017

Vanessa Alexandra Morais Sardinha **The influence of gliotransmission on higher cognitive functions**

Universidade do Minho
Escola de Medicina

Vanessa Alexandra Morais Sardinha

The influence of gliotransmission on higher cognitive functions

Tese de Doutoramento em Ciências da Saúde

Trabalho efetuado sob a orientação do
Professor Doutor João Filipe Pedreira de Oliveira
e do
Professor Doutor Nuno Jorge Carvalho Sousa

DECLARAÇÃO

Nome: Vanessa Alexandra Morais Sardinha

Endereço electrónico: vanessasardinha@med.uminho.pt

Número do Cartão do Cidadão: 13444795

Título da tese:

The influence of gliotransmission on higher cognitive functions

Orientadores:

Doutor João Filipe Pedreira de Oliveira
Professor Doutor Nuno Jorge Carvalho Sousa

Ano de conclusão: 2017
Doutoramento em Ciências da Saúde

Universidade do Minho, 21 / 09 / 2017

Assinatura: _Vanessa Alexandra Sardinha_

DECLARAÇÃO DE INTEGRIDADE

Declaro ter atuado com integridade na elaboração da presente tese. Confirmo que em todo o trabalho conducente à sua elaboração não recorri à prática de plágio ou a qualquer forma de falsificação de resultados.

Mais declaro que tomei conhecimento integral do Código de Conduta Ética da Universidade do Minho.

Universidade do Minho, 21 de Setembro de 2017

Nome completo: Vanessa Alexandra Morais Sardinha

Assinatura: _Vanessa Alexandra Sardinha_

À Rosa, Fátima e Thiago por me fazerem ver sempre o lado positivo da vida e pelas gargalhadas que partilhamos tão frequentemente, agora com a Carolina a mostrar-nos que há tanto para viver;

Aos meus pais por me terem ajudado a chegar aqui, sempre a fazer acreditar que o amanhã vai ser melhor que hoje; era aos meus pais a quem ligava sempre que o trabalho não corria bem, obrigada por me ouvirem sempre sem questionar os meus argumentos;

Por fim ao Bé, és o meu herói aconteça o que acontecer.

"You never fail, until you stop trying."

Albert Einstein

x

The influence of gliotransmission on higher cognitive functions

Abstract

In recent years, the understanding of synaptic modulation by neuron-astrocyte interactions has evolved considerably, contributing to build up the concept of the "tripartite synapse". This concept is based on the dynamic dialogue between astrocytes and neurons that complements and modulates the communication between pre- and post-synaptic structures. However, it remains elusive how this interaction between neurons and astrocytes translates into network computation of behavior. Astrocytes were described to release gliotransmitters (such as glutamate, GABA, ATP or D-Serine) by means of several mechanisms, being exocytosis the more extensively studied. This process is mediated by the vesicular machinery and SNARE complex formation between vesicles and the target membrane, ultimately resulting in the release of the vesicular content. Transmitter release is essential for astrocyte signaling and a disruption of this phenomenon is expected to impact on the function of neuronal networks, with consequences for the computation of higher brain functions. In this thesis, our main goal was to evaluate the influence of transmitter release by astrocytes on brain circuits responsible for cognitive functions, such as learning and memory.

Throughout this work, we studied the transgenic dnSNARE mouse model that displays a conditional blockade of transmitter release by exocytosis, selectively in astrocytes. This was achieved by allowing the conditional expression of the dominant negative domain of vesicular SNARE protein synaptobrevin II (dnSNARE), which interferes with the SNARE complex formation, impairing vesicular release. Four weeks after the induction of transgene transcription, the levels of transgenic protein reached its maximum. The dnSNARE transgenes are expressed exclusively by astrocytes and display inter-subject variability. The quantification of dnSNARE transgene expression levels allowed to discriminate high "expressor" subjects to be analyzed throughout.

Mice were first evaluated by performing *in vivo* electrophysiological recordings of local field potentials from neuronal populations of cognitive related brain regions: dorsal hippocampus and prefrontal cortex. This functional network evaluation was followed by a thorough assessment of cognitive ability of these mice, by performing a battery of behavioral tests. These tests addressed different cognitive tasks mainly dependent from the performance of the hippocampus-prefrontal network. This functional assessment was complemented by a morphological characterization of neurons and astrocytes to address structural correlates of network function.

Our findings demonstrated a specific neural desynchronization in the theta rhythm between the dorsal hippocampus and prefrontal cortex in the dnSNARE mice, without any alteration of levels of neuronal activity. Moreover, the blockade of gliotransmitter release in astrocytes triggers a critical cognitive impairment in tasks classically attributed to neuronal circuits of the hippocampus-prefrontal cortex network. More specifically, dnSNARE mice faced an increased difficulty when performing in reference memory tasks of Morris water maze (MWM) and hole-board test (HB), and revealed a clear deficit in tasks involving spatial recognition and long-term memory, such as the novel object recognition (NOR) and two-trial place recognition (2TPR) tests. Further analysis of electrophysiological recordings showed a direct correlation between the loss of theta coherence in dorsal hippocampus-prefrontal link and poor consolidation of reference memory. The structure evaluation of the dorsal hippocampus and prefrontal cortex revealed that the neuronal dendritic trees appear to be intact in dnSNARE mice. However, astrocytes undergo drastic process atrophy, specifically in GFAP+ cells that also express dnSNARE transgenes.

Interestingly, the intraperitoneal supplementation with the NMDAR co-agonist D-serine — that is known to be released by exocytosis in astrocytes and to be significantly decreased in the brains of dnSNARE mice — completely restored theta synchronization and rescued the learning and memory deficits in transgenic mice.

In conclusion, this PhD thesis provides the evidence of a mechanism by which astrocytic signaling is required for entrainment of distant cortico-limbic circuits, being mandatory for cognitive performance. Moreover, our findings suggest that D-serine may be the gliotransmitter maintaining the synchronization of the theta rhythm between these circuits required for learning and memory consolidation. Further studies should be performed to unravel the astrocytic contribution to different cognitive tasks, as well as the therapeutic potential of astrocyte signaling to the development of new approaches to treat disorders of the central nervous system, characterized by cognitive decline.

A influência da gliotransmissão sobre as funções cognitivas superiores

Resumo

Nos últimos anos, a compreensão da modulação sináptica através de interações neurónio-astrócito tem evoluído consideravelmente, contribuindo para o aparecimento do conceito da "sinapse tripartida". Este conceito é baseado no diálogo dinâmico entre astrócitos e neurónios que complementa e modula a comunicação entre as estruturas pré e pós-sinápticas. No entanto, continua por esclarecer de que forma essa interação entre neurónios e astrócitos se traduz na produção de comportamentos pelo cérebro. Os astrócitos libertam gliotransmissores (tais como glutamato, GABA, ATP ou D-serina) através de diversos mecanismos, sendo a exocitose o mais amplamente estudado. Este processo é mediado pela maquinaria vesicular e pela formação do complexo SNARE entre vesículas e a membrana alvo, resultando, em última instância, na libertação do conteúdo vesicular para o exterior. A libertação de transmissores é essencial para a sinalização dos astrócitos e seria de esperar que a interrupção desse fenómeno afectasse a função das redes neuronais, com consequências para a computação de funções cerebrais superiores. Assim, o principal objetivo deste trabalho foi avaliar a influência da libertação de transmissores pelos astrócitos nos circuitos cerebrais responsáveis pelas funções cognitivas, como a aprendizagem e o processamento de memória.

Ao longo deste trabalho utilizámos o modelo de murganho transgénico dnSNARE que apresenta um bloqueio condicional da libertação de transmissores por exocitose, selectivamente em astrócitos. A ocorrência deste bloqueio é devida à expressão condicional do domínio negativo dominante da sinaptobrevina vesicular II (dnSNARE), que interfere com a formação do complexo SNARE e, consequentemente, com a libertação vesicular. O transgene atinge o seu pico de expressão quatro semanas após a indução da sua expressão. A mesma é exclusiva dos astrócitos e apresenta variabilidade entre indivíduos. A quantificação da expressão do transgene dnSNARE permitiu identificar os animais com níveis elevados de expressão transgénica, que foram utilizados ao longo do trabalho para comparação com os respectivos controlos.

Os murganhos dnSNARE, e respectivos controlos, foram primeiramente avaliados através da realização de registos electrofisiológicos de potenciais de campo locais, *in vivo*, de populações neuronais de regiões do cérebro implicadas na função cognitiva: o hipocampo e o córtex pré-frontal. Esta análise funcional da integridade da rede foi complementada com uma avaliação completa da capacidade cognitiva destes animais, procedendo-se para esse fim, à realização de

uma bateria de testes comportamentais. Os testes utilizados abrangiam diferentes funções, principalmente dependentes do desempenho da rede hipocampo–cortex pré-frontal. Além desta caracterização funcional, procedeu-se ainda a uma caracterização morfológica de neurónios e astrócitos, com o intuito de avaliar possíveis correlatos estruturais das funções da rede.

Os resultados principais desta tese demonstram uma desincronização neuronal específica no ritmo teta, entre o hipocampo dorsal e o córtex pré-frontal em murganhos dnSNARE, sem qualquer alteração dos níveis basais de atividade neuronal. Além disso, o bloqueio da libertação de gliotransmissores em astrócitos desencadeia um défice cognitivo severo em tarefas classicamente atribuídas aos circuitos neuronais do hipocampo dorsal e do córtex pré-frontal. Mais especificamente, os murganhos dnSNARE enfrentaram uma maior dificuldade na realização de tarefas de memória de referência no teste da pisicna de *Morris* (MWM) e no teste do *Hole-Board* (HB). Estes animais revelaram ainda um claro défice em tarefas que envolviam o reconhecimento espacial e memória de longo prazo nos testes de reconhecimento de novos objectos (NOR) e espaços (2TPR). Análises adicionais de registros electrofisiológicos mostraram a existência de uma correlação significativa entre a perda de coerência teta na ligação hipocampo dorsal-cortex pré-frontal e a consolidação de memória de referência. A análise estrutural do hipocampo dorsal e do córtex pré-frontal revelou que a estrutura neuronal permance intacta nos murganhos dnSNARE. No entanto, os astrócitos GFAP-positivos que também expressam transgenes dnSNARE parecem sofrer uma drástica atrofia.

Curiosamente, a suplementação intraperitoneal com D-serina – um co-agonista dos receptores NMDA, libertado por exocitose nos astrócitos e significativamente diminuído nos cérebros de murganhos dnSNARE – restaurou completamente a sincronização em teta e, recuperou os défices de aprendizagem e memória nos mesmos animais.

Em conclusão, esta tese de doutoramento apresenta resultados relativos à evidência de um mecanismo pelo qual a sinalização astrocítica é necessária para o estabelecimento da comunicação entre circuitos cortico-límbicos distantes, revelando a sua importância para o desempenho cognitivo. Estes resultados sugerem que a D-serina pode ser o gliotransmissor responsável pela sincronização do ritmo teta entre os circuitos necessários para os processos de aprendizagem e consolidação de memória. Estudos adicionais deverão ser realizados para dissecar a contribuição astrocítica para outras tarefas cognitivas e, para avaliar o potencial terapêutico da sinalização de astrócitos para o desenvolvimento de novas abordagens, capazes de tratar distúrbios do sistema nervoso central caracterizados pelo declínio cognitivo.

Abbreviations list

AMPA	–	α-amino-3-hydroxy-5-methyl-4-isoxazolepropionic acid
ANOVA	–	Analysis of variance
AS	–	Acoustic startle
ATP	–	Adenosine triphosphate
CA1	–	Cornu Ammonis 1
CA3	–	Cornu Ammonis 3
cDNA	–	complementary DNA
CNS	–	Central nervous system
DG	–	Dentate gyrus
dHIP	–	dorsal Hippocampus
dnSNARE	–	dominant negative domain of vesicular SNARE
Dox	–	Doxycycline
EGFP	–	Enhanced green fluorescent protein
EPM	–	Elevated plus maze
FST	–	Forced swim test
GFAP	–	Glial-fibrillary acidic protein
GFP	–	Green fluorescent protein
GLAST/EAAT1	–	Glutamate aspartate transporter/excitatory amino acid transporter 1
GLT-1/EAAT2	–	Glutamate transporter/excitatory amino acid transporter 2
GluRs	–	Ionotropic glutamate receptors
HB	–	Hole-board
HIP	–	Hippocampus
i.p.	–	intraperitoneal
LDB	–	Light/dark box
LFP	–	Local field potential
lGFP	–	low GFP
LTP	–	Long-term potentiation
mGluRs	–	metabotropic glutamate receptors
mPFC	–	medial Prefrontal Cortex
mRNA	–	messenger Ribonucleic acid

MWM	–	Morris water maze
NeuN	–	Neuronal nuclei
NMDA	–	N-methyl-d-aspartate
NMDAR	–	N-methyl-d-aspartate receptors
NOR	–	Novel object recognition
OF	–	Open field
PBS	–	Phosphate-buffered solution
PCR	–	Polymerase chain reaction
PFC	–	Prefrontal Cortex
PNS	–	Peripheral nervous system
RM	–	Reference Memory
RT-PCR	–	Reverse transcription PCR
SEM	–	Standard error of the mean
SIC	–	Slow inward current
SNARE	–	Soluble N-ethylmaleimide–sensitive factor attachment protein receptor
tetO	–	tetracycline operator
TST	–	Tail suspension test
tTA	–	tetracycline transactivator
VAMP2	–	vesicle-associated membrane protein 2/synaptobrevin II
VAMP3	–	cellubrevin
vHIP	–	ventral Hippocampus
WM	–	Working memory
WT	–	Wild-type
2TPR	–	two trial place recognition

Contents

CHAPTER 1

1   Introduction

For many years, neurons were recognized as the main type of cells in the brain, characterized by their ability to transmit fast electrical signals under the form of action potentials. Neurons are organized in circuits and communicate through intercellular adhesion sites called synapses, which are specialized chemical junctions. In the second half of the nineteenth century, Rudolf Virchow spread the concept and term of 'neuroglia' for a different group of cells that could be distinguished in the nervous system. At that time, glial cells were postulated as supportive cells to neuronal populations, functioning as a simple glue filling in the space between neurons that is responsible for maintaining stability and the overall architecture of the nervous system, suggesting a passive function for these cells (Kettenmann and Verkhratsky, 2008; McIver et al., 2013; Dimou and Gotz, 2014). However, the wide and persistent research on the field has been progressively revealing their importance as functional partners of neurons, sharing a symbiotic relationship and contributing to the formation, operation and adaptation of neural circuitry (Allen and Barres, 2009; Navarrete and Araque, 2014).

Glial cells do not fire action potentials and their impulses spread through the tissue at a slower rate altering neuronal activity, neurotransmitter kinetics, metabolic activity, blood flow and the extracellular environment. Since glia and neurons are in contact across almost every part of their membranes, they interact and influence each other in a tight, reciprocal relationship. But in vertebrates, glial cells are not all the same and could be classified based on their morphology and function in microglia – fundamental in phagocytosis and defense; oligodendrocytes and Schwann cells – the myelinating glial cells in the CNS and in the peripheral nervous system (PNS), respectively; NG2-glia, involved in the formation of perineuronal nets (dense arrangements of extracellular matrix); and in astrocytes – the main focus of this thesis (Araque et al., 1999; Kettenmann and Verkhratsky, 2008; Wang and Bordey, 2008; Dimou and Gotz, 2014; Guillamon-Vivancos et al., 2015).

The main goal of this thesis was to assess the involvement of astrocytic signaling in the modulation of brain circuits that process cognitive function. Therefore, a detailed introduction will be now provided addressing the main topics: astrocyte and gliotransmission, brain networks and cognitive function.

1.1 Astrocytes

Astrocytes are the most abundant type of glial cells in the CNS playing major roles in neuronal function (Bayraktar et al., 2015). These cells are termed astrocytes because they are recognized for their star-shaped and densely ramified form, being broadly distributed in the brain and spinal cord (Oberheim et al., 2012; Hu et al., 2016). In the adult brain, each astrocyte occupies a precise domain with minimal overlap of cell processes, meaning that each synapse will only be regulated by one astrocyte (Allen, 2014). One single astrocyte is then capable to interact with many neurons (Watson et al., 2010) covering thousands of synapses by extending their fine processes (Watson et al., 2010; Clarke and Barres, 2013; Allen, 2014). Astrocytes lack structures such as axons and dendrites and do not present electrical excitability since they are not capable to generate action potential, being their activity mediated by ionic changes in the environment. These cells express ion channels, receptors and other cell surface molecules. Both potassium (K^+) and sodium (Na^+) channels are present in astrocytes. However, their high expression of inwardly rectifying K^+ channels turns these cells into strong passive K^+ buffers that allows to keep the required low extracellular levels of K^+ (Wang and Bordey, 2008).

Astrocytes can couple to neighboring astrocytes through gap junctions formed by connexins (Cxs), namely the Cx30 and Cx43, forming networks that integrate intra- and extracellular signals to modulate and scale network activity and synaptic plasticity (Giaume et al., 2010; Pannasch et al., 2011; McIver et al., 2013; López-Hidalgo and Schummers, 2014). This communication also allows the transmission of small molecules and ions among neighboring astrocytes establishing an astrocyte network, that can be highly flexible and dynamic depending on brain region and age (Allen and Barres, 2009; Matyash and Kettenmann, 2010; Sofroniew and Vinters, 2010).

1.1.1 Origin

The primary neural stem cells to produce neurons and glia throughout the brain have their origin in the neuroepithelium and are called radial glia (RG) (Rowitch and Kriegstein, 2010; Bayraktar et al., 2015). The neuroepithelial cells, that line the cerebral ventricles and spinal canal, give rise to neurogenic RG that generate different subtypes of neurons in a sequential manner and, at later stages of embryonic development, RG become gliogenic to produce astrocytes (Figure 1.1) (Allen, 2014; Bayraktar et al., 2015). After the period of neuronal migration along their radial fibers, in most regions of the CNS occurs a retraction of RG processes to transform themselves into star-

shaped astrocytes, during the perinatal period (Wang and Bordey, 2008). Astrocytes differentiation comprise the expression of vimentin, glial fibrillary acidic protein (GFAP), two astrocyte-specific glutamate transporters (GLAST and GLT-1) and glutamine synthase. Astrocyte progenitors spread from the ventricular-subventricular zone or the pial surface through the entire brain parenchyma where they continue to proliferate within regional constraints, as they largely migrate radially, covering homogeneously the neuropil (Dimou and Gotz, 2014).
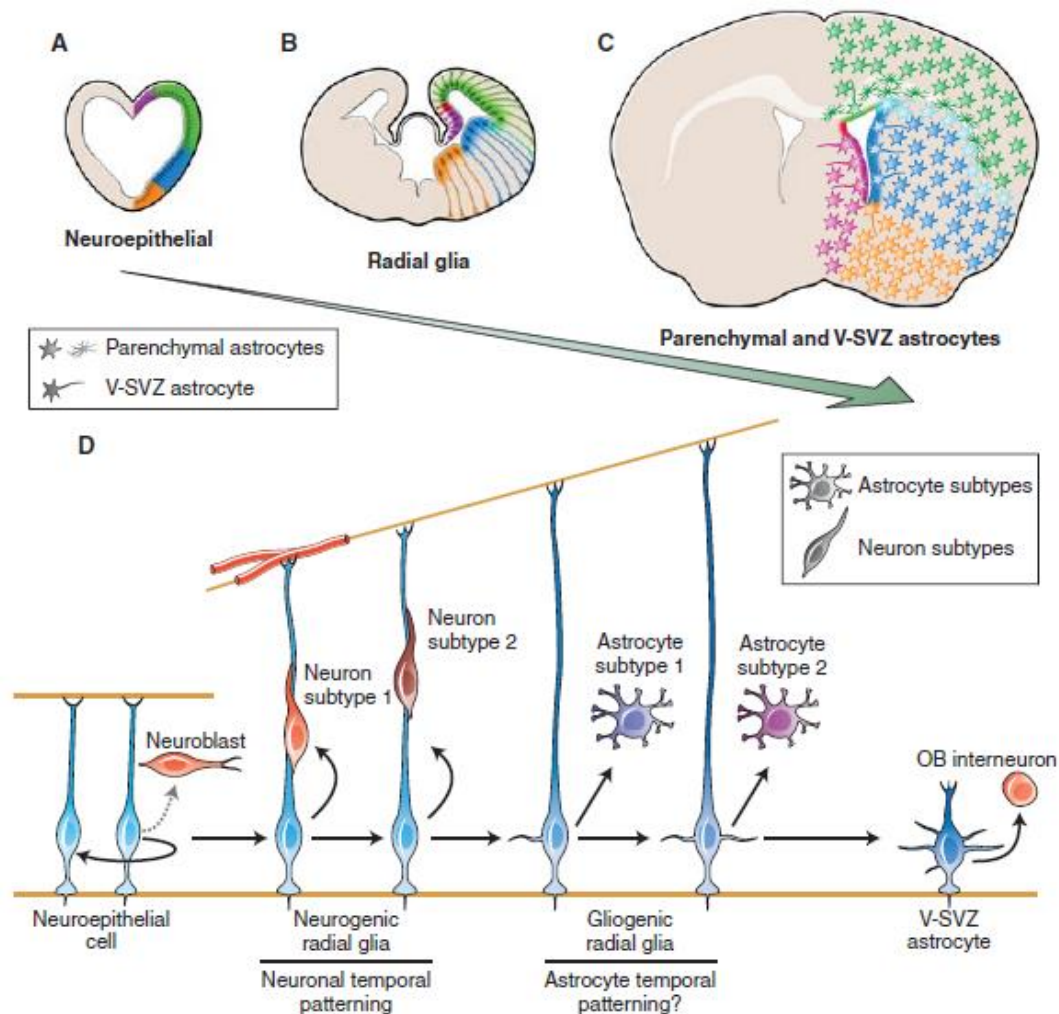
Figure 1.1. Developmental origins of astrocyte heterogeneity. (A) The regional specification of neuroepithelial cells (NE), (B) radial glia (RG), and (C) ventricular-subventricular zone (V-SVZ) and parenchymal astrocytes; (D) during development. NE and RG cells at different regions of the developing forebrain generate adult V-SVZNSCs and parenchymal astrocytes that retain key positional information cues to control the progeny they produce and function, respectively. (D) Neural stem cell lineage progression in brain development. NE origin neurogenic RG able to generate different neuronal subtypes sequentially, and at later stages of embryogenesis, neurogenic RG become gliogenic to produce astrocytes. RG also give rise to V-SVZ astrocytes that produce different subtypes of olfactory bulb (OB) interneurons depending on the region in which they are located (Adapted from Bayraktar et al., 2015).

1.1.2 Morphological and molecular heterogeneity

Since Ramon y Cajal prompted the existence of variability in astrocytes morphology, based on brain region and circuit location, a growing piece of evidence has been supporting the concept of morphological and molecular differences between astrocytes depending on their derivation from regionally patterned RG, and their specialization according to their brain location (López-Hidalgo and Schummers, 2014; Khakh and Sofroniew, 2015). In fact, the molecular and functional heterogeneity in astrocytes might be an enlightenment for the capacity of the CNS to retain embryonic positional information into adulthood. Thus, their heterogeneity is presented in a spatio-temporal manner encompassing development, gene expression, physiological and functional properties, and even how these cells respond in a pathological condition or brain injury (Zhang and Barres, 2010; Bayraktar et al., 2015; Hu et al., 2016). During development, the spread of astrocytes results from a local proliferation, already proposing a regional heterogeneity of fundamental functional importance (Dimou and Gotz, 2014).

In adult brain, astrocytes can be mainly divided in protoplasmic and fibrous. The protoplasmic astrocytes are present in the gray matter, involved with neuronal cell bodies and synapses, and exhibit a dense ramification of fine processes. The fibrous astrocytes are found in the white matter associated with neuronal axons by their long fiber-like processes (Allen and Barres, 2009; Matyash and Kettenmann, 2010; Sofroniew and Vinters, 2010; Hu et al., 2016). In addition to these two classes, more specialized astrocytes were defined based on their regional-specific differences in morphology and function, being categorized as tanycytes, Müller glia, Bergmann glia, velate glia, marginal glia, ependymal glia, perivascular and radial astrocytes (Emsley and Macklis, 2006; Hu et al., 2016). These different types of cells share with astrocytes the ability to become reactive in response to CNS insults. Moreover, human astrocytes can be distinguished in protoplasmic, interlaminar, polarized and fibrous, based on their distinct morphologies and distribution in the adult human temporal lobe (Oberheim et al., 2009; Hu et al., 2016). In comparison to rodent astrocytes, the human ones are three-fold larger and about 10-times more complex and diverse structurally (Oberheim et al., 2009; Matyash and Kettenmann, 2010; Sofroniew and Vinters, 2010; Allen, 2014), varying according to the relative complexity of the neural network (McIver et al., 2013).

Cortical and hippocampal astrocytes have their own non-overlapping territory that is composed by fine processes that surround neuronal membranes and capillary walls (Bushong et al., 2002). The bushy nature of astrocytes allows the establishment of distinct domains within the neuropil in the

brain (Bushong et al., 2004; Watson et al., 2010). Despite of the non-overlapping territories, the stimulation of one astrocyte can lead to the subsequent activation of a specific subset of neighboring astrocytes, suggesting the existence of different networks with different functional significance (Bardehle et al., 2013). These networks were suggested to work as functional islands of synapses in which neighboring synapses confined within the boundaries of an individual astrocyte can be modulated by signals derived from that same astrocyte (Halassa et al., 2007b). Astrocyte signaling can be manifested at synapses relatively distant from active synapses, a process termed lateral astrocyte synaptic regulation that is essentially dependent on the morphological and functional features of astrocytes (Covelo and Araque, 2016). Moreover, a recent work demonstrated that in basal ganglia pathway, there are astrocyte subpopulations that selectively regulate either homotypic or heterotypic synapses through metabotropic glutamate receptor activation suggesting that there is a specificity in the communication between astrocytes, neurons and synapses (Martín et al., 2015).

Different markers have been used to study the molecular identity and heterogeneity of astrocytes. The most commonly used is GFAP, an intermediate filament protein expressed in astrocytes that has cyto-architectural functions. Ten different forms and splice variants of GFAP are known (α, β, γ, δ, ζ, κ, Δexon7, GFAPΔ135, GFAPΔexon6 and GFAPΔ164) and may be variably expressed in different astrocytes (Hol and Pekny, 2015). The immunohistochemistry anti-GFAP labels the main stem branches as GFAP is completely absent from the cytoplasm and from fine processes of astrocytes. It is important to note that not all astrocytes are GFAP-positive and not all cells in the CNS that express GFAP are astrocytes, like neural stem cells of the subventricular zone, although they do not meet the criteria for phenotypic assignment as astrocytes (Wang and Bordey, 2008; Sofroniew and Vinters, 2010; Oberheim et al., 2012; Guillamon-Vivancos et al., 2015; Khakh and Sofroniew, 2015). However, this is a less-time consuming tool that gives an overall assessment of astrocyte main structure and allows a prompter detection of critical morphological alterations. Alternatives to GFAP immunohistochemistry to allow a detailed morphological analysis would be the Golgi staining, transgenic approaches to drive the expression of reporter proteins, or single-cell filling with fluorescent dyes with sharp/patch-clamp electrode, or single cell electroporation (Wang and Bordey, 2008; Sofroniew and Vinters, 2010). Besides GFAP, other markers with growing application are S100β, Aldh1L1 (aldehyde dehydrogenase 1 family member L1), glutamine synthetase and Aldoc (Aldolase C) (Kimelberg, 2004; Cahoy et al., 2008; Wang and Bordey, 2008; Oberheim et al., 2012; Guillamon-Vivancos et al., 2015).

1.1.3 Functions

Astrocytes play a wide range of key functions for the maintenance of the brain network. In general, their main functions include governing capillary flow and traffic between neural tissue and the bloodstream, buffering the extracellular environment, tending synapses, metabolic regulation and intercellular signaling (Wang and Bordey, 2008; Watson et al., 2010).

Astrocytes are important during development of both gray and white matter, since their molecular boundaries guide the migration of developing axons and certain neuroblasts (Sofroniew and Vinters, 2010). Moreover, astrocytes were shown to be actively involved in the regulation of synaptogenesis during development through the release of molecular signals such as thrombospondin (Pfrieger, 2010; Sofroniew and Vinters, 2010; Allen, 2014).

Regarding the regulation of the microvasculature and brain microcirculation, astrocytes appose fine processes named end-feet that involve blood vessels controlling the blood flow and thus the supply of oxygen and glucose to active brain regions (Allen and Barres, 2009). This regulation is mediated by specific molecules such as prostaglandins, nitric oxide and arachidonic acid that are produced by astrocytes to regulate CNS blood vessel diameter and blood flow in a synchronized way (Sofroniew and Vinters, 2010). The ability of astrocytes to function as barrier is also crucial for the establishment of the blood brain barrier (BBB) (Sofroniew and Vinters, 2010; Cabezas et al., 2014).

Astrocytes contribute to the regulation of the neuronal microenvironment through a tight control of fluid, local ion concentrations, pH and transmitter homeostasis. There are different ways for proton shuttling to occur in astrocytes: by Na^+/H^+ exchangers, bicarbonate transporters, monocarboxylic acid transporters and by the vacuolar-type proton ATPase. Moreover, both aquaporin 4 (AQP4) water channel and channels for the uptake of K^+ are abundant in astrocyte processes (Sofroniew and Vinters, 2010).

The clearance of byproducts of metabolism and neurotransmitters from the extracellular space is one important function of astrocytes (Wang and Bordey, 2008; Verkhratsky et al., 2015). In the adult brain, the removal of neurotransmitters from synaptic cleft occurs via transporter-mediated uptake into cells. For instance, glutamate is taken by specific transporters that are in control of excitatory neurotransmission, preventing glutamate-mediated excitotoxicity, and include the glutamate transporter-1 (GLT-1/EAAT2) and glutamate-aspartate transporter (GLAST/EAAT1) (Kreft et al., 2009). GLT-1 is the predominant glutamate transporter expressed in the adult brain supporting 90% of glutamate uptake in the CNS, and is highly expressed in hippocampus, cerebral

cortex and striatum, at the endfeet of astrocytes. On the other hand, GLAST has a higher expression in cerebellum, being primarily assembled within astrocyte cell body. The uptake process is affected by Na^+ and K^+ concentrations and then, by the membrane potential of the astrocyte (Allen, 2014). The potassium buffering by astrocytes avoids excessive basal excitability of neighboring neurons, being this process mediated particularly by the inwardly rectifying potassium $K_{ir}4.1$ and also by TREK channels (Matyash and Kettenmann, 2010; Allen, 2014). According to this, it was shown that the ablation of astrocytes from specific brain regions of rodents, *in vivo*, leads to neuronal degeneration and death, suggesting that the failure to uptake excitatory neurotransmitters or K^+ in excess may lead to excessive activation of glutamate receptors and excitotoxicity (Wagner et al., 2006; Lima et al., 2014).

Astrocytes also participate in the recycling process of neurotransmitters by the glutamate-glutamine cycle. Briefly, glutamate is taken by astrocytes via glutamate transporters and converted to glutamine by the glutamine synthetase, localized in the cytosol. Glutamine is then released back to extracellular space by the transporter SN1 and uptaken by neighboring neurons, where it is converted to glutamate and GABA within the mitochondrial membrane, by phosphate-activated glutaminase, and repackaged into vesicles (Hertz, 2013; Allen, 2014; Verkhratsky et al., 2015).

Also, astrocytes produce and release L-lactate as a potential source of energy for neurons, in particular for glutamatergic activity, being implicated in the astrocyte-neuron lactate shuttle. After the glycolysis, pyruvate is converted to lactate and shuttled to the surrounding neurons to produce ATP by oxidative phosphorylation, during periods of intense neuronal activity (Hertz, 2004; Pellerin and Magistretti, 2012; Tang et al., 2014).

Perisynaptic processes of astrocytes can act as physical barriers for spillover and diffusion into the extrasynaptic space of locally released, potentially active molecules, such as glutamate and GABA. This effect may limit the crosstalk between neighboring synapses, while favoring specificity of synaptic transmission, resulting in regulation of synapse development and modulation of synaptic strength (Potokar et al., 2007; De Pittà et al., 2016).

1.2 Astrocyte-derived signaling and gliotransmission

Across the years, new information has been pointing out an involvement of astrocytes in the active control of neuronal activity and thus on synaptic neurotransmission, being currently accepted that, just like neurons, astrocytes are capable to release transmitters through a process called

gliotransmission (Halassa et al., 2007a; McIver et al., 2013). Astrocyte-neuron communication through gliotransmission was proposed to take part in synaptic mechanisms and memory, sensory perception, neuroendocrine function, circadian rhythm regulation, breathing and pain modulation (Zhang and Haydon, 2005; Ben Achour and Pascual, 2012). The detection of local and rapid basal synaptic transmission by astrocytes suggest an aptitude to discriminate different levels of communication, from basal synaptic activity up to complex patterns of plurisynaptic network interactions. Therefore, through gliotransmission, astrocytes participate in information processing by linking neuronal activities occurring at different spatial and temporal dimensions in order to achieve a higher level of integration of brain function (Araque et al., 2014).

1.2.1 The concept of the tripartite synapse

The bidirectional communication between neurons and astrocytes occurs between neuronal elements (presynaptic and postsynaptic) and the astrocyte projection, surrounding the synaptic cleft. Briefly, the neurotransmitter release by neurons, under a depolarization at the pre-synaptic terminal, activates astrocytic receptors triggering signaling cascades (namely, calcium-dependent) in astrocytes which, in turn, release neuroactive substances signaling back to neurons and forming a feedback loop. This tight spatial relationship led to propose the tripartite synapse concept (Figure 1.2) (Araque et al., 1999; Ni et al., 2007; Perea et al., 2009; Allen, 2014).

Astrocytes are able to sense activity changes in the adjacent neurons through ion channels, receptors and also transporters present on their surface. Astrocytes express a large range of receptors, including G-protein coupled and ionotropic receptors, for typical neurotransmitter and neuromodulator molecules such as glutamate, acetylcholine, ATP, GABA, norepinephrine and endocannabinoids (Verkhratsky et al., 2015; De Pittà et al., 2016). The activation of these receptors leads to an increase in astrocytic intracellular calcium that may conduct the release of many different transmitters, such as neurotransmitters and neuromodulators collectively called gliotransmitters (Harada et al., 2015; De Pittà et al., 2016; Petrelli and Bezzi, 2016; Zorec et al., 2016). There are several astrocyte-derived secretory substances such as: Adenosine/ATP, glutamate, GABA, BDNF, D-serine or TNF-α (Araque et al., 2014; Yoon and Lee, 2014; Petrelli and Bezzi, 2016; Verkhratsky et al., 2016). Gliotransmitters are synthesized by and/or stored in astrocytes and their release is regulated by a physiological or pathological stimuli. Once released, these transmitters rapidly (milliseconds to seconds) interact and activate the surrounding cells,

specifically modulating neuronal firing frequency and synaptic transmission (Parpura and Zorec, 2010; Oberheim et al., 2012; Allen, 2014).
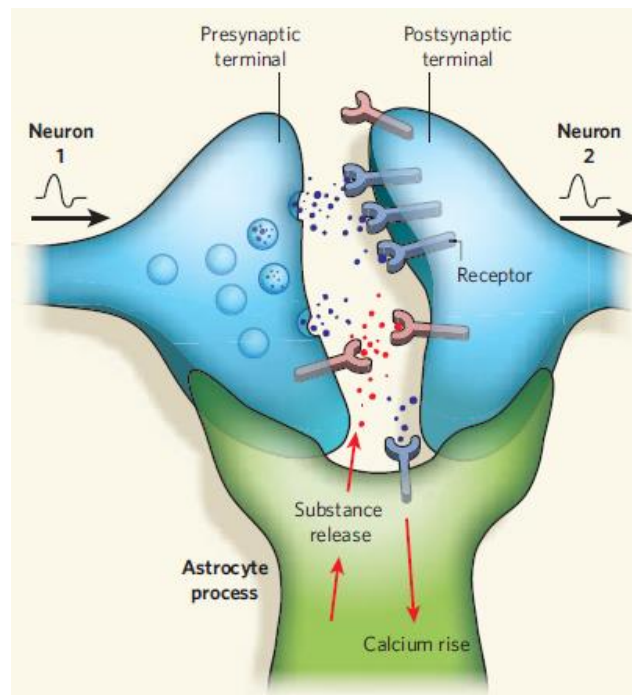
Figure 1.2. The tripartite synapse and gliotransmission. Astrocytes express several neuronal receptors and once neurotransmitters are released from the presynaptic terminal of a neuron, astrocytic receptors are able to sense them. This process results in astrocytic activation and leads to an intracellular rise of calcium levels with the subsequent release of various active substances, such as ATP and D-serine, which feedback on neurons to either inhibit or enhance neuronal activity. Astrocytes also participate in the synapse formation, presynaptic function regulation and modulation of the response of the postsynaptic neuron to neurotransmitters (Adapted from Allen and Barres, 2009).

The calcium signaling is considered a substrate for glial excitability and simple changes in astrocytic calcium levels can activate the astrocyte-to-neuron signaling pathways (Parpura and Haydon, 2000; Perea and Araque, 2007; Di Castro et al., 2011). The hallmark of the cytosolic excitability of astrocytes is the calcium concentration transient elevation. In one hand, these elevations in astrocyte intracellular calcium concentration that trigger gliotransmission, can be originated by intrinsic oscillations, resultant from the release of Ca^{2+} from intracellular stores. On the other hand, the release of transmitters from astrocytes can elicit neurotransmitters release during synaptic activity, triggering receptor mediated currents in neurons that, in turn, propagate to neighboring astrocytes, prompting intracellular calcium elevations in these cells (Perea et al., 2009; Sofroniew and Vinters, 2010; Oberheim et al., 2012). One of the main mechanisms described to trigger calcium oscillations in astrocytes works via activation of metabotropic G protein-coupled receptors. Upon activation, these receptors stimulate phospholipase C and lead to the

formation of inositol (1,4,5)-triphosphate (IP$_3$) molecules. These will in turn mediate calcium release from intracellular stores at the smooth endoplasmic reticulum via IP$_3$ receptor activation (Perea et al., 2009; Agulhon et al., 2012; Harada et al., 2015). Recent studies support alternative types of intracellular Ca^{2+} signaling by demonstrating that spontaneous Ca^{2+} signals can occur not only in somata, but also in astrocytic fine processes far away from the intracellular Ca^{2+} stores. It was shown that, under stimulation of the Schaffer collateral fibers in acute hippocampal slices from adult mice, Ca^{2+} signals are faster and of higher amplitude in the fine processes than those in somata of astrocytes, probably due to the larger surface/volume ratio of processes (Tang et al., 2015). Nevertheless, it is now clear that astrocytes exhibit calcium domains in different cell compartments resultant from localized calcium activity, triggered by different inputs (Di Castro et al., 2011; Kanemaru et al., 2014; Asada et al., 2015; Srinivasan et al., 2015). These data sets highlight the high-sensitivity of astrocytic processes to neuronal activity detection, providing evidence for astrocytic integration in local synaptic functioning.

1.2.2 Transmitter release by astrocytes

The exact mechanisms of release and which gliotransmitters are assuredly released from astrocytes are still topics under discussion (Malarkey and Parpura, 2009; Perea et al., 2009; Parpura and Zorec, 2010; Martineau, 2013; Allen, 2014; Sahlender et al., 2014; Verkhratsky et al., 2016). Nonetheless, it is generally accepted that astrocyte mechanisms for transmitter release can be divided based on two main routes: Ca^{2+} regulated exocytosis and non-exocytotic release from cytosolic pools. We will briefly refer to the latter, and proceed in detail to the first, due to its relevance and amount of studies supporting the release of transmitters by astrocytes through exocytosis.

Non-exocytotic release from cytosolic pools may occur by diffusion through volume-regulated anion channels (Kimelberg et al., 2006), Ca^{2+}-dependent anion channel bestrophin 1 (Park et al., 2013), two-pore potassium channels (Zhou et al., 2009), hemichannels/connexins (Montero and Orellana, 2015) or pore-forming P2X7 receptors (Duan et al., 2003); or mediated by specific transporters [cysteine-glutamate exchanger, reversal of uptake by glutamate (GLT-1 and GLAST) and GABA transporters (GAT-3)] (Hamilton and Attwell, 2010) (Figure 1.3). There is evidence of astrocytic glutamate release by volume-regulated anion-cannels (VRAC), an intracellular Ca^{2+}-dependent mechanism, demonstrated to be more predominant in pathological conditions such as stroke and

depression (Gundersen et al., 2015). The diffusive flux of molecules from the cytoplasm to the extracellular space can also occur by gap junction hemichannels, formed by connexins or pannexins, but this mechanism was also suggested to be independent of fluctuations in astrocytic $[Ca^{2+}]_i$ (Ye et al., 2003). The P2X7 receptors activation leads to a pore formation that is permeable to specific gliotransmitters (Virginio et al., 1999). Moreover, reversal of uptake carriers through plasma membrane transporter, is a mechanism that is Ca^{2+}-independent and for instance, blocking glutamate transporters does not affect glutamate release from astrocytes, suggesting that this mechanism has a minor contribution to gliotransmitters release (Hamilton and Attwell, 2010).
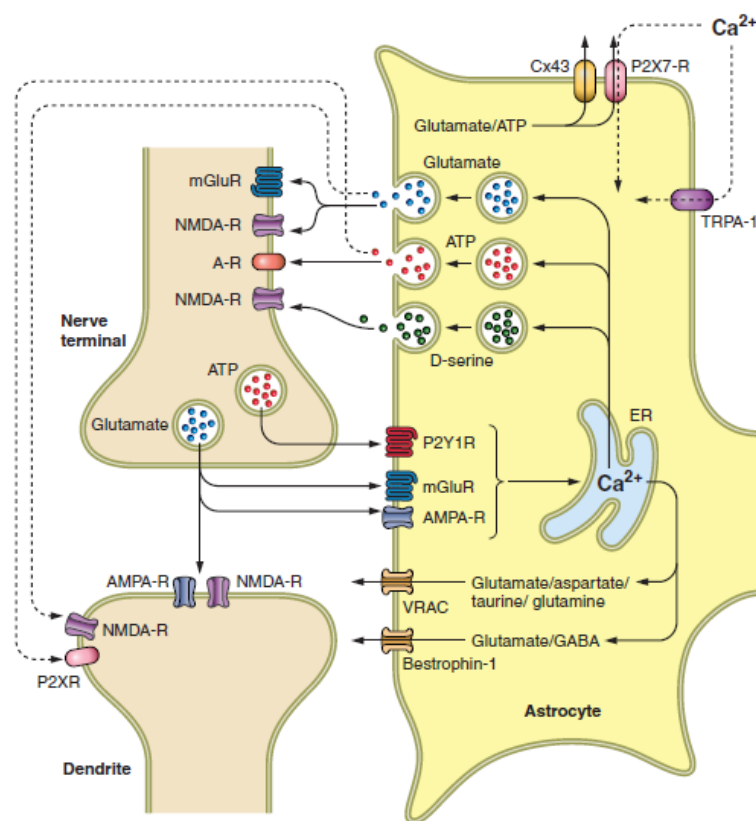
Figure 1.3. Signaling mechanisms. Schematic synopsis of the mechanisms responsible for the increase of intracellular Ca^{2+} and release of gliotransmitters in astrocytes, and the effects of gliotransmitters on synaptic activity. Synaptically released glutamate and ATP activate metabotropic glutamate and ATP receptors on neighboring astrocytic processes, or AMPA receptors on astroglial cells. This receptor activation mobilizes the release of Ca^{2+} from endoplasmic reticulum (ER). Alternatively, Ca^{2+} can flux into astrocytes from the extracellular fluid via P2X receptors or TRPA-1 channels. The increase in the cytosolic Ca^{2+} concentration is a trigger for exocytotic release of gliotransmitters or channel-mediated release via bestrophin-1 and volume-regulated anion channels (VRACs). Gliotransmitters can also be released through Ca^{2+}-independent opening of P2X7 ATP receptors or Cx43 hemichannels (Adapted from Gundersen et al., 2015).

Ca^{2+} regulated exocytosis appears as the most studied mechanism, in which gliotransmitters are released through vesicle or lysosome fusion. The traffic of vesicles in astrocytes is commonly associated with cell morphology, determining the signaling potential and metabolic support for

13

neighboring cells. The cargo contained and carried by these vesicles is quite diverse, counting with neurotransmitters, neuromodulators, transporters, water channels and receptors. Regulated exocytosis of the astrocytic vesicles content is a slower process in comparison to neurons (Guček et al., 2012) and if such a slow constitutive plasma membrane turnover occurs in astrocytes *in vivo*, one would expect that the slightest imbalance in the rate of vesicle delivery to, against the rate of retrieval from the plasma membrane, could progressively affect the properties of astrocytes and their responsiveness to physiological and pathological stimuli. Furthermore, the vesicular motility can be primarily controlled by the cytoskeleton dynamics and thus, synaptic transmission can be also affected by changes in shape and volume of astrocytic processes (Araque et al., 1999; Reichenbach et al., 2010). The retraction or expansion of these processes can consequently alter the extracellular space geometry, interfering with the astrocyte-neuron signaling (Theodosis et al., 2008). With the increased knowledge about the nature of vesicle mobility in astrocytes in both health and disease (reviewed in Vardjan et al., 2015), and taking advantage from the slowness of this process, has been emerging the development of new drugs affecting vesicle traffic that could be used in the treatment of neurological disorders. For instance, multiple sclerosis treatment was attempted by the use of fingolimod, a drug used to interfere with vesicular mobility, decreasing it (Chun and Brinkmann, 2011; Trkov et al., 2012).

Based on these evidences, vesicular exocytosis is an essential mechanism for the astrocyte-to-neuron communication in the brain (Kreft et al., 2009; Verkhratsky et al., 2012; Thorn et al., 2016). There are several transporters such as V-ATPase (for ATP), VGLUTs 1-3 (for glutamate) and VSERT (for D-serine) responsible for the vesicular upload of transmitters (Montana et al., 2006; Verkhratsky et al., 2012; Martineau, 2013), and numerous proteins that provide an excitation-secretion coupling in astrocytes (Vardjan et al., 2016).

The vesicular fusion encompasses: (i) the transport of vesicular cargo and membrane proteins inside cells; (ii) the release of their content to the extracellular space after fusion with plasma membrane and, (iii) membrane repair (Ropert et al., 2016). For exocytosis to occur, a fusion pore connecting the vesicle lumen with the extracellular space should be formed (Kreft et al., 2016).
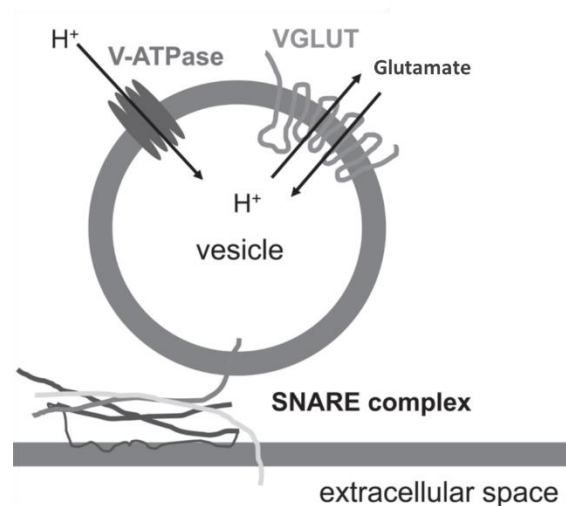
Figure 1.4. SNARE complex formation in astrocytes. Gliotransmitters such as glutamate and D-serine are packaged in vesicles and its release from the astrocyte occurs when the vesicle fuses with the plasma membrane. This fusion process is mediated by synaptotagmin 4 and SNARE complex proteins such as syntaxin 1, synaptobrevin II and synaptosome-associated protein of 23 kDa (SNAP-23) (Adapted from Montana et al., 2014).

The soluble N-ethylmaleimide-sensitive factor attachment protein receptor (SNARE) machinery is the responsible for the mediation of this fusion/secretory process and is composed by vesicular- and target membrane-associated proteins constituted by α-helices that bind to form a stable four-helix bundle and then, the so called SNARE complex (Weber et al., 1998). The astrocytic SNARE complex mainly comprises the following proteins: synaptobrevin II (also referred to as vesicle-associated membrane protein 2 – VAMP2; its homologue cellubrevin (VAMP3); syntaxin 1 (isoforms A and B); synaptosome-associated protein (SNAP23) and the auxiliary protein synaptotagmin 4 (Figure 1.4) (Schubert et al., 2011; Singh et al., 2014; Vardjan et al., 2016). It was shown that in mice knock-out (KO) for the expression of synaptobrevin II there is a significant decrease in synaptic vesicle fusion and in fast Ca^{2+}-triggered fusion, supporting the role of this protein in stabilizing fusion intermediates and in fusion catalysis (Schoch, 2001). More specifically, the inactivation of synaptobrevin II by either Tetanus neurotoxin (TeNT) or Botulinum neurotoxin B (BoNT/B) (Pellizzari et al., 1999) abolished the release of glutamate (Araque et al., 2000; Bezzi et al., 2004; Jourdain et al., 2007) or D-serine (Henneberger et al., 2010) from astrocytes. Additionally, the expression of the dominant negative domain of the cytosolic portion of synaptobrevin II selectively in astrocytes is accompanied by a drastic reduction in the release of glutamate, in cell cultures (Zhang et al., 2004). The same strategy was employed to suppress exocytosis in mice, through the generation of the dnSNARE mouse model by Philip Haydon's Lab (Pascual et al., 2005). Astrocytes cultured from this mouse displayed a decrease of vesicular fusion events down to 9% (Sultan et al., 2015). This was accompanied by a decrease of ATP release, measured in brain slices from either

15

hippocampus or cortex (Cao et al., 2013; Pankratov and Lalo, 2015) and D-serine, measured in cell culture, brain slices and *in vivo* (Pankratov and Lalo, 2015; Sultan et al., 2015). Consequently, alterations in synaptic transmission and plasticity were seen in this model (Pascual et al., 2005; Hines and Haydon, 2013; Nadjar et al., 2013; Turner et al., 2013; Lalo et al., 2014a). These studies suggest a clear involvement of astrocytic synaptobrevin II-dependent exocytosis in information transfer in the brain.

The exocytotic release of transmitters is a Ca^{2+}-dependent mechanism and the main source of cytosolic Ca^{2+} is primarily derived from internal stores, the endoplasmic reticulum and mitochondria (Montana et al., 2006; Parpura et al., 2011; Verkhratsky et al., 2012). After exocytosis, vesicles are re-endocytosed, recycled and refilled with transmitters. Different types of astrocytic secretory organelles can be identified based on their characteristics. The synaptic-like microvesicles, with a diameter of 30-100 nm, are typically generated by intracellular fusion of smaller vesicles and/or organelles either in response to an increase in $[Ca^{2+}]_i$ or to mechanical stimulation, and primarily store D-serine and glutamate. The dense-core vesicles are present in astrocytes in a smaller fraction, with a diameter of 100-600 nm. The fusion of both types of vesicles is mediated by synaptobrevin II and VAMP3. Secretory lysosomes are also found in astrocytes and were described to participate in the storage and Ca^{2+}-dependent exocytosis of ATP. Lysosomes diameter can vary between 300 and 500 nm and they coexist with synaptic-like microvesicles within the same astrocyte. Additionally, extracellular vesicles may also be released from astrocytes and are commonly loaded with several bioactive substances such as cytokines, signaling proteins, mRNA and microRNA. They can be broadly divided into exosomes (produced by the formation of multi vesicular bodies and subsequent fusion with the plasma membrane), and ectosomes, that are formed and released by shedding off the plasma membrane (Verkhratsky et al., 2016).

1.2.3 Gliotransmitters released by exocytosis

Among the several transmitters proposed in the literature, there are three well characterized gliotransmitters described to be stored in astrocytes secretory vesicles and to be released by exocytosis: ATP, glutamate and D-serine.

ATP

ATP is one of the main neurotransmitters released by astrocytes that takes part in the mediation of the neuroglial chemical signaling (Newman, 2003; Zhang et al., 2003; Verkhratsky et al., 2012; McIver et al., 2013). Astrocytic ATP is stored in vesicles, namely synaptic-like microvesicles. Despite of its fast hydrolyzation into adenosine in the extracellular space, once released ATP can modulate individual neuronal activity and also coordinate both neuronal and astrocytic networks. For instance, the vesicular release of ATP from astrocytes can produce an excitatory signaling in the neighboring neurons, operating through purinergic P2X receptors (Lalo et al., 2014a). Moreover, the release of ATP by astrocytes may also activate P2Y1 receptors in neighboring astrocytes generating calcium waves across the astrocytic network, providing a mechanism for rapid intercellular communication across broad domains (Bowser and Khakh, 2007).

The first study using the transgenic mouse model dnSNARE, with impaired gliotransmission and consequent reduction of ATP release, showed that enhanced synaptic transmission in these mice was due to the absence of tonic presynaptic inhibition of synaptic transmission that is mediated by neuronal adenosine A_1 receptors (Pascual et al., 2005). Moreover, the same lab showed that astrocyte-derived adenosine plays an important role in driving the homeostatic sleep response and the effects of sleep deprivation on memory processing (Halassa et al., 2009b; Florian et al., 2011). In normal conditions, there is an increase in extracellular concentration of adenosine, in response to wakefulness and sleep loss, which is accompanied by an increase in the expression levels of A_1 receptors. Though, in dnSNARE mice these increases are prevented, and the wakefulness-dependent changes in synaptic and network regulation by A_1 receptors are attenuated (Schmitt et al., 2012). However, astrocytic ATP was demonstrated to act in a bidirectional fashion to regulate neuronal excitability depending on concentration. Using a mouse model containing an astrocyte-selective mutation and displaying an overexpression of hGFAP, it was verified that a small increase in the release of ATP results in the suppression of inhibitory GABAergic transmission, enhancing the excitability of neuronal circuitry and lowering the threshold for LTP induction, in comparison to controls (Lee et al., 2013). Another work in the hippocampal CA1 region confirmed the role of astrocytic ATP in the facilitation of heterosynaptic long-term depression (Chen et al., 2013). ATP was pointed also as the key factor involved in astrocytic modulation of depressive-like behavior in adult mice. Briefly, Cao and colleagues showed that ATP is decreased in the brain of mice susceptible to chronic social defeat and that administration of exogenous ATP induces a rapid antidepressant-like effect in the same animals. Moreover, they found that stimulating endogenous

ATP release from astrocytes reverts the depressive-like behavior in mouse models of depression (Cao et al., 2013). A different study revealed that exogenous ATP is able to rescue the deficits observed in synapse elimination in inositol 1,4,5-trisphosphate receptor type 2 knockout (Itpr2$^{-/-}$) mice, lacking somatic Ca^{2+} signaling in astrocytes. These findings suggest that astrocytes release ATP in an IP$_3$R2-dependent manner in order to regulate synapse elimination (Yang et al., 2016).

Glutamate

Glutamate is the major excitatory neurotransmitter in the regulation of synaptic plasticity and LTP, and thus deeply involved in functions such as cerebral development and motor and cognitive functions, being astrocytes the main cell type enrolled in the maintenance of physiological glutamate concentration in CNS (Kandel et al., 2012). Glutamate was suggested to be stored in astrocytic vesicles that release the gliotransmitter through an exocytotic pathway in a Ca^{2+}-dependent manner (Araque et al., 2000; Bezzi et al., 2004; Zhang et al., 2004). More specifically, a study showed by immunogold cytochemistry of the adult hippocampus, that glutamate accumulates in synaptic-like microvesicles in the perisynaptic processes of astrocytes (Bergersen et al., 2012). The uptake of cytoplasmic glutamate into astrocytic vesicles is mediated by VGLUTs, driven by a photon gradient produced by vacuolar-type H$^+$ ATPases (Harada et al., 2015). The glutamate release by astrocytes can occur spontaneously or in response to neuronal activity (Malarkey and Parpura, 2008), modulating synaptic transmission through the activation of either presynaptic, synaptic or extrasynaptic glutamate receptors (López-Hidalgo and Schummers, 2014). These receptors can be ionotropic – GluRs, such as AMPA, kainate and NMDA receptors (NMDAR); or metabotropic – mGluRs.

Importantly, a study showed the crucial role that glutamate released specifically by astrocytes, plays in the maintenance of a synchronized activity from hippocampal neurons. The astrocyte-derived glutamate was described to act on the adjacent neuronal processes, controlling simultaneously the excitability of several neighboring pyramidal cells (Angulo et al., 2004). Moreover, the glutamate released by astrocytes was also shown to trigger a coordinated Ca^{2+} response in CA1 neurons (Fellin et al., 2004; Sun et al., 2013); to increase the frequency of excitatory postsynaptic potentials (Fiacco and McCarthy, 2004), or to lead to a decreased synaptic failure in response to minimal stimulation of the Schaeffer collaterals (Navarrete and Araque, 2010).

Besides the activation of neuronal receptors, astrocyte-derived glutamate may also virtually activate astrocytes receptors. The AMPA type glutamate receptor is highly expressed by astrocytes while NMDAR were only found in astrocytes from cortex (Lalo, 2006) and in spinal cord (Ziak et al., 1998) of rodents. Evidence of the existence of functional NMDAR expression in human astrocytes was also given by Lee and colleagues using primary astrocyte cultures (Lee et al., 2010). Metabotropic receptors are greatly expressed in astrocytes, and are mainly represented by mGluR3 and mGluR5 (Verkhratsky et al., 2012; Araque et al., 2014). While there is a lack of studies showing relevant activation of astrocytic glutamate receptors upon glutamate release form astrocytes, one should not discard this possibility.

D-serine

A growing piece of evidence established D-serine as a key signaling molecule used for the astrocyte-neuron metabolic crosstalk, supplying energy for neurons through the regulation of synaptic glutamate (Wolosker, 2011). D-serine is an aminoacid that acts as primary endogenous positive modulator (coagonist) of cortical and hippocampal NMDAR activity – acting on their glycine site (Hashimoto et al., 1993; Mothet et al., 2000, 2015; Papouin et al., 2012). The biosynthesis of D-serine occurs in the cytoplasm of astrocytes and primarily depends on 3-Phosphoglycerate dehydrogenase (PHGDH) that catalyzes the first committed step in L-serine biosynthesis, in both neurons and astrocytes (Ehmsen et al., 2013). L-serine is an amino acid and the predominant source of one-carbon groups for the *de novo* synthesis of purine nucleotides and deoxythymidine monophosphate (De Koning et al., 2003). D-serine synthesis also requires the interaction between serine racemase (SR), an enzyme that transforms L-serine to D-serine and that is abundant in astrocytes from cerebral cortex of rodents and humans (Verrall et al., 2007), with glyceraldehyde 3-phosphate dehydrogenase (GAPDH), a glycolytic enzyme that catalyzes the sixth step of glycolysis (Suzuki et al., 2015). D-serine is stored within synaptobrevin II-bearing vesicles and its release occurs via Ca^{2+} regulated exocytosis from astrocytes (Mothet et al., 2005; Bergersen et al., 2012; Verkhratsky et al., 2012; Martineau et al., 2013; McIver et al., 2013). Free D-serine can be found at a high concentrations in all brain regions, but cerebellum (Hashimoto et al., 1993; Pernot et al., 2012), being highly concentrated in areas enriched in NMDAR (Mothet et al., 2000). Its selective elimination in the forebrain tissues has been reported to result in marked attenuation of the NMDAR function both *in vitro* and *in vivo* in rodents (Wolosker, 2007). The regulation of the extracellular level of D-serine in mammals brain occurs by means of D-amino-acid-oxidase (DAO), a flavoenzyme

that catalyzes the oxidation of D-amino acids, described to be mainly located in the astrocytes from brain stem, cerebellum and spinal cord (Horiike et al., 1994; Mothet et al., 2000; Pilone, 2000; Park, 2006) and to neurons at dorsolateral prefrontal cortex and hippocampus (Verrall et al., 2007).

The main cellular origin of D-serine is still under debate (Papouin et al., 2017b). Primarily, it was believed that D-serine was exclusively synthetized and expressed by astrocytes (Figure 1.5). Martineau and colleagues found that SR is anchored to the membrane of vesicles in rat cortical astrocytes, allowing local generation of D-serine and suggesting D-serine uptake as an astrocyte-specific function (Martineau et al., 2013). Importantly, SR was also found to be highly expressed by astrocytes from human subiculum (Suzuki et al., 2015). There is some evidence available describing a neuronal source for D-serine (Rosenberg et al., 2010). In fact, a recent study demonstrated that neuronal SR is implicated in the regulation of the extracellular D-serine signaling in the hippocampus of neuron-specific SR gene deficient mice, that exhibited a hypoactivity of the hippocampal NMDAR and lower basal content of extracellular D-serine, in comparison to their littermates (Ishiwata et al., 2015). Nevertheless, the extensive literature specifying the roles of
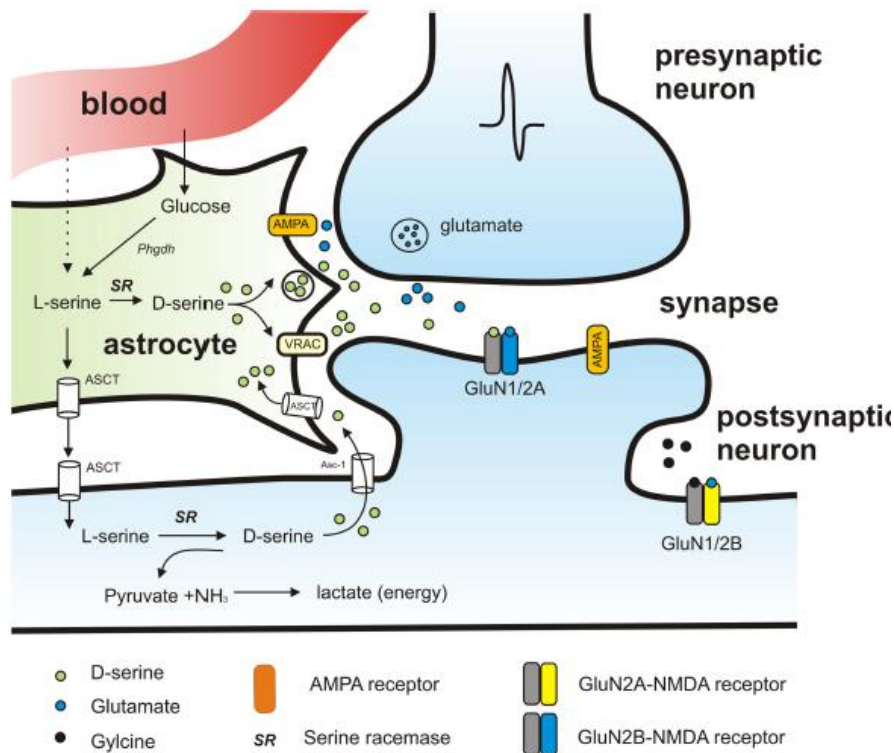
Figure 1.5. Schematic model of the proposed pathways mediating D-serine synthesis and release. The activation of a presynaptic neuron leads to the release of glutamate that binds to AMPA receptors on neighboring astrocytes conducting to the subsequent release of D-serine. In neurons, SR synthesizes D-serine from L-serine. L-serine is shuttled to neurons from astrocytes through aminoacid transporters (ASCT) (Adapted from Van Horn et al., 2013).

astrocyte-derived D-serine are very strong. D-serine was shown to impact long-term potentiation (LTP) by enhancing NMDAR activation and enabling LTP induction in cultures of neurons fed with glial conditioned medium. Furthermore, in hippocampal slices, the induction of LTP at Schaffer collateral–CA1 pyramidal cell synapses was shown to depend on the presence of intact glial cells and extracellular D-serine (Yang et al., 2003). Later, Panatier and colleagues demonstrated that the concentration of D-serine in the synaptic cleft and thus the occupancy of the glycine site at synaptic NMDAR was strongly dependent on the amount of synapses covered by astrocytes, in agreement with a possible role of D-serine on long-term synaptic plasticity (Panatier et al., 2006). Following this study, Henneberger and colleagues reinforced that Ca^{2+}-dependent release of astrocytic D-serine is in control of NMDAR-plasticity in thousands of excitatory synapses in the hippocampus (Henneberger et al., 2010). Like so, astrocytic D-serine has been suggested to be involved in synaptic mechanisms of learning and memory as, for instance, the ones occurring with aging progression that is characterized by a deficit in NMDAR activation and by an impairment in D-serine biosynthesis pathway (Mothet et al., 2006). One study indicating that acute stress leads to a decrease of D-serine levels in the brain and to a behavioral deficit, demonstrated that by administering exogenous D-serine the stress-induced impairments in memory consolidation in mice can be prevented (Guercio et al., 2014).More specifically, it was demonstrated that the inhibitory effect of the astrocyte-selective toxin fluoroacetate (FAC) on synaptic transmission and plasticity (Zhang et al., 2008) can be fully prevented by D-serine addition to slices of the medial prefrontal cortex of adult rats (Fossat et al., 2012). In accordance, a recent study restored the FAC-induced spatial and contextual fear learning and memory impairment, with a systemic treatment with D-serine that restored the hippocampal LTP in rats (Han et al., 2015b).

1.2.4 The dnSNARE mouse model

The dnSNARE mouse model was generated at the lab of Prof. Philip Haydon (Tufts University, USA) and is being used as a tool to dissect the role of gliotransmitter release in the function of brain circuits and consequent behavior modulation. These mice express a dominant-negative SNARE protein that interferes with the vesicular release by exocytosis selectively in astrocytes, causing a deficient gliotransmission, but a normal neurotransmission. The behavioral consequences of this impairment in gliotransmission have been explored in different conditions. Originally, the Haydon lab demonstrated that astrocytes are crucial in the regulation of synaptic transmission and

modulation of plasticity through the purinergic signaling (Pascual et al., 2005). Later, they also described that the expression of dnSNARE transgenes in astrocytes decreases the tyrosine phosphorylation of Src kinase and NR2 subunits (Deng et al., 2011). In a normal circuit, protein phosphorylation participates in the regulation of glutamate receptors trafficking and specifically, the phosphorylation of tyrosine residues on NR2A and NR2B potentiates NMDAR-mediated currents (Petralia et al., 2009). The reduction in tyrosine phosphorylation of NR2 enhances the interactions with the core plasma membrane adaptor AP2, a protein that is required for the endocytosis of these subunits. So, an increased rate of endocytosis of NMDAR may justify the reduction of its surface expression in the current mouse model. These modulatory capacities of astrocytes ultimately impact the sleep homeostasis, by the regulation of sleep pressure accumulation and its cognitive consequences. Briefly, in dnSNARE mice, the blockade of gliotransmission attenuates the cognitive deficits observed in wild-type animals under sleep deprivation, exhibiting then a better performance in spatial cognitive tasks (Fellin et al., 2009; Halassa et al., 2009b; Florian et al., 2011; Nadjar et al., 2013). Moreover, Turner and coworkers tested dnSNARE mice in behavioral paradigms examining cocaine-induced behavioral plasticity and found that gliotransmission is required for the reinstatement of drug-seeking behaviors by cocaine or associated cues (Turner et al., 2013). Since in dnSNARE mice there is an attenuation of the progressive increase in seizure frequency *in vivo*, astrocytes were shown to contribute to the development of temporal lobe epilepsy by the control of synaptic NMDAR (Clasadonte et al., 2013). Similarly, Hines and Haydon demonstrated an attenuation of damage following stroke in dnSNARE mice that had a reduced lesion volume and an improved behavioral performance after photothrombosis (Hines and Haydon, 2013). Furthermore, dnSNARE mice exhibit a reduced nociceptive threshold in response to mechanical stimulation under baseline conditions, providing evidence that gliotransmission modulates the baseline mechanical nociception and hence, the physiological pain behavior (Foley et al., 2011). More recently, an elegant study also using the dnSNARE mouse, confirmed the influence of niche-constituting astrocytes in the maturation of adult-born hippocampal neurons, demonstrating that astrocytic signaling regulates synapse formation in newborn neurons (Sultan et al., 2015).

In spite of being used in different labs (Oliveira et al., 2015), this mouse model validity was challenged (Fujita et al., 2014). Nevertheless, its validation and reliability were reestablished by our data and by others (Pankratov and Lalo, 2015; Sultan et al., 2015; Papouin et al., 2017a;

Wagner et al., 2017). The data gathered so far indicates that this model is an excellent tool to study the impact of astrocyte signaling to the modulation of brain circuits.

1.3 Brain networks

Astrocytes were proposed to represent an additional and complementary neuromodulatory system, with its own time and space domains, due to their particular intrinsic properties of calcium signaling. Astrocytes have a lower time scale of operation in comparison to neurons. Typically, neurotransmission occurs in milliseconds while astrocytes can transiently control the synaptic strength during seconds. Astrocytes have the ability to enhance the frequency of spontaneous and evoked activity of excitatory synaptic currents through glutamate by, activation of mGluRs or NMDAR. Furthermore, astrocytes can induce the potentiation or depression of inhibitory synaptic transmission (Perea et al., 2009). So, the contact with thousands of synaptic inputs and the ability to receive multiple signals and homeostatic information from different origins allow astrocytes to perform several and complex modulation of neuronal functions. These abilities of astrocytes point out their potential to the enrichment of information processing in the brain by the modulation of synaptic activity and plasticity (Figure 1.6) (Araque et al., 2014; Jones, 2015).

Synaptic plasticity is the capacity of a preexisting connection between two neurons to change in strength as a function of neural activity, and astrocytes are involved in three main forms of synaptic plasticity in the brain (De Pittà et al., 2016). First, they can regulate short-term plasticity – a transient alteration in the strength of a synaptic connection – by interfering with the neurotransmitter release from the presynaptic terminal under the arrival of an action potential (Perea and Araque, 2007; Sibille et al., 2015). This process is mediated by ATP that is hydrolyzed to adenosine in the extracellular space. Adenosine either has a tonic effect when acting through presynaptic A_1 receptors, decreasing the release probability and suppressing synaptic transmission, or an excitatory effect when binding to the A_{2A} receptors, thus strengthening the connection (Pascual et al., 2005; Florian et al., 2011; Panatier et al., 2011). Second, astrocytes participate in long-term potentiation (LTP – a long-lasting increase in the strength of specific synaptic connections) (Perea and Araque, 2007). This modulation could be mediated by the release of the NMDA receptor co-agonist D-serine that activates NMDAR in the presence of glutamate (Henneberger et al., 2010; Shigetomi et al., 2013). Third, astrocytes can regulate homeostatic synaptic scaling which is a long-term change in the strength of all synapses on a given neuron, in response to prolonged changes in cell's electrical activity (Allen, 2014). Specifically, scaling is due to alterations in

receptor content at synapses and, is largely mediated by the pro-inflammatory cytokine tumor necrosis factor-α (TNF-α). TNF-α ensures the maintenance of the relative strength of synapses by controlling the astrocytic input to glutamatergic transmission by the modulation of synaptic AMPA and GABA$_A$ receptor levels (Stellwagen and Malenka, 2006; Santello et al., 2011).

Since neuronal and glial activity are mediated by changes in electrical potentials, it is possible to collect information about how the nervous system codes and processes information, in terms of action potentials, through electrical recording techniques. Thus, the arrangement between a molecular genetic approach and imaging and electrophysiological techniques such as patch-clamp, has a huge potential to disentangle the complexity of astrocytes contribution to the CNS function.
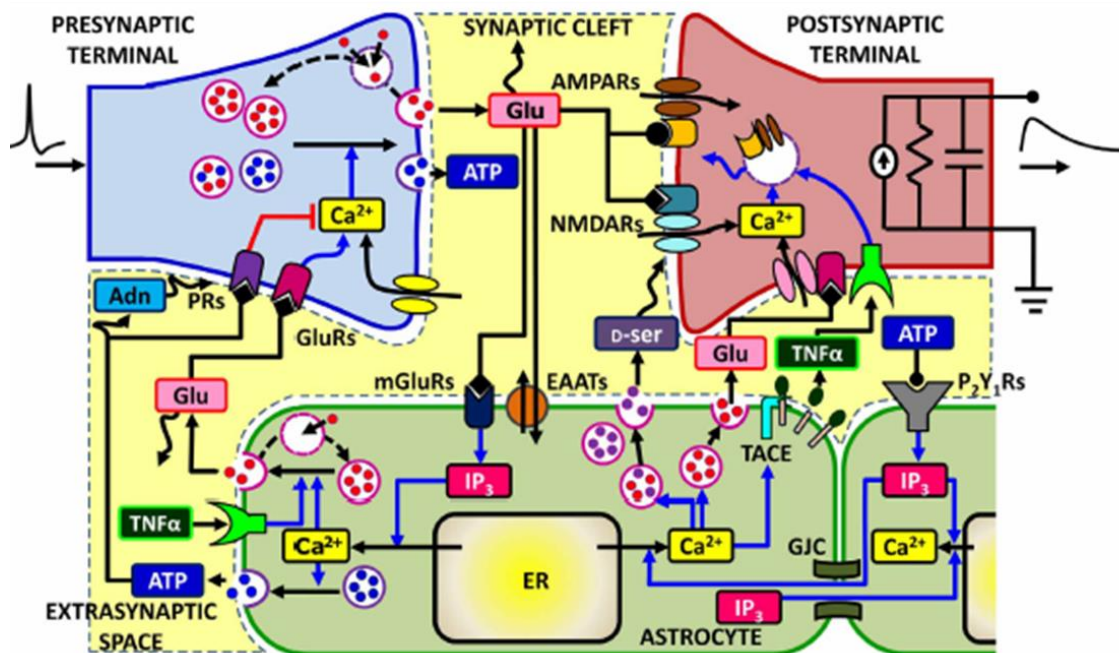
Figure 1.6. The signaling network of astrocyte-synapse interactions. Scheme of the different signaling pathways between synaptic terminals and astrocytes for the excitatory synapses in the hippocampus. The arrival of an action potential to the presynaptic terminal triggers the release of glutamate, which can spillover from the synaptic cleft. Perisynaptic astrocytes take up glutamate using their plasma membrane transporters (EAATs) while glutamate, acting on astrocytes metabotropic receptors (mGluRs), triggers Ca^{2+} signaling in the astrocyte due to efflux of this ion from the endoplasmic reticulum (ER). At some synapses, Ca^{2+} signaling could also be mediated by astrocytic purinergic P2Y$_1$ receptors, likely activated by synaptically released ATP. Astrocytic Ca^{2+} excitability can in turn lead to the exocytotic release of neuroactive substances such as glutamate (glu), D-serine (D-ser) or ATP which can target specific receptors on pre-and post-synaptic terminals, differentially modulating synaptic transmission. Glutamate acting on presynaptic GluRs could enhance synaptic release, while ATP and its derivate adenosine (Adn) could express it (red path) through presynaptic purinergic receptors (PRs). On the postsynaptic spines (RC circuit), the following effect of gliotransmitters could modify postsynaptic currents by enhancing activation of NMDA receptors (D-serine) or by altering expressions of AMPA receptors therein. Astrocytes could also release TNFα by Ca^{2+}-dependent activation of the matrix metalloprotease TNFα-converting enzyme (TACE), while extracellular TNFα could in turn regulate glutamate release from the astrocyte as well as postsynaptic AMPAR expression (Adapted from De Pittà et al., 2012).

1.3.1 Neuronal oscillations

Brain rhythms are periodically fluctuating waves of neuronal activity considered a fundamental mechanism for the modulation, filter, and redirection of information in the nervous system, being these oscillations central for the dynamical coupling observed between brain areas (Benchenane et al., 2010). They reflect the synchronized activity of neurons and are considered important for several cognitive functions such as learning, memory and attention (Colgin, 2016). So, understanding their mechanisms and function is quite relevant to understand how the brain executes complex behaviors. Different frequency ranges denote different brain activity states and are involved in shaping the temporal structure of neural activity. This way, they act as carriers for the communication between different brain regions (Buzsáki, 2006). Conventionally, human neuronal oscillations are classified into delta (0-4 Hz), theta (4-8 Hz), alpha (8-12 Hz), beta (12-20 Hz) and gamma (low: 20-40 Hz; high: > 40 Hz) (Xu et al., 2013). In rodents, the functional relevance of each frequency band is generally maintained, yet the theta frequency is considered to range in 4-12 Hz, disregarding the alpha rhythm (O'Neill et al., 2013). Each type of rhythm can be observed during specific behaviors, and generated by particular mechanisms in association with characteristic neuronal firing properties (Colgin, 2016). Theta, beta and gamma rhythms are typically seen in the cortex during active behaviors. The theta rhythm is a large amplitude coherent oscillation, prominent during immobility and exploratory movements, and closely linked to the formation, storage and retrieval of memory. It was described to play an important role in specific inter-regional communication in the brain, such as the hippocampal-prefrontal interaction (Buzsáki, 2002; Ujfalussy and Kiss, 2006; O'Neill et al., 2013). Both beta and gamma rhythms are typically associated with attention, perception and cognition (Cannon et al., 2014). Neural oscillations are then critical for information processing, and provide the nervous system with a mechanism that allow dynamic coupling within and between brain regions (Buzsáki, 2004).

Theta oscillations were shown to travel along the septotemporal axis demonstrating that the firing of hippocampal neurons is patterned in time and across anatomical space (Cappaert et al., 2009; Lubenov and Siapas, 2009). In rodents, theta-frequency ranges from 4 to 12 Hz and can be broadly separated in two subtypes, type I from 7-12 Hz, more related to movement and sensitive to anesthetics; and the type II, from 4-7 Hz, that occurs during immobility, is resistant to anesthetics and has a cholinergic nature confirmed by its sensitivity to atropine sulfate, a muscarinic receptor blocker (Adhikari et al., 2010; Kowalczyk et al., 2013, 2014). The last one corresponds more

closely to human theta frequency (as hippocampal theta oscillations are slower in humans in comparison to rodents), behavioral correlates and epoch duration (Jacobs, 2013; Watrous et al., 2013; Hoffmann et al., 2015). Theta oscillations play a pivotal role in the function of the hippocampus and in its association to cortical regions. They are a result of a concerted work of both rhythm generators and oscillators in different locations (Buzsáki, 2002). Cholinergic and GABAergic, as well as the recently described glutamatergic afferents (Huh et al., 2010) originating from the medial septum-diagonal band of Broca, provide the main extrinsic rhythm inputs to support theta oscillations, by modulation of interneurons, and CA1 and CA3 pyramidal neurons. Input originating from CA3 and entorhinal cortex add up to the establishment of the CA1 theta rhythm (Buzsáki, 2002). In spite of being classically accepted as oscillators, CA1 pyramidal neurons are also included in an intrinsic loop circuit, which is able to self-generate theta rhythm (Goutagny et al., 2009). In these septal-entorhinal-hippocampal circuits, glutamatergic modulation via NMDA receptors appears to mediate theta oscillations, at least partially. Glutamatergic neurons play a role in hippocampal theta generation through local modulation of septal neurons (Robinson et al., 2016). Moreover, the pharmacological inhibition of NMDA receptors significantly impairs hippocampal theta oscillations *in vivo* (Lazarewicz et al., 2010), while the paired activation of NMDA and GABA receptors are able to generate theta oscillations *in vitro* (Kazmierska and Konopacki, 2013). More importantly, the genetic deletion of NMDA receptors in parvalbumin-positive interneurons interfered with theta oscillations, decreasing theta-gamma phase locking, with impact in spatial memory (Korotkova et al., 2010). Finally, a transgenic mouse line lacking the NR1 NMDAR subunit fails to reshape hippocampal theta rhythms after the switch between place and sequence representations in a spatial navigation task (Cabral et al., 2014). These studies denote the importance of NMDA-mediated theta oscillations for behavior performance. Due to their ubiquitous distribution and close apposition of processes endowed with machinery to send and interpret physiological signals resulting in modulation of hippocampal NMDA receptors (Henneberger et al., 2010; for review: Araque et al., 2014), astrocytes are in a good position to modulate theta oscillations. Despite the lack of literature in this sub-field, a recent work suggests that the physiological activation of astrocytes leads to the release of signals that may add up to hippocampal theta. The deletion of GABA B receptors specifically in astrocytes leads to a decrease in hippocampal theta oscillations (Perea et al., 2016). Moreover, septo-hippocampal cholinergic input to hilar astrocytes leads to hilar interneuron activation and consecutive dentate gyrus

inhibition (Pabst et al., 2016), while cholinergic input to CA1 astrocytes leads to release of D-serine and modulation of CA1 pyramidal neuron activation (Papouin et al., 2017a).

Network oscillations can be measured extracellularly as LFPs. LFP data can serve as an extremely useful mesoscopic measurement of neuronal cooperation, with gamma band and lower frequency activities providing signatures of local processing within neural circuits. Simultaneous recording of LFP and spiking of isolated pyramidal cells and interneurons confers a greater ability to assess both the involvement of different cell populations in the coordinated activity reflected in the LFP and the directionality of communication (Buzsáki and Schomburg, 2015). Moreover, the importance of oscillatory coupling for a task performance was already shown (Igarashi, 2015).The simultaneous recording of LFPs from multiple brain regions allows then, the evaluation of the network by the coupling of oscillations in distributed brain circuits.

1.3.2   Neuronal synchronization: the cortico-limbic circuit

The functional communication between hippocampus (HIP) and medial PFC (mPFC) depends on the monosynaptic projections from ventral CA1 and subiculum subfields of the HIP to mPFC that projects back to the HIP via entorhinal cortex (Tierney et al., 2004; Parent et al., 2010; Colgin, 2011). Several studies have been nourishing the idea that the HIP-PFC link underlies memory processes. For instance, Spellman and colleagues recently demonstrated that the direct input from ventral HIP (vHIP) to mPFC is crucial for the encoding of spatial cues in a working memory task (Spellman et al., 2015). When evaluating a connection between two brain regions, authors commonly assess the neural synchronization that translates activity changes that occur together over time between brain areas. The spectral coherence is a traditional measure of synchrony between two brain regions that gives information about the temporal consistency and strength of a correlation between two neural signals. It comprises both phase synchronization and co-variation of power of neural oscillations (Fell and Axmacher, 2011; Gordon, 2011). In 2005, Jones and colleagues demonstrated a correlated firing in the hippocampal CA1 and prefrontal cortex that was selectively enhanced during behavior recruiting spatial working memory, and that this process was accompanied by an enhanced coupling of the two structures in the theta frequency range (Jones and Wilson, 2005). Later, another group, suggested that hippocampal-prefrontal coherence could lead to synchronization of reward predicting activity in prefrontal networks (Benchenane et al.,

2010). Additionally, the synchronization of synaptic activity in specialized brain regions, during the performance of tasks that require memory acquisition and retrieval have also been reported. Sigurdsson and colleagues demonstrated that there is an increase in the synchrony between mPFC and dHIP during the execution of a spatial working memory task, and this observation was disrupted in a mouse model of schizophrenia (Sigurdsson et al., 2010). Moreover, recordings of local field potentials (LFPs) from vHIP and mPFC of anesthetized rats, previously submitted to a chronic stress protocol and to a behavior assessment, revealed the existence of a correlation between the decrease in coherence with the stress-induced behavioral deficits observed in a spatial reference memory task (Oliveira et al., 2013). In general, synchrony between oscillations of hippocampal dorsal or ventral sub-regions, and PFC has been related respectively to cognitive (O'Neill et al., 2013) and emotional behavior (Adhikari et al., 2010; Oliveira et al., 2013; Mateus-Pinheiro et al., 2016; Kafetzopoulos et al., 2017).

The gathered data suggests that the coordination of theta rhythm plays a critical role as a general mechanism through which the relative timing of neural activity can be controlled. Accordingly, specialized brain structures can encode information in an independent manner and interact selectively based on the current behavioral demands.

Although, there is still uncertainty about the fundamental processes behind this coordinated activity of neurons. Astrocytes have been suggested to regulate neural synchronization since the spontaneous activity of glial cells was shown to shape the excitability of hippocampal pyramidal neurons, by evoking slow inward currents (SICs) through activation of NMDAR under glial glutamate and D-serine release, leading to a synchronized activity of neighboring neurons, in slices of rats (Angulo et al., 2004; Fellin et al., 2004) and of humans (Navarrete et al., 2013). This piece of evidence indicates that gliotransmission increases neuronal excitability, suggesting a non-synaptic mechanism for neuronal synchronization. For instance, Poskanzer and co-workers demonstrated that astrocytes are involved in triggering a slow neural rhythm via regulation of extracellular glutamate, being implicated in the synchronization of cortical circuits (Poskanzer and Yuste, 2016). Moreover, another recent study using Cx30 and 43-deficient mice, showed evidences for the synchronization of neuronal assemblies bursting through Cx-mediated astrocyte networks, suggesting that astrocytic disconnection prevented optimal coordination of neuronal activity (Chever et al., 2016). Remains to dissect whether this astrocytic contribution to neuronal synchronization is specific to some cognitive tasks than others, in order to better understand and treat brain disorders implicating cognitive deficits (Tewari and Parpura, 2015).

1.3.3 Role of theta frequency in learning and memory processing

In the current years, a growing body of evidence has been supporting that information can be processed by mPFC neurons by phase-locking to theta hippocampal oscillations (Hyman et al., 2011). Theta oscillations are observed in LFPs and spiking of single neurons, being the predominant frequency domain during active behavior, which supports a link between theta rhythm and behavioral encoding of space (Hasselmo and Stern, 2014). Since the communication with the hippocampus appears to be dependent mostly on theta oscillations, theta coherence between HIP and PFC have been described as crucial for spatial working memory and to be involved in the selection of important information to be stored in long-term memory processing (Benchenane et al., 2011; Hyman et al., 2011). An increase in the cortico-limbic coherence implies a deep reorganization of the dynamics of neural ensembles, in order to achieve a synchronized activation of groups of cells (Benchenane et al., 2010, 2011). The timing of spikes within the theta cycle and the cell's firing rate have been shown to correlate with animal's position in space and also with the performance level. For instance, the coherence in theta oscillations between dHIP and mPFC of rats, was shown to be critical for the performance of tasks that recruit spatial memory (Winson, 1978), working memory (Jones and Wilson, 2005; Siapas et al., 2005; O'Neill et al., 2013) and in tasks of rule learning (Benchenane et al., 2010). These data demonstrated that theta rhythm is selectively enhanced during mnemonic processes and is accompanied by a prefrontal phase locking to hippocampal theta oscillations, suggesting theta coupling as a mechanism for prefrontal cell assembly formation. Importantly, it was already shown that slow theta oscillations were able to predict successful episodic-memory encoding also in humans (Lega et al., 2012). More recently, memory integration in humans was shown to be supported by the amplitude and coupling strength of theta oscillations in the HIP and mPFC (Backus et al., 2016). Other studies supporting the interregional coupling of theta oscillations, demonstrate that bidirectional interactions between the PFC and the medial temporal lobe are crucial to mediate human memory processes (Anderson et al., 2010), while theta synchronization between mPFC and cerebellum contribute to the adaptive performance of associate learning behavior in guinea-pigs (Chen et al., 2016). Additionally, LFP recordings from the vHIP and PFC of freely behaving mice revealed that theta coherence also plays a key role in the modulation of anxiety-like behavior (Adhikari et al., 2010; Zhan, 2015).

In parallel to theta frequency, gamma oscillations can also occur during the same behavioral states, suggesting an intimate relationship between activity of both frequency bands (Butler and Paulsen, 2015). The phase of the ongoing slower theta oscillations modulates the amplitude of the gamma

rhythm (Jensen and Colgin, 2007; Burke et al., 2013; Bott et al., 2015). Because of conduction delays, low frequency oscillations (theta) have been suggested to synchronize large neuronal spatial domains over long distances while fast oscillations (gamma), are thought to synchronize cell assemblies over rather short spatial scales being this cross-frequency coupling suggested to be implicated in learning and memory processes (Buzsáki and Draguhn, 2004).

All these findings suggest that theta oscillations are involved in the orchestration of learning and memory processing, being critical for cognitive functions, essentially dependent on hippocampus and prefrontal cortex. However, the contribution of astrocytes in these processes remains unclear.

Hassanpoor and colleagues suggested that astrocytes are important for theta rhythm generation, theta phase precession and formation and then to the construction and consolidation of spatial memory (Hassanpoor et al., 2014). The speculative nature of this hypothesis requires now further research and validation.

1.4 Cognitive function - Learning and memory

The cognitive neural science comprises specific domains such as perception, action, motivation, attention, learning and memory (Kandel et al., 2012). In the current thesis, the main focus was directed to learning and memory processing.

Human brain has the ability to recall previous events and to use them for guidance of future behavior based on previous experience, which modulates the nervous system response, being this a form of learning. Alterations in the connectional structure of networks of neurons, more specifically on their synapses, is the predominant type of change that is assumed to underlie the basic mechanisms of learning and memory (Watson et al., 2010; Kandel et al., 2014). Based on evidences, memories are created after learning, by phenomena that drive synaptic plasticity that may be stabilized within hours or days with structural changes on dendritic spines at postsynaptic sites. Memory consolidation is the process through which recently acquired information is gradually transformed in enduring stable memories. We can distinguish short-term memory when these changes in synaptic transmission are temporary and reversible (from minutes to hours), and long-term memory if changes are persistent and require gene expression and synthesis of new proteins (from days to weeks) (Lamprecht and LeDoux, 2004; Mizuno and Giese, 2005; Kandel et al., 2014). Memory is organized in multiple systems involving distinct brain areas or circuitries (Maviel,

2004). Thus, lesions in specific brain regions result in severe learning injuries in certain memory tasks, but not in others, both in humans and animals.

There are two main types of memory described in the literature: (1) explicit (declarative) memory for facts, events, people, places or objects – mainly requiring the hippocampus and adjacent cortex; and (2) implicit (nondeclarative) memory for perception and motor skills – mostly relying on other brain regions such as cerebellum, striatum and amygdala (Kandel et al., 2014).

In this work we will focus on forms of explicit memory since most of the studies reporting the involvement of astrocytes in synaptic plasticity were performed in the hippocampus or cerebral cortex. To provide a conceptual framework for interpreting the dissociation in explicit memory processes observed in both humans and animals, different forms of memory (dependent on the function of these brain regions) can be acknowledged. For instance, Reference memory (RM) depends mainly in the presence of an appropriate discriminative stimulus, such as visual cues, representing the spatial, contextual and factual aspects of a task that remains constant among trials. Working memory (WM) is involved in a temporary maintenance of representations from previously experienced events (Buccafusco, 2001). Disturbance of memory can affect cognitive function, especially in the development of children or throughout aging.

1.4.1 The hippocampus

The hippocampal formation includes the hippocampus, dentate gyrus, and subiculum (Kandel et al., 2012). The hippocampus itself plays a key role in complex forms of memory including spatial learning, declarative memory and processes underlying the establishment of relational representations (Buccafusco, 2001; Purves and Williams, 2004). Specific studies revealed that hippocampal neurons of rats have spatially specific firing, considering hippocampal pyramidal neurons as *place cells* that encode a map of the animal's spatial location (Ciocchi et al., 2015). Long-term potentiation (LTP) in the hippocampus was discovered to play a significant role in memory in the mammalian brain (Bliss and Collingridge, 1993). It basically consisted in a high-frequency electrical stimulation of the perforant path input to the hippocampus, resulting in an increased strength of stimulated synapses that lasted longer. Also, the long-term depression (LTD) is another form of synaptic plasticity that results in the weakening of synaptic strength. Both mechanisms were already described to play a central role in the linkage of ensembles of neurons

31

encoding different environmental features thereby forming memory associations (Malenka and Bear, 2004; Han et al., 2012; Kandel et al., 2014).

Among other brain areas, the hippocampus directly projects to PFC by axons originating in the subiculum and ventral CA1 subfields that terminate in the pyramidal cells and interneurons of the medial PFC. The projections conduct specific neuronal communication: the dorsal hippocampus is primarily associated to spatial navigation and episodic memory, while ventral hippocampus is described for its role in emotional and motivated behaviors (Adhikari et al., 2010; Fanselow and Dong, 2010; Ciocchi et al., 2015). By interfering with the synaptic activity between hippocampus and PFC, one can modulate the synergistic regulation of learning/memory processes. Damage to the hippocampus is described to profoundly affect cognition in common neurological disorders such as Alzheimer's disease, epilepsy and stroke, by interfering with synaptic plasticity and astrocytic functions (Jones, 2015). For instance, astrocytes were shown to be critical for the NMDAR-dependent maturation, synaptic integration and survival of adult-born hippocampal neurons, pointing out the astrocytic fundamental role in the regulation of adult brain plasticity (Sultan et al., 2015). Moreover, another study recently demonstrated the implication of astrocytes in the mediation of hippocampal long-term memory specifically through the β2-adrenergic receptors (Gao et al., 2016).

1.4.2 The prefrontal Cortex

The cerebral cortex is responsible for the analysis, prediction and response to environmental events which allow a sophisticated shaping of behavior. The cortex learns from previous experience gathering information from different sensory systems and mental states (Watson et al., 2010). More specifically, the prefrontal cortex (PFC) plays a key role for the representation, planning and execution of actions at the highest level of cognitive ability, sitting at the top of the sensorimotor cortical hierarchy. This brain region is mainly involved in: working memory – the temporary storage of information as a buffer for internal manipulation; attentional processes; inhibitory control; processing of emotional stimuli; decision-making; rule learning and behavior flexibility (Goldman-Rakic, 1995; Clark et al., 2004; Cerqueira et al., 2007; Benchenane et al., 2011). All different prefrontal tasks participate in the orchestration of neural activity through PFC connections with cortical, subcortical, and neuromodulatory structures (Goldman-Rakic, 1995).

Astrocytes have been described for their implication in the maintenance of prefrontal cortex functional integrity. Ablation of astrocytes in this brain region was shown to be sufficient for depressive-like behavior induction, similarly to the behavioral consequences of chronic stress (Banasr and Duman, 2008). Furthermore, our lab showed that an impairment in prefrontal cortex astrocytes impairs the cognitive function of rats, affecting the attentional set-shifting, working memory and reversal learning (Lima et al., 2014). These results point out the pathological role of astrocytes dysfunction in several conditions.

1.4.3 Cognitive assessment in rodent models

The similarity between the brains of mammals across species is very relevant and helpful in order to understand how the human brain works. The cerebral cortex in humans is highly developed in comparison to other mammals. Nevertheless, all mammals share many functional details allowing the use of rodents to dissect connections and mechanisms (Watson et al., 2010). Much of the scientific improvement achieved until our days was revealed by experimental studies on rats and mice. More precisely, the interest in working with mouse models comes from the extensive knowledge about the mouse genome (and tools to modify it) and in the large number of available genetically modified strains. There are currently several mouse models of human cognitive disorders involving memory deficits that could yield new basic insights into human brain disorders. In fact, the development of transgenic and knock-out mice to study the astrocytic function *in vivo* is a valuable option to elucidate the actual impact of gliotransmission on cognitive behavior, allowing to advance in understanding how alterations in synaptic transmission, cells and circuits can contribute to mnemonic deficits (Oliveira et al., 2015).

The selection of appropriate cognitive tasks for mice requires primarily awareness of strain differences and is also dependent on gender and age. In particular, learning and memory may be assessed by a variety of mazes (Figure 1.7), where different tasks address specific forms of memory. For instance, to study the role of the hippocampus in explicit memory, tasks requiring place learning, such as T-maze, radial arm maze and water maze where distal cues are used for animals to reach a goal location, should be performed, since these are hippocampal dependent tasks (Kandel et al., 2014). More specifically, water maze tasks have been used to measure spatial learning and memory processes being the Morris water maze (MWM) a challenging task that involves mnemonic processes encompassing the acquisition and spatial localization of visual cues

to successfully navigate and find a hidden platform to escape from the water (Morris, 1984; Buccafusco, 2001). This is a versatile paradigm that can be used to study both spatial/discriminative learning and working memory processes therefore contributing to the understanding of cognitive processes, not only in healthy subject, but also in the study of neurodegenerative diseases such as Alzheimer's and Parkinson's diseases which feature cognitive decline (Terry, 2009).
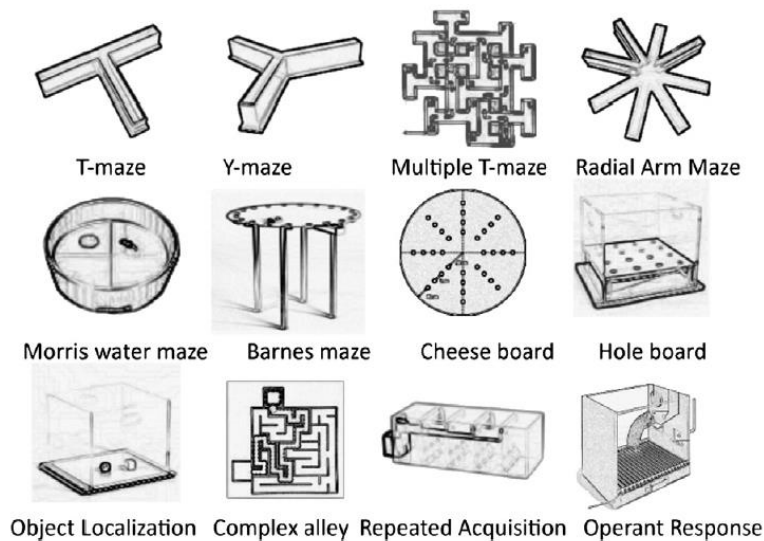

Figure 1.7. Examples of mazes used for cognitive assessment. The evaluation of spatial learning and memory processing can be assessed by numerous behavioral paradigms and applied to the study of cognitive function in mice (Adapted from Sharma et al., 2010).

 Most behavioral tests for rodents require some positive or negative emotion to motivate the animal's response. For instance, in the MWM, mice will perform the task driven by the fact that they feel uncomfortable in the water (despite of being great swimmers). In the hole-board test, animals are expected to explore a maze where food pellets are hidden in a specific manner inside holes and thus, a food deprivation protocol is applied before and during the test. Also, in the contextual fear conditioning, an aversive electric shock is used so the animals can associate the shock with a specific context. Finally, in the Y-Maze the drive for exploring novelty will be used to perform the task. The combination of a battery of cognitive tasks driven by different motivations is the key to maximize the number of functional domains assessed during test sessions. Moreover, different behaviors will specifically represent the function of particular brain regions. A stringent control of environmental conditions comprising animal welfare, room temperature, background noise, odors, cage cleanness and light conditions should be followed. In parallel, the regular

handling of animals should be accomplished in order to allow the adequate habituation to experimental manipulation.

1.5 Astrocytes and cognition: early cues

An emerging body of evidence has been proposing that astrocytes modulate actively brain processing, both during development and in adulthood, suggesting that astrocyte functions and dysfunctions may contribute to behavioral mechanisms and behavioral disorders (Chung et al., 2015; Oliveira et al., 2015) (Figure 1.8). Their role in the regulation of emergence, maturation and function of neuronal networks make astrocytes essential elements in learning and memory formation processes (reviewed in Gibbs et al., 2008; Pannasch and Rouach, 2013; Fields et al., 2014; Perea et al., 2014). For instance, the aging process carries some structural and functional changes which ultimately result in a progressive cognitive impairment that was shown to be paralleled with alterations on astrocytes phenotype (Bernal and Peterson, 2011). The absence of gliotransmitter release from astrocytes or blockade of adenosine A1 receptor, was shown to affect neuronal plasticity and cortical oscillations, promoting resilience to sleep pressure and spatial long-term memory impairments, as a consequence of sleep deprivation (Pascual et al., 2005; Fellin et al., 2009; Halassa et al., 2009b; Florian et al., 2011).Suzuki and colleagues reported that astrocytic glycogen breakdown and lactate release are in charge of the long-term memory formation and are crucial for the maintenance of LTP under the astrocytic lactate transporters (monocarboxylate transporter 4 (MCT4) or MCT1) (Suzuki et al., 2011). Other study demonstrated that the inhibition of astrocyte calcium-signaling in mice leads to memory-deficits in hippocampal-dependent long-term memory tasks (Tanaka et al., 2013). In addition, ablation of astrocytes from mPFC of rats was shown to have a negative impact in cognitive functions including working memory, reversal learning and attentional set-shifting (Lima et al., 2014). The maintenance of spatial working memory and *in vivo* long-term depression was proposed to be specifically dependent of astrocytic, but not neuronal, type-1 cannabinoid receptors (Han et al., 2012). There is also evidence supporting that gliotransmission is critical for the integrity of spatial recognition memory, as confirmed by the poor performance of mice with an inducible impairment in astrocytes vesicular release, in the novel object recognition test (Lee et al., 2014). At last, the transplantation of human glial progenitor cells into mice brain showed an enhanced ability to perform behavioral tasks by the rodents, possibly due to the larger coverage of synaptic inputs by engrafted astrocytes, which were significantly larger (Han et al., 2013). As such, the assessment of human glial chimeric

mice may provide new insights into the role of astroglial cells in human cognitive processing in a near future (Goldman et al., 2015).
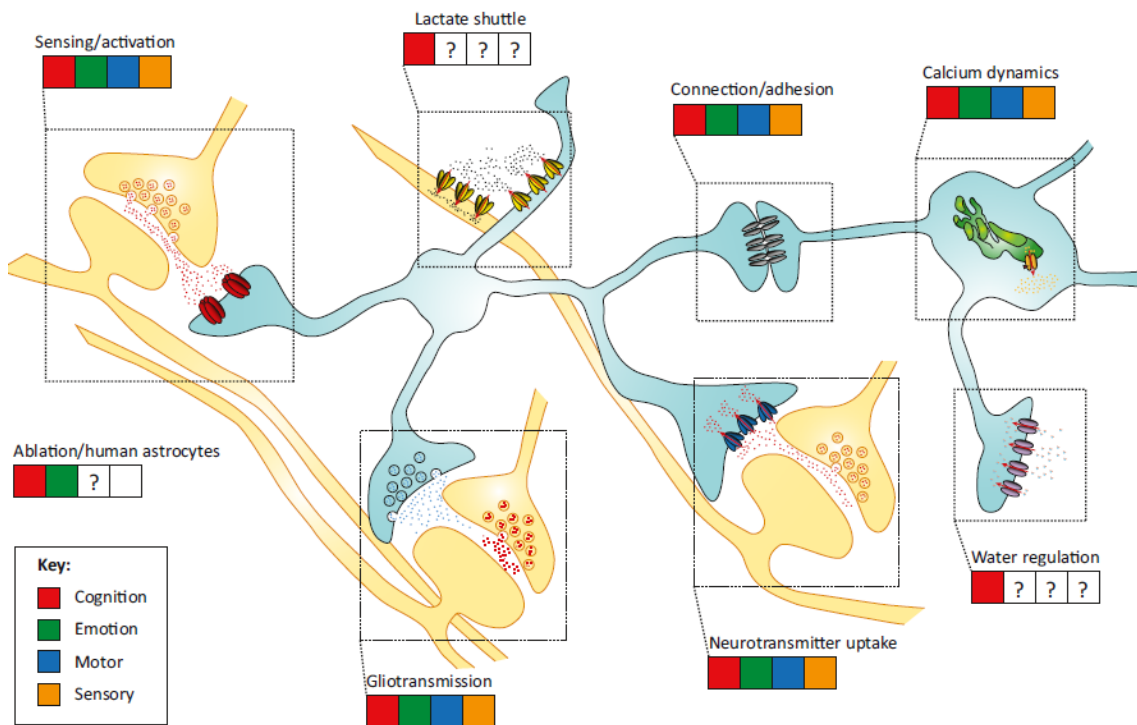

Figure 1.8. Behavioral dimensions affected by different astrocytic functions. Scheme illustrating different behavioral dimensions and how they can be affected by astrocytic function modulation. Each frame of four squares represents the behavioral dimensions (from left to right): cognition (red); emotion (green); motor activity and coordination (blue) and sensory processing (orange). A colored square indicates that at least one study has implicated astrocytes in that particular behavioral dimension. White squares refer to dimensions not affected by astrocyte modulation, while question marks identify dimensions that are yet to be assessed. Neurons in yellow; astrocytes in blue. Depicted structures: G-protein-coupled receptors (red); lactate transporters (yellow); glutamate transporters (blue); aquaporin channels (purple); connexins/adhesion molecules (gray); inositol triphosphate (IP_3) receptors (orange). Molecules: neurotransmitters (red dots); gliotransmitters (blue dots); lactate (black dots); water (red/blue dots); IP_3 (orange) (Adapted from Oliveira et al., 2015).

1.5.1 The role of astrocytes in brain disorders with cognitive deficits

Astrocytes are central elements of neuropathology playing key roles in the pathogenesis of neurodegenerative diseases (Allaman et al., 2011). Their contribution arises from the number of studies showing an impact that an imbalance in gliotransmitters release, along with the regulation of synapse development, plasticity and function would have in neuronal activity (Halassa et al., 2007a; Chung et al., 2015). In neuropathologies, astrocytes are typically affected by degenerative alterations able to suppress their functional and neuroprotective ability, which enables the disease

progression (Verkhratsky et al., 2015). Simultaneously, astrocytes can respond to CNS insults by a process called astrogliosis, in which these cells undergo substantial changes. It is a multi-stage and complex defensive response characterized by an alteration on the structure and functional plasticity of reactive astrocytes, namely by an increase in the number of processes and hypertrophy of soma and processes, consequent overlapping of processes, and substantial up-regulation of GFAP. Ultimately, a glial scar might occur (Sofroniew, 2015; Verkhratsky et al., 2015; Hu et al., 2016; Pekny et al., 2016). Reactive astrocytes exhibit a substantial heterogeneity in gene expression, cell morphology and function, on their response to different specific signaling events (Anderson et al., 2014). Astrogliosis is one of the inflammatory processes mostly proposed to play a central role in many pathological conditions such as in schizophrenia (Catts et al., 2014), autism spectrum disorders (McDougle et al., 2015) and in Alzheimer's disease (Osborn et al., 2016).

The described pathology-driven alterations in cellular morphology are hand-in-hand with modification of cell signaling observed in multiple disorders. Specifically, schizophrenia is typically associated with a hypofunction of NMDAR, arising from alterations of normal functions of astrocytes at synapses since failure in the normal uptake of glutamate by astrocytes directly affects synaptic and behavioral function (Balu and Coyle, 2015; Chung et al., 2015). In Alzheimer's disease, a neurodegenerative disorder characterized by irreversible memory loss and cognitive impairments, astrocytes were shown to alter their gene expression pattern consequently leading to synaptic dysfunction and behavioral deficits at early stages of the disease (Parpura et al., 2012; Orre et al., 2014). This can be derived from an upregulation of adenosine A_{2A} receptors that contributes to long-term memory loss (Orr et al., 2015). Additionally, astrocytes were pointed out to contribute to epilepsy, where recurrent spontaneous seizures can occur due to hyperexcitability and hypersynchrony of brain neurons under an astrocytic deregulation of ions, water and neurotransmitters (Devinsky et al., 2013). Regarding major depressive disorder, there is clear evidence of astrocyte degeneration and cell number decrease, accompanied by the reduction of astrocyte-specific glutamate transporter, in patients, and in the number of astrocytic GFAP-positive cells, in animal models (Han et al., 2015a; Peng et al., 2015). These changes were previously correlated to the induction of anhedonia and spatial memory impairment in rats (Bechtholt-Gompf et al., 2010). The subarachnoid hemorrhage (SAH), a subtype of stroke that can result from the rupture of an aneurysm, can lead to early brain injury and delayed cerebral ischemia under gliosis activation, ultimately conducting to cognitive impairments covering visual and verbal memory, among other functions. These impairments may have their origin in a decrease in GLT-1 and KIR4.1

expression in astrocytes, leading to excitotoxicity and changes in neurovascular coupling (Van Dijk et al., 2016). Furthermore, astrocytic TNF receptor type 1 signaling has been implicated in the synaptic and cognitive impairments observed in a mouse model of multiple sclerosis (Habbas et al., 2015).

1.6 Aims of the study

The findings reported in last two decades clearly showed that astrocytes are able to modulate information processing in the CNS, namely in cognitive function. Nonetheless, the specific circuits and machinery underlying this interaction are still unclear. Astrocyte exocytosis is until now widely described as the main route for the release of chemical messengers that typically affect neighboring cells, resulting in a dynamic dialogue between neurons and astrocytes, also known as tripartite synapse. The main goal of this thesis was to investigate the potential role of gliotransmission on higher cognitive functions, and for that we took advantage of a mouse model of gliotransmission impairment, obtained by conditional blockade of exocytosis in astrocytes, the dnSNARE mice. We employed a multimodal approach to assess and dissect the implication of astrocyte exocytosis-dependent signaling in the processing of complex cognitive tasks, essentially settled in the performance of two brain areas: the hippocampus and the prefrontal cortex.

More specifically, this work aimed to address the following key objectives:

(i) Characterize and validate the dnSNARE model in the regions under study **(Chapter 2.1)**;

(ii) Characterize the electrophysiological activity of the cortico-limbic network with the purpose of obtaining an *in vivo* fingerprint of the regional activity and of temporal synchronization between brain regions intimately related to cognitive processing **(Chapter 2.2)**;

(iii) Evaluate the influence of gliotransmission on cognitive processing, assessing the mice performance in complementary and specific behavioral paradigms **(Chapter 2.3)**;

(iv) Identify histological/morphological correlates that could explain the impact that impairing gliotransmission could have in the network activity and behavior performance (**Chapter 2.4**);

(v) Clarify the potential role of astrocytic signaling and of D-serine as network modulator, and evaluate its contribution towards cognitive function restoration, under the blockade of astrocytic exocytosis (**Chapter 2.5**).

CHAPTER 2

Experimental work

2.1 Validation of the dnSNARE mouse model to study gliotransmission

Introduction

As described above, the most prominent mechanism used by astrocytes to release signaling molecules is SNARE-dependent exocytosis. Therefore, the dnSNARE mouse model was elected to pursue the goals of this study, since it allows the inducible blockade of exocytosis selectively in astrocytes. In this sub-chapter, we aimed to perform a complete characterization of the dnSNARE mouse model by: (1) confirming the co-expression of dnSNARE and reporter transgenes; (2) validating the tet-Off system used to control the induction of transgene expression in dnSNARE mice; (3) confirming the astrocyte specificity in this model; (4) assessing the transgene expression levels among brain regions and subjects. This validation of the model will allow to drive away some inconsistencies raised by Fujita and colleagues (Fujita et al., 2014), that have been recently rebutted (Pankratov and Lalo, 2015; Sultan et al., 2015).

Materials and Methods

Animals

All experimental procedures were conducted in accordance with the guidelines for welfare of laboratory animals, as described in the Directive 2010/63/EU, and were approved by the local ethical committee (SECVS 075/2015) and national authority for animal experimentation (DGAV).

The generation of transgenic dominant-negative SNARE (dnSNARE) mice, a model of gliotransmission impairment, was performed as previously described (Figure 2.1) (Pascual et al., 2005). Mice were obtained by crossing two transgenic founder lines: GFAP-tTA, in which the expression of tetracycline transactivator (tTA) is driven by the astrocyte-specific human glial fibrillary acidic protein (hGFAP) promoter; and tetO-dnSNARE, in which the cytosolic portion of the SNARE domain of VAMP2/Synaptobrevin II (amino acids 1 to 96), as well as the reporters enhanced green fluorescence protein (EGFP) and β-galactosidase gene (LacZ) are coexpressed under the control of the tetO promoter. Developmental expression of dnSNARE was prevented by breeding the animals in the presence of doxycycline (Dox, Sigma-Aldrich) in the drinking water (100 µg/ml; water bottles covered with aluminum foil to avoid light exposure), which was removed six weeks before the beginning of the behavior experiments. The conditional expression of the dnSNARE transgenes interfered with the endogenous SNARE complex formation resulting in a blockade of exocytosis, specifically in astrocytes [dnSNARE astrocytes expressing the transgene displayed a 91% reduction

in the number of fusion events (Sultan et al., 2015)], impairing the vesicular release of gliotransmitters.

Founders of both mice lines were kindly supplied by Prof. Philip Haydon (Tufts University, USA), and were maintained in a C57Bl6/J background and C57Bl6/J littermates were used as wild type (WT) controls. All mice had *ad libitum* access to food and water in their home cages (maximum 5 mice per cage) and lights were maintained on a 12 h light/dark cycle (lights on from 8:00 A.M. to 8:00 P.M.). In order to exclude possible confounder behavior effects of hormonal variability in females, we used only male mice throughout the experiments included in this thesis, within ten to twelve weeks-old. Their genotype was confirmed by means of polymerase chain reaction (PCR): mice negative or positive for both transgenes (GFAP-tTA, tetO-dnSNARE) were tested (WT and dnSNARE, respectively), while mice expressing single transgenes were not included in the experimental groups. Mice of both genotypes were visually indistinguishable and were kept in the housing cages mixed. Each mouse received a numbered tag which remained constant throughout the experiment and allowed to perform the complete electrophysiological, behavior, histological and molecular analysis in a blind manner.

Molecular analysis

Mouse genotyping

Mice genotype was confirmed by PCR using either tail or ear samples. A mixture of 300 µl of Cell Lysis and 1.5 µl of proteinase K (200mg/mL) were added to each sample, followed by a spin down. The samples were left overnight at 55°C, for tissue dissociation. Next, 100 µl of Protein Precipitation Solution was added to the cell lysis and, after a quick vortex for homogenization, samples were centrifuged at 14000 rpm during 5 min. The addition of 300 µl of Isopropanol 100% to each sample was performed to induce DNA precipitation, followed by a centrifugation (14.000rpm; 5min). The supernatant was carefully discarded and 300 µl of Ethanol 70% was added to the pellet. Samples were centrifuged (14.000rpm; 1min), the supernatant removed and the pellet left to dry at room temperature for 60 min. In the last step, H_2O miliQ was added to the samples and left to incubate at 65°C for 15 min. Nanodrop was used to quantify the RNA level and the concentration of all samples was adjusted to 50ng/µl.

The PCRs were performed in a MyCycle thermal cycler (Eppendorf), and the amplified PCR products were separated on a 2% agarose gel prepared in SGTB agarose electrophoresis buffer

that was heated before the addition of the Greensafe Premium dye (3μl/100ml; NzyTech). DNA size marker (0.5μg/μl; GeneRuler 1Kb; Fermentas) and the samples were loaded in the gel, and electrophoresis at 150V run for 1h. Gel pictures were taken using a transilluminator (Alpha Innotech Corporation, BioRad). For the PCR we used three independent sets of primers. Transgenic mice were identified using specifically one for the tTA: tTA-forward 5'-ACT CAG CGC TGT GGG GCA TT-3' and tTA-reverse 5'-GGC TGT ACG CGG ACC CAC TT-3'; and a second one specific for tetO identification: TSL-forward 5'-TGG ATA AAG AAG CTC ATT AAT TGT CA-3' and TSL-reverse 5'-GCG GAT CCA GAC ATG ATA AGA-3'. Transgenic mice should present both tTA and tetO to be considered a dnSNARE mouse. A third set for HSF-1, a constitutive mouse gene was used as positive control to confirm the identification of WT mice: HSF-1-forward 5'-TCT CCT GTC CTG TGT GCC TAG C-3' and HSF-1-reverse 5'-CAG GTC AAC TGC CTA CAC AGA CC-3'. The amplified fragments were of ≈ 200, 850 and 500 bp, respectively, and distinguished by electrophoresis through a 1.2% agarose gel.

Quantification of transgenic RNA levels

In order to assess the transcription levels of the dnSNARE and EGFP transgenes, relative mRNA levels of both genes were quantified by RT-PCR. Mice were first anesthetized with a mixture of ketamine (75 mg/kg, i.p.; Imalgene 1000, Merial, EUA) and medetomidine (1 mg/kg, i.p.; Dorbene Vet, Pfizer, EUA) and transcardially perfused with 0.9% saline. Brains were carefully removed and macrodissected, and tissue samples were stored at −80 °C until further analysis. To avoid experimenter-dependent bias, all brains were macrodissected by a single investigator.

Total RNA was isolated from macrodissected tissue of the prefrontal cortex of dnSNARE mice (n=15), using the Direct-zol RNA miniPrep kit (Zymo Research, USA), according to manufacturer's instructions. Briefly, tissue was mechanically homogenized with a syringe and 20G needle using the NZYol reagent (NZYTech, Portugal).

Total RNA (500 ng) was reverse-transcribed using qScript™ cDNA SuperMix (Quanta Biosciences, USA). The following primers were designed using PRIMER-BLAST (NCBI, http://www.ncbi.nlm.nih.gov/tools/primer-blast/) and used for expression quantification of EGFP: EGFP-forward 5'- CCCGACAACCACTACCTGAG-3' and EGFP-Reverse 5'- ACTTTGACCATCAGAGGACATT-3'; and for dnSNARE: dnSNARE-Forward 5'- TACCAGTAACAGGAGACTGC-3' and dnSNARE-Reverse 5'- ACTTTGACCATCAGAGGACATT-3'.

Quantifications were performed using the Fast Real-Time PCR System (Applied Biosystems, USA) and 5x HOT FIREPol® EvaGreen® qPCR Mix Plus, ROX (Solis Biodyne, Estonia). Target gene expression levels were normalized against the housekeeping gene 18S rRNA and the relative expression was calculated using the ΔΔCt method.

Quantification of transgenic protein levels

It is very difficult to quantify dnSNARE protein levels in brain tissue, since available antibodies detect similarly both the exogenous and endogenous forms of synaptobrevin II. Given the fact that the EGFP levels observed were highly correlated with the EGFP mRNA, which in turn were directly correlated with the dnSNARE mRNA levels, the quantification of GFP by WB was used throughout to screen the transgene protein expression levels in all mice tested. Quantification of relative EGFP levels was performed in brain samples containing the hippocampus that were lysed in cold HEPES-buffered sucrose (0.32M sucrose, 4mM HEPES, pH 7.4) with 1% Nonidet-P40, 0.5% SDS, and a mixture of protease inhibitors (cOmplete, EDTA-free, Roche, Switzerland). Then, samples were sonicated for 10 s and centrifuged at 10000 rpm during 25 min at 4°C. The supernatant was collected and protein concentrations were determined using the Bradford protein assay (Bio-Rad, USA). Total lysates were denatured in 2x Laemmli buffer (Bio-Rad, USA) by heating for 5 min at 95-100°C. Each sample was centrifuged during 10 s before loading. Equal protein amounts (50 µg) were loaded into SDS-PAGE (10%) gels and then transferred to a nitrocellulose membrane (Trans-blot Turbo Kit, Bio-Rad, USA). Membranes were blocked in 5% dry milk/TBS (1 h) to prevent non-specific background bindings of antibodies, before incubation overnight at 4°C with the primary antibodies: mouse anti-α-tubulin (1:500, DSHB, USA); goat anti-GFP (1:2000, Abcam, UK). After washing with TBS-T, membranes were incubated with secondary antibodies: anti-mouse HRP (1:15000; Bio-Rad, USA) and anti-goat HRP (1:5000, Bio-Rad, USA), respectively. Detection of the chemiluminescent signal was performed with the Clarity Western ECL substrate kit (Bio-Rad, USA) using a gel blot imaging system (Chemidoc, Bio-Rad, USA). Band quantification was assessed using the Image Lab software (Bio-Rad, USA), and all the samples were normalized according to the loading control (α-tubulin). To confirm the induction of expression of dnSNARE transgenes after Dox removal from the diet, groups of 2 dnSNARE mice were sacrificed at different timepoints (on Dox and 1, 2, 3, 4 and 8 weeks after Dox removal). Additionally, 2 WT littermates were used as negative control. Protein extracts were obtained from hippocampus lysates. In order to quantify the relative levels of GFP across brain regions and across mice (Figure 2.7), the brains of 13 dnSNARE

mice were macrodissected 6 weeks after Dox removal, and each brain region was processed independently by WB as described above.

Immunofluorescence analysis

Brain tissue of the tested mice was stained by immunofluorescence to visualize the expression of transgene reporters and to study the co-expression with astrocytic and neuronal markers. Mice were deeply anesthetized with the ketamine and medetomidine mix, and readily perfused transcardially with 4% paraformaldehyde (PFA). Brains were carefully removed and immersed during 48 h in 4% PFA. After cryopreservation with 30% sucrose PBS solution (at 4°C, until sinking), brains were frozen by immersion in isopentane, cooled with liquid nitrogen in Neg-50 medium (ThermoFisher Scientific, USA) and stored at -20 °C. The immunofluorescence procedures were performed in coronal brain sections (20 μm thick) obtained by means of a cryostat (Leica, Germany). The double staining protocol started with three washes with PBS followed by a permeabilization with 0.3% v/v Triton X-100 in PBS. Sections were washed over again and submitted to an antigen retrieval step, with a citrate buffer solution (10 mM, pH 6.0, Sigma-Aldrich) during 20 min at 100 W microwave potency. Once cooled, slices were rinsed in PBS and incubated with 10% fetal bovine serum (FBS) in PBS blocking solution (to reduce unspecific bounds) for 30 min at room temperature (RT), followed by the overnight incubation, at 4°C, with combinations of the primary antibody goat polyclonal anti-GFP (1:300, Abcam, UK) and one of the following: rabbit polyclonal anti-GFAP (1:200, DakoCytomation, Denmark), or rabbit polyclonal anti-S100β (1:200, DakoCytomation, Denmark) for staining of astrocytes; and with mouse polyclonal anti-NeuN (1:100, Millipore, Germany), rabbit polyclonal anti-Calbindin (1:300, Abcam, UK), or mouse monoclonal anti-βIII-tubulin (1:1000, Millipore, Germany) for staining of mature neurons; all prepared in PBS with 0.3% Triton X-100 and 4% fetal bovine serum (FBS). On the next morning tissue sections were rinsed in PBS and then incubated with the respective species-specific secondary antibodies: Alexa Fluor® 488 donkey anti-goat, Alexa Fluor® 594 donkey anti-rabbit, Alexa Fluor® 594 chicken anti-mouse and Alexa Fluor® 594 donkey anti-mouse (1:1000, ThermoFisher Scientific, USA) in PBS with 4% FBS, during 2 h at room temperature. After rinsing the brain slices with PBS, the nucleic acids were indiscriminately labeled by 10 min incubation with DAPI (1:1000, Invitrogen, USA) in the dark. After a final series of rinses in PBS, slides were mounted using Immu-mount (ThermoFisher Scientific, USA) mounting media and evaluated

through confocal microscopy imaging (FV1000, Olympus, Japan) and FIJI open-source software (http://fiji.sc/Fiji).

Statistical analysis

Pearson coefficients were calculated to assess correlations between the mRNA relative levels of EGFP and dnSNARE transgenes and between EGFP mRNA and protein levels (GraphPad Prism 6 Software Inc., USA). Correlations were considered statistically significant whenever $p < 0.05$. Results are presented as mean ± SEM (Standard Error of the Mean).

Results

The dnSNARE model expresses a truncated form of synaptobrevin II (dnSNARE transgene) that corresponds to the cytosolic portion of endogenous synaptobrevin II. The available antibodies target both proteins indiscriminately, thus the quantification of transgene expression is achieved by measuring the levels of transgene reporter (EGFP). Since the transgenes are not linked in the mouse genome (Figure 2.1), one should validate the use of EGFP to confirm the actual expression of dnSNARE transgene. Previous studies showed that the dnSNARE and EGFP transgenes are highly co-expressed (97.3% in cultured astrocytes) and, in agreement with our own data, that EGFP specifically co-localizes with the astrocytic marker GFAP in brain slices (Halassa et al., 2009b; Florian et al., 2011). .
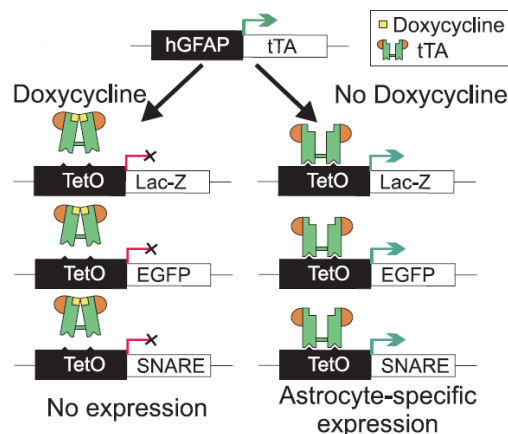

Figure 2.1. Scheme depicting the controlled expression of dnSNARE transgenes in GFAP+ astrocytes. The tetracycline transactivator (tTA) ins expressed under the control of the hGFAP promoter. In the absence of doxycycline (right panel), the tet-operator will drive the expression of the transgenes SNARE, EGFP, and lacZ. In the presence of doxycycline the expression of transgenes is blocked (left panel), therefore mice have intact astrocytic vesicular release (Pascual et al., 2005).

In order to overcome the technical difficulties associated to the identification and quantification of the transgenic protein, we investigated whether the dnSNARE transgene and EGFP reporter were expressed in the same proportion in each brain region. One could expect that the expression of the three genes inserted in dnSNARE mice genome (dnSNARE, EGFP and LacZ) - was of the same order of magnitude, since all genes are GFAP-driven and then their expression should be regulated by the same cellular mechanisms. We quantified the relative expression levels of dnSNARE and EGFP mRNA by RT-PCR in one set of dnSNARE mice (n = 15; Figure 2.2A). A strong correlation was observed between the amount of transcripts of both mRNAs suggesting that the transcription of both transgenes should indeed undergo similar regulatory mechanisms, in line with the previously described co-expression in this model (Halassa et al., 2009b). Moreover, the quantification of the relative levels of EGFP by western blot (Figure 2.2B), using anti-GFP antibody for the same mice, demonstrated a strong direct correlation between the relative levels of protein and mRNA in the dnSNARE mice. Together, these data indicate that mice expressing high levels of dnSNARE also express high levels of EGFP mRNA, which in turn translates into increased levels of EGFP in the same mice. Based on this, EGFP relative levels and GFP staining were employed throughout this work, as a correlate of dnSNARE transgene expression.
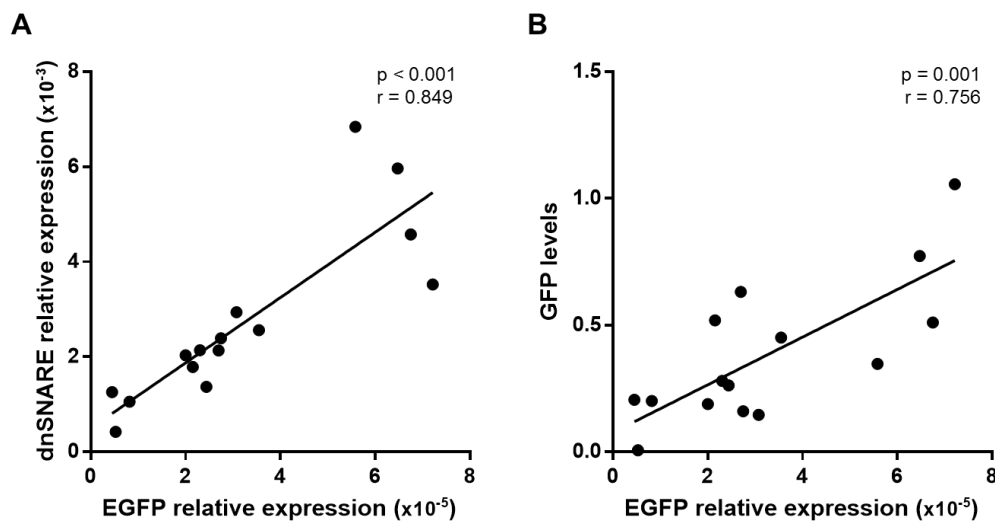

Figure 2.2. GFP reporter is a good readout of dnSNARE transgene expression and inter-subject variability. (A) Direct correlation between relative expression levels of EGFP mRNA and dnSNARE mRNA and (B) between relative expression levels of EGFP mRNA and GFP protein levels, measured in the same set of dnSNARE mice (n = 15).
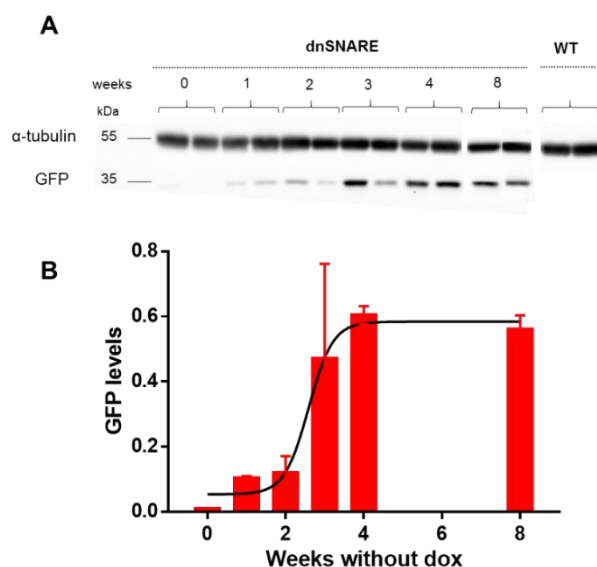
Figure 2.3. Validation of tet-Off system. Doxycycline removal from the mice diet triggers transgene expression specifically in dnSNARE mice, as assessed by the quantification of GFP (35 kDa) expression on the hippocampus of dnSNARE mice by western blot analysis at 0, 1, 2, 3, 4 and 8 weeks after doxycycline (Dox) removal from drinking water. Tubulin (55 kDa) was used as control (n = 2 / time point); Wild-type (WT) mice were used as negative controls; data plotted as mean ± SEM.

To validate the tet-Off system used to generate the dnSNARE mice and to further confirm the absence of dnSNARE expression during development, we quantified the GFP levels from mice in which Dox was removed from their diet at different timepoints (n = 2 per timepoint). The removal of Dox from the mice diet triggered the expression of the transgenes that reached its maximum at weeks 3-4, remaining stable in time while in WT littermates the transgene was completely absent (Figure 2.3). These observations are in accordance with previous studies using doxycycline-controlled systems, where it was already shown that the metabolism of Dox requires three to four weeks in order to reach a complete elimination from mice's body (Nakashiba et al., 2008; Halassa et al., 2009b).

The expression of transgenes occurred throughout the brain displaying in a typical mosaic-like distribution as described previously (Figure 2.4) (Florian et al., 2011; Sultan et al., 2015). We verified the astrocyte specificity of transgene expression by performing immunofluorescence staining of brain slices containing the hippocampus and the prefrontal cortex, regions object of study in this thesis.
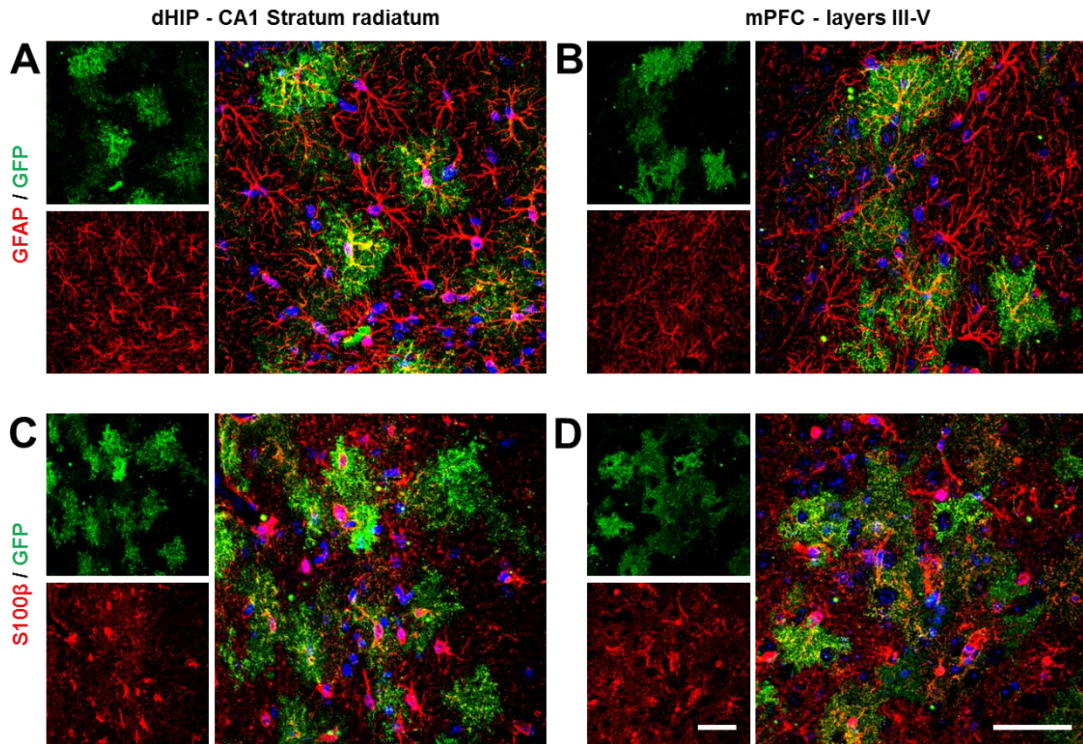
Figure 2.4. Transgene expression is astrocyte specific. (A-B) Confocal micrographs illustrating co-expression of GFP reporter transgenes (green) with GFAP (red) in the dorsal CA1 (A, stratum radiatum) and mPFC (B, layers III-V) of dnSNARE mice; (C-D) Confocal micrographs illustrating co-expression of GFP reporter transgenes (green) with S100β (red) in the dorsal CA1 (C, stratum radiatum) and mPFC (D, layers III-V) of dnSNARE mice. DAPI staining, blue. Scale bars = 50 μm.

Specific antibodies were used to label the EGFP in combination with either astrocytic or neuronal markers. The GFP staining revealed only the characteristic bushy astrocytic structure (Pascual et al., 2005; Florian et al., 2011; Khakh and Sofroniew, 2015). These structures were regularly positive for the astrocyte-specific marker GFAP both in CA1 region of the dorsal hippocampus (dHIP) and in the medial prefrontal cortex (mPFC), in agreement with previous reports (Halassa et al., 2009b; Florian et al., 2011) (Figure 2.4A, B). Further confirmation was accomplished with the astrocyte cytosolic marker S100β (Pfrieger and Slezak, 2012; Khakh and Sofroniew, 2015) in both brain regions (Figure 2.4C,D). Together, the typical astrocytic arborization evidenced by GFP fluorescence in confocal micrographs and the double immunostainings reveal that the transgenes are expressed by astrocytes of both populations. Moreover, to support astrocyte specificity and to exclude neuronal expression of dnSNARE transgenes, double immunostainings were performed against GFP and the neuronal specific nuclear protein marker, NeuN, in the same brain regions (Figure 2.5). The detailed observation of images of each confocal section excluded staining overlap between GFP and NeuN both at the dHIP and mPFC. Also, further double-immunostainings

including GFP and two additional neuronal markers were performed: the βIII Tubulin that stains neuritis and Calbindin, found in neuronal cytosol (Figure 2.6). One can clearly observe that the neurites that originate in the pyramidal layer and spread across the radiatum layer are devoid of GFP staining, which remains restricted to the bushy-like astrocyte structure (Figure 2.6A).
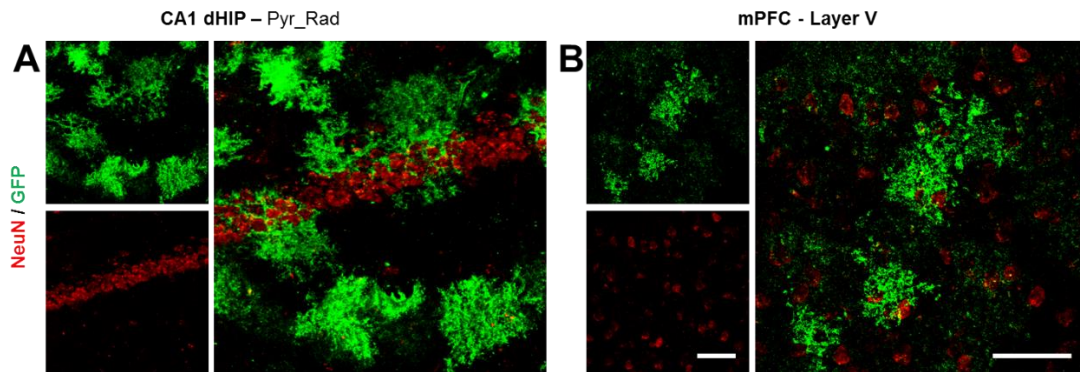

Figure 2.5. Transgene expression is absent in NeuN+ neurons in dnSNARE mice. (A-B) Confocal micrographs illustrating double staining of GFP reporter transgenes (green) and NeuN (red) in the dorsal CA1 (A, oriens, pyramidal and radiatum layers), and mPFC (B, layer V) of dnSNARE mice. DAPI staining, blue. Scale bars = 50 μm.
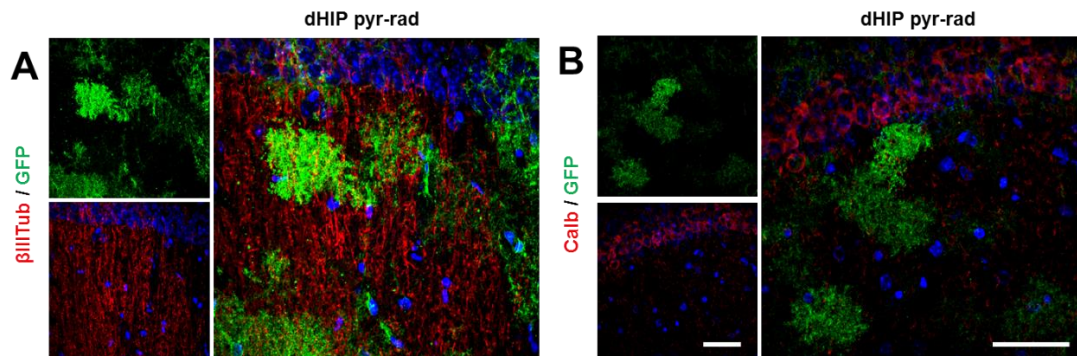
Figure 2.6. Neurons of dnSNARE mice do not express the transgene in the dendrites or cytosol. Confocal micrographs illustrating double staining of GFP reporter transgenes (green) with βIII tubulin (red, A; cytoskeleton marker) and with calbindin (red, B; cytosolic marker) in the dorsal CA1 (pyramidal and radiatum layers) of dnSNARE mice. Scale bars = 50 μm.

For the double-immunostainings using calbindin (Figure 2.6B), we failed to find co-localization of staining in the same cellular structures. Since EGFP expression is expected to be also found in the cellular cytosol, by using this combination, we definitely excluded the expression of transgenes in neurons.

Absence of co-staining in microglia, NG-2 positive cells and oligodendrocytes also ruled out co-expression in these cells (Fellin et al., 2009; Sultan et al., 2015). These observations were

rigorously consistent across brain areas and experimental sets (n = 5 mice screened per group) supporting the specific expression of dnSNARE transgenes in astrocytes described previously (Pascual et al., 2005; Florian et al., 2011; Pankratov and Lalo, 2015; Sultan et al., 2015), ruling out possible expression in neurons (Fujita et al., 2014).

We next aimed to characterize the regional distribution of dnSNARE transgenes and examined whether the transgene reporter expression was homogeneous among the brain of dnSNARE mice. To address this question we quantified by WB the EGFP levels across several brain regions such as hippocampus, dentate gyrus, prefrontal cortex, cortex, amygdala, cerebellum and in the remaining tissue of the brain, macrodissected from dnSNARE mice (n = 13). Interestingly, results showed a variable expression of transgenes across mice but a proportional oscillation of EGFP levels was maintained between brain regions of each animal, meaning that a mouse has higher levels of expression they will be reflected for all brain regions, while a mouse presenting lower levels of EGFP expression in one region will also present lower levels of expression in the remaining brain regions (Figure 2.7). Since the expression of truncated synaptobrevin II (dnSNARE) rules the level of exocytosis blockade, it would be expectable that only mice displaying high levels of the transgene would present an effective gliotransmission impairment. According to this, we stratified mice into two groups based on the relative expression of EGFP (normalized to the housekeeping gene, α-tubulin): the low (lGFP) and the high transgene "expressors" (dnSNARE) (Figure 2.8).
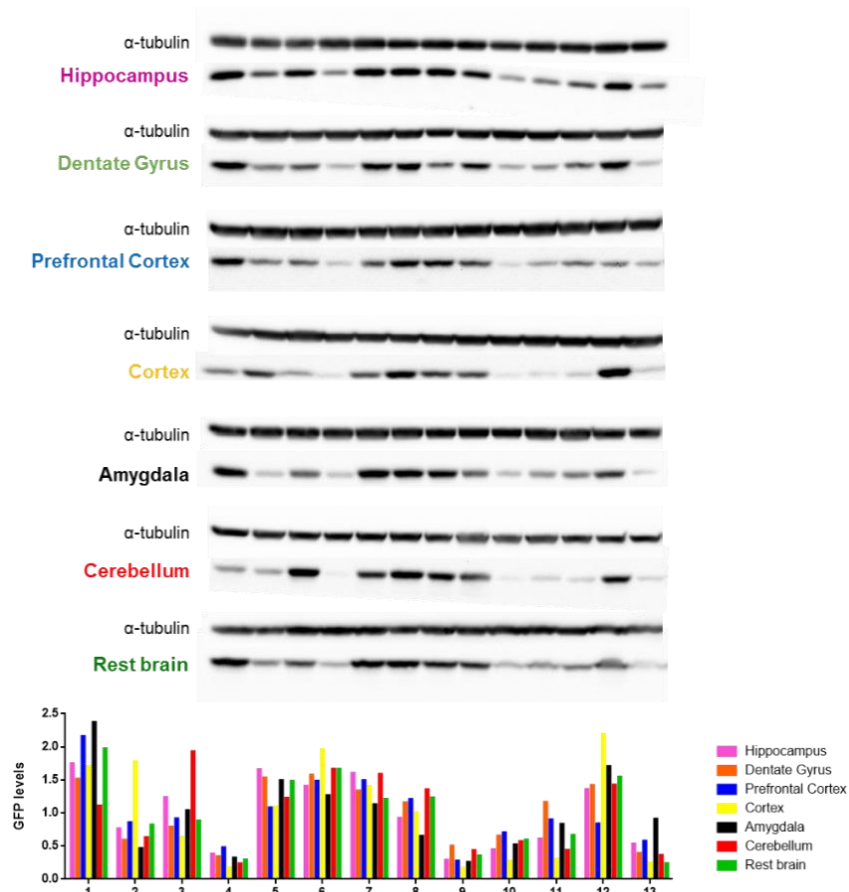
Figure 2.7. The dnSNARE mice display inter-subject variability of transgene reporter levels.
Quantification of GFP expression levels in different brain regions of dnSNARE mice (one mouse per column; n = 13) by western blot analysis (35 kDa), relatively to tubulin (55 kDa); hippocampus (pink), dentate gyrus (orange), prefrontal cortex (blue), cortex (yellow), amygdala (black), cerebellum (red) and rest of the brain (green).
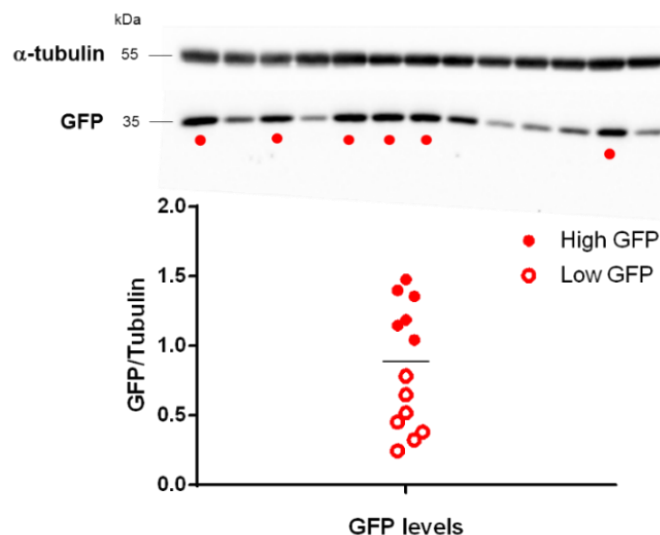
Figure 2.8. Quantification of the transgene reporter GFP from the hippocampus of dnSNARE mice.
Western blot analysis was performed for each set of mice after behavioral and electrophysiological assessment. GFP levels were quantified (35 kDa) relatively to tubulin (55 kDa) and the mean value of GFP expression, black dash, was used as criteria to separate two clusters of animals in each set: the high and the low "expressors" of the transgenes. (n = 13, representative sample).

56

Since we were interested in hippocampal-dependent behaviors, we quantified the relative EGFP levels in the hippocampus of every mouse that carried both tTA and tetO transgenes (double-transgenic). This quantification was repeated for each animal set, and only those mice who expressed higher levels of EGFP transgenes than the group mean were included in the dnSNARE group, being compared to their WT littermates throughout.

The analysis of GFP levels was performed after the sacrifice, being the experimenter simultaneously blind to the animal genotype, and to its relative level of transgene expression. Therefore, the data including the lGFP mice will be presented throughout for the verification of transgene level-dependent loss of function.

2.2   Electrophysiological characterization of the hippocampal-prefrontal network

Introduction

The investigation of the hippocampus of the mammalian cerebral cortex revealed a functional heterogeneity among regions. Sequentially, this finding occasioned the segmentation of hippocampus in the dorsal and ventral subregions. The ventral region of hippocampus (vHIP) projects directly to the mPFC while its dorsal subregion is not directly connected to mPFC (Preston and Eichenbaum, 2013; Jin and Maren, 2015). These direct and indirect communication pathways allow a neural synchronization between both hippocampal subregions and mPFC. The strength of hippocampal–prefrontal synchrony is demanded for the performance of specific tasks dependent on these brain regions. Specifically, the involvement of this hippocampal-prefrontal link in cognition and emotional regulation is well-established (Jones and Wilson, 2005; Sigurdsson et al., 2010; Spellman et al., 2015). However, the contribution of astrocytes to the maintenance of a synchronized neural activity between these two distant regions is still unclear. The involvement of astrocyte signaling in synaptic plasticity have been demonstrated in both hippocampus (Pascual et al., 2005; Jourdain et al., 2007; Henneberger et al., 2010) and cortex (Takata et al., 2011; Min and Nevian, 2012) through different regulatory mechanisms, and the release of gliotransmitters from astrocytes was previously shown to modulate synaptic communication between both regions (Araque et al., 2014; Perea et al., 2014; Petrelli and Bezzi, 2016). The correct dialog between these two regions is important to process cognitive function (Jones and Wilson, 2005; Siapas et al., 2005; Anderson et al., 2010; Benchenane et al., 2010; Oliveira et al., 2013; O'Neill et al., 2013; Zhan, 2015). Therefore, one might expect that the cellular modulation accomplished in the dnSNARE mouse model could impact the function of these circuits, by interfering with neuronal communication. In this sub-chapter, we aim to clarify if gliotransmission, specifically by vesicular exocytosis, is playing a starring role in the maintenance of the HIP-PFC synchronization. To address this hypothesis, we characterized the electrophysiological fingerprints of this network in vivo, by analyzing LFPs (oscillations that result from coordinated rhythmic activity of neuronal populations) recorded simultaneously from both the dorsal or ventral CA1 region of hippocampus and mPFC of dnSNARE mice and their WT littermates (Figure 2.9).
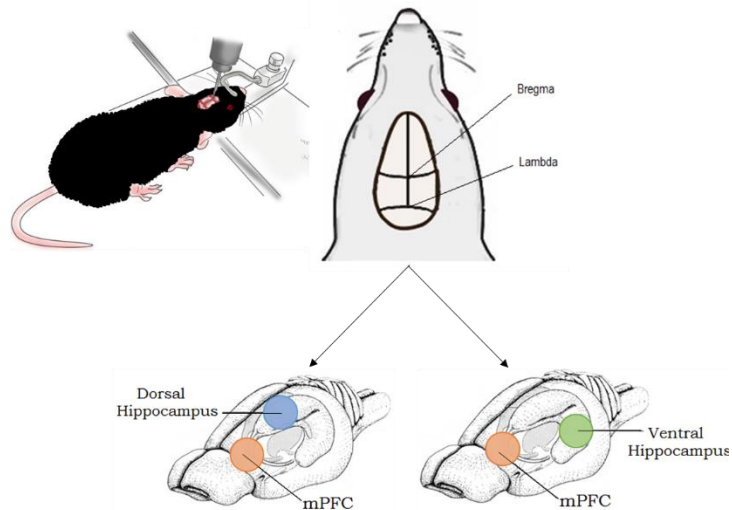
Figure 2.9. Approach to recording the hippocampal-prefrontal cortex links. Scheme of stereotaxic mounting of a mouse for the recording of electrophysiological activity. LFP signals were simultaneously recorded from the mPFC and either the dHIP or vHIP CA1 region in order to address both HIP-PFC links.

Materials and Methods

Surgery

The dnSNARE mice and WT littermates were anesthetized with Sevofluorane (4%, SevoFlo, Abbott, USA) and the body temperature was maintained at 37°C by a homoeothermic blanket (Stoelting, Ireland). When deeply anesthetized each animal was mounted on the stereotaxic apparatus (KOPF, USA). To avoid local pain during the surgery, Lidocaine (2%, B. Braun, Germany) was injected subcutaneously in the area of incision. The eyes were covered with an ophthalmic cream (Duratears Z, Alcon, USA) to avoid dehydration. Experimental procedures for electrode implantation were performed as previously described (Oliveira et al., 2013). Briefly, concentric platinum/iridium recording electrodes (400 μm shaft diameter; 50-100 KΩ impedance; Science Products, Germany) were placed in the prelimbic area (PL) of the mPFC (coordinates: 1.94 mm anterior to bregma, 0.4 mm lateral to the midline, 2.5 mm below bregma) and in either the dorsal or the ventral CA1 subregion of hippocampus (dorsal CA1 coordinates: 1.94 mm posterior to bregma, 1.2 mm lateral to the midline, 1.5 mm below bregma; ventral CA1 coordinates: 3.4 mm posterior to bregma, 3.35 mm lateral to the midline, 3.25 mm below bregma), according to the mouse brain atlas (Paxinos and Franklin, 2004).

Local field potential recording and analysis

Local field potential (LFP) signals from the mPFC and either the dHIP or vHIP were acquired and analyzed as previously described (Oliveira et al., 2013). These signals were simultaneously amplified, filtered (5000x; 0.1–300 Hz; LP511 Grass Amplifier, Natus, USA), acquired (Micro 1401mkII, CED, UK) and recorded on a personal computer running Signal Software (CED, UK). After surgery and a resting period of 20 min, 100 s of LFP were recorded at the sampling rate of 1000 Hz. The power of mPFC and hippocampal regions, as well as the coherence assessment between both pairs of regions (dHIP-mPFC and vHIP-mPFC), were performed on LFP signals acquired for each mouse. Each measure was applied on 1 s long segments and the average of all segments was considered for statistical analysis. All LFP recordings were thoroughly inspected and those that presented significant noise corruption were excluded from further analyses. Power and coherence were calculated with custom-written MATLAB-based programs (MathWorks, USA) and scripts, using the Chronux toolbox (http://www.chronux.org) (Mitra and Pesaran, 1999), for all frequencies up to 40 Hz. For power quantification the squared magnitude of Fourier data of each region was evaluated. Coherence analysis was based on multi-taper Fourier analysis and calculated for each segment (1 s). For group comparison, 3 frequency bands were analyzed based on previously described functional relevance (Gordon, 2011; Oliveira et al., 2013): theta (4–12 Hz); beta (12–20 Hz) and low gamma (20–40 Hz). Delta frequency was also analyzed (< 4 Hz).

Analysis of recording locations

After the electrophysiological protocol, animals were euthanized with a lethal dose of sodium pentobarbital (150 mg/Kg, i.p). A biphasic stimulus (5 s; 0.7 mA for mPFC, 0.8 mA for HIP) was delivered to the electrodes in order to mark the local of recording. Brains were carefully removed and the left hemisphere (electrodes location) was immersed in 4% PFA in PBS (0.1 M, pH 7.4) for tissue fixation. Twenty-four hours later, each brain was sectioned in 50 µm slices using a vibratome (Leica Biosystems, Germany) and processed with Cresyl Violet staining to identify the electrolytic lesion at the recording sites. Whenever at least one of the electrodes of each pair missed the target region, mice were discarded from the analysis (about 15% of the recordings). The right hemisphere was macrodissected and cryopreserved for molecular analysis. (Final number of animals after confirmation of electrodes position, n = 6-9 per group).

Statistical analysis

Statistical significance of the comparisons for each statistical test was set with a confidence interval of at least 95%. All data sets passed the normality tests for Gaussian distributions (D'Agostino & Pearson for n > 7; Kolmogorov-Smirnov for n = 5-6). Therefore, parametric tests were applied. Two-way ANOVA with uncorrected Fisher's LSD post-hoc tests were applied to analyze the genotype effect in different frequencies (theta, beta or low gamma). Unpaired two-sided t-tests were used to compare data between the main groups of study (WT and dnSNARE) and one-way analysis of variance (ANOVA) to compare data between 3 groups (WT, dnSNARE and lGFP). Pearson coefficients were calculated to assess correlations between the GFP protein levels and electrophysiological activity (GraphPad Prism 6 Software Inc., USA). All results were considered statistically significant when $p < 0.05$. Results are presented as mean $\pm$ SEM.

Results

In order to evaluate the synchrony among regions, the confirmation of electrodes correct position was our first approach to ensure that the mice used in this study were recorded in the regions of interest. Significant variations can occur during the adjustment of the antero-posterior coordinates while positioning and lowering the electrodes due to the softness of brain tissue and the small size of the mouse brain. Hence, the selection of subjects was based on the inflexible criteria that only the electrodes concurrently located in the prelimbic area of mPFC and in the CA1 region of hippocampus (either dorsal or ventral) of each animal could be accepted (Figure 2.10).
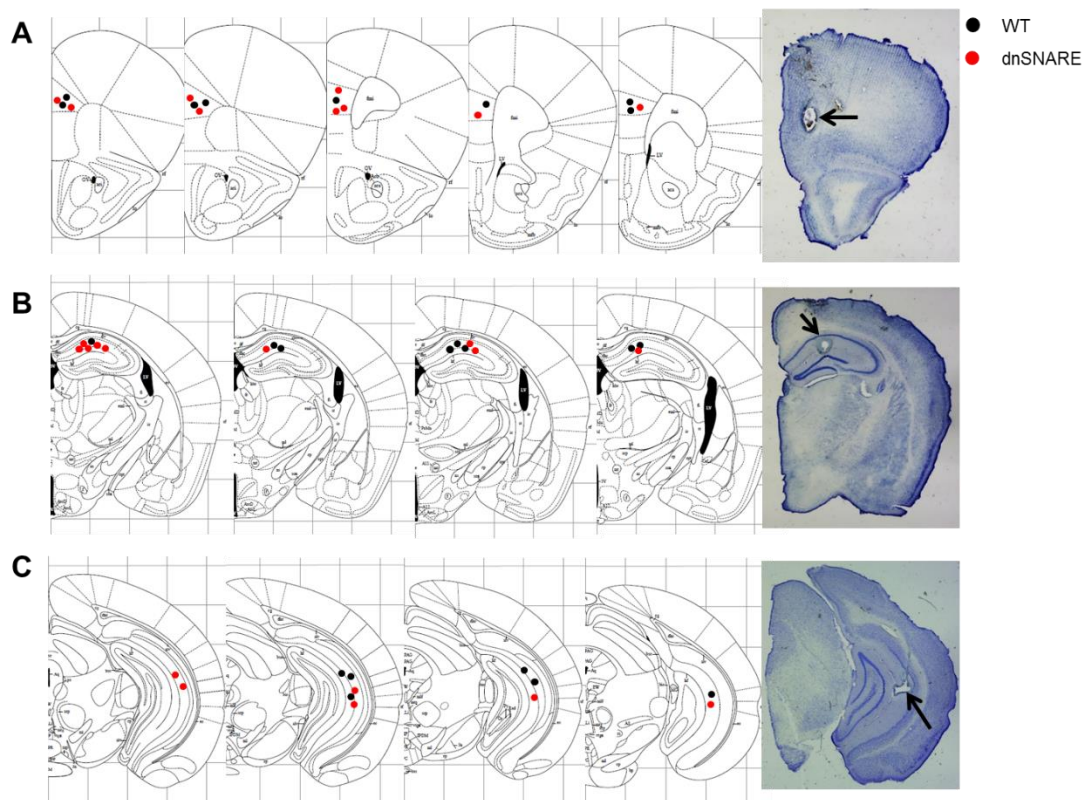
Figure 2.10. Representation of electrode recording sites. Left panel, recording site location in WT (n = 6-8, black circles) and in dnSNARE mice (n = 6-9, red circles), within the (A) mPFC, from 2.22 mm to 1.70 mm from bregma, (B) CA1 dHIP, from -1.70 mm to -2.06 mm from bregma, and (C) CA1 vHIP, from -3.28 mm to -3.88 mm from bregma according to the mouse brain atlas. Right panel, representative Cresyl Violet stained sections (50 μm). Black arrows indicate the electrolytic lesion after the recording.

To dissect the impact of gliotransmission on higher cognitive functions, we firstly recorded neuronal activity from dHIP and mPFC of both dnSNARE and WT mice (Figure 2.11A-B).

Figure 2.11. Recording oscillations in the dorsal hippocampal-prefrontal link of dnSNARE mice. (A) Scheme depicting the electrodes position for recording of LFPs in the mPFC (orange) and CA1 region of dHIP (blue); (B) representative LFP traces recorded from the mPFC and dHIP of WT (black) and dnSNARE mice (red; scale bars: 100 µV, 1 s).

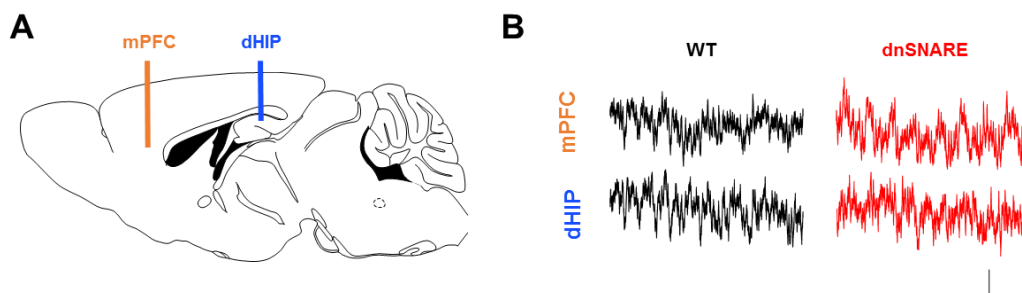The individual analysis of the LFP power on the frequency domain gives an estimate of the amplitude of network activity for a given frequency in the basal condition. The measurement of the LFP power in the dHIP of WT and dnSNARE mice revealed it to be similar between genotypes across all frequencies (Figure 2.12A, left). For all mice, the dHIP power tends to be higher for lower frequencies, possibly because there is a progressive increase in low-frequency and high amplitude activity as the level of general anesthesia deepens. The analysis of power activity by specific frequency bands defined by their functional relevance (Gordon, 2011; Oliveira et al., 2013), confirmed the power similarities between both genotypes for all frequency bands (theta: $t_{15} = 0.769$, $p = 0.454$; beta: $t_{15} = 1.307$, $p = 0.211$; low gamma $t_{15} = 1.436$, $p = 0.172$; Figure 2.12A, right). The analysis of the distribution of power across frequency bands revealed that theta oscillations represent most the activity recorded in the dHIP and mPFC. The same measurements were performed for the mPFC (Figure 2.12B). Similarly to the dHIP, no differences were found in the mPFC power activity between WT and dnSNARE mice for any of the frequencies under study (theta: $t_{15} = 0.793$, $p = 0.440$; beta: $t_{15} = 1.296$, $p = 0.215$; low gamma: $t_{15} = 1.220$, $p = 0.241$), suggesting the existence of an equivalent amount of energy of the neuronal oscillations at the given frequencies, within each region. These results are in line with previous observations of electroencephalogram data (Fellin et al., 2009).
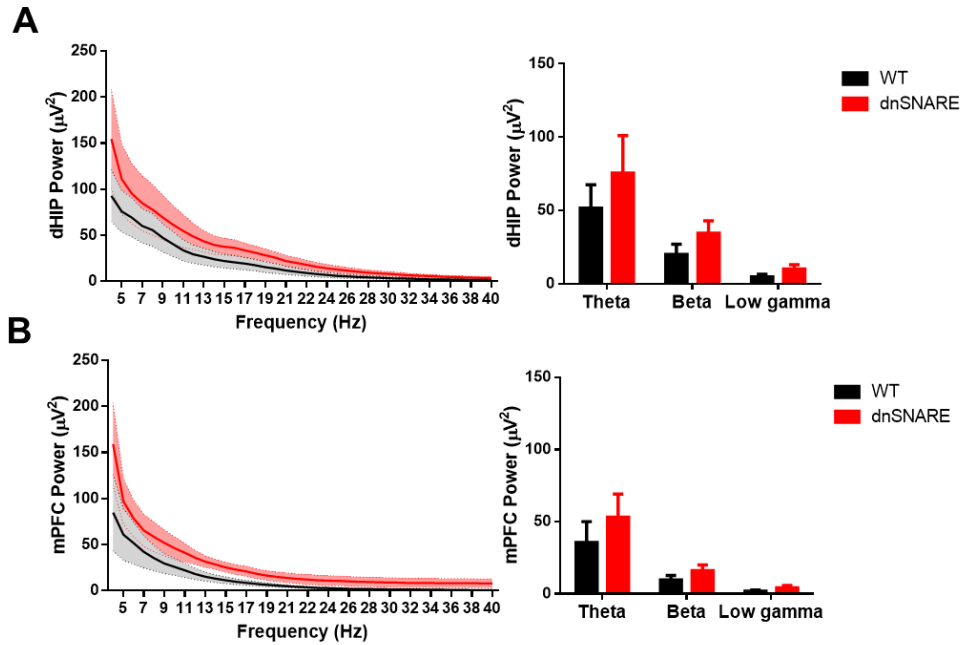
Figure 2.12. LFP power analysis between WT and dnSNARE mice. Power spectra (left) and power analysis by frequency bands (right; theta: 4-12 Hz; beta: 12-20 Hz; low gamma: 20-40 Hz) for dHIP (A) and for mPFC (B). WT mice are represented in black and dnSNARE mice in red lines and bars. Data plotted as mean ± SEM (n = 8-9 per group).

Next, we addressed the coherence between the LFPs recorded from the dHIP and mPFC, as a measure of phase and amplitude synchronization between these regions. Interestingly, dnSNARE mice displayed decreased levels of dHIP-mPFC coherence in the lower frequencies which were significantly different from their WT counterparts for the theta frequency band (Figure 2.13A, theta, $t_{15} = 2.279$, $p = 0.038$), as visible by the superposition of theta-filtered LFP traces (Figure 2.13B). The level of decrease of dHIP-mPFC theta coherence found in dnSNARE mice is in line with previous reports from us and others linking this synchrony measure to comparable cognitive deficits (Benchenane et al., 2010; Sigurdsson et al., 2010; Oliveira et al., 2013).
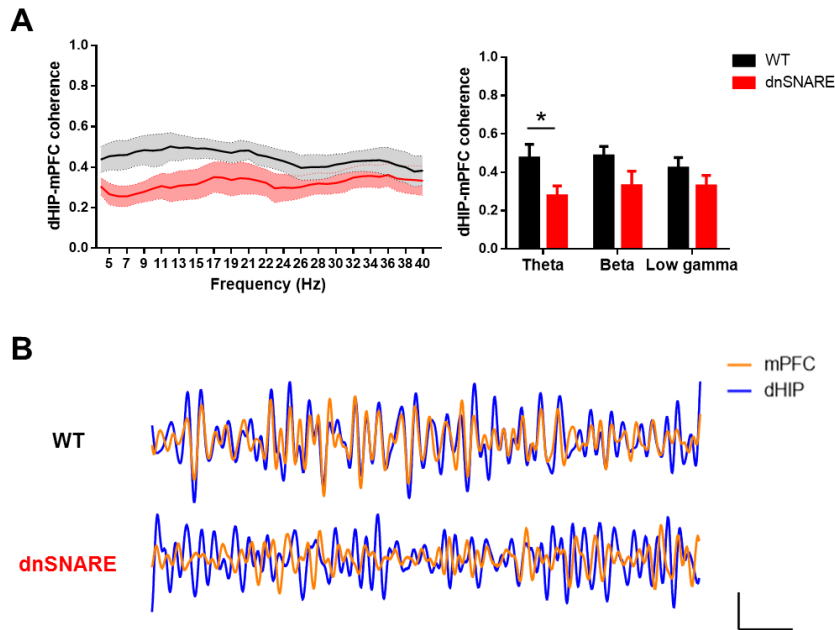
Figure 2.13. Gliotransmission impairment compromises theta coherence in the dorsal hippocampal-prefrontal pathway in dnSNARE mice. (A) Analysis of synchrony between dHIP and mPFC with dHIP-mPFC coherence spectra (left) and measured by frequency bands (right). (B) Overlap of representative theta filtered LFP traces of mPFC (orange) and dHIP (blue), recorded from WT and dnSNARE mice (scale bars: 50 μV, 500 ms). WT mice are represented in black and dnSNARE mice in red lines and bars. Data plotted as mean $\pm$ SEM. *$p < 0.05$ (n = 8-9 per group).

The inclusion of the IGFP mice in the analysis led to the verification that both power and coherence for the same range of frequency bands were not altered in this group. Indeed, when plotting the low expressors of the transgenes, these mice presented similar electrophysiological activity to WT littermates behaving as WT resembles (Figure 2.14A, B). The establishment of a negative correlation between electrophysiological performance and GFP expression levels confirmed that there is a transgene-dependent loss of function, specifically for the synchronization of theta oscillations in the dHIP-PFC link (Figure 2.14C). In accordance, the higher the expression of the transgene, the lower the theta coherence in the dHIP-mPFC connection.

Together, these results suggest that astrocyte signaling is required for the maintenance of a basal theta synchronization between cortico-limbic regions that might be important for cognitive performance.

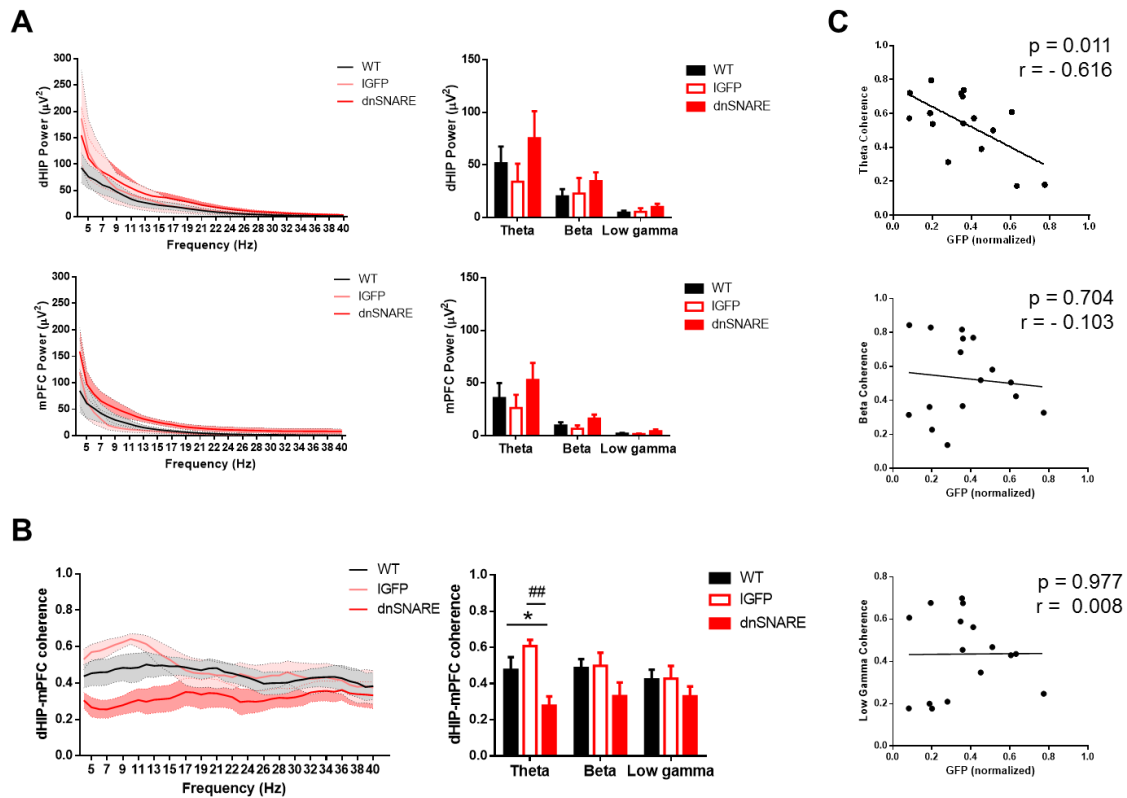**Figure 2.14. The low expressors of the transgene present similar electrophysiological activity to WT mice.** (A) Power spectra (left) and power analysis by frequency bands (right; theta: 4-12 Hz; beta: 12-20 Hz; low gamma: 20-40 Hz) for dHIP (top) and for mPFC (bottom). (B) Analysis of synchrony between dHIP and mPFC with dHIP-mPFC coherence spectra (left) and measured by frequency bands (right). (C) Direct correlation between GFP protein levels and electrophysiological activity in theta, beta and low gamma frequency bands, measured in the same set of mice (dnSNARE and lGFP mice; n = 16). WT are represented in black, lGFP in pink lines and white bars, and dnSNARE mice in red lines and bars. Data plotted as mean ± SEM. *Denotes the comparison between WT and dnSNARE mice; #Denotes the comparison between lGFP and dnSNARE mice. *p < 0.05; ##p < 0.01 (n = 7-9 per group).

Based on the most recent evidence from Poskanzer and Yuste, showing that astrocytes activation can switch the cortical circuit to a state of slow oscillations considered to be important for slow-wave sleep and memory consolidation (Poskanzer and Yuste, 2016), we included in our analysis the evaluation of the delta activity of dnSNARE mice. Disregarded from the beginning due to a suspicious influence of anesthetics in delta power, our measurements of basal delta activity revealed similar levels of power between the three groups under study (WT, lGFP and dnSNARE mice; Figure 2.15A, B). Furthermore, there were no significant changes in delta coherence (Figure 2.15C). These results suggest that the basal delta oscillations in dHIP and mPFC are not explicitly modulated by the astrocytic vesicular exocytosis.
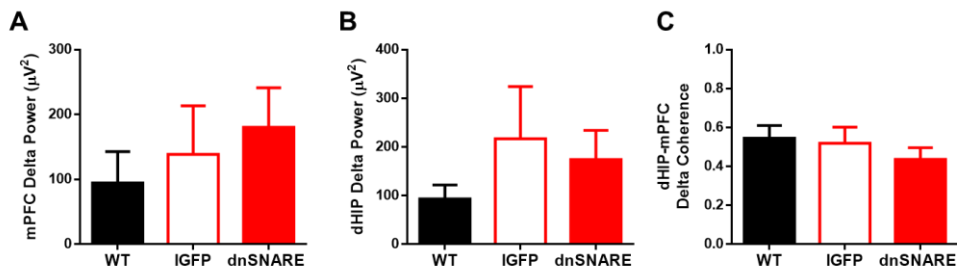
Figure 2.15. Delta oscillations are not affected by the gliotransmission impairment. No differences were found in slow oscillations (Delta: < 4 Hz) in the (A) mPFC, (B) dHIP and for (C) dHIP-mPFC coherence among groups. WT are represented in black, IGFP in white and dnSNARE mice in red bars. Data plotted as mean ± SEM (n = 7-9 per group).

The vHIP typically modulates anxiety- and depressive-like behaviors such as emotional and affective processes or even stress responses (Adhikari et al., 2010; Fanselow and Dong, 2010; Padilla-Coreano et al., 2016). In order to perform a more complete screening of the hippocampal-prefrontal network, we explored the vHIP-mPFC link. For this purpose, we recorded simultaneously the neuronal activity from vHIP and mPFC of both dnSNARE and WT mice (Figure 2.16).
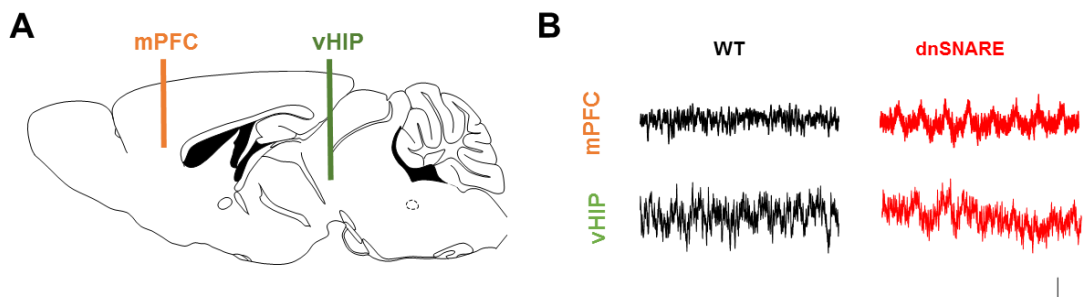
Figure 2.16. Recording oscillations in the ventral hippocampal-prefrontal link. (A) Scheme depicting the electrodes position for recording of LFPs in the mPFC (orange) and CA1 region of vHIP (green); (B) representative LFP traces recorded from the mPFC and vHIP of WT (black) and dnSNARE mice (red; scale bars: 100 μV, 1 s).

The measurement of the distribution of power across the whole spectrum of frequencies revealed no differences between genotypes, even when performing a more detailed analysis including the IGFP mice. These absence of alterations was consistent when taking a closer look to each frequency band separately (theta, beta and low gamma), for both the vHIP (Figure 2.17A, top) and the mPFC (Figure 2.17A, bottom). Likewise, the coherence between these two regions was shown to be intact

for all animals, as confirmed either by the distribution across the whole frequency range (Figure 2.17B, top) or by frequency bands (Figure 2.17B, bottom). These data reinforce that vesicular exocytosis from astrocytes does not interfere with the vHIP-mPFC link and, on that basis, one would expect that there will be no relevant impact in the emotional behavior of dnSNARE mice. Despite of these results, there are still studies supporting that the vHIP-mPFC link plays a central role in behavioral performance, mainly due to the existence of a monosynaptic projection between both regions (Oliveira et al., 2013; Spellman et al., 2015). Moreover, O'Neill and colleagues disclosed a potential vHIP mediation of the hippocampal-prefrontal theta synchrony (O'Neill et al., 2013).
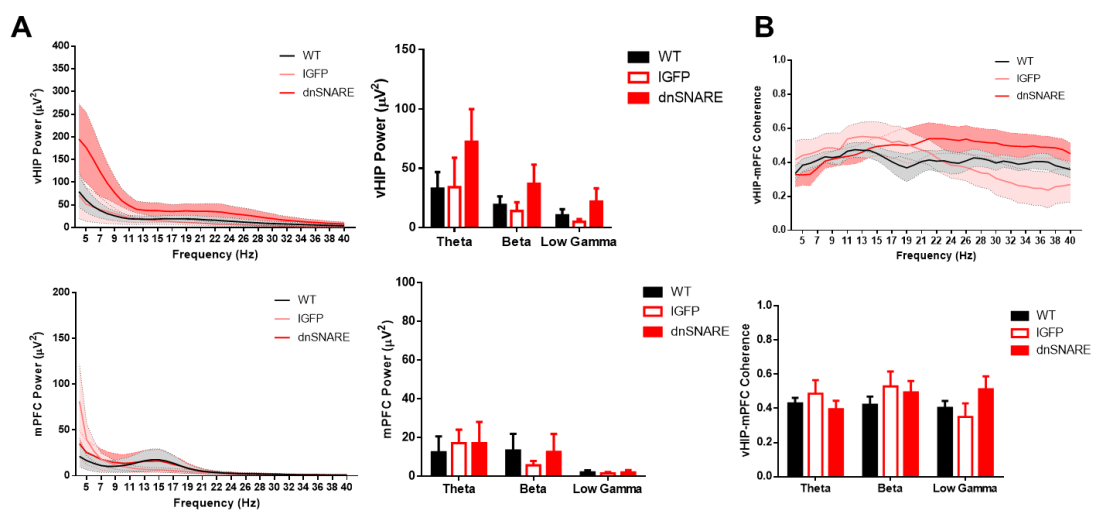
Figure 2.17. The blockade of gliotransmission does not interfere with the ventral hippocampal-prefrontal link in dnSNARE mice. (A) Power spectra (left) and power analysis by frequency bands (right; theta: 4-12 Hz; beta: 12-20 Hz; low gamma: 20-40 Hz) for vHIP (top) and for mPFC (bottom). (B) Analysis of synchrony between vHIP and mPFC with vHIP-mPFC coherence spectra (top) and measured by frequency bands (bottom). WT are represented in black, IGFP in pink lines and white bars, and dnSNARE mice in red lines and bars. Data plotted as mean ± SEM (n = 6 per group).

2.3 Evaluation of the role of astrocyte-derived signaling in cognitive function

Introduction

Based on the available evidence linking dHIP-mPFC correct dialog and cognitive processing (Jones and Wilson, 2005; Siapas et al., 2005; Anderson et al., 2010; Benchenane et al., 2010; Oliveira et al., 2013; O'Neill et al., 2013; Hoffmann et al., 2015; Zhan, 2015), we hypothesized that the observed loss of dHIP-mPFC theta synchronization might underlie a cognitive loss in mice lacking astrocyte signaling. To address this idea, independent sets of mice were submitted to tasks that assess spatial learning and reference memory in different environments and conditions. These tasks are highly dependent on cortico-limbic networks, namely on the interaction between the hippocampus and prefrontal cortex. The goal of this sub-chapter was to extract from behavioral correlates of the blockade of gliotransmission in dnSNARE mice.

Materials and Methods

Both dnSNARE and WT littermates were submitted to a battery of behavioral tests. Cognitive functions mainly dependent on either dHIP (spatial learning and recognition, and reference memory tasks) or PFC (behavior flexibility and working memory tasks), were evaluated by different tests including the Morris water maze (MWM), hole board (HB), novel object recognition (NOR) or the two-trial place recognition (2TPR) tasks.

Furthermore, to exclude a behavior phenotype that could bias the cognitive assessment, we performed a screening for anxious- and depressive-like behavior. Anxious phenotype characterization included the elevated-plus maze (EPM), light/dark box (LDB) and open field (OF) tests while learned helplessness (a hallmark of depressive-like behavior) was assessed by the forced swim (FST) and tail suspension (TST) tests.

All tests were performed during the light phase of the day. Prior to experimentation, mice were handled daily for at least 5 minutes, throughout one week, and habituation to testing rooms was performed 1 h before the beginning of each test.

Cognitive function

Morris water maze (MWM)

MWM was used to assess spatial reference memory and behavior flexibility. The test was conducted under dim light in a dark circular pool (106 cm diameter) filled with water at 23°C ± 1 °C, with

extrinsic visual cues (square, triangle, horizontal stripes and cross). In order to increase the contrast to detect the mice, water was made opaque with the addition of non-toxic titanium dioxide (Sigma-Aldrich; 250 mg/L). A circular escape platform (10 cm diameter, 22 cm height) was placed in one of four imaginary quadrants of the pool, submerged 1 cm below the water surface.

Reference memory task: The first 4 days of protocol consisted in a hippocampal-dependent task whose goal was to assess the ability of mice to learn the position of the hidden platform kept always in the same position (Figure 2.18A). Each day, mice performed 4 consecutive trials (maximum of 60 s, with a 30 s inter-trial interval) being placed in the pool facing the maze wall and oriented to each of the extrinsic cues in random order. The cut-off time for a trial was when the animal found the platform or when the escape did not occur within the 60 s of test. Whenever mice failed to reach the platform, they were manually guided to the platform for 30 s before being positioned at a new starting point.

Reversal Learning Task: On the fifth day, the platform was placed inside the pool but in the opposite quadrant, and mice were gently guided to the new position of their escape (Figure 2.18B). Right after, animals performed a reversal learning (RL) task during a set of 3 more trials, of 60 seconds each one with an inter-trial interval of 30 seconds, similarly to the first 4 days of test. This task assessed the formation of a prefrontal cortex dependent-memory, related to behavior flexibility which can be evaluated by the capacity of mice to learn that the platform has a new position, and can be assessed by measuring the amount of time spent by each animal looking for the platform in the old and new quadrants.

Escape latencies, distances swum and swim pattern were monitored and analyzed using a video camera and the EthoVision XT 11.5 software (Noldus, Netherlands).

Hole-board test (HB)

The HB task was performed to assess spatial orientation, namely reference and working memory (Castilla-Ortega et al., 2010). Transgenic mice and WT littermates were food restricted for 4 days before the beginning of the test to achieve a body weight drop to 80-85% of their free-feeding weights and food deprivation lasted through the whole behavioral experiment. The behavioral test was performed in a hole-board containing sixteen equidistant holes (6 cm apart, 1.5 cm diameter, 2.5 cm depth; MedAssociates, USA). The hole-board was placed inside a maze with Plexiglas walls with a different cue in each wall for orientation. All mice were submitted to 3 days of habituation (1 daily session of 10 min) and one food pellet was placed in each of the 16 holes to attract mice

to explore holes and eat the pellets. In the following 4 days, only a fixed set of 4 holes was baited with a pellet in a pattern that remained constant (2 sessions per day with an inter-session interval of 2 h, each session consisting in 2 trials with an inter-trial interval of 45 s) (Figure 2.20A). Each trial had a maximum duration of 5 min, finishing whenever the animal found all 4 rewards. Mice were manually placed inside the HB arena at one of four random starting locations. Arenas were cleaned with 10% ethanol between trials. Tests were evaluated by tracking mice trail with an infrared detection system and a computer interface. The following measures were analyzed: RM ratio (number of visits to the baited set of holes over the number of visits to all holes – provides an index for the ability of mice to discriminate between baited and unbaited holes); and WM ratio (number of rewarded visits over the number of visits to the baited set of holes – reflects the ability of the mice to avoid re-visits to baited holes during a trial).

Novel object recognition test (NOR)

The NOR task (Leger et al., 2013) was conducted under dim white-light illumination in a lusterless white box (30 x 30 x 30 cm) (Figure 2.21A). Habituation to the empty box was performed in three consecutive days for 20 min. In the fourth day of the task mice were submitted to a training phase consisting in the exploration of two equal objects (glass bottles) for 10 min. In the fifth day, for the novel object recognition phase, one of the familiar objects was replaced by a novel (Lego® brick) and mice were placed in the arena and allowed to explore both for 10 min. This trial assesses the ability to recognize a novel object 24 h after the first exposition, evaluating long-term recognition memory. After an interval of 1 h in their home cages, the novel object was displaced to the opposite side of the box and mice were allowed to explore this new configuration. This trial allowed the assessment of the spatial recognition memory of the subjects. In the following day, to evaluate the short-term recognition memory, mice were again submitted to two consecutive trials of 10 min each, now with an inter-trial interval of only 1 h. The first trial consisted in a training phase with two equal objects to explore, and in the second trial one of the familiar objects was replaced by a novel.

Boxes were cleaned between trials and subjects with 10% ethanol. Behavior was video-recorded and analyzed using EthoVision XT 11.5 software (Noldus, Netherlands). Exploration time of the novel or displaced objects over the total exploration time was used as measure of object preference.

Two-trial place recognition test (2TPR)

The 2TPR task is based on the innate predisposition of rodents to explore novel environments and is a test performed in a Y-Maze arena to assess spatial recognition memory, a form of episodic-like memory in rodents (Costa-Aze et al., 2012). It does not require learning of a rule being useful in particular for the study of genetic influences on the response to spatial novelty. The Y-maze consisted in an apparatus made of white Plexiglas with three identical arms (33.2 L x 7 W x 15 cm H) which were randomly designated start (S), familiar (F) and novel (N) arms (Figure 2.22A). Visual cues were placed at the end of each arm of the maze. In the first trial mice were placed in the start arm and allowed to explore only two arms (S and F) for 5 min. Mice were replaced in their home cages for a period of 30 s, and then they were placed in the start arm of the maze and allowed to explore the three arms for 2 min for memory retrieval. The maze was cleaned with 10% ethanol between trials and subjects, and the test was performed in a dim light room. Mice trail was video-recorded and analyzed using EthoVision XT 11.5 software (Noldus, Netherlands). The percentage of time spent in the distal third of the novel arm was considered as a measure of spatial recognition memory.

Anxious-like behavior and locomotor activity

Elevated-plus maze (EPM)

EPM is described as a method used to assess anxiety responses of rodents (Belzung and Griebel, 2001; Bourin et al., 2007). This test is commonly used to investigate the psychological and neurochemical basis of anxiety as well as to screen anxiety-modulating drugs or mouse genotypes, having in consideration the greater avoidance response from mice to elevated open alleys in comparison to closed ones (Bourin et al., 2007). Transgenic dnSNARE mice anxiety-related behavior was assessed by EPM test. The EPM consists in a four arms structure, two open (50.8 x 10.2 cm) and two enclosed (50.8 x 10.2 x 40.6 cm) arranged to form a plus shape elevated 72.4 cm above the floor (Figure 2.25A). EPM is based on rodents' tendency toward dark, enclosed arms, and in an unconditioned fear of heights and natural aversion for open spaces, open arms (Walf and Frye, 2007). Thus, avoidance of open arms reflects an anxious-like behavior of animals. Mice were individually placed in the arena and left to explore the plus maze in one single trial of 5 minutes. A system of infrared photo-beams connected to a video tracking interface was used to

record the crossings of each animal along with the time spent in the open arms, hub and closed arms. The test was performed under bright white light.

Light/dark box (LDB)

The LDB test was also used to assess anxiety-like behavior. This test is centered on the innate aversion of rodents to brightly illuminated areas and allows the assessment of the spontaneous exploratory behavior of rodents in response to mild stressors such as novel environment and light. The LDB is performed in the open field arena, and the apparatus comprises two equally divided compartments connected by an opening: one dark and safe, and another one illuminated (Figure 2.25B) (Bourin and Hascoët, 2003; Miller et al., 2011). The dark compartment (black Plexiglas box) was entirely enclosed within the apparatus dimly illuminated. Mice were gently placed in the middle of the illuminated compartment facing toward the dark compartment and allowed to explore the maze for 10 minutes. The percentage of time and distance spent in the open arena was monitored by infrared beams (MedPCIV) and used as an index of anxiety-like behavior.

Open-field test (OF)

The OF test was performed to assess animal's motor and spontaneous activity, exploratory behavior and anxious-like behavior in an open field arena (Prut and Belzung, 2003; Sargin et al., 2013). Through this test is possible to investigate a variety of behavior patterns such as thigmotaxis – the tendency to rely on the periphery of the arena without entering the center (Bourin et al., 2007). The test was performed in a Plexiglas box enclosing a white arena (43.2 x 43.2 x 30.5 cm; Figure 2.26A). The arena was illuminated with bright white light while performing the test. Mice were individually placed in the middle of the open field arena and left to freely explore the space for 5 minutes. To evaluate the anxious-like behavior of these mice, the total time and distance spent in the center of the arena was assessed using a system of two 16-beam infrared arrays connected to a computer. Total distance and average velocity were an indicative of locomotor activity. The number of rearings was also recorded.

Depressive-like behavior

Depression can be clinically defined as a pathological sum of psychological, neuroendocrine and somatic symptoms. Though, in animal models these symptoms can only be evaluated by measurable behaviors. Two tests commonly used to estimate a depressive mood in mice are the forced swim (FST) and tail suspension tests (TST) as standard assessments used to test learned helplessness (Yoshikawa et al., 2002; Petit-Demouliere et al., 2004; Bessa et al., 2008).

Forced swim test

To perform FST, mice were individually placed within glass cylinders, with approximately 20 cm in diameter, filled with water at 24 °C to a depth such that animals were not able to touch the bottom of the cylinder (Figure 2.27A). Mice were forced to swim for 6 min. Time of latency, mobility and immobility time of each animal were assessed for the final 4 min of test. Immobility was considered the absence of struggling movements, only the necessary ones to keep the animal head above water, and can be taken as an indicator of animals learning that there is no way of escaping from this stressful situation. Thus, a short latency to immobility and a longer time of immobility were considered as signs of learned helplessness behavior (Bessa et al., 2008; Castagné et al., 2011).

Tail suspension test

The TST is essentially based on the observation that rodents tend to develop an immobile position when placed in an unavoidable stressful situation. In TST this stressful situation is accomplished by suspending the animal by the tail (Figure 2.27B) (Cryan et al., 2005). To perform the test, mice were suspended by their tails to the edge of a shelf 80 cm above the floor using adhesive tape, for 6 minutes. The period of latency, immobility and mobility times were assessed for the final 4 min of test, for each animal. Latency to immobility corresponded to the time point in which the animal stopped for the first time.

Statistical analysis

Results are presented throughout as mean ± SEM and the statistical significance of the comparisons for each statistical test was set with a confidence interval of at least 95%. All data sets passed the normality tests for Gaussian distributions (D'Agostino & Pearson for n > 7; Kolmogorov-Smirnov for n = 5-6), therefore parametric tests were applied. Two-way ANOVA was used to analyze

the performance of mice in behavioral tests. Sidak post-hoc tests were applied to the analysis of the MWM and HB. Uncorrected Fisher's LSD post-hoc tests was used to evaluate the arm effect in the 2TPR task. In the remaining experiments, unpaired two-sided t-tests were applied to compare data between the main groups of study (WT and dnSNARE) and one-way ANOVA was used to compare data between three groups (WT, dnSNARE and lGFP). Pearson coefficients were calculated to assess correlations between behavior performance and electrophysiological activity. Statistical analysis was performed using the GraphPad Prism 6 (GraphPad Software Inc., USA).

Results

Cognitive function of dnSNARE mice

The MWM test enclosed tasks to assess reference memory (RM) and behavioral flexibility, by the performance of a reversal learning task (RL) (Figure 2.18). In the RM task, the analysis of the learning curves showed that WT mice learnt to follow the external cues in order to reach the platform as confirmed by the decreasing latencies and distances swum during the four trials of each day. On the other hand, dnSNARE mice needed to swim longer to reach the same platform, especially in the last days of the task (Figure 2.18A; escape latency: genotype, $F_{1,27} = 26.14$, $p < 0.001$; days of test, $F_{3,81} = 37.70$, $p < 0.001$; day 2, $t_{108} = 3.011$, $p = 0.013$; day 3, $t_{108} = 3.259$, $p = 0.006$; day 4, $t_{108} = 4.551$, $p < 0.001$). Similarly, the distance swum by dnSNARE mice was higher than WT mice especially in the third and fourth days of test (distance swam: genotype, $F_{1,27} = 8.649$, $p = 0.007$; days of test, $F_{3,81} = 18.42$, $p < 0.001$; day 3, $t_{108} = 2.560$, $p = 0.047$; day 4, $t_{108} = 4.167$, $p < 0.001$). These data suggest the blockade of gliotransmitter release as the main responsible for the deficits observed in the reference memory acquisition of dnSNARE mice. Moreover, the analysis of the RL task, reveals no alterations in dnSNARE mice behavioral flexibility since both genotypes spent more time in the new quadrant of the platform (Quadrants, escape latency: $F_{1,54} = 6.827$, $p = 0.012$; distance swam: $F_{1,54} = 4.303$, $p = 0.043$; Figure 2.18B).
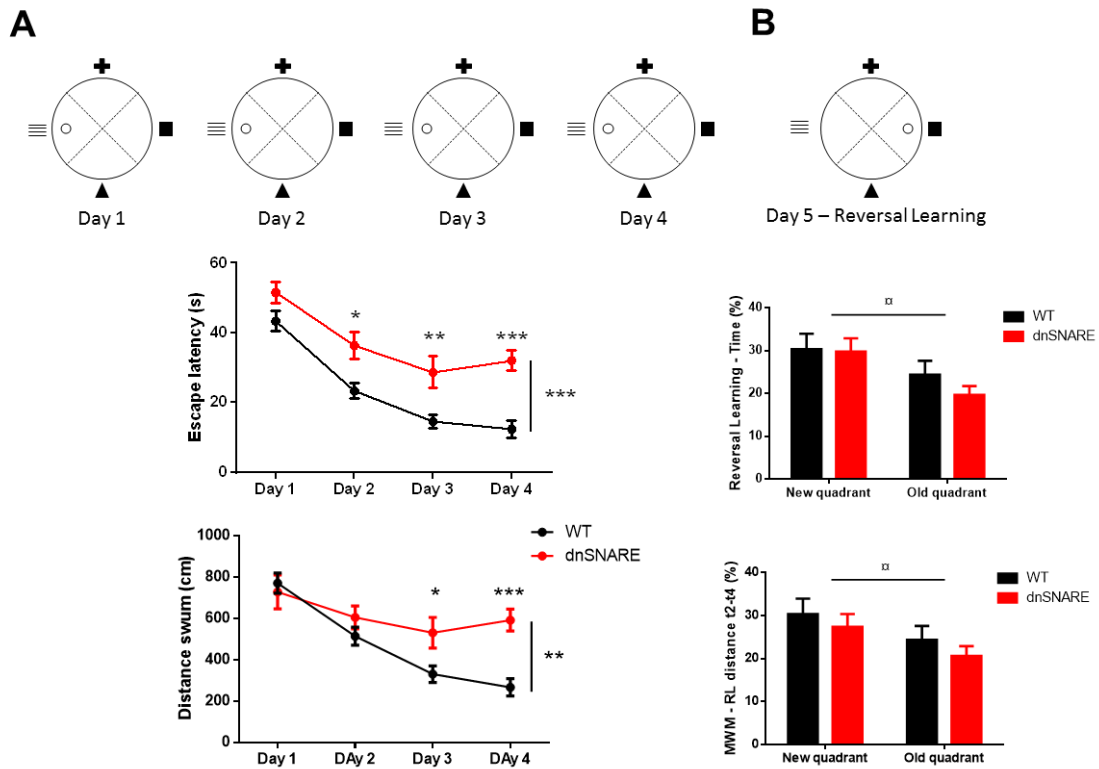
Figure 2.18. Gliotransmission impairment compromises spatial learning and reference memory of dnSNARE mice in the MWM task. (A) Reference memory task scheme (RM, top) and learning curves showing escape latencies and distances swum (bottom); (B) Reversal learning scheme (top) with the percentage of time and distance spent in the new quadrant of the platform (bottom). WT mice are represented in black and dnSNARE mice in red lines and bars. Data plotted as mean ± SEM. *, ¤ $p < 0.05$, **$p < 0.01$; ***$p < 0.001$ (n = 14-15 per group).

For a complete characterization of dnSNARE mice performance in the MWM test, we analyzed the different strategies used to reach the escape platform during the four days of the RM task. This evaluation was established according to already described and prototypical tracks of different behavioral categories of strategies used in the MWM (Graziano et al., 2003; Figure 2.19A, B).

In accordance with previous results, the analysis of strategies used to reach the platform revealed that dnSNARE mice failed more often to reach the platform within the 60 s of each trial (Figure 2.19C, left; $t_{27} = 4.366$, $p < 0.001$), and whenever they reached it, they employed rather random searching and scanning strategies indicating a poor spatial orientation throughout the four days of test (Figure 2.19C, right; $t_{27} = 2.586$, $p = 0.015$). Additionally, from Figure 2.19D one can observe the progressive evolution in the type of strategies used to reach the platform, from trial to trial. The transition of type of strategies used during the whole test occurred in a more efficient way in WT than in dnSNARE mice, in agreement with a deleterious effect of astrocyte exocytosis impairment in the hippocampal function of dnSNARE mice.
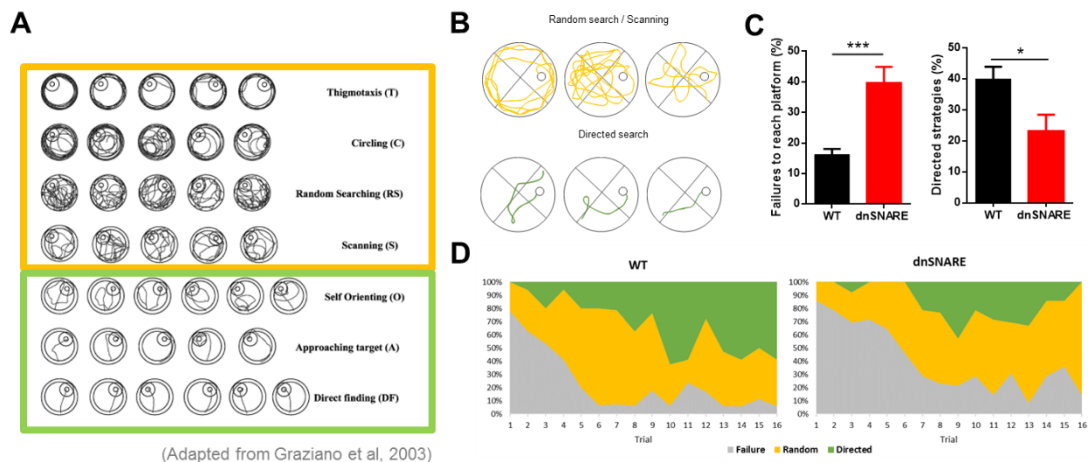
Figure 2.19. The dnSNARE mice use less goal-oriented strategies in the MWM task. (A) Prototypical tracks of different behavioral categories of strategies used in the MWM; (B) representative swim tracks used to reach the hidden platform, of random search/scanning (yellow) and directed search strategies (green); (C) Percentage of failures (left) and cue-based/directed strategies to reach the platform in RM (right); (D) stacked area charts displaying the percentage of failures (gray) and strategies used to reach the platform over the 16 trials of RM for wild-type (WT, left) and dnSNARE mice (right). WT mice are represented in black and dnSNARE mice in red bars. Data plotted as mean ± SEM. *$p < 0.05$; ***$p < 0.001$ (n = 14-15 per group).

In order to get further confirmation of the behavior results observed in the RM task of MWM, additional experiments were conducted and RM was complementarily tested using the HB task (Castilla-Ortega et al., 2010). HB test was performed in a different environment, using food deprivation as motivation to learn the location of hidden food pellets with the help of spatial cues. In this test, WT mice learnt to perform the task, as indicated by the increasing RM ratio measured along the days. However, dnSNARE mice with impaired gliotransmission, faced difficulties to discriminate between baited and unbaited holes, even with the help of spatial cues, supporting an impairment in RM of transgenic mice (day 1, $t_{84} = 3.700$, $p = 0.002$; day 2, $t_{84} = 6.053$, $p < 0.001$; day 3, $t_{84} = 7.789$, $p < 0.001$; day 4, $t_{84} = 4.634$, $p < 0.001$) (Figure 2.20B, left). Moreover, two-way ANOVA revealed a significant effect on genotype ($F_{1,21} = 79.530$, $p < 0.001$) for the performance in the RM task. Curiously, the calculation of WM ratios (more dependent on the function of the prefrontal cortex) (Castilla-Ortega et al., 2010; Lima et al., 2014) also pointed out an impairment of this function in the dnSNARE mice (Figure 2.20B, right). In comparisons within each test day, dnSNARE mice presented a pronounced dysfunction in WM comparatively to controls, namely in the first days of test (day 1, $t_{84} = 3.839$, $p < 0.001$; day 2, $t_{84} = 4.528$, $p < 0.001$; day 3, $t_{84} = 4.817$, $p < 0.001$). In the WM task, dnSNARE mice did a random exploration of the maze independently of the holes being baited or not. Statistical analysis showed a genotype effect for the WM task ($F_{1,21} = 39.950$, $p < 0.001$). The obtained results were in line with previous ones from MWM, holding an impairment in RM, a task mainly dependent on hippocampus function.

In addition, these data suggest the implication of astrocyte signaling in the mPFC function, as one main region involved in working memory processing (Goldman-Rakic, 1995; Lima et al., 2014).
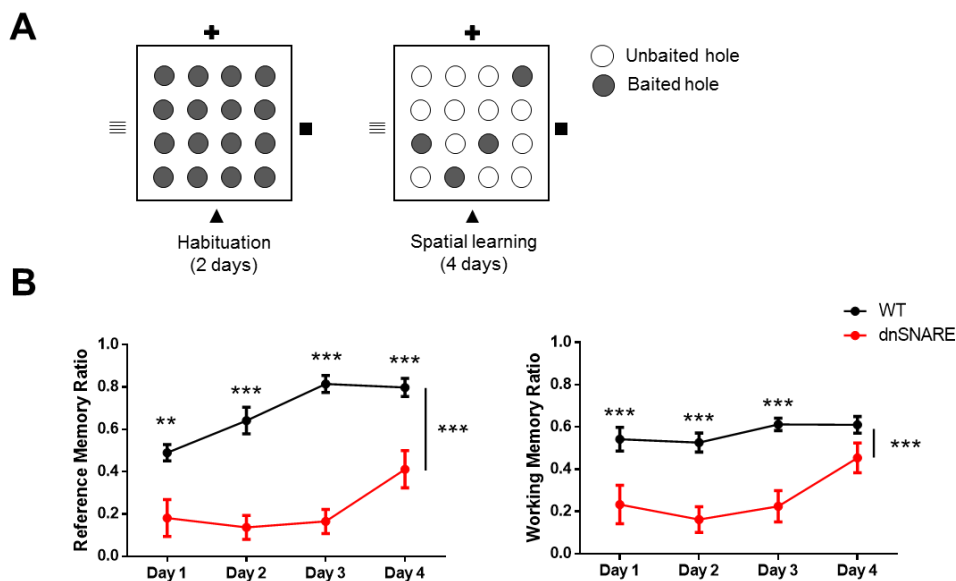

Figure 2.20. Spatial reference and working memory deficits in dnSNARE mice. (A) Hole-board task scheme (baited holes, gray; unbaited holes, white); (B) RM and working memory (WM) ratios for WT and dnSNARE mice. RM ratio: number of visits to the baited holes/total number of visits; WM ratio: number of rewarded visits/number of visits to the baited holes. WT mice are represented in black and dnSNARE mice in red lines. Data plotted as mean ± SEM. **$p < 0.01$; ***$p < 0.001$ (n = 9-14 per group).

Next the NOR test was performed to assess long-term memory, spatial recognition memory and short-term memory of dnSNARE and WT mice (Figure 2.21A-B). These behavior paradigms are driven by novelty exploration (Leger et al., 2013), processes critically dependent on hippocampal and cortical networks. Long-term memory was evaluated by exposing mice to a novel object 24h after an exposition to two identical objects. In this test, WT mice dedicated higher percentages of time exploring the novel object (around 75% of the total exploration time), which was not the case of the dnSNARE mice that performed an indiscriminate exploration of both objects ($t_{14} = 4.889$, $p < 0.001$). For dnSNARE mice, these results were an indicator of a deficit in their ability to recognize the previously experienced object or to detect differences between the objects (Bevins and Besheer, 2006; Ennaceur, 2010) as a consequence of astrocyte dysfunction. Spatial recognition memory was assessed by means of displacing one of two objects to the opposite side of the box, in a second trial with 1h delay. Regarding the time spent exploring the displaced object, although WT mice appear to still prefer the displaced object, this observation was not statistically different ($t_{15} = 1.198$, $p = 0.249$). Additionally, in the assessment of short-term memory, where animals explored a new pair of similar objects and, 1 h later, one of the familiar objects was replaced by a new one, no

differences were found between genotypes ($t_{14} = 1.484$, $p = 0.160$). These observations support a specific impairment on long-term recognition memory that matches with the hippocampal-related deficits observed in the previous tasks.
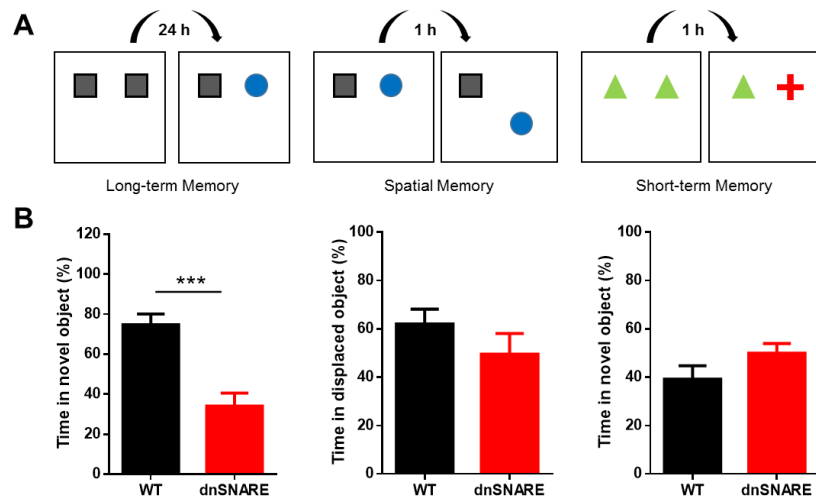
Figure 2.21. Blockade of gliotransmission induces long-term memory deficits. (A) Novel object recognition task schemes (top) for the assessment of long-term (left), spatial (middle), and short-term (right) recognition memories; (B) Percentages of exploration time of the novel and displaced objects. WT mice are represented in black and dnSNARE mice in red bars. Data plotted as mean ± SEM. ***$p < 0.001$ (n = 7-9 per group).

Finally, we examined the spatial recognition memory of WT and dnSNARE mice in the 2TPR task (Figure 2.22A). Mice performed a two trial place recognition task in which they were expected to preferentially explore and spend more time in a novel arm marked by spatial cues. This configuration allowed the assessment of both dHIP and mPFC functions (Costa-Aze et al., 2012). The analysis of the percentage of time spent in the distal third of the three arms showed that mice spent longer time in the novel arm ($F_{2, 57} = 12.930$, $p < 0.001$). Moreover, our data showed that dnSNARE explore the novel arm significantly less than their WT mice littermates ($t_{57} = 2.388$, $p = 0.020$), which reveals deficits on place recognition memory in the latter (Figure 2.22B).

Together, the results of the behavior analysis indicate a striking cognitive deficit, namely on functions that rely on the dHIP and its interaction with the mPFC.
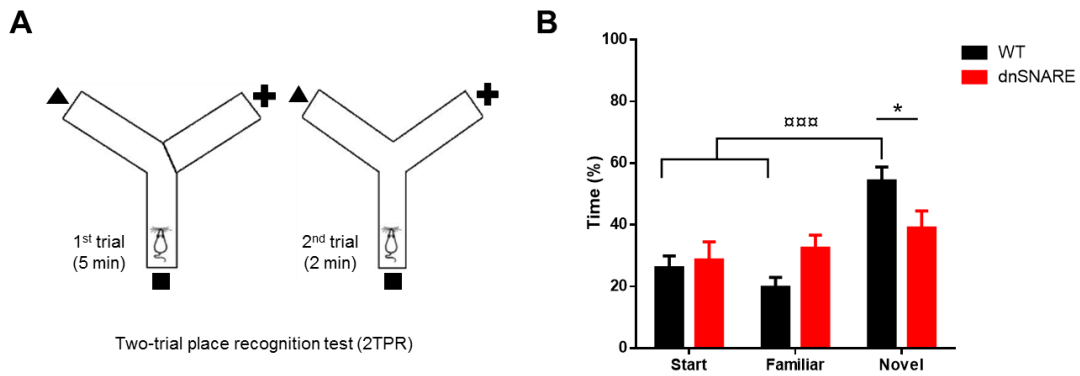
Figure 2.22. The performance of dnSNARE mice in a spatial recognition memory task in the Y-maze is affected by the gliotransmission impairment. (A) Two-trial place recognition task scheme; (B) Percentage of time spent in the distal third of start, familiar or novel arms in the retrieval trial. WT mice represented in black and dnSNARE mice in red bars. Data plotted as mean ± SEM. *$p < 0.05$; ¤¤¤ $p < 0.001$ (n = 9-12 per group).

Next, we took advantage of the variable transgene expression levels observed between subjects to verify whether the performance in the cognitive tasks was modulated by the level of transgene expression. Indeed, double-transgenic mice that display low levels of expression perform in the different tasks similarly to controls, being significantly different from strongly expressing-dnSNARE mice. This is true for the four tasks carried out: MWM (Figure 2.23A; day 3, $t_{164} = 3.067$, $p = 0.030$; day 4, $t_{164} = 5.159$, $p < 0.001$); HB (Figure 2.23B; day 2, $t_{136} = 3.339$, $p = 0.003$; day 3, $t_{136} = 4.177$, $p < 0.001$); NOR (Figure 2.23C; $t_{19} = 2.958$, $p = 0.024$) and 2TPR task (Figure 2.23D; novel arm: $t_{90} = 2.506$, $p = 0.033$). It is noteworthy that the levels of expression in double-transgenic mice strongly correlate with a worse performance in the tests that rely on the cortico-limbic link, supporting the use of dnSNARE mice for in vivo testing (Figure 2.23A-D, bottom). This means that, the higher the expression of truncated synaptobrevin II by astrocytes *in vivo*, the stronger the cognitive impairment.

Figure 2.23. The individual performance in the cognitive tasks by transgenic mice correlates directly with the respecti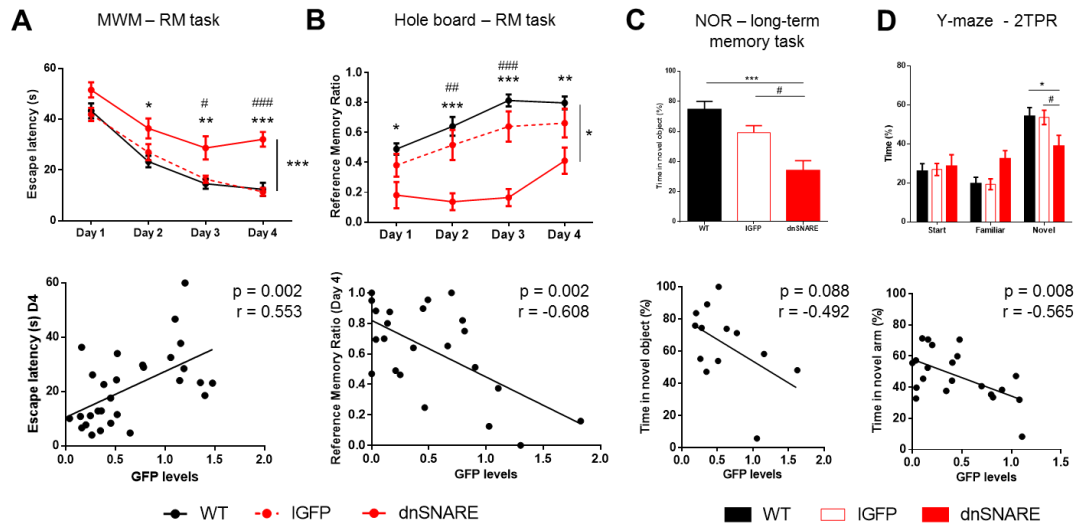ve hippocampal transgene expression levels. Graphs of performance (top panels) in the RM task of MWM (A, Latency to platform; n = 14-15 per group), RM task of HB (B, RM ratio; n = 9-14, per group), long-term memory task of NOR (C, percentage of time exploring novel object; n = 6-9, per group) and Two-trial place recognition task (D, percentage of time spent in the distal third of novel arm; n = 9-12, per group). The bottom panels include the correlation plots between relative GFP levels in the hippocampus and performance in each behavior task for each transgenic mouse tested and p-values are indicated for each Pearson correlation. WT are represented in black, lGFP in dashed lines and white bars, and dnSNARE mice in red lines and bars. Data plotted as mean ± SEM. *Denotes the comparison between WT and dnSNARE mice; #Denotes the comparison between lGFP and dnSNARE mice. *.#$p < 0.05$; **.##$p < 0.01$; ***.###$p < 0.001$.

Correlation between behavior and electrophysiological activity

So far, our results raised the possibility of the existence of a link between the impairment in the cortico-limbic synchronization and the poor performance in cognitive tasks that rely on those areas. In order to confirm this idea, we performed a functional characterization of the cohort of mice that performed in MWM test by recording the electrophysiological activity of mPFC and dHIP of both dnSNARE and WT mice. We measured the dHIP-mPFC synchrony and investigated for possible correlates between the levels of dHIP-mPFC synchronization and behavior measures (Figure 2.24). Analysis of Pearson's correlations between both factors showed that the lower levels of theta coherence directly correlate with the poor performance after the third day of the RM task, expressed by longer latencies and distance swum (day 3, escape latency: $p = 0.048$, $r = -0.557$, distance: $p = 0.014$, $r = -0.661$; day 4, escape latency: $p = 0.022$, $r = -0.625$, distance: $p = 0.003$, $r = -0.746$), with the use of directed strategies ($p = 0.027$, $r = 0.634$) and with the success to reach the platform ($p = 0.020$, $r = -0.660$; Figure 2.24A-C). Moreover, this effect was quite specific, since the dHIP-mPFC coherence in the beta band only seems to be significantly correlated with the distance swum in day 1 ($p = 0.027$, $r = -0.608$) or the success to reach the platform ($p = 0.041$,

r = -0.595; Figure 2.24D-F), and low gamma coherence fails to correlate with any of the parameters measured (Figure 2.24G-I). We and others showed previously that the HIP-PFC theta coherence is crucial for reference memory processing (Jones and Wilson, 2005; Siapas et al., 2005; Benchenane et al., 2010; Oliveira et al., 2013). Now, on behalf of our findings, we specify that gliotransmission, through the astrocytic release of signaling molecules, is critically required to support the cortico-limbic theta synchronization underlying memory consolidation.
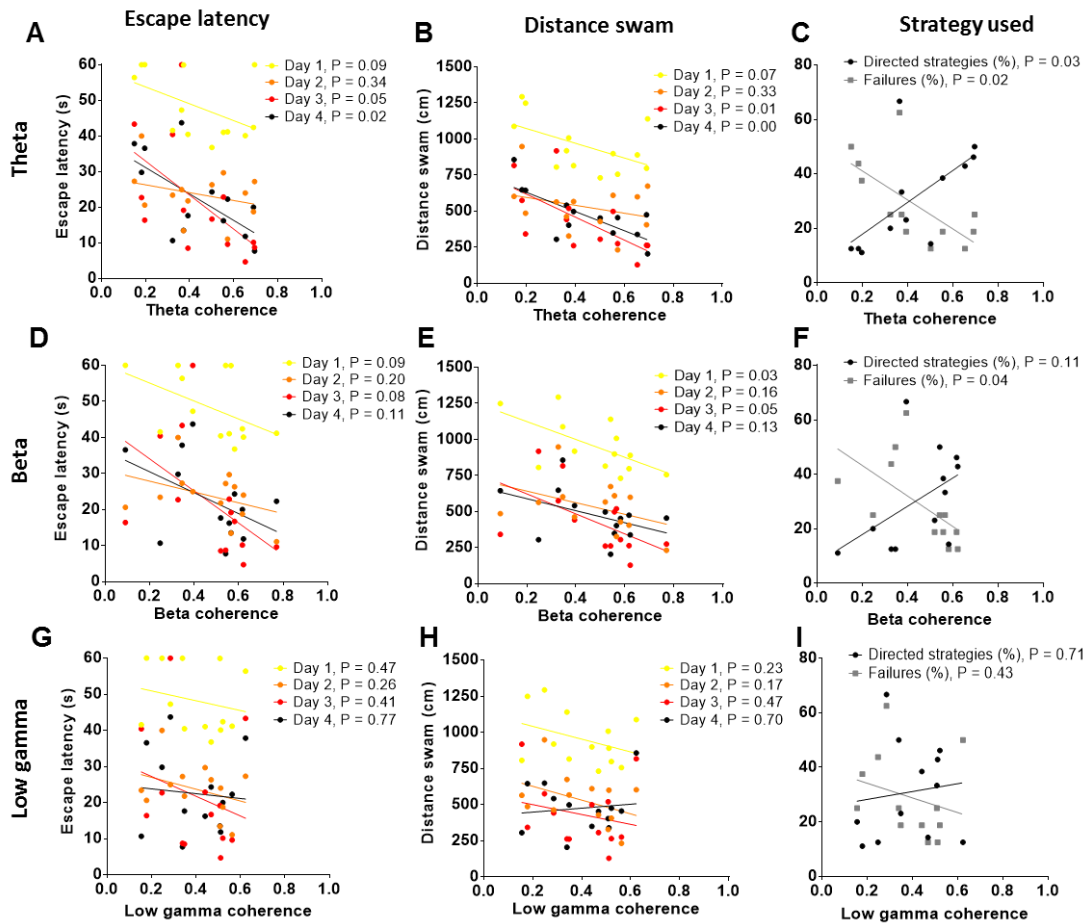
Figure 2.24. Theta dHIP-mPFC coherence correlates with the consolidation of reference memory. Correlation plots between behavior parameters analyzed for the reference memory (RM) task (escape latency, distance swam, directed strategies and failures to reach platform) and levels of dHIP-mPFC coherence measured in those mice that performed the RM task for (A-C) theta; (D-F) beta and (G-I) low gamma frequency bands, and the respective p-values for Pearson correlations. Performance of day 1 in yellow, day 2 in orange, day 3 in red, day 4 in black. The percentage of use of directed strategies is plotted in black and percentage of failures to reach platform is plotted in gray (n = 6-7 per group).

Locomotion and emotional state of dnSNARE mice

Ultimately, we performed a screening of locomotor activity, anxiety and depressive-like phenotypes in order to discard a putative influence on the cognitive testing. Anxiety in rodents is usually

assessed through paradigms such as the EPM and OF. Several studies with either lesion or local drug infusion lines, have shown the relevance of hippocampus for normal anxiety-like behavior in these environments (Bannerman et al., 2003; Adhikari et al., 2010). In a first approach, we evaluated the anxious-like behavior in the EPM. In this test, the percentage of time spent by mice in the open arms was used as a measure of their anxiety level. The longer in the open arms, the less anxious animals should be considered. Our data showed no significant differences between WT and dnSNARE mice, also when the lGFP mice were included in the analysis ($F_{2, 27} = 0.152$, $p = 0.860$; Figure 2.25A). Secondly, as a complementary study to assess the tendency of rodents to stay in darker and safer places to avoid their exposure to predation we performed the LDB test (Bourin and Hascoët, 2003; Takao and Miyakawa, 2006). We observed that mice of the three groups spent similar time in the lightened area ($F_{2, 12} = 0.020$, $p = 0.980$; Figure 2.25B). Additionally, we evaluated mice performance in the OF test (Figure 2.26A). This test takes advantage of the tendency of rodents to avoid brightly lit open spaces and allows to assess the general locomotor function and exploratory behavior of mice (Tatem et al., 2014; Seibenhener and Wooten, 2015). Also in this test, mice of the three groups performed similarly in all the parameters under study (thigmotaxis – tendency to spend their time near the walls and corners of the arena: $F_{2, 27} = 2.043$, $p = 0.149$; total distance: $F_{2, 27} = 2.917$, $p = 0.071$; number of rearings: $F_{2, 27} = 2.308$, $p = 0.119$; average velocity: $F_{2, 27} = 2.920$, $p = 0.071$; Figure 2.26B-E).
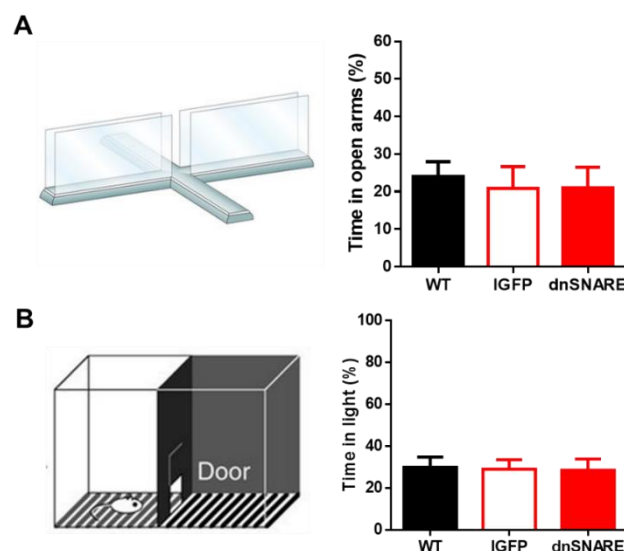
Figure 2.25. The dnSNARE mice do not display anxious-like behavior. (A) The Elevated Plus Maze (EPM) showing the percentage of time spent in the open arms (n = 7-15 per group); (B) Light/Dark Box test showing the percentage of time spent in the light chamber (n = 5 per group). WT are represented in black, lGFP in white and dnSNARE mice in red bars. Data plotted as mean ± SEM.
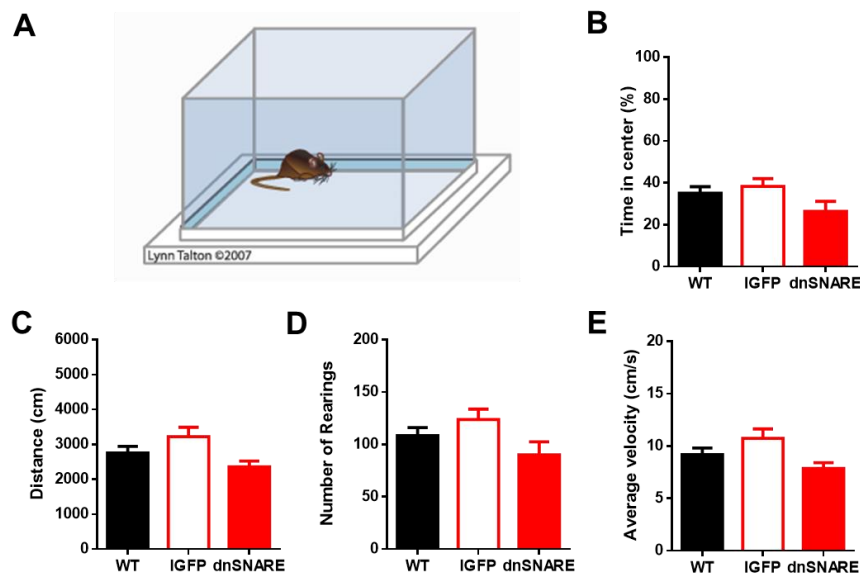
Figure 2.26. The dnSNARE mice display normal exploratory behavior and general motor function.
(A) Open-field test scheme; (B) Percentage of time spent in the center of the chamber; (C) Total distance (cm); (D) Number of rearings and (E) Average velocity (cm/s). WT are represented in black, IGFP in white and dnSNARE mice in red bars. Data plotted as mean ± SEM (n = 7-15 per group).

Next, our behavior assessment for depressive-like phenotype included the performance of the FST (Figure 2.27A) and the TST (Figure 2.27B) tests (Can et al., 2012a, 2012b). In both paradigms we analyzed the latency to immobility and immobility times as a measure of learned helplessness. Generally, WT mice tried to escape from a forced swimming condition, as well as from tail suspension, by engaging in energetic movements or trying to hold to their own tails, becoming immobile after a few minutes. The faster they stop moving, expressed by a shorter latency to immobility and a longer immobility time of the animal, the more depressive-like phenotype can be associated. The analysis of the results showed no significant differences between groups for any of the parameters, both in FST (latency: $F_{2,27} = 0.025$, $p = 0.975$; Immobility: $F_{2,27} = 1.183$, $p = 0.322$; Figure 2.27A) and in TST tests (latency: $F_{2,27} = 0.419$, $p = 0.662$; Immobility: $F_{2,27} = 3.243$, $p = 0.055$). These results excluded a depressive-like state for dnSNARE mice.
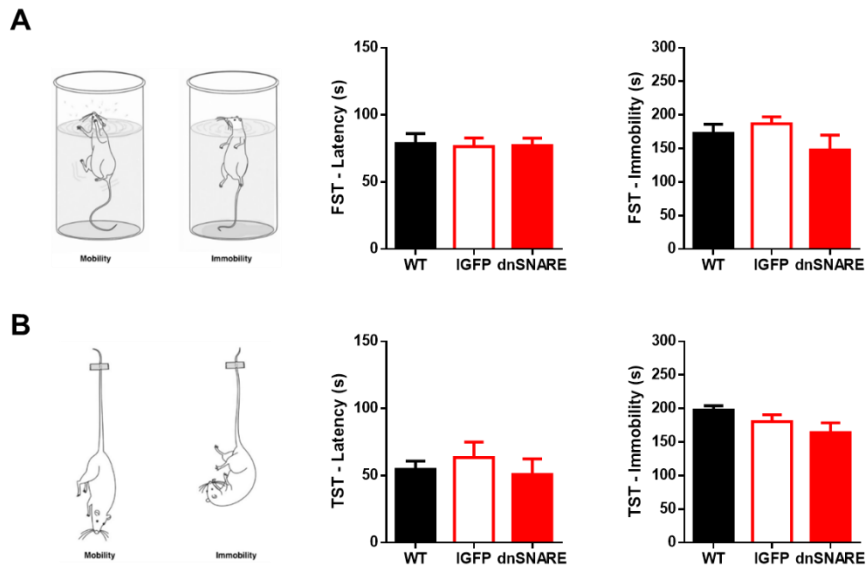
Figure 2.27. The dnSNARE mice do not display depressive-like behavior. (A) Forced swim test and (B) Tail suspension test schemes showing latency to immobility (s) and total immobility time (s), for each test. WT are represented in black, IGFP in white and dnSNARE mice in red bars. Data plotted as mean ± SEM (n = 7-15 per group).

These observations are in agreement with the lack of alterations in terms of electrophysiological activity in the vHIP, or in its synchronization to the mPFC, described above (Chapter 2.2). It is known that the vHIP is required for anxiety-like behavior and that theta-frequency synchronization between the vHIP, but not dHIP, and the mPFC plays a role in anxiety (Adhikari et al., 2010). Thus, our data goes in line with this assumption since our results showed an undamaged synchrony in the vHIP-mPFC link the dnSNARE mice. Altogether, the results suggest that at least in the dnSNARE model, interfering with astrocyte signaling affects neither the emotional state of dnSNARE mice, nor their motor function.

2.4   Analysis of morphological and structural correlates of the electrophysiological and behavior deficits

Introduction

Astrocytes have the ability to maintain a dialog with neurons resulting in synaptic modulation. This dialog is only possible due to astrocytic morphologic features, namely their complex ramification, which allows the close apposition of astrocytic processes to functional synapses and blood vessels. At these sites, astrocytes can sense, process, and release neuroactive molecules in order to modulate synaptic communication and blood flow (Perea et al., 2009; Reichenbach et al., 2010; Araque et al., 2014), ultimately impacting the network function and behavior processing (Oliveira et al. 2015). The results obtained with dnSNARE mice hitherto prompted us to seek for morphological correlates that could justify the loss of function observed. Therefore, assessing morphologic features of both neurons and astrocytes of dnSNARE mice in the HIP-PFC network will help to better understand the mechanisms underlying the desynchronized theta activity, as well as the consequent impairment in cognitive tasks dependent on this link.

Materials and Methods

Golgi-Cox impregnation and 3D dendritic reconstruction of neurons

All procedures employed to assess the morphology of neurons were previously described (Lima et al., 2014). In order to assess dendritic morphology of hippocampal neurons a set of mice (n = 5 WT and n = 5 dnSNARE) were perfused with 0.9% saline under deep anesthesia (ketamine and medetomidine mix) and the brains were processed for Golgi–Cox staining. Briefly, brains were removed and immersed in Golgi–Cox solution (1:1 solution of 5% potassium dichromate and 5% mercuric chloride diluted 4:10 with 5% potassium chromate) for 14 days; transferred to a 30% sucrose solution (minimum 3 days) and sectioned by means of a vibratome. Coronal sections (200 μm thick) were collected in 6% sucrose and blotted dry onto gelatin-coated microscope slides, subsequently alkalinized in 18.7% ammonia, developed in Dektol (Kodak, USA), fixed in Kodak Rapid Fix, dehydrated and xylene cleared, mounted and coverslipped. All incubation steps were performed in a dark room.

Three dimensional (3D) reconstruction of Golgi-Cox impregnated neurons was performed in the CA1 and dentate gyrus (DG) subregions of the dHIP and in the mPFC, following the mouse brain atlas (Paxinos and Franklin, 2004). CA1 pyramidal neurons were readily identified by their characteristic triangular soma-shape, apical dendrites extending toward the stratum radiatum, whereas granule neurons from DG extend their dendritic trees into the molecular layer. Neurons

were selected for reconstruction following these criteria: (i) identification of soma within the pyramidal layer of CA1, granular layer of DG and layer V of mPFC (ii) full impregnation along the entire length of the dendritic tree; (iii) no morphological changes attributable to incomplete dendritic impregnation of Golgi–Cox staining or truncated branches. To avoid selection bias, brain slices containing the region of interest were randomly searched and the first 6 neurons from each animal were reconstructed from at least 3 brain slices (containing both hemispheres). The dendritic reconstruction was performed by using a motorized microscope controlled by the Neurolucida software (MBF Bioscience, USA) under 100x magnification. The analyzed dendritic branch features were total length, number of endings and nodes and Sholl analysis (number of dendrite intersections at radial intervals of 20 µm). Dendritic spine densities were also assessed for the CA1 and DG of dHIP, in randomly selected 30 µm segments of 3 proximal and 3 distal dendritic branches per neuron, and were categorized in 4 types (thin, mushroom, wide and ramified). The features of the reconstructed neurons and spines were quantified using NeuroExplorer software (MBF Bioscience, USA).

GFAP-structure reconstruction of astrocytes

To study the astrocytic main structure, 3D reconstructions of GFAP-stained cells were performed using Simple Neurite Tracer (Longair et al., 2011; Tavares et al., 2016), an open-source FIJI plugin (http://fiji.sc/Simple_Neurite_Tracer). Brain slices containing the dorsal hippocampus of both WT and dnSNARE mice were stained by immunofluorescence for the GFAP (the intermediate filament protein used as specific marker of astrocyte structure (Khakh and Sofroniew, 2015) and for DAPI, for cell nuclei identification, as described in sub-chapter 2.1 (n = 5 WT and n = 5 dnSNARE). The dnSNARE brain slices were also stained for the GFP to identify the transgene expressing astrocytes (n = 3 dnSNARE). Z-stacks of images (2 per brain region from 2 brain slices per animal) obtained from the CA1 and DG of dHIP were acquired by means of a confocal microscope (FV1000, Olympus, Japan). Each image stack was acquired with 1 µm z-step interval, 640x640 pixel resolution, under 60x oil magnification (field size 211.51 x 211.51 µm). Astrocytes were readily identified by their characteristic GFAP-positive ramified shape, displaying thicker processes around the DAPI-stained nucleus. The selection criteria used to pick astrocytes for reconstruction were: (i) the whole GFAP-stained structure was clearly identified and was located within the region of interest (stratum radiatum of CA1 and molecular layer of DG); (ii) GFAP-stained structure enclosed a single DAPI-stained nucleus and (iii) main structure without truncated processes. To minimize selection

bias, the first 10 cells per animal that fulfilled the criteria were reconstructed, by a maximum of 4 cells per randomly selected Z-stack. The structural features analyzed were: total process length, number of processes, process thickness, and radial distance from soma of last intersection, and Sholl analysis.

Astrocytes density

In order to determine the density of GFAP-positive (GFAP+) astrocytes, 1 μm spaced confocal image stacks were obtained from the representative brain sections selected for astrocyte reconstruction using a 20x magnification objective (1024x1024 pixel resolution; field size 635.28 x 635.28 μm). Each of the dHIP subregions were outlined according to the mouse brain atlas (Paxinos and Franklin, 2004). All GFAP+ astrocytes were counted using the "Cell counter" plugin of Image J (http://fiji.sc/Fiji). Only cells that displayed co-localization of GFAP with DAPI were considered for counting.

Statistical analysis

Results are presented throughout as mean ± SEM (Standard Error of the Mean) and the statistical significance of the comparisons for each statistical test was set with a confidence interval of at least 95%. Unpaired t-tests were used to compare the total length, number of nodes, endings, spine density and types of spines for neuronal 3D reconstructions, and to compare the total length, number of processes and process thickness between groups for astrocytic 3D morphologic reconstructions. Two-way ANOVA and Sidak post-hoc tests were applied to the Sholl analysis data for neurons and astrocyte 3D reconstructions (factors: genotype and radial distance from soma). Statistical analysis was performed using the GraphPad Prism 6 (GraphPad Software Inc., USA).

Results

In the present sub-chapter, we characterized the morphologic features of neurons of the hippocampus and prefrontal cortex. We focused on the neurons of subregions typically relevant for the operation of hippocampal-prefrontal networks and cognitive processing: the CA1, DG in the dorsal hippocampus and layer 5 of the prelimbic prefrontal cortex (Cerqueira et al., 2007; Bessa et al., 2008; Lima et al., 2014; Sultan et al., 2015).

Tridimensional reconstruction of pyramidal neurons in the dCA1 subregion (Figure 2.28A) showed that WT neurons are similar to dnSNARE neurons for all parameters analyzed (Figure 2.28B), namely the total dendritic length (t_{59} = 1.222, p = 0.227), the number of nodes (t_{59} = 1.488, p = 0.142) and endings (t_{59} = 1.543, p = 0.128), and complexity given by the number of intersections at increasing radial distances from the soma ($F_{1,60}$ = 0.591, p = 0.445). The lack of major structural alterations prompted us to analyze the spine distribution to assess subtler alterations that could have an impact in synaptic communication. The analysis covered the determination of spine density in apical proximal and apical distal segments of the reconstructed neurons and the categorization of spines in thin, mushroom, thick and ramified (Figure 2.28C). The spine distribution according to maturity criteria remained constant in mice of both genotypes, without statistical differences in spine density in either proximal (t_{47} = 0.455, p = 0.651) or distal segments (t_{46} = 0.331, p = 0.742). Furthermore, and as expected for the WT mice, most of the spines were the mushroom type and this result was also obtained for the dnSNARE mice. However, the blockade of vesicular exocytosis in astrocytes did not affect the proportion of spines of each morphological category in both proximal and distal segments of the apical dendritic trees (proximal – thin: t_{39} = 0.458, p = 0.649; mushroom: t_{39} = 0.541, p = 0.591; thick: t_{39} = 0.333, p = 0.741; ramified t_{39} = 0.245, p = 0.807; distal – thin: t_{39} = 0.483, p = 0.631; mushroom: t_{39} = 0.091, p = 0.928; thick: t_{39} = 0.673, p = 0.505; ramified t_{39} = 0.309, p = 0.759). These results support the general integrity of the neuronal and spine structures notwithstanding the lack of surrounding gliotransmitters in the dCA1.
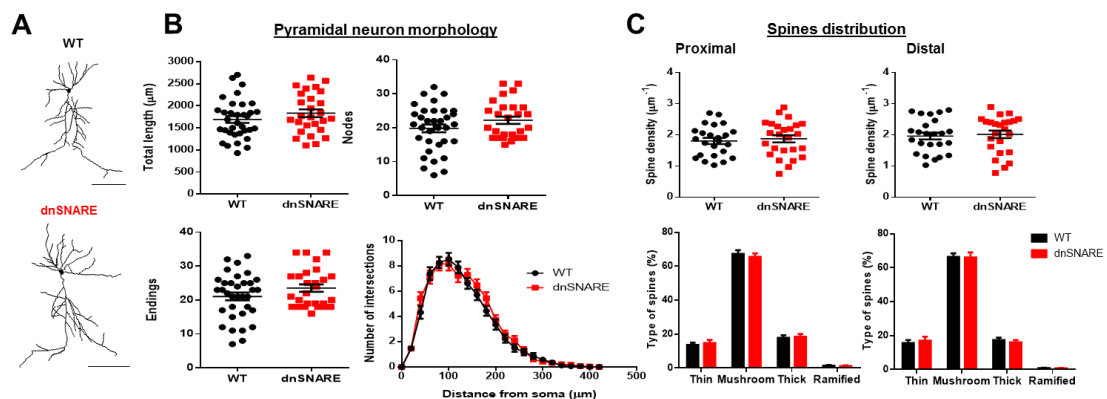
Figure 2.28. The dnSNARE mice display an intact neuronal morphology in the CA1 region of the dorsal hippocampus. (A) Representative 3D reconstructions of dorsal CA1 pyramidal neurons of WT (top) and dnSNARE mice (bottom); scale bars = 100 μm; (B) Characterization of the 3D structure of apical dendrites by analysis of total dendritic length, number of nodes and endings, and Sholl intersections (n = 27-34 neurons; 5 mice per group); (C) Density of spines (top) and proportions of spine types (bottom) at proximal and distal portions of the apical dendrites (n = 19-25 neurons; 5 mice per group). WT mice represented in black and dnSNARE mice in red dots and bars. Data plotted as mean ± SEM.

In order to evaluate whether the preservation of neuronal structures was common in other subregions of the hippocampus, we extended the evaluation of neuronal morphology to granule cells of the dentate gyrus (Figure 2.29A). In this subregion, the structures of granule neurons of WT and dnSNARE mice were also analogous, as given by every measure analyzed regarding dendritic morphology: total dendritic length ($t_{42} = 1.606$, $p = 0.116$), number of nodes ($t_{42} = 1.267$, $p = 0.212$), number of endings ($t_{42} = 1.372$, $p = 0.178$), and arbor complexity assessed by Sholl analysis ($F_{1, 40} = 1.283$, $p = 0.264$) (Figure 2.29B). In the same way, the distribution of spines in the DG was similar between both genotypes in either proximal ($t_{48} = 0.224$, $p = 0.824$) or distal segments ($t_{48} = 0.944$, $p = 0.350$). Moreover, like previously observed for the dCA1 subregion, also in the DG there were no differences in the proportion of spines of each morphological category, in proximal and distal segments of the apical dendritic trees of both WT and dnSNARE mice (proximal – thin: $t_{43} = 1.264$, $p = 0.213$; mushroom: $t_{43} = 1.400$, $p = 0.169$; thick: $t_{43} = 0.381$, $p = 0.705$; ramified $t_{43} = 0.752$, $p = 0.456$; distal – thin: $t_{42} = 0.222$, $p = 0.825$; mushroom: $t_{42} = 1.374$, $p = 0.177$; thick: $t_{42} = 1.650$, $p = 0.106$; ramified $t_{42} = 0.378$, $p = 0.707$; Figure 2.29C). These results suggest that the general morphology of neurons in the hippocampus is untouched by the lack of gliotransmitters, as well as the spine distribution in their dendrites.
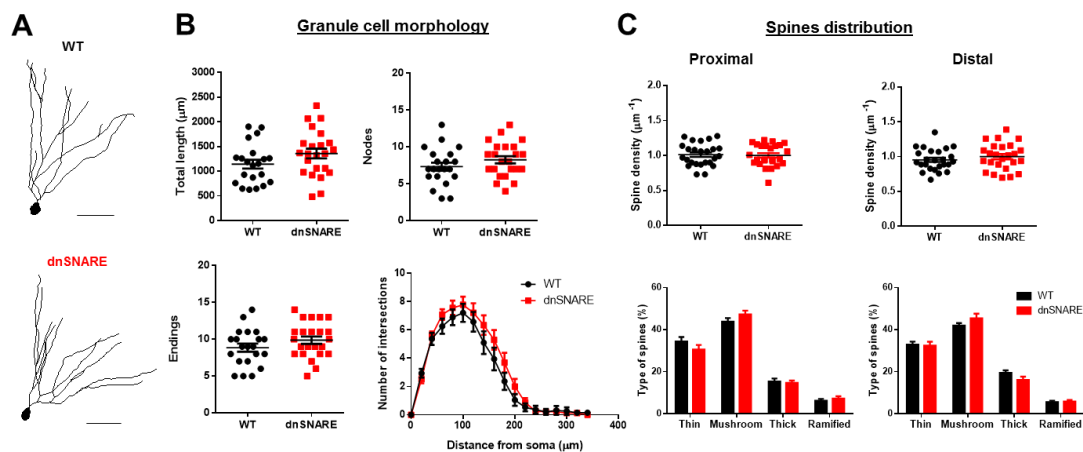
Figure 2.29. The dnSNARE mice display an intact general neuronal morphology in the dentate gyrus (DG) of the dorsal hippocampus. (A) Representative 3D reconstructions of dorsal DG neurons of WT (top) and dnSNARE mice (bottom); scale bars = 50 µm; (B) Characterization of the 3D structure of neurons from the granular layer by analysis of total dendritic length, number of nodes and endings, and Sholl intersections (n = 19-23 neurons; 5 mice per group); (C) Density of spines (top) and proportions of spine types (bottom) at proximal and distal portions of the apical dendrites (n = 24-25 neurons; 5 mice per group). WT mice represented in black and dnSNARE mice in red dots, lines and bars. Data plotted as mean ± SEM.

A final analysis covered the tridimensional reconstruction of pyramidal neurons of the mPFC of the studied mice, in order to verify whether the neuronal structures were also preserved (Figure 2.30A).

The data showed that prefrontal neurons of WT and dnSNARE mice are similar in all morphologic measures analyzed, independently of the assessment being performed for basal (total dendritic length: $t_{33} = 0.673$, $p = 0.506$; number of nodes: $t_{33} = 0.078$, $p = 0.938$; number of endings: $t_{33} = 0.482$, $p = 0.633$; Sholl analysis: $F_{1, 32} = 0.479$, $p = 0.494$; Figure 2.30B) or apical dendrites (total dendritic length: $t_{33} = 0.686$, $p = 0.498$; number of nodes: $t_{33} = 0.680$, $p = 0.501$: number of endings: $t_{33} = 0.765$, $p = 0.450$; Sholl analysis: $F_{1, 32} = 1.457$, $p = 0.236$; Figure 2.30C).

This set of data is in agreement with previous results supporting that, as in the dHIP, the shutdown of astrocyte exocytosis signaling does not interfere with general neuronal morphology.
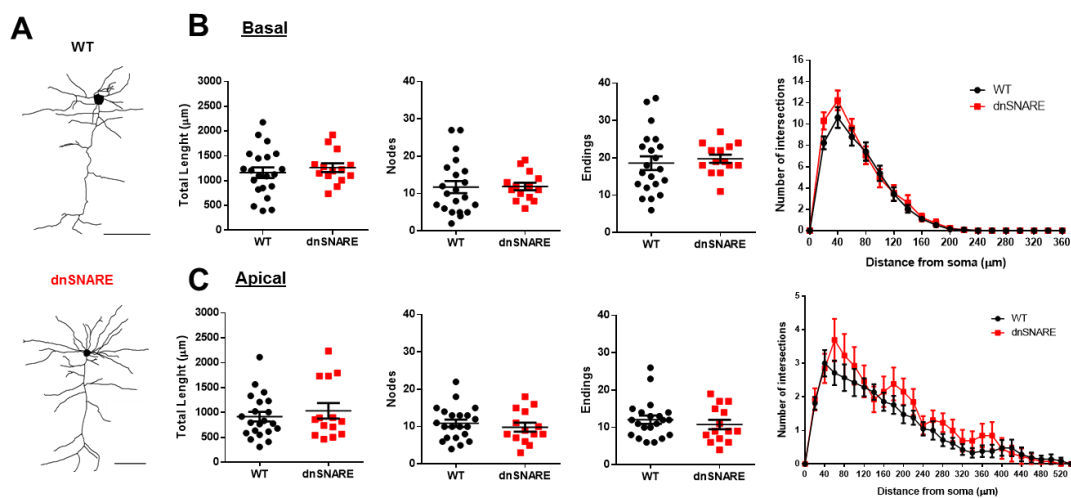
Figure 2.30. The dnSNARE mice display an intact neuronal morphology in layer V of the medial prefrontal cortex. (A) Representative 3D reconstructions of pyramidal neurons of WT (top) and dnSNARE mice (bottom); scale bars = 100 μm; (B) Characterization of the 3D structure of basal and (C) apical dendrites by analysis of total dendritic length, number of nodes and endings, and Sholl intersections (n = 14-21 neurons; 5 mice per group). WT mice represented in black and dnSNARE mice in red dots and lines. Data plotted as mean ± SEM.

After observing the lack of morphological alterations in neurons, we sought for alterations of astrocyte morphologic features. In order to accomplish that, we performed a tridimensional reconstruction of the main GFAP-structure of astrocytes in the dorsal hippocampus, namely on the CA1 and DG subregions. Interestingly, astrocytes from the CA1 subregion (Figure 2.31A) present less complex structures comparatively to their WT littermates, which is translated into a decrease in: total length of the processes ($t_{85} = 5.033$, $p < 0.001$); number of processes (given by the total number of segments; $t_{85} = 4.419$, $p < 0.001$); GFAP-stained thickness ($t_{85} = 5.525$, $p < 0.001$); and arbor complexity (given by Sholl analysis of the arbor; $F_{1, 95} = 10.96$, $p = 0.001$) (Figure 2.31B-E, respectively). However, no differences were seen in the distance from soma of the last intersection in Sholl analysis ($t_{94} = 1.236$, $p = 0.22$; Figure 2.31F). This observation suggests that the territorial

boundaries of astrocytes are not affected in the dCA1 of dnSNARE mice. In order to understand whether this astrocytic atrophy was dCA1-specific, we further evaluated astrocytic structures in the vicinal dDG (Figure 2.32A). In this subregion, astrocyte processes displayed a similar reduction in the exactly same parameters analyzed in the dCA1 (total process length: $t_{61} = 5.040$, $p < 0.001$; number of processes: $t_{61} = 4.333$, $p < 0.001$; process thickness: $t_{61} = 3.031$, $p = 0.004$; arbor complexity ($F_{1,55} = 14.46$, $p < 0.001$) (Figure 2.32B-E, respectively). Once again, no differences were seen between dDG astrocytes of WT and dnSNARE, in the distance of last Sholl intersections ($t_{55} = 0.051$, $p = 0.96$; Figure 2.32F).

For further confirmation of the role of transgene expression on astrocyte morphology, we next evaluated whether this reduction of process arbor complexity observed in dorsal hippocampus was specifically related to the expression of dnSNARE transgenes.
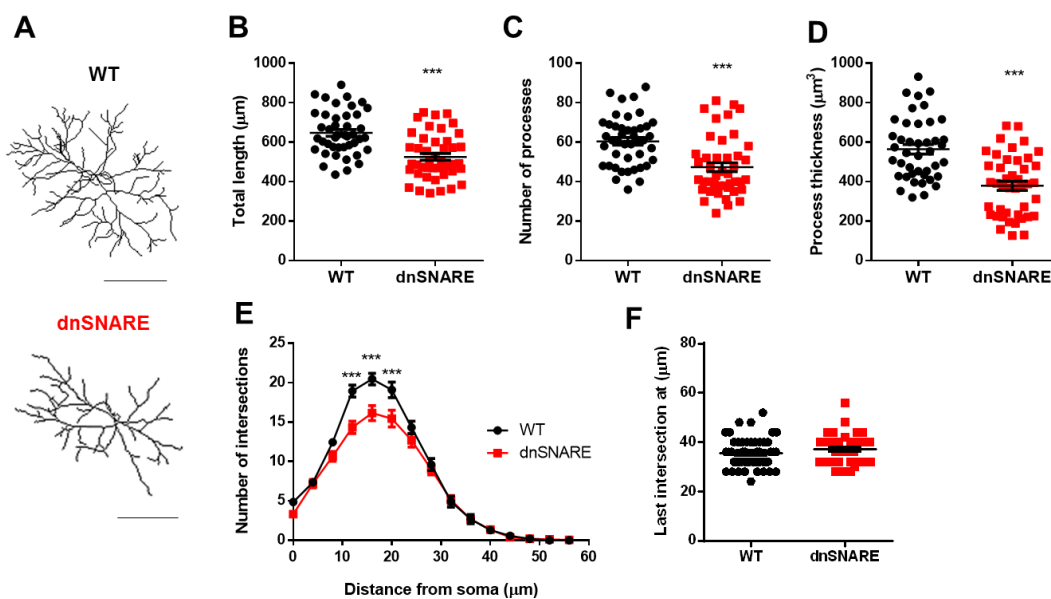
Figure 2.31. Astrocytes of dnSNARE mice, but not neurons, exhibit an altered morphologic structure in the CA1 of dHIP. (A) Representative 3D reconstructions of CA1 dHIP GFAP+ astrocytes of WT (top) and dnSNARE mice (bottom); scale bars = 20 μm; (B-F) Characterization of the 3D structure of astrocytes by analysis of (B) total length, (C) number of processes, (D) process thickness, (E) Sholl intersections and (F) length of the last intersection (n = 42-50 astrocytes; 5 mice per group). WT mice represented in black and dnSNARE mice in red dots and lines. Data plotted as mean ± SEM. ***$p < 0.001$.
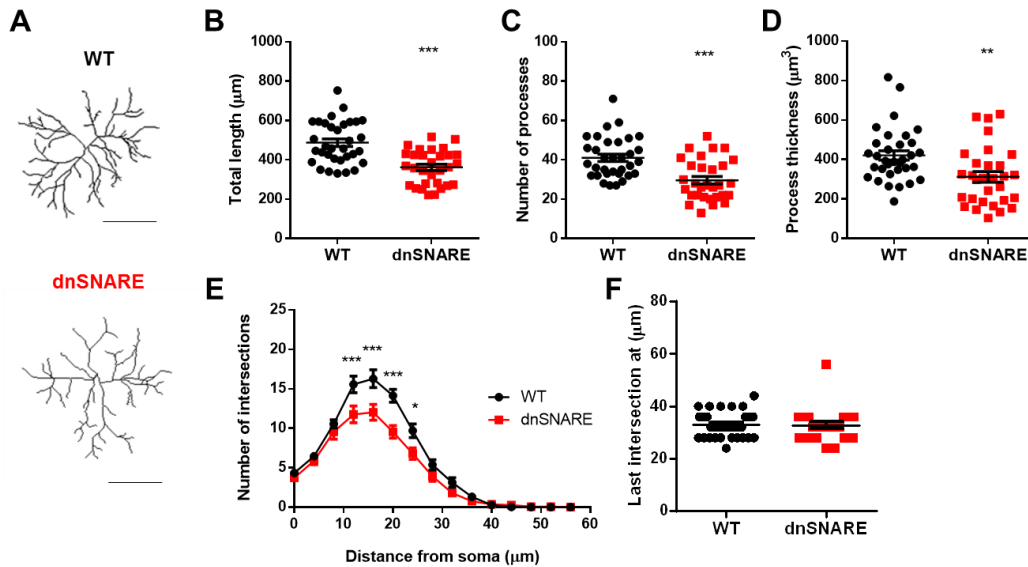
Figure 2.32. Structural changes of dnSNARE mice astrocytes are sustained in the DG region of hippocampus. (A) Representative 3D reconstructions of DG dHIP GFAP+ astrocytes of WT (top) and dnSNARE mice (bottom); scale bars = 20 μm; (B-F) Characterization of the 3D structure of astrocytes by analysis of (B) total length, (C) number of processes, (D) process thickness, (E) Sholl intersections and (F) length of the last intersection (n = 25-33 astrocytes; 5 mice per group). WT mice represented in black and dnSNARE mice in red dots and lines. Data plotted as mean ± SEM. *$p < 0.05$; **$p < 0.01$; ***$p < 0.001$.

Taking advantage of the immunofluorescent double-staining of GFP reporter and GFAP structure, we compared the structure of GFAP+GFP+ astrocytes (astrocytes expressing the dnSNARE transgenes) and GFAP+ astrocytes (astrocytes with none or negligible expression of dnSNARE transgenes) subregion in the same set of dnSNARE brain slices previously used for dCA1 astrocytic reconstruction (Figure 2.33A). This analysis pointed out that GFAP+GFP+ astrocytes are less complex than native counterparts, as indicated by the shorter total process length (t_{37} = 3.307, p = 0.002), decreased number of processes (t_{37} = 2.695, p = 0.011), thinner processes (t_{37} = 2.172, p = 0.036), and decreased arbor complexity ($F_{1,37}$ = 11.3, p = 0.002) (Figure 2.33B-E, respectively). Interestingly, the mean radial distance at the last intersection is once again similar between the GFAP+ and GFAP+GFP+ groups of cells (35.39 ± 1.8 μm and 32.00 ± 1.1 μm, respectively; t_{38} = 1.703, p = 0.097; Figure 2.33F). Of notice, and according to the parameters analyzed, GFAP+ astrocytes in dnSNARE mice are structurally identical to those of WT mice in all parameters analyzed. These sets of data support that the astrocytic atrophy is dependent on the dnSNARE transgene expression.
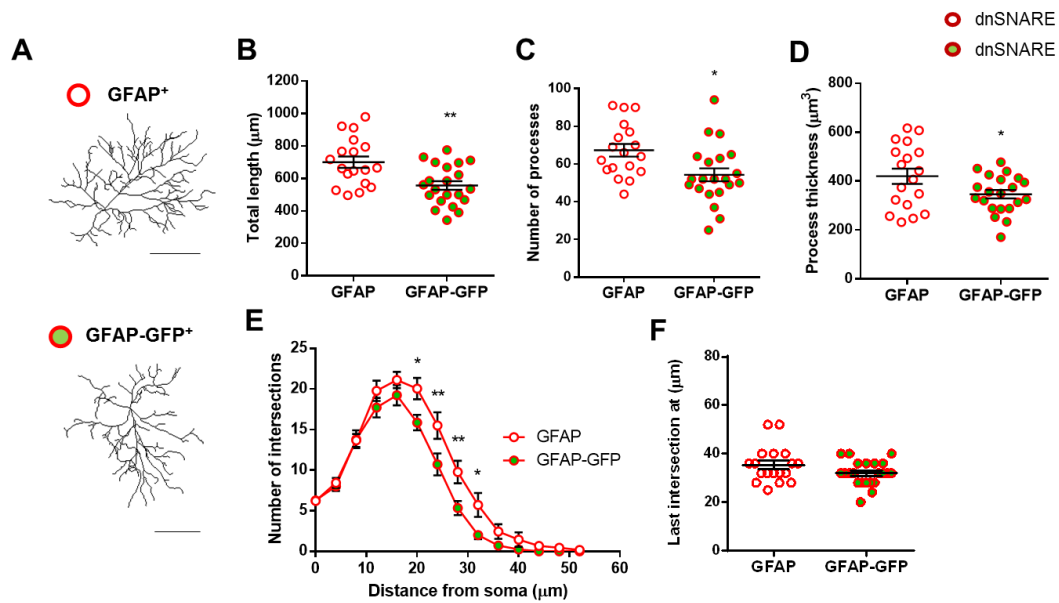
Figure 2.33. The structural changes in dnSNARE mice astrocytes are restricted to GFAP+GFP+ cells.
(A) Representative 3D reconstructions of CA1 dHIP GFAP+ only (top) and GFAP+GFP+ cells of dnSNARE mice (bottom); scale bars = 20 μm; (B-F) Characterization of the 3D structure of dnSNARE mice astrocytes by analysis of (B) total length, (C) number of processes, (D) process thickness, (E) Sholl intersections and (F) length of the last intersection (n = 18-21 astrocytes; 3 mice per group). GFAP+ cells represented in red and white, and GFAP+GFP+ cells in red and green dots and lines. Data plotted as mean ± SEM. *p < 0.05; **p < 0.01.

We next evaluated the astrocyte densities in both subregions of the dorsal hippocampus analyzed above (CA1 and DG) to evaluate a putative alteration of the astrocyte networks (Figure 2.34A-B). In this case, we verified that both genotypes display similar astrocyte densities for each cellular layer, from both dHIP (Pyramidal: t_{24} = 0.476, p = 0.638; Radiatum: t_{28} = 0.323, p = 0.750) and dDG (Granular: t_{26} = 1.713, p = 0.099; Molecular: t_{41} = 0.584, p = 0.563; Hilus: t_{41} = 0.024, p = 0.981), suggesting these results the maintenance of the astrocyte networks in the dnSNARE mice.
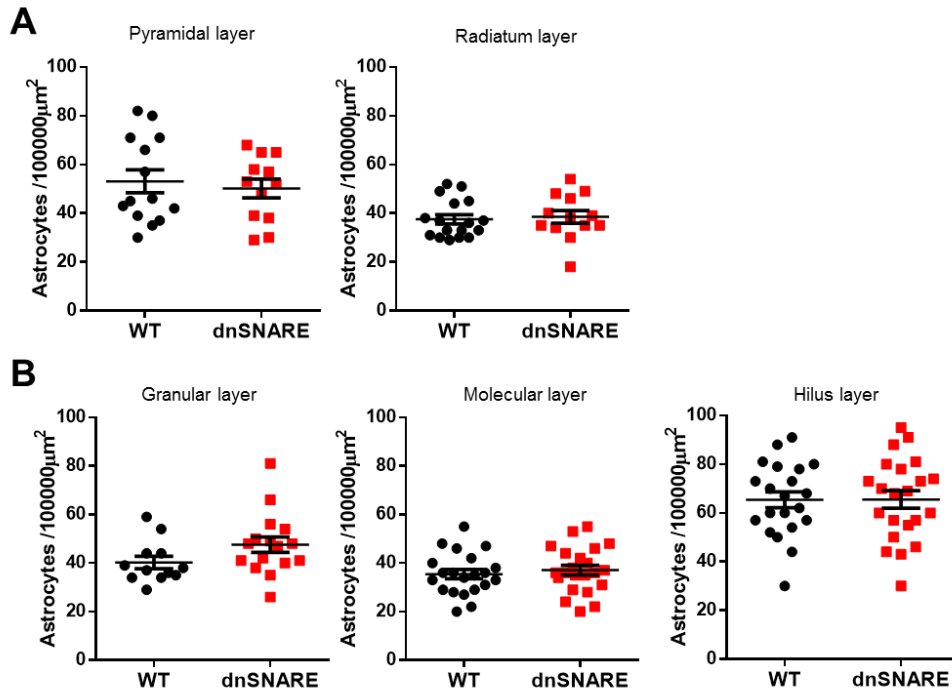
Figure 2.34. Blockade of vesicular release by exocytosis does not affect astrocytes density in the CA1 and DG regions of the hippocampus. Estimated number of astrocytes in (A) pyramidal and radiatum layers of dHIP (n = 12-17 mice per group) and in (B) granular (n = 12-16 mice per group), molecular and hilus layers (n = 21-22 mice per group) of dorsal DG. WT mice represented in black and dnSNARE mice in red dots. Data plotted as mean ± SEM.

As a whole, these data sets support the idea that, under the impairment of gliotransmission in dnSNARE mice, the neuronal circuitry appears to keep its structure intact, while the transgene-expressing astrocytes undergo process atrophy. This structural alteration of astrocytes most likely implies their processes retraction from several synaptic sites, with a consequent loss of signaling to neurons and synapses. These morphological changes, along with the decreased exocytosis represent a hardening of the gliotransmission impairment in the hippocampus of the dnSNARE mice. This could in turn underlie the loss of theta coherence in the cortico-limbic link and the poor cognitive performance of these mice.

2.5   Evaluation of the ability of D-serine to rescue cortico-limbic theta synchronization and cognitive function

Introduction

In previous chapters, we have described that the lack of exocytosis-dependent signaling from astrocytes is critical for the maintenance of dHIP-mPFC synchrony, which in turn is impacts learning and memory consolidation. Gliotransmitters such as ATP, glutamate or D-serine were shown to modulate the strength of neighboring synapses with functional consequences to the network output. In particular, D-serine, a potent NMDA-receptor co-agonist released by astrocytes (Kang et al., 2013; Martineau et al., 2013) is critical for (i) the maintenance of hippocampal synaptic plasticity (Fellin et al., 2009; Henneberger et al., 2010; Han et al., 2015b), (ii) involved in synaptic modulation in the hippocampus and cortex (Yang et al., 2003; Panatier et al., 2006; Henneberger et al., 2010; Takata et al., 2011; Fossat et al., 2012) and (iii) for dendritic maturation of newly-born neurons in the hippocampus (Sultan et al., 2015). Taking advantage of the specific dnSNARE transgene expression in astrocytes of the hippocampus and cortex, we next sought for the molecular mechanism of the alterations reported so far. Recent literature showed that the release of gliotransmitters is significantly decreased in dnSNARE mice and that their transgene expressing astrocytes release significantly less D-serine (Cao et al., 2013; Pankratov and Lalo, 2015; Sultan et al., 2015). Therefore, D-serine arises as a good candidate to explain the effects observed in this work. To test whether D-serine was implicated in the dnSNARE loss of dHIP-mPFC theta synchrony, and consequent cognitive deficits, we re-assessed these functions in independent sets of both WT and dnSNARE mice supplemented with an intraperitoneally administration of either saline or D-serine, an approach described to increase the intracerebral levels of D-serine (Takata et al., 2011; Guercio et al., 2014).

Materials and Methods

Drugs

In order to test the rescue of functional impairments displayed by dnSNARE mice, D-serine (Sigma-Aldrich, USA; 1 g/kg of body weight, 10 ml/kg of body weight, in 0.9% saline, i.p.) was administered to mice of both genotypes prior/during electrophysiology and behavior experiments, as described below.

Rescue of dHIP-mPFC theta synchrony

For the electrophysiological experiments, surgical procedures and electrodes positioning were performed as described in sub-chapter 2.2 (n = 6-7 per group). After the surgery and resting period, 15 periods of 100 s of local field activity were recorded in 5 min frames. D-serine was administered i.p. after the third recording window, and the effect of D-serine was observed during the next twelve recordings (total of 60 min). The first three recordings represented the basal activity, while the twelve following recordings illustrated the longitudinal effect of D-serine administration. The recording locations were verified as described in sub-chapter 2.2.

Rescue of cognitive deficits

For the behavior experiments, either D-serine or saline were administered, to an independent set of mice, 20 min before the first trial on each day in the MWM, reference memory task (n = 6-9 per group), or 20 min before the training session in the NOR task (n = 6-8 per group) to address the impact of exogenous D-serine in long-term memory. Despite of the i.p. injection, mice behaved normally and no signs of distress or potential drug side effects were observed, therefore no animal was excluded for those reasons.

Rescue of astrocytic structure

To address the effects that exogenous administration of D-serine could have on the morphological structure of astrocytes, we performed 3D reconstructions of astrocytes from the WT and dnSNARE mice that participated in the cognitive rescue experiment, using Simple Neurite Tracer (Longair et al., 2011) as described in sub-chapter 2.4. Brain slices containing the dorsal hippocampus of both WT and dnSNARE mice were stained by immunofluorescence for the GFAP and for DAPI (n = 2-3 mice per group), and dnSNARE brain slices were also stained for the GFP to identify the transgene-expressing astrocytes. Z-stacks of images (2 per brain region from 2 brain slices per animal) obtained from the CA1 of dHIP were acquired by means of a confocal microscope (FV1000, Olympus, Japan). Each image stack was acquired with 1 μm z-step interval, 640x640 pixel resolution, under 60x oil magnification (field size 211.51 x 211.51 μm). The selection criteria used to select astrocytes for reconstruction were already described above, in sub-chapter 2.4. The structural features analyzed were: total process length, number of processes, process thickness and Sholl analysis.

Statistical analysis

Results are presented throughout as mean ± SEM (Standard Error of the Mean) and the statistical significance of the comparisons for each statistical test was set with a confidence interval of at least 95%. All data sets passed the normality tests for Gaussian distributions (D'Agostino & Pearson for n > 7; Kolmogorov-Smirnov for n = 5-6), therefore parametric tests were applied. Two-way ANOVA was used to analyze the performance in rescue experiments (factors: treatment and genotype). Uncorrected Fisher's LSD post-hoc tests were applied to analyze the genotype effect and Sidak's post-hoc tests to analyze the treatment effect (saline or D-serine). Unpaired t-tests were used to compare the total length, number of processes, process thickness and radial distance from soma of last intersection between groups, for astrocytic tridimensional reconstructions. Sholl analysis of astrocyte tridimensional reconstructions was performed by two-way ANOVA (factors: genotype and radial distance from soma). Statistical analysis was performed using the GraphPad Prism 6 (GraphPad Software Inc., USA).

Results

To test whether D-serine was implicated in the dnSNARE loss of dHIP-mPFC theta synchrony, and consequent cognitive deficits, we first performed the simultaneous recording of LFPs from the dHIP and mPFC of WT and dnSNARE mice. First, the levels of power of each region were longitudinally measured during D-serine administration. From Figure 2.35A-C and Figure 2.36A-C one can see that, supplementation with D-serine leads to an increase of the spectral power, comparatively to saline, that was similar in WT and dnSNARE mice, in all analyzed frequency bands for both dHIP (theta: $F_{1,11}$ = 43.97, p < 0.001; beta: $F_{1,11}$ = 51.46, p < 0.001; low gamma: $F_{1,11}$ = 63.57, p < 0.001; Figure 2.35) and mPFC (theta: $F_{1,11}$ = 63.05, p < 0.001; beta: $F_{1,11}$ = 18.64, p = 0.001; low gamma: $F_{1,11}$ = 31.97, p < 0.001; Figure 2.36). These data suggest that exogenous D-serine has the ability to enhance neuronal activity, possibly by the enhancement of NMDA receptor activation.
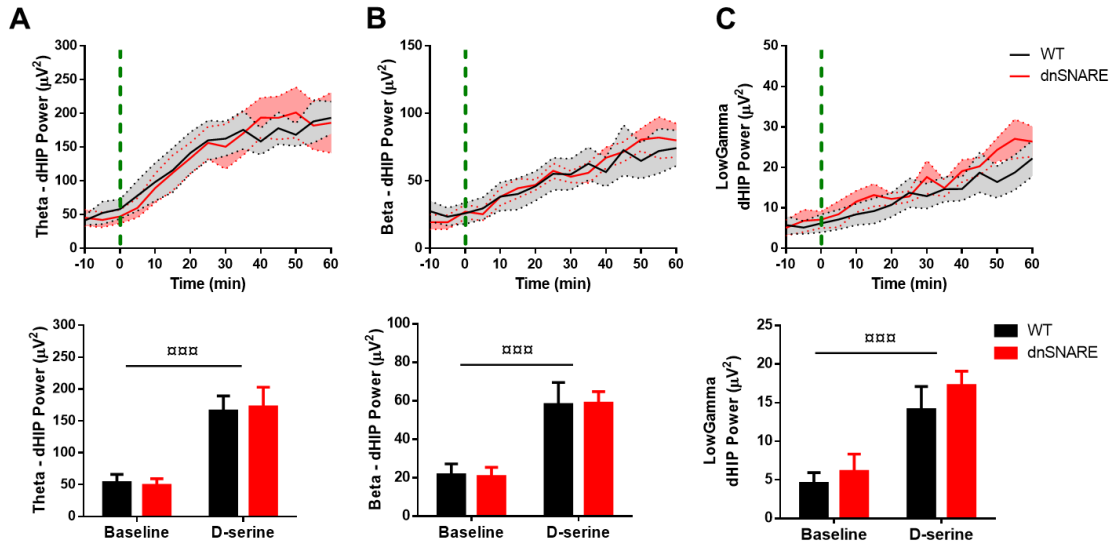
Figure 2.35. Exogenous D-serine leads to an increase of neuronal power in the dHIP, regardless of the mouse genotype. (A-C) Evolution of dHIP power for (A) theta, (B) beta and (C) low gamma frequencies in WT and dnSNARE mice over time (top; dashed line: administration of D-serine); and values of dHIP power at baseline (average of 3 recordings before injection) and after D-serine administration (average of 3 recordings 30 min after injection) (bottom). WT mice represented in black and dnSNARE mice in red lines and bars. Data plotted as mean ± SEM. ¤¤¤ $p < 0.001$ (n = 6-7 per group).
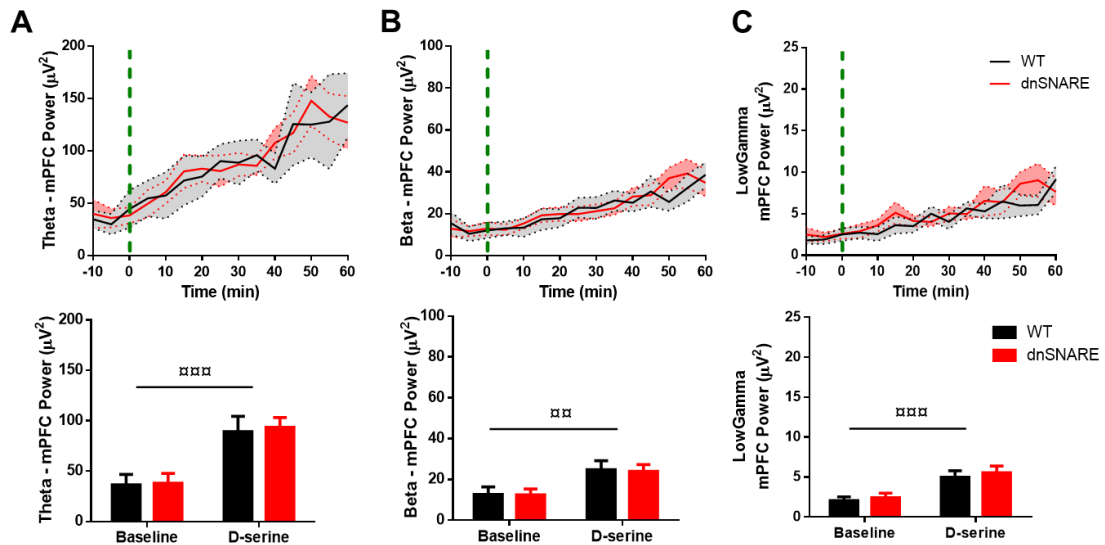
Figure 2.36. Exogenous D-serine leads to an increase of neuronal power also in the mPFC, regardless of the mouse genotype. (A-C) Evolution of mPFC power for (A) theta, (B) beta and (C) low gamma frequencies in WT and dnSNARE mice over time (top; dashed line: administration of D-serine); and values of mPFC power at baseline (average of 3 recordings before injection) and after D-serine administration (average of 3 recordings 30 min after injection) (bottom). WT mice represented in black and dnSNARE mice in red lines and bars. Data plotted as mean ± SEM. ¤¤ $p < 0.01$; ¤¤¤ $p < 0.001$ (n = 6-7 per group).

Following, the coherence between both regions was evaluated (Figure 2.37). The dHIP-mPFC theta coherence recorded in WT mice remained fairly stable over time in levels similarly to those recorded previously (Figure 2.13), even after the administration of D-serine. Interestingly, dHIP-mPFC theta

110

coherence recorded in dnSNARE displayed a sustained increase about 20 minutes after D-serine administration, to similar levels of those recorded from WT mice in the same conditions, and significantly larger than at baseline (Figure 2.37A-C). The quantification of this effect showed that D-serine administration restored specifically the theta coherence (t_{22} = 2.151, p = 0.043 from WT; t_{11} = 2.965, p = 0.026 from dnSNARE baseline; Figure 2.37C, right). No significant variations were recorded for coherence in beta frequency band (Figure 2.37D) and low gamma coherence decreased in WT mice during the protocol, however dnSNARE mice displayed levels of coherence similar to WT before and after D-serine administration (t_{11} = 3.178, p = 0.018; Figure 2.37E, right). The specific rescue of dHIP-mPFC coherence in the theta frequency band only in the dnSNARE mice (while WT mice display stable levels of coherence after D-serine administration), confirms the relevance of the spectral coherence readout as a robust measure of inter-regional neural synchrony, independently of the increasing amplitude of neuronal oscillations recorded.
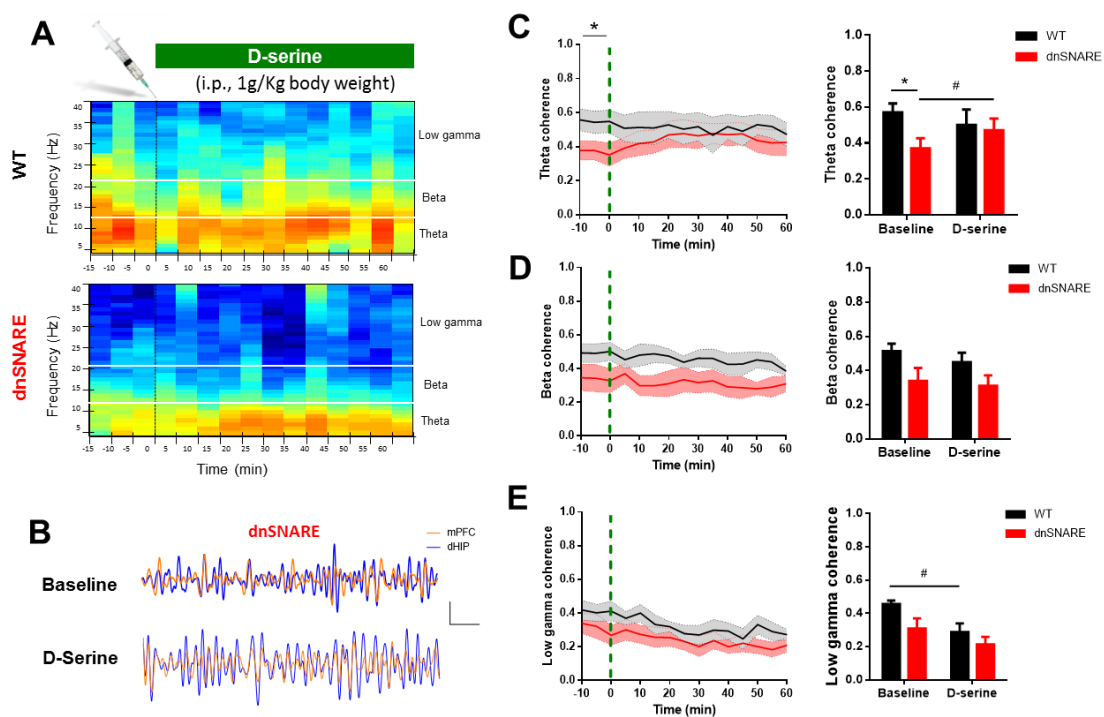
Figure 2.37. D-serine supplementation restores dHIP-mPFC theta synchronization in dnSNARE mice. (A) Representative heatmaps of spectral dHIP-mPFC coherence for WT (top) and dnSNARE mice (bottom) over time; syringe and dashed line indicates the moment of D-serine administration; each spectrogram represents the dHIP-mPFC coherence calculated in intervals of 5 min for 4-40 Hz (theta, 4-12Hz; beta, 12-20 Hz; low gamma, 20-40 Hz); color range: 0, dark blue; 1, red; (B) Representative theta filtered LFP traces of mPFC (orange) and dHIP (blue), recorded from dnSNARE mice at baseline or after D-serine administration (scale bars: 50 µV, 500 ms); (C-E) Evolution of dHIP-mPFC coherence for (C) theta, (D) beta and (E) low gamma frequencies in WT and dnSNARE mice over time (left; dashed line: administration of D-serine); values of dHIP-mPFC coherence at baseline (average of 3 recordings before injection) and after D-serine administration (average of 3 recordings 30 min after injection) (right). WT mice are represented in black and dnSNARE mice in red lines and bars. Data plotted as mean ± SEM. *p < 0.05 from WT; #p < 0.05 from baseline (n=6-7 per group).

The succeeding question was if the rescue of the dHIP-mPFC theta synchronization by D-serine supplementation would also revert the cognitive impairments observed in dnSNARE mice, mainly in hippocampal-dependent tasks. In the RM task of MWM, dnSNARE mice treated with saline confirmed the previous deficits observed in the reference memory task of MWM, as noted by the longer latencies and distances swam, the higher percentage of failures and use of random strategies to reach the hidden platform (Figure 2.38). However, the administration of D-serine 20 min before the beginning of the first trial, in the four days of MWM (Figure 2.38A), rescued the poor performance of dnSNARE mice in the reference memory task (Figure 2.38B-D). D-serine completely restored the capacity of dnSNARE mice to learn a spatial task, taking as much time as WT mice to reach the hidden platform. In accordance, dnSNARE mice swum similar distances to their WT counterparts (dnSNARE, D-serine vs saline for escape latency: $F_{1,13} = 4.987$, $p = 0.044$, Figure 2.38C top; distance swam: $F_{1,13} = 4.684$, $p = 0.048$, Figure 2.38C bottom). These results were further confirmed by the decrease in the percentage of failures and by the use of strategies to reach the platform analogous to WT (Saline: % of failures: $t_{25} = 3.776$, $p = 0.002$, Figure 2.38D top; % of directed strategies: $t_{25} = 4.582$, $p < 0.001$, Figure 2.38D bottom). It is noteworthy, that the supplementation with D-serine did not affect the performance of WT mice (WT, D-serine vs saline for escape latency: $F_{1,12} = 0.594$, $p = 0.456$, Figure 2.38C top; distance swam: $F_{1,12} = 0.0004$, $p = 0.984$, Figure 2.38C bottom).
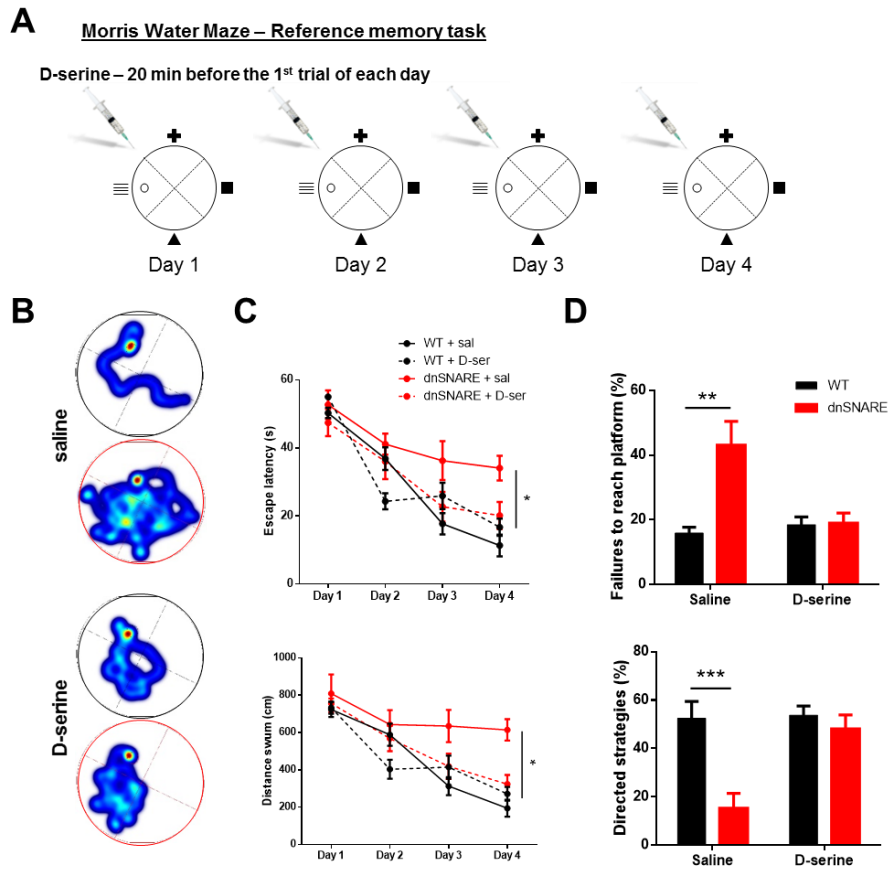
Figure 2.38. D-serine supplementation rescues the reference memory deficits observed in dnSNARE mice. (A-D) Reference memory rescue in the MWM; (A) Scheme of D-serine administration; (B) Representative heatmaps of cumulative trajectories at day 4 of WT (black pool) and dnSNARE mice (red pool) under saline (top) and D-serine administration (bottom); (C) Escape latency (top) and distance swum (bottom) to reach the hidden platform after administration of saline (line) or D-serine (dashed line); (D) Percentage of failures to reach the platform (top) and of directed strategies used to find the platform (bottom), after administration of saline or D-serine. WT mice are represented in black and dnSNARE mice in red lines and bars. Data plotted as mean ± SEM. *$p < 0.05$; **$p < 0.01$; ***$p < 0.001$ (n = 6-9 per group).

In accordance, D-serine administration 20 min prior to the training session of the NOR test (Figure 2.39A) restored the long-term recognition memory in the dnSNARE mice, as seen by the increase of time spent by transgenic mice exploring the novel object in the test session, to the performance of the control group (Saline: $t_{23} = 3.611$, $p = 0.003$; Figure 2.39B-C).
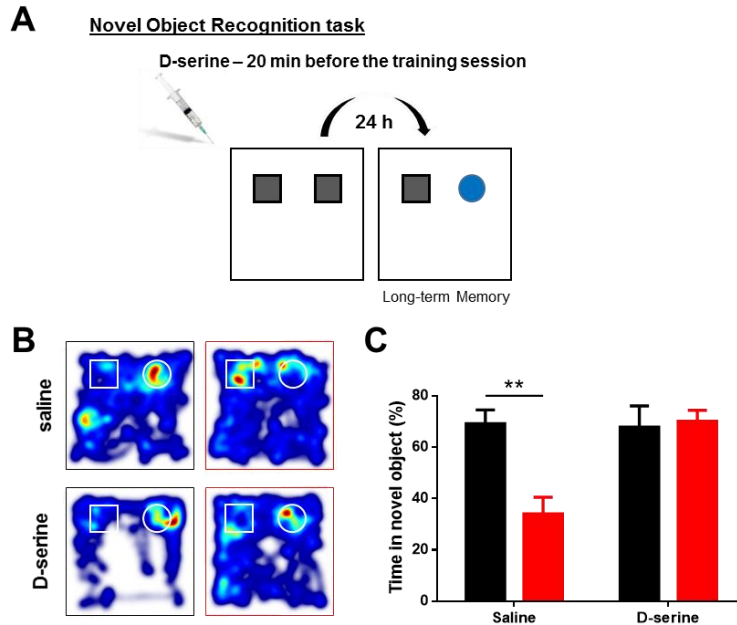
Figure 2.39. D-serine supplementation rescued the long-term memory deficits of dnSNARE mice. (A-C) Long-term memory rescue in NOR; (A) Scheme of D-serine administration; (B) Representative heatmaps of cumulative exploration of a familiar (square) and novel (circle) objects in the long-term memory task, for WT (black arenas) and dnSNARE mice (red arenas), after saline (top) or D-serine administration (bottom); (C) Percentage of exploration time of novel object by WT and dnSNARE mice, after saline or D-serine administration. WT mice represented in black and dnSNARE mice in red bars. Data plotted as mean ± SEM. **$p < 0.01$ (n = 6-8 per group).

In addition, the performance of low dnSNARE transgene "expressors" supplemented with either saline or D-serine was also similar to WT, as observed in the latency they needed to reach the platform (Figure 2.40A-B). As expected, the correlation between GFP levels in the hippocampi of low and high dnSNARE transgene "expressors" and their respective poor performance the RM task disappeared under D-serine administration. A similar effect was observed in the NOR test, where both low and high dnSNARE transgene "expressors" spend longer exploring the novel object (Figure 2.40C-D), breaking the relationship between GFP expression and performance. These observations suggest, that exogenous D-serine fulfilled the network signaling needs, despite of the variable extracellular levels due to the different levels of exocytosis blockade.
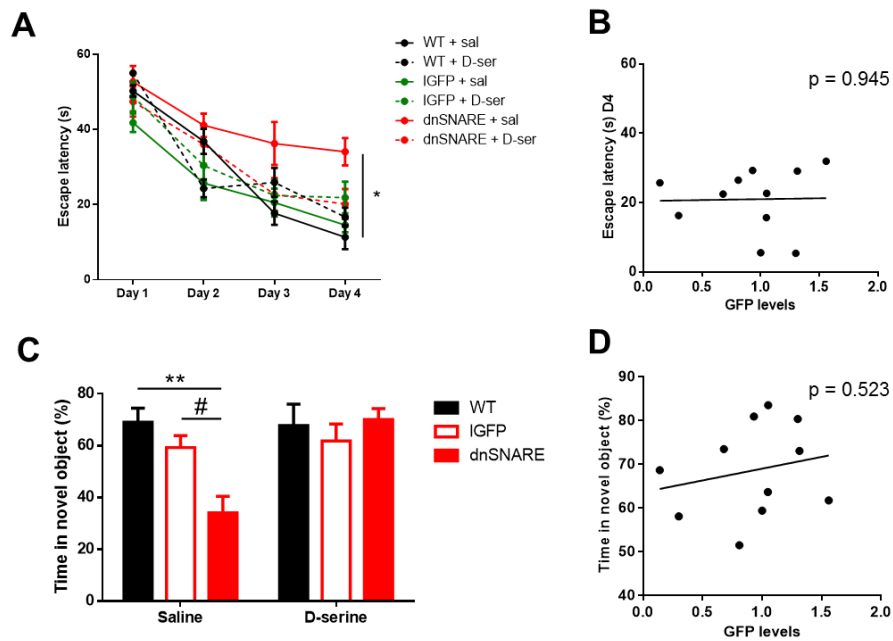
Figure 2.40. D-serine supplementation rescues the cognitive impairment independently of the dnSNARE transgene expression levels. (A-B) Reference memory (RM) rescue in the MWM (n = 5-9 per group); (A) Escape latency to reach the hidden platform after administration of saline (line) or D-serine (dashed line); (B) Correlation plot between the performance of total transgenic mice that received D-serine in the RM task and relative levels of transgene expression in the hippocampi of the same mice (n = 5-6 per group); (C-D) Long-term memory rescue in NOR task (n = 6-8 per group); (C) Percentage of exploration time of novel object by WT and dnSNARE, after saline or D-serine administration; (D) Correlation plot between the performance of total transgenic mice that received D-serine in the NOR task and relative levels of transgene expression in the hippocampi of the same mice (n = 5-6 per group). The p-values are indicated for each Pearson correlation. WT mice represented in black, IGFP in green and white and dnSNARE mice in red lines and bars. *Denotes the comparison between WT and dnSNARE mice; #Denotes the comparison between IGFP and dnSNARE mice. Data plotted as mean ± SEM. *·#$p < 0.05$; **$p < 0.01$.

Taking into account all the data so far, we next investigated the impact that D-serine could have in astrocytes morphology, in order to better understand if such alterations in astrocytes main structure could also support the restoration of the network coherence and behavior performance, in dnSNARE mice. A first approach consisted in the morphologic characterization of control astrocytes from WT and dnSNARE mice (GFAP+ only in the latter case) to explore the general effect of D-serine administration. As observed in Figure 2.41, and from two-way ANOVA analysis, there is a clear effect of the treatment with exogenous D-serine in all the parameters under analysis including the total length (Figure 2.41A, $F_{1, 64} = 12.30$, $p < 0.001$), number of processes (Figure 2.41B, $F_{1, 64} = 7.685$, $p = 0.007$), process thickness (Figure 2.41C, $F_{1, 64} = 12,74$, $p < 0.001$) and distance from soma of the last intersection (Figure 2.41E, $F_{1, 64} = 8.644$, $p = 0.005$). Furthermore, when looking to the arbor complexity of astrocytes, through Sholl analysis, we found that either under saline or D-serine there were no differences between WT and dnSNARE GFAP+ astrocytes (saline: $F_{1, 30} = 0.001$, $p = 0.975$; D-serine: $F_{1, 32} = 1.062$, $p = 0.311$). However, the treatment with D-serine

caused an increase in the number of dendritic intersections in both genotypes (WT: $F_{1,29} = 9.922$, $p = 0.004$; dnSNARE: $F_{1,33} = 4.304$, $p = 0.046$; Figure 2.41D).
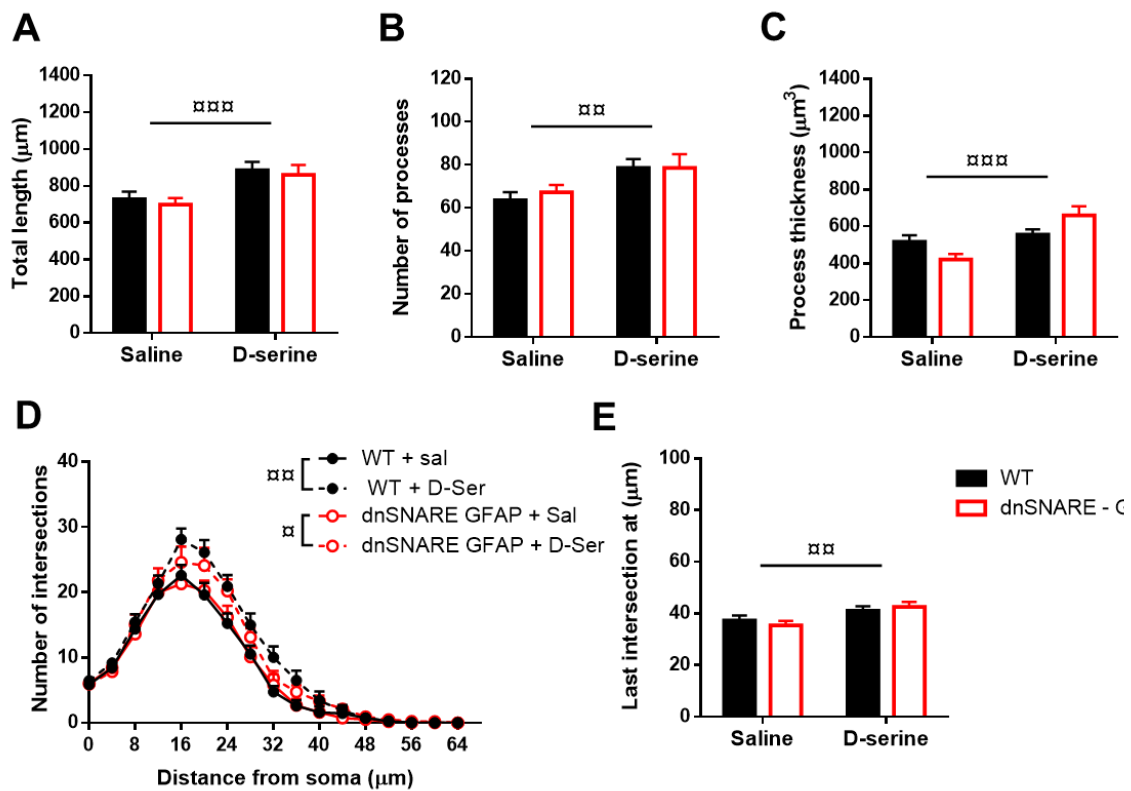
Figure 2.41. The administration of exogenous D-serine increased the complexity of the morphological structure of control astrocytes in the dHIP CA1, of both WT and dnSNARE mice. (A-E) Characterization of the 3D structure of control astrocytes of WT and dnSNARE mice (GFAP+ cells only, not expressing the transgene) by analysis of (A) total length, (B) number of processes, (C) process thickness, (D) Sholl intersections and (E) length of the last intersection (n = 15-19 astrocytes; 2-3 mice per group). WT mice represented in black and dnSNARE mice (GFAP+ cells) in red and white lines and bars. Data plotted as mean ± SEM. ¤ Denotes the treatment effect. ¤$p < 0.05$; ¤¤ $p < 0.01$; ¤¤¤$p < 0.001$.

Considering the effect exerted by D-serine in GFAP+ astrocytes where gliotransmission should be intact, we next investigated whether the administration of exogenous D-serine would be enough to recover the main structure of transgene expressing astrocytes (GFAP+GFP+) in dnSNARE mice. For this purpose, a morphological characterization similar to the described above was performed (Figure 2.42A-E). In agreement with previous data, in saline conditions, the transgene expressing cells present a smaller total length (Figure 2.42A, $t_{62} = 3.437$, $p = 0.001$), less number of processes (Figure 2.42B, $t_{62} = 2.474$, $p = 0.016$) and thinner processes (Figure 2.42C, $t_{62} = 3.145$, $p = 0.003$), and a shorter distance from soma of the last intersection than WT astrocytes (Figure 2.42E, $t_{62} = 2.054$, $p = 0.044$). Interestingly, D-serine supplementation clearly restored the main

structure of GFAP+GFP+ astrocytes to the levels of WT mice (D-serine: Figure 2.42A, $t_{62} = 1.345$, $p = 0.184$; Figure 2.42B, $t_{62} = 0.123$, $p = 0.902$; Figure 2.42C, $t_{62} = 1.253$, $p = 0.215$; Figure 2.42E, $t_{62} = 0.488$, $p = 0.627$). Two-way ANOVA showed a clear treatment effect in all the parameters under analysis including the total length (Figure 2.42A, $F_{1,62} = 27.94$, $p < 0.001$), number of processes (Figure 2.42B, $F_{1,62} = 28.60$, $p < 0.001$), process thickness (Figure 2.42C, $F_{1,62} = 10.49$, $p = 0.002$) and distance from soma of the last intersection (Figure 2.42E, $F_{1,62} = 14.89$, $p < 0.001$).
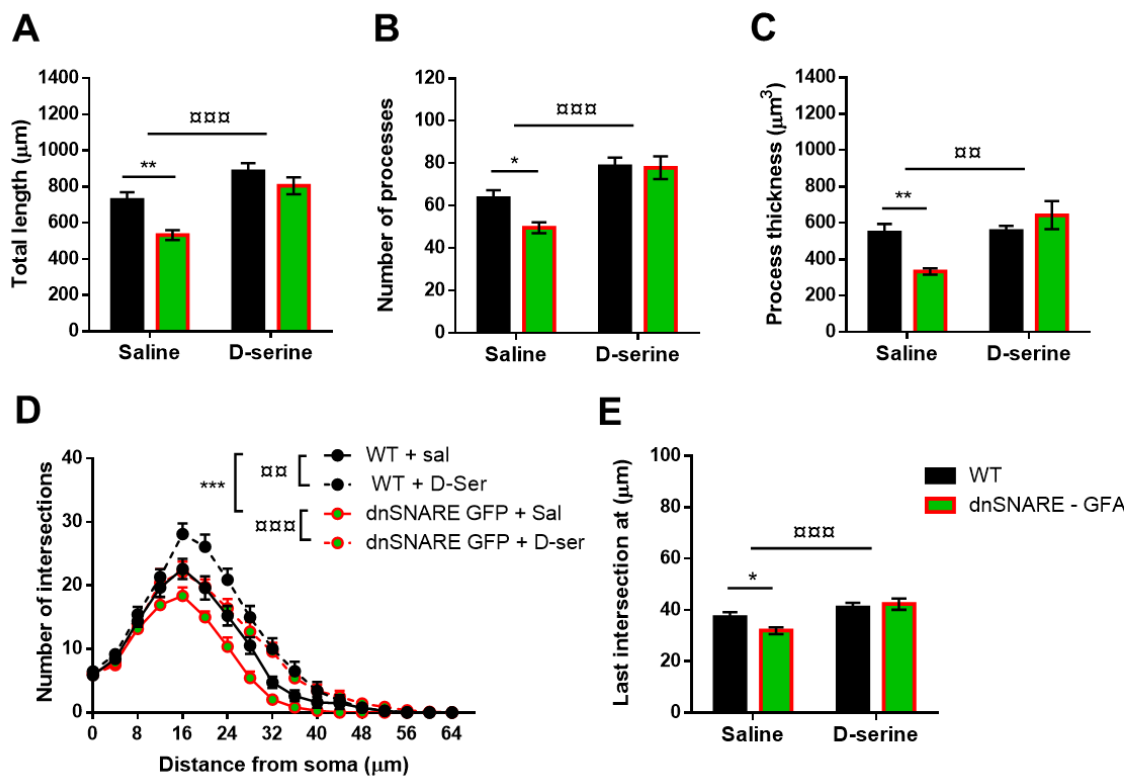
Figure 2.42. Application of exogenous D-serine restores the morphological features of transgene expressing astrocytes in the dHIP CA1 of dnSNARE mice. (A-E) Characterization of the 3D structure of dnSNARE mice transgene expressing astrocytes (GFAP+GFP+ cells) by analysis of (A) total length, (B) number of processes, (C) process thickness, (D) Sholl intersections and (E) length of the last intersection (n = 15-18 astrocytes; 2-3 mice per group). WT mice represented in black and dnSNARE mice (GFAP+GFP+ cells) in red and green lines and bars. Data plotted as mean ± SEM. *Denotes the comparison between genotypes; ¤ Denotes the treatment effect. *$p < 0.05$; ¤¤ $p < 0.01$; ***. ¤¤¤$p < 0.001$.

Additionally, the treatment with exogenous D-serine caused an increase in the number of dendritic intersections in both genotypes (WT: $F_{1,29} = 9.922$, $p = 0.004$; dnSNARE: $F_{1,33} = 25.46$, $p < 0.001$; Figure 2.42D). Moreover, the differences observed between astrocytes from WT and dnSNARE mice, under saline conditions ($F_{1,32} = 13.33$, $p < 0.001$), were lost with D-serine administration ($F_{1,30} = 3.499$, $p = 0.071$). D-serine restored the arbor complexity of GFAP+GFP+ astrocytes of

dnSNARE mice, in all radial intervals, to similar number of dendritic intersections from WT astrocytes.

Together, these results suggest that astrocyte-derived signaling is demanding for the integrity of astrocytes main structure, which may account for theta hippocampal-prefrontal coherence, ultimately supporting acquisition and consolidation of spatial memory. Thereby, depletion or disruption of exocytosis in astrocytes may underlie the malfunctioning of the network and the cognitive impairments observed in the dnSNARE mice.

CHAPTER 3

3.1 General Discussion

Throughout this thesis, we have sought for new insights on the role of astrocyte signaling in the modulation of cognitive processing using a complementary of electrophysiological, behavioral and molecular approaches. In order to achieve that goal, we used the dnSNARE mouse model to shut down gliotransmission, specifically through astrocytic exocytosis, to address the impact of astrocyte-derived signaling in cognitive behavior. In chapter 2.1, we validated this mouse model as a reliable tool to target specifically astrocytes and defined a sub-group that displayed high levels of dnSNARE transgenes to assess their effect *in vivo*. These dnSNARE mice presented a decreased theta synchrony in the neuronal oscillations of the hippocampal-prefrontal pathway (chapter 2.2), that highly correlated with deficits in cognitive tasks used to evaluate learning and memory consolidation (chapter 2.3). Moreover, the correlation observed was regionally specific since no differences were observed in theta synchrony when assessing the direct link between vHIP and mPFC of dnSNARE mice. In agreement with the integrity of this link that is typically related to emotional behavior, dnSNARE mice do not display anxious- or depressive-like phenotypes when compared to their WT littermates. Furthermore, morphological analysis of neuronal and astrocytic morphologies in the brain regions of interest (dHIP and mPFC), revealed that the neuronal structure was preserved, while a clear shrinkage of the main structure of astrocytes was observed, as shown by the decrease in total length, number of processes, their thickness and the reduction of general GFAP-positive arbor complexity (chapter 2.4).

In summary, we found that the astrocytic signaling through exocytosis modulates distant networks by allowing a synchronized neuronal firing, specifically in the theta frequency range. Thereby, astrocytes become neuronal partners in the modulation of cognitive processing. The shutdown of the astrocyte-to-neuron dialogue by interfering with vesicular fusion in astrocytes triggers an imbalance through the sequence of events above described, that we believe to be linked to each other in a causal relationship, as summarized in Figure 3.1.

Finally, the administration of exogenous D-serine to WT and dnSNARE mice triggered a general circuit activation in both genotypes, translated in a general increase of neuronal activity in the three frequency bands analyzed, in both regions recorded (dHIP and mPFC). This observation was accompanied by a morphologic empowerment of astrocytes in the same brain regions. Despite of these indiscriminate alterations, D-serine administration was enough to restore specifically the dHIP-PFC theta desynchronization and cognitive deficits observed in dnSNARE mice (as shown in chapter 2.5).

Based on the observations of this study and on the available literature, we suggest a possible signaling cascade triggered by the shutdown of astrocyte signaling, that leads to the cognitive impairments in dnSNARE mice (summarized in Figure 3.2). In accordance, we suggest that this cascade of events is bypassed by the supplementation of D-serine as indicated in Figure 3.3.

We will now discuss specifically the validity of the dnSNARE mouse model and the three main relationships (Figure 3.1 A, B and C) that link our experimental observations and support the cascade of events.
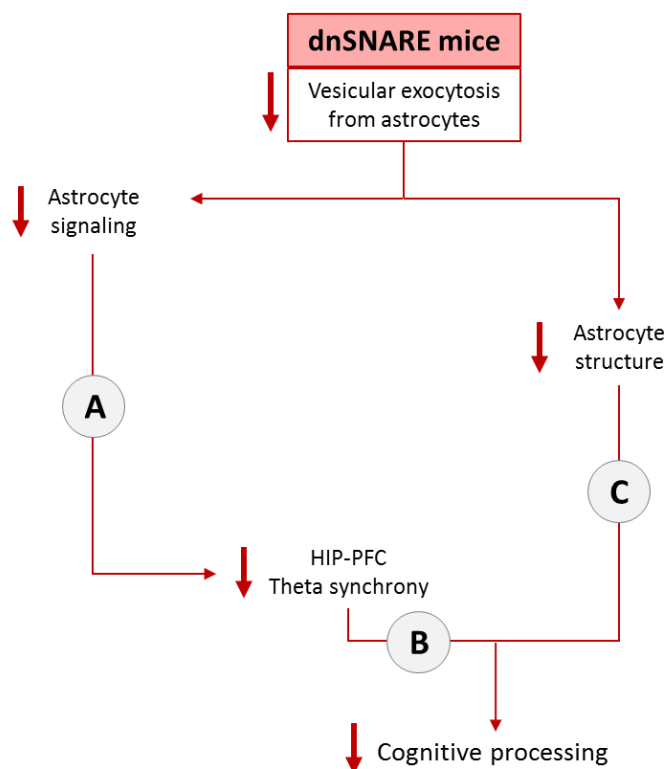
Figure 3.1. Summary of the proposed sequence of events that explain the cognitive deficits of the dnSNARE mouse model. (A) Astrocyte signaling seems to participate in the generation of theta synchrony playing a critical role on its maintenance in the dorsal hippocampal-prefrontal (dHIP-PFC) link. (B) The loss of dHIP-PFC theta synchrony may account for a large extent of the cognitive deficits observed in dnSNARE mice. (C) The blockade of vesicular release from astrocytes resulted in the atrophy of these cells, possibly contributing additionally to the impairment in cognitive processing.

3.1.1 The dnSNARE mouse model

Since 2005, when the dnSNARE mouse model was first described (Pascual et al., 2005), several laboratories have been taking advantage of its main feature, the blockade of astrocytic exocytosis, to better understand how this process contributes to the modulation of the function of synapses and circuits (Fellin et al., 2009; Halassa et al., 2009b; Deng et al., 2011; Florian et al., 2011; Foley et al., 2011; Cao et al., 2013; Hines and Haydon, 2013; Lalo et al., 2014b). However, in

2014, the mouse model validity was challenged mainly due to an allegedly leaky expression of the dnSNARE transgenes in neuronal populations (Fujita et al., 2014). A variety of inconsistent data in the work of Fujita and colleagues was pointed out by other authors. For instance, the claim that astrocytes have a vestigial expression of synaptobrevin II is in contradiction with other evidences of this protein expression in astrocytes (Pascual et al., 2005; Martineau et al., 2013). In fact, the expression of dnSNARE transgenes that interfere with the SNARE-complex formation is, in our hands, restricted to astrocytes as confirmed by the bushy (astrocyte typical) morphology of all GFP-labeled structures and by the analysis of double immunostainings of the GFP reporter and cellular markers performed by us and others (Fellin et al., 2009; Sultan et al., 2015). Consistently, immunostainings against GFP followed by confocal microscopy in the pyramidal and radiatum layers of the dCA1, the molecular and the granule cell layers of the DG, and in layers III to V of the mPFC, revealed a strong expression of GFP in astrocytes but not in neurons or other cell types. We confirmed the selectivity of transgene expression in astrocytes of dnSNARE mice by monitoring the EGFP fluorescence and by the confirmation of its co-localization with the astrocytic markers GFAP and S100β, but not with markers of different neuronal structures (NeuN, calbindin and βIII-tubulin). Further studies have also excluded the co-expression of EGFP with NG2, aspartocyclase or Iba1, which are markers of NG2-positive glia, oligodendrocytes, and microglia, respectively (Fellin et al., 2009; Halassa et al., 2009b).

Several studies have been describing the gliotransmitters which release is impaired in dnSNARE mice, such as glutamate (Zhang et al., 2004), ATP (Pascual et al., 2005; Cao et al., 2013; Pankratov and Lalo, 2015) and D-serine (Pankratov and Lalo, 2015; Sultan et al., 2015). As further confirmation of the impairment of exocytosis being specifically in astrocytes, Sultan and colleagues examined exocytosis in vitro on hippocampal astrocytes, using total internal reflection fluorescence (TIRF) microscopy. In comparison to WT, the authors found that astrocytes from dnSNARE mice present a 91% reduction in the number of fusion events (Sultan et al., 2015). These observations support that the expression of dnSNARE transgenes drastically reduced the number of fusion events and release of D-serine in astrocytes from dnSNARE mice, explaining the decreased levels of extracellular D-serine observed in the hippocampus and cortex of dnSNARE mice by the same study and by others (Pankratov and Lalo, 2015; Sultan et al., 2015).

Also, three additional pieces of evidence in this thesis support the specificity of the transgene expression. First, the analysis of the power spectra of dHIP and PFC indicates that neuronal oscillations ranging from delta to gamma frequencies are intact in the dnSNARE mice. This

evidence suggests that neuronal communication by exocytotic release of transmitters is preserved in dnSNARE mice, which is not observed in the mouse strains studied Fujita and colleagues (Fujita et al., 2014), supporting the hypothesis that they might have studied a different mouse strain. Second, the structural alterations observed in astrocytes were exclusive of transgene-expressing astrocytes (GFAP+GFP+), specifying the GFAP+ cells as the cellular target for transgene expression. Finally, our data revealed a direct relationship between the amount of transgene being expressed in astrocytes and the aggravation of theta synchrony and cognitive function. This last observation establishes a functional dependence between manipulation of astrocytic exocytosis and the deficits observed in the different approaches, that also supports the validity of the genetic manipulation.

3.1.2 Astrocyte-derived signaling modulates dHIP-PFC theta synchrony

In this sub-chapter we will discuss the relationship between astrocyte derived signaling and the modulation of theta synchrony in the dorsal hippocampus-prefrontal cortex network (Figure 3.1, A).

Astrocyte-dependent NMDA receptor modulation and D-serine

Exocytosis-dependent astrocyte signaling was suggested to modulate neuronal communication in different studies (Araque et al., 2014; Petrelli and Bezzi, 2016). The lab that generated the dnSNARE mouse model performed an electrophysiological characterization of these animals using acutely isolated hippocampal slices (Pascual et al., 2005). Several important issues were described back in that time including the demonstration that under an evoked stimulation, dnSNARE mice present a larger slope of Schaffer collateral CA1, suggesting that basal synaptic transmission is influenced by a SNARE-dependent process specifically in astrocytes. The authors suggested, that a tonic activity of extracellular adenosine under A_1 receptors exerts a presynaptic inhibition of the excitatory synaptic transmission. The expression of dnSNARE transgene reduced the release of ATP from astrocytes and thus its extracellular concentration, interfering with adenosine levels and reducing the activation of adenosine A_1 receptors, possibly justifying the increase in slope. Moreover, the authors showed that the magnitude of theta-burst LTP was smaller in comparison to WT, which was indicative of an astrocytic regulation of the strength of synaptic plasticity. Fellin and colleagues excluded any alterations in astrocytic supportive functions that could come from the inhibition of gliotransmission in dnSNARE mice by performing whole-cell recordings from astrocytes in hippocampal slices (Fellin et al., 2009). The authors confirmed that glia from both

dnSNARE and WT mice have similar electrophysiological properties such as highly negative resting potentials, an absence of action potential firing on depolarizing current injection, a linear I-V relationship, a low input resistance, and an unaltered total surface expression of EAAT2. In our results, the neuronal oscillations measured as power activity in the dorsal hippocampus are intact, which suggests that these might not be dependent on classic synaptic plasticity mechanisms. In fact, Halassa and co-workers described that cortical oscillations in dnSNARE mice, under baseline conditions are not affected, which is in agreement with our observations (Halassa et al., 2009b). Since the intrinsic hippocampal population activity appears to be normal, we sought for alternative mechanisms, that could justify that the selective inhibition of gliotransmission results only in the alteration of synchrony between specific brain regions and in a specific frequency range, while the power activity measured remains intact *in vivo*.
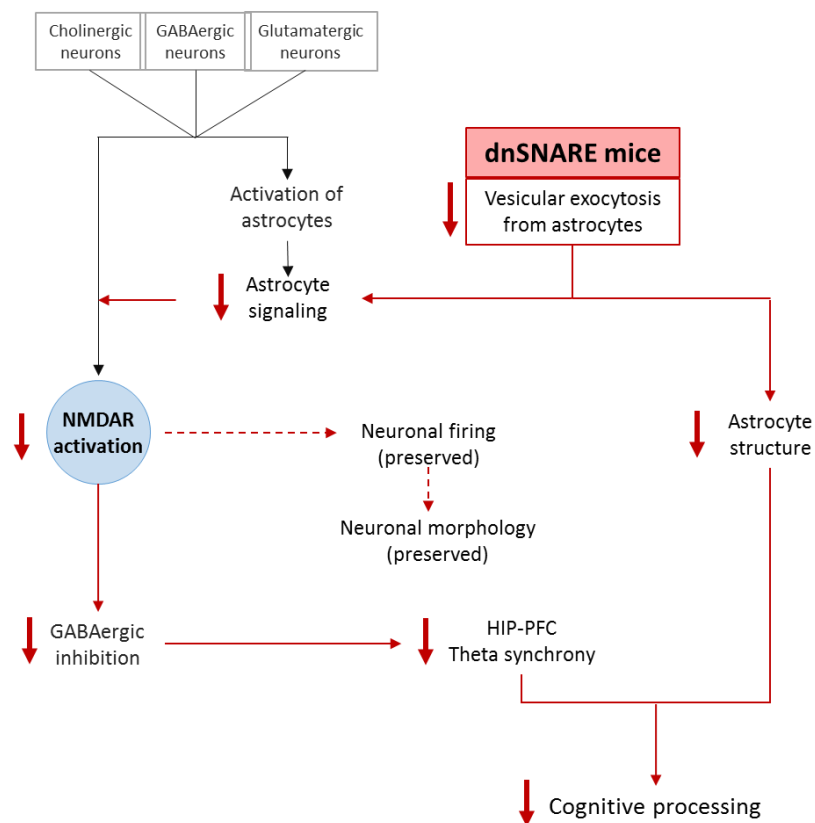
Figure 3.2. Hypothetical model summarizing the mechanisms through which gliotransmission by exocytosis affects the cognitive function, based on the main findings of this thesis.

The NMDAR-mediated signaling appears as a good candidate to link astrocytic signaling and theta synchrony (Figure 3.2). NMDAR are central for structural and synaptic plasticity as well as cognitive functions, requiring their activation the binding of both glutamate and a co-agonist (Meunier et al.,

2016). The Haydon lab, described an interesting hypofunction of post-synaptic neuronal NMDAR under astrocytic dnSNARE expression (Fellin et al., 2009). The authors quantified the total protein expression of the AMPA receptor subunits GluR1, GluR2 and NMDA receptor subunits NR1, NR2A and NR2B from somatosensory cortical slices and showed no alteration in dnSNARE mice. However, a selective reduction of the NR2A and NR2B subunits inserted in the plasma membrane of dnSNARE astrocytes was confirmed, holding a reduced activity of the NMDAR. To revert this condition, D-serine was applied to slices preparation, restoring the NMDA currents and, partially, the AMPA/NMDA ratio in dnSNARE mice, while in slices from WT, no alterations were observed in the presence of exogenous D-serine. This work suggests that the changes seen in cortical slow oscillations are a consequence from alterations in synaptic receptor function. NMDAR hypofunction is typically associated with a range of effects on cognition and behavior in whole animal and human studies (Newcomer and Krystal, 2001). Hence, the results suggested that NMDA receptor hypofunction can preferentially affect neural mechanisms regulating the efficiency of encoding and consolidation into longer-term storage. Sultan and colleagues recently claimed to observe a strong reduction of synaptic AMPA EPSCs in the adult hippocampus of dnSNARE mice. The NMDAR-mediated EPSCs were also reduced, but less than AMPA EPSCs resulting in a consequent increase in the NMDA/AMPA ratio (Sultan et al., 2015).

Why D-serine?

Several gliotransmitters acting by themselves or *en masse* could be responsible for the observed phenotypes. Independent studies already showed that ATP, glutamate and D-serine are the main three gliotransmitters significantly decreased in the extracellular space in brain slices (either cortical or hippocampal) from dnSNARE mice (Zhang et al., 2004; Pascual et al., 2005; Cao et al., 2013; Pankratov and Lalo, 2015; Sultan et al., 2015). These are studies proposing the involvement of astrocytic synaptobrevin II-dependent exocytosis in information transfer in the brain.

Functioning as one of the co-agonists of NMDAR and thus as endogenous synaptic modulator, D-serine was described for its impact in cognitive enhancement (Collingridge et al., 2013). However, little is known about the influence of D-serine that is released from astrocytes and in which proportion its absence can impact neuronal function. Based on this, we chose to dissect the role of D-serine in the phenotypes observed in the dnSNARE mice. D-serine was shown to be stored in vesicles that rely in the perisynaptic processes of hippocampal and cortical astrocytes (Martineau, 2013). Astrocytes modulate the activity of NMDAR through the release of glutamate and D-serine.

The release of D-serine can be elicited by activation of glutamatergic and bradykininergic receptors that lead to an intracellular Ca^{2+} increase in astrocytes (Martineau, 2013). Astrocyte-derived D-serine was already shown to be critical for the induction of synaptic plasticity (Yang et al., 2003; Henneberger et al., 2010). D-serine was shown in different studies to interact with the different NMDAR subunits, namely NR1 and NR3 (Dzamba et al., 2013) or NR2B (Hahn et al., 2015). D-serine is a co-agonist of NMDAR and its systemic administration was described to increase the intracerebral levels of D-serine and rescue functional deficits in different contexts and independent laboratories (Takata et al., 2011; Guercio et al., 2014; Han et al., 2015b). The fine tuning of the extracellular levels of D-serine, that can be accomplished by several molecular machineries and signaling pathways, is crucial for the maintenance of the correct NMDAR functions. D-serine is thus mandatory for long-term changes in synaptic strength, memory, learning and social interactions (Martineau et al., 2014). This amino acid may be released by astrocytes, neurons or both, but the mechanisms underlying D-serine release dynamics and consecutive NMDAR modulation are poorly understood. Despite of the ability of neurons to release D-serine (Wolosker et al., 2016), astrocytes play a critical role in D-serine mediated functions (Yang et al., 2003; Henneberger et al., 2010). Moreover, Le Bail and colleagues proposed that D-serine would function as a coagonist of more mature synapses (Le Bail et al., 2015). One would expect that, under this close contact, astrocytes would be able to supply neurons with D-serine to modulate synaptic transmission and plasticity.

Modulation of theta oscillations

The use of complementary electrophysiological and behavior analysis to assess the involvement of astrocyte-derived gliotransmitters on cognition, suggests that astrocyte signaling is critical for the synchronization of theta oscillations between the dHIP and mPFC, which underlies performance in spatial learning and memory tasks. The involvement of astrocyte-derived D-serine in theta dHIP-mPFC synchronization is supported by several pieces of evidence. Theta desynchronization was observed in dnSNARE mice that have blocked exocytosis specifically in astrocytes. The expression of dnSNARE transgenes that interfere with the SNARE-complex formation is restricted to astrocytes. Since astrocytic D-serine was shown to assure synaptic potentiation in the hippocampus and cortex (Yang et al., 2003; Henneberger et al., 2010; Takata et al., 2011; Fossat et al., 2012), and the hippocampus is able to self-generate theta oscillations, or to generate them after rhythmic input from entorhinal and subicular regions (Buzsáki, 2002; Jackson et al., 2014; Hoffmann et al., 2015), it is plausible that the dHIP-PFC desynchronization is related to decreased extracellular

levels of astrocyte-derived D-serine. Indeed, supplementation with D-serine was enough to restore theta synchronization between both regions (Figure 3.3).
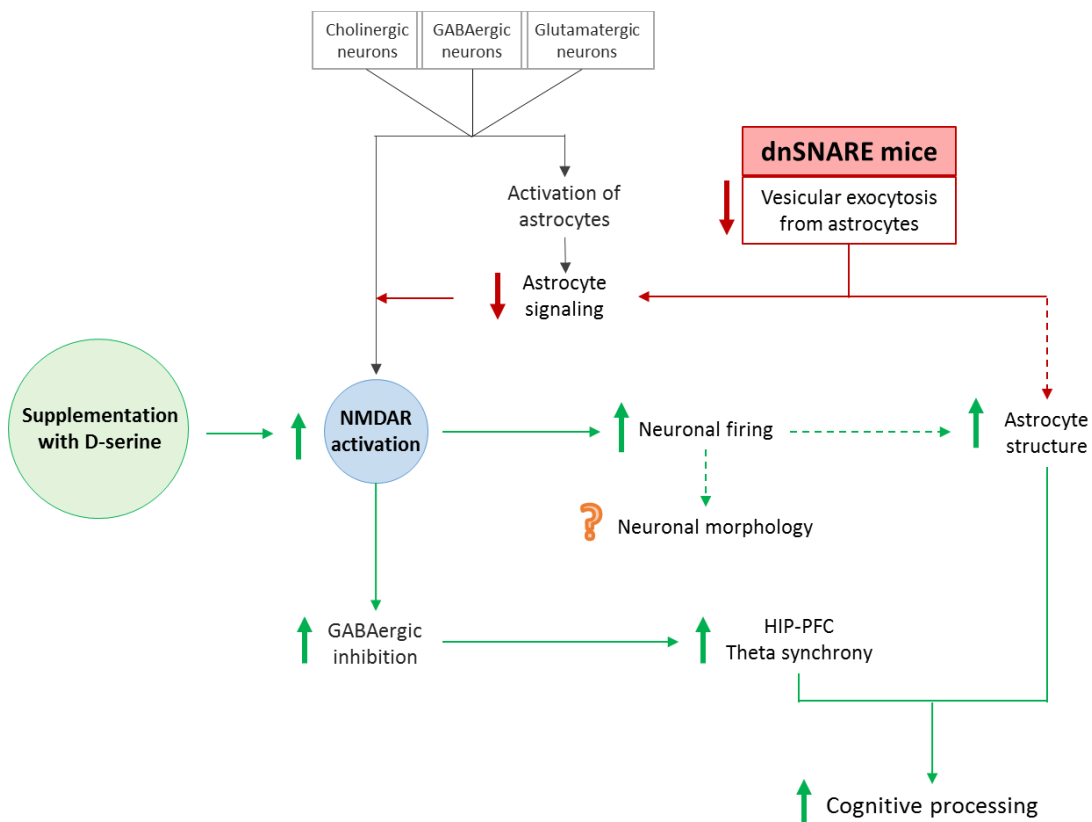
Figure 3.3. Hypothetical model summarizing the effects of supplementation with D-serine in the reverse of dnSNARE mice cognitive deficits.

A subpopulation of medial septum (MS) GABAergic neurons was shown to serve as pacemakers of hippocampal theta, conducting rhythmic activity from the MS to the hippocampus and providing a critical feedback circuit that promotes the modulation of theta within the hippocampus. On the course of theta synchronization, septo-hippocampal GABAergic pacemaker neurons inhibit all known subsets of hippocampal interneurons, causing the disinhibition of pyramidal cells and producing an alternating charge flow along the soma-dendritic axis of pyramidal cells, leading to the generation of field theta activity. A hippocampo-septal backprojection to the septo-hippocampal GABAergic cells, further enhances synchrony of MS GABAergic cells (Hangya et al., 2009). The activity of hippocampal interneurons was shown by Kang and colleagues to activate astrocytes, by eliciting a $GABA_B$-receptor mediated elevation of astrocytic Ca^{2+}, that results in a long-lasting enhancement of inhibitory synaptic transmission, through glutamate release and consequent activation of kainate receptors in inhibitory terminals (Kang et al., 1998). Moreover, the Ca^{2+}-

dependent release of gliotransmitters from astrocytes was shown to modulate synaptic transmission (Di Castro et al., 2011). All together, these data sets suggest that astrocytes might be an intermediary in activity-dependent modulation of both inhibitory and excitatory synapses in the hippocampus (Figure 3.3). Mariotti and colleagues showed recently that also cortical astrocytes in the mouse brain can sense the activity of GABAergic interneurons contributing to the distinct roles played by the different subsets of GABAergic interneurons (Mariotti et al., 2016). Moreover, an elegant study from Perea and colleagues showed that astrocytes are in control of the impact of GABAergic signaling also in excitatory transmission, both in an activity- and time-dependent manner (Perea et al., 2016). The conditional ablation of astrocyte-GABA$_B$ receptors completely abolished the excitatory synaptic potentiation by interneuron stimulation and this was accompanied by a significant reduction in theta and gamma rhythms. Also, selective ablation of NMDA receptors in parvalbumin-positive interneurons was shown to cause the reduction of theta phase-locking of gamma oscillations and, impairments in spatial working and spatial short- and long-term recognition memory (Korotkova et al., 2010). The CA1 pyramidal cells are paced by interneurons also during spontaneous theta oscillations, and a subset of these cells also receives excitatory inputs from other pyramidal cells (Goutagny et al., 2009). Together, these studies suggest the participation of astrocytes in different forms of synaptic regulation and suggest the existence of an activity-dependent interplay between interneuron-astrocyte-synapses. Since D-serine is of huge relevance in the maintenance of glutamatergic transmission via NMDAR, we believe that astrocyte-derived D-serine may play an important role in the theta oscillations entrainment between pyramidal cells and interneurons, in CA1. This phenomenon could be achieved through the establishment of a balance between both the excitatory and inhibitory synaptic transmission, allowing the occurrence of the mutual inhibitory loop between MS and hippocampus which forms the core of the theta generating circuitry. This way, D-serine released by astrocytes could modulate specifically the phase and/or amplitude of basal theta oscillations, that may entrain unit or ensemble firing between the hippocampus and connected cortical areas (Yang et al., 2003; Jones and Wilson, 2005; Siapas et al., 2005; Anderson et al., 2010; Benchenane et al., 2010; O'Neill et al., 2013; Hoffmann et al., 2015) (Figure 3.3).Since we did not observe a decrease in theta oscillation amplitude (given by the power analysis), a strong possibility for the loss of theta coherence in the dHIP-mPFC link of dnSNARE mice is that the communication between both regions may be affected by the coherence of the oscillations in both the sender and receiver networks. Two studies using either *in vitro* or *in vivo* approaches showed that variations in the peak

coherence of theta, does not affect hippocampal theta power, suggesting that multiple theta oscillators with different frequencies coexist along the longitudinal axis of CA1 (Goutagny et al., 2009; Benchenane et al., 2010). Therefore, astrocytes may modulate specifically certain oscillators that reshape the phase of the oscillations leading to the decrease of long distance synchronization. While the literature provides substantial amount of information on the generation of hippocampal theta oscillations, the same is not true for the understanding of synchronization of theta between the hippocampus and other brain regions, such as the cortex (Lisman and Jensen, 2013). In our study, dnSNARE mice exhibit lower levels of dHIP-mPFC theta synchronization, whereas the two regions produce similar amounts of theta oscillations of WT controls. Since coherence measures the synchrony of both phase and amplitude of the signals, one might speculate that astrocyte modulation of NMDA receptors might have a role on the phase component of the theta produced, which could be synchronized by supplementing D-serine. Further experiments are needed to specifically address this issue. Together, these correlational evidences support the hypothesis that D-serine released by astrocytes modulates specifically basal theta synchronization, that may entrain unit or ensemble firing in anatomically connected cortical areas (Yang et al., 2003; Jones and Wilson, 2005; Siapas et al., 2005; Anderson et al., 2010; Benchenane et al., 2010; O'Neill et al., 2013; Hoffmann et al., 2015)

3.1.3 The dHIP-PFC theta synchrony modulated by astrocytes supports cognitive function

Astrocyte signaling appears to be important for the modulation of cortical oscillations (Lee et al., 2014; Poskanzer and Yuste, 2016). However, the modulation of neuronal oscillations that allow the entrainment of deep brain areas required for cognitive computation remained elusive. Here, we described that dnSNARE mice display a basal dorsal hippocampus-prefrontal desynchronization and strong deficits in cognitive functions dependent on this circuit (Figure 3.1, B). Based on our own data and the available literature, we do believe that these observations are causally related (Figure 3.2).

Cognitive phenotype and electrophysiological underpinnings

Cognition links different processes such as memory, association, language, attention, concept formation and problem solving. Memory is related to the capacity of an individual to remember

past experiences and retain perceptions, reflecting many processes such as acquisition, consolidation, retention, retrieval and performance (Abel and Lattal, 2001). Many studies already proved the influence of hippocampus in memory formation in rodents, settling the significance of this region on the creation of spatial representations in the brain (De Bruin et al., 1994; Mizuno and Giese, 2005). Hippocampus is connected to the PFC by axons projected from the CA1 field and subiculum and the modulation of synaptic activity in this connection is responsible for the regulation of learning/memory processes unravelling its impact on cognition processing (Goldman-Rakic, 1995; Cerqueira et al., 2007). Blockade of neurotransmitter release from astrocytes in vivo was shown to induce an unexpected cognitive modulation, namely affecting sleep homeostasis, in dnSNARE mice (Florian et al., 2011; Pascual et al., 2005; Halassa et al., 2009a, 2009b). In light of these observations, astrocyte function seems to be implicated in cognitive functions such as learning or memory processing through gliotransmission. The use of transgenic mice with controllable astrocytic vesicular release was of great help to address the impact of gliotransmission in the formation of memory processes. In this work, the dnSNARE mice presented a slower learning curve in the RM task of MWM than WT mice. This might suggest that dnSNARE mice developed a strategy to escape from water, such as by swimming away from the side walls to increase the likelihood of contacting the platform by chance, instead of a true spatial learning of the location of the platform. The RL task assesses behavior flexibility, which is a PFC-dependent function consisting in the adaptation of behavior according to changes in stimulus-reward possibilities and was not particularly affected in our mouse model. The HB test is based in a food rewarding system and allows the assessment of several parameters including both RM and WM. The first task keeps information that is exclusively relevant within a specific trial while the last holds information about the solution of a spatial discrimination task, retaining its relevance across many trials. In accordance to what was observed in the MWM, dnSNARE mice present a slight increase in both RM and WM ratios, however, transgenic mice only get closer to the WT ratios in the fourth day of test, showing a clear deficit in both dimensions. The average weight of the mice was maintained during the course of the test suggesting that these results might represent a lack of exploration of the maze rather than a decreased motivation to eat. Another test was the 2TPR task in the Y-maze, where the expected from rodents was to visit the two first arms in a training session, for memory acquisition, and to remember them in the second trial in order to preferentially explore the novel arm during the retrieval session. This test allows the assessment of spatial recognition memory of mice and to dissect if gliotransmission through exocytosis is critical for its maintenance. Once

again, dnSNARE mice explored the three arms of the maze randomly, demonstrating a lack of recognition memory for the novel arm. Additionally, Halassa and colleagues tested dnSNARE mice in the NOR task to evaluate the recognition memory of these mice under sleep pressure (Halassa et al., 2009b). The authors did not see differences between genotypes when mice were undisturbed, which might be conflicting with our own data. This discrepancy is explained by the fact that, in that study high and low expressor dnSNARE mice were pooled together in one group and this might have diluted the basal cognitive deficit.

Synchrony in the hippocampus-prefrontal cortex network is known to support cognitive processing. The dHIP is connected to the PFC indirectly. The loop closes by a multi-synaptic circuit, being the PFC also indirectly connected to the dHIP (Preston and Eichenbaum, 2013). Despite of these indirect connections, O'Neil and colleagues demonstrated that dHIP theta oscillations are synchronized with theta oscillations in the mPFC, and that theta synchrony is critical for a spatial memory task (O'Neill et al., 2013). Interestingly, both single units and ensembles in the PFC appear to entrain with the theta rhythm from the dHIP. This type of memory task was previously shown to be dependent on the synchronization of theta oscillations between the hippocampus and prefrontal cortex (Jones and Wilson, 2005; Siapas et al., 2005; Benchenane et al., 2010). Our data shows, that the good consolidation of reference memory directly correlates with high basal theta coherence presented by a given dnSNARE mouse, which is in accordance with previous reports showing that the pathological decrease of theta coherence triggered this cognitive deficit (Gordon, 2011; Oliveira et al., 2013). On the other hand, the higher expression of dnSNARE transgenes in the hippocampus strongly correlates with a worse cognitive performance, suggesting that those impairments are due to the lack of astrocyte-secreted signals. Again, that this variability of genetic modulation may explain negative results or the absence of effects in studies in which mice displaying variable levels of transgene expression or genomic recombination were pooled together as one single group (Oliveira et al., 2015).

The cognitive deficits observed in dnSNARE mice are likely a consequence of the loss of HIP-PFC synchrony in these animals, as D-serine supplementation also restored behavioral function in dnSNARE mice. However, and despite the specificity of basal desynchronization for theta frequency range in this link, we should not exclude the possibility that the hippocampus may be desynchronized with other brain regions, which could help to explain the cognitive deficits observed.

The absence of an emotional phenotype

In order to exclude a possible bias of the cognitive assessment caused by an emotional phenotype that could reduce the motivation of dnSNARE mice to perform the tasks, we analyzed this behavior dimension together with the electrophysiological evaluation of the ventral hippocampus-prefrontal link that is classically related with emotional behavior. Anxiety empowers the recognition of danger and the fear of dealing with an unknown internal or external threat. The assessment of the anxious-like behavior of the used animal model was important to look for any mood alterations that could condition the execution of specific tests for cognition processing, working as a preclinical research. EPM, LDB and OF tests allow a quick anxiety screening of laboratory rodents without training sessions, focusing on the locomotor activity and exploratory behavior. From our observations, no differences in anxious-like behavior were seen between dnSNARE and WT mice. Furthermore, we assessed if the lack of gliotransmission was enough to induce depressive-like behavior per se. FST and TST were used to perform a screening of learned helplessness, a hallmark of depressive-like behavior, and this phenotype was completely discarded for dnSNARE mice. Interestingly, Cao and colleagues suggested that dnSNARE mice present a depressive-like behavior based on the lower levels of extracellular ATP, measured in PFC and hippocampal slices, and in the higher immobility time in the FST, in comparison to WT mice (Cao et al., 2013). These intriguing phenotype collides not only with our own data but also with a study from the same year, using dnSNARE mice to assess the impact of sleep deprivation as one rapid intervention to alleviate depressive symptoms, in major depressive disorder (Hines et al., 2013). In this study, authors suggest astrocyte-dependent adenosine mediated signaling as the central pathway for sleep deprivation to exert its antidepressive effects. Both FST and TST tests were performed and the basal immobility times were similar between dnSNARE and WT mice, in agreement with our results and supporting the exclusion of a depressive-like phenotype in this mouse model.

The absence of an emotional phenotype was backed up by the intact basal function of vHIP-prefrontal link, translated in normal power and synchrony between both regions. Astrocytes my act differently in both sub-regions of the hippocampus and this fact may explain the different electrophysiological observations between dorsal and ventral connections. A recent study gathered evidences on astrocytes ability to maintain region-associated expression of specific genes and functions (Haim and Rowitch, 2017). Furthermore, Molofsky and colleagues showed that astrocytes from the dorsal and ventral spinal cord display striking transcriptomic differences, being responsible for a region-specific phenotype (Molofsky et al., 2014), that may be translated in

different functions. The regional specificity of theta synchrony for the dHIP-mPFC, and not for the vHIP-mPFC link, observed in dnSNARE mice could be, in part, justified by interregional heterogeneity between existing astrocytes from dorsal and ventral subregions of hippocampus.

3.1.4 Network structure correlates

The role of astrocytes in information processing is translated in the concept of multipartite synapse where perysynaptic astroglial processes closely enwrap the synaptic structure, participating in several features of synaptic transmission. Memory formation in the brain is settled on the remodeling of synaptic connections that may result in the rewiring of neural network (Heller and Rusakov, 2015; Zorec et al., 2016). Astrocytes are in a tight relationship with neurons at synapses. Therefore, based in the functional deficits in the network as well as in the cognitive performance observed for dnSNARE mice, one would expect to see modifications of the network structure translated in alterations in neuronal and/or astrocytic morphologies (Figure 3.1, C).

Neuronal morphology is preserved

The dendritic morphology of neurons was mainly evaluated using 3D reconstruction and Sholl analysis. Interestingly, no alterations were found in dendritic arborization of individual neurons of dnSNARE mice, in both hippocampal (dCA1 and dDG) and prefrontal cortex regions (Figure 3.2). On one hand, this data is in support of the specificity of transgene expression in astrocytes. On the other hand, finding no differences between dnSNARE and WT mice neurons was not in complete agreement with already published data, showing that newborn neurons from hippocampal DG of dnSNARE mice present less complexity and number of protrusions in comparison to WT littermates (Sultan et al., 2015). In fact, Sultan and co-workers demonstrated that astrocyte signaling is required for the maturation of the dendrites and spines of newly-formed neurons. Assuming the principle that the direct contact with astrocyte regulates the stabilization and maturation of dendritic spines (Nishida and Okabe, 2007), the group elegantly describe that newly formed neurons display different spine distribution in the territory of a GFP-expressing astrocyte, in dnSNARE mice, having also shorter dendrites and less branched morphology. These data suggest a local regulation of synapse formation within specific dendritic segments of newborn neurons. While this evidence supports their mechanistic proof-of-concept, the authors also show that the dendrites of mature neurons (the large majority of functionally connected DG neurons) and all dendrite segments of

newly-formed neurons that lay outside the territories of a GFP-expressing astrocytes are intact. Moreover, their effect shall be restricted to the DG due to lack of neurogenesis in the remaining hippocampal subregions, namely the hippocampal CA1, where the neural dendrites are intact in dnSNARE mice as demonstrated by our analysis since our LFP recordings were obtained by electrodes implanted in the pyramidal/radiatum layers of the CA1, where no neurogenesis occurs. The poorer synaptogenesis within the territories of GFP-expressing astrocytes in the DG may also account in a certain extent for our readouts. Nevertheless, we believe that the critical behavior and electrophysiological impairments observed in dnSNARE mice are mainly due to the general decrease of astrocyte-exocytosis throughout. In this way, our results support that dnSNARE transgene expression does not alter the neuronal structure explicitly of mature neurons that should compose the majority of the septal-hippocampal-prefrontal network.

Astrocyte structure atrophy

A similar analysis of the main structure of astrocytes revealed that, in contrary to what happened to neurons, astrocytes significantly decreased their GFAP-positive arbor complexity under dnSNARE transgene expression (Figure 3.2). Although we did not perform experiments to understand the causes of the astrocytic atrophy, one could suggest two possible explanations: an intrinsic mechanism of structure stability related to exocytosis and/or a mechanism dependent on astrocyte/neuron signaling.

The astrocytic atrophy is specific of transgene expressing astrocytes (GFAP+GFP+), which suggests an intrinsic mechanism related to the blockade of exocytosis. While the process of endocytosis leads to a subtraction of membrane, exocytosis is known to involve the reposition of phospholipid bilayer to the plasma membrane, resulting both processes in membrane area fluctuations (Kreft et al., 2004). Lee and colleagues, using a mouse model with an overexpression of hGFAP, showed that there was an increased release of ATP suggesting that GFAP intermediate filaments are a major determinant of vesicle traffic in astrocytes (Lee et al., 2013). In our model, where there is a blockade of vesicular release by exocytosis, selectively from astrocytes, interfering with gliotransmission results in a significant decrease of gliotransmitters release, such as ATP and D-serine. This impairment in astrocytic fusion events was already shown to be very strong (shutdown of about 91% of the fusion events) (Sultan et al., 2015). Accordingly, this blockade in exocytosis accompanied by a normal endocytosis process, would potentially lead to a reduction of membrane surface, with a possible consequence to the main structure of the transgene expressing astrocytes,

135

by an imbalance in the compensatory mechanisms for the restoration of the cell membrane. Moreover, the progressive decrease of the cell membrane due to impaired exocytosis could justify the accentuated decrease of GFAP detected in dnSNARE mice transgene-expressing astrocytes. The fusion of vesicles with the plasma membrane can be assessed by controlling the increase in the membrane capacitance (C_m), which is reflected in the increase of plasma membrane surface due to a net addition of vesicular membrane to the plasma membrane (Kreft et al., 2004; Zorec et al., 2012; Martineau, 2013). For instance, evoked glutamate release from astrocytes was shown to be accompanied by an increase in C_m in all cells (Zhang et al., 2004). More specifically, Kreft and colleagues showed in cultures of astrocytes, that these cells exhibit Ca^{2+}-dependent membrane increases due to regulated vesicular exocytosis, that are abolished by the treatment with tetanus toxin, which cleaves synaptobrevin II in a similar fashion to what happens in the dnSNARE mouse model (Kreft et al., 2004). Based on this data, one would anticipate that dnSNARE mice, for having a compromised astrocytic exocytosis, also have a decreased rate of C_m and thus, a decrease in their astrocytes plasma membrane surface, complementarily justifying the decrease in these cells arborization and complexity of main structure. Therefore, it could be a possible approach to check this hypothesis. Despite of the apparent distance between the levels of alteration (single vesicle in the order of tens of nanometers and process atrophy in the range of the tens of micrometers), the huge release blockade (≈90%) might explain these alterations, at least partially.

The other hypothesis to explain the astrocytic structure atrophy is a mechanism dependent on astrocyte/neuron signaling. Synaptic plasticity was shown to promote significant and important ultrastructural modifications on dendritic spines, presynaptic terminal and associated glial processes. Specifically, after LTP induction in an organotypic slice culture model, the proportion of synapses receiving glial coverage rapidly increases (Lushnikova et al., 2009). Furthermore, Tanaka and colleagues showed that the synaptic coverage by astrocytic processes is reduced in mice lacking the IP3-mediated astrocytic Ca^{2+} signaling (Tanaka et al., 2013), a critical step for the astrocytes vesicular-regulated exocytosis that is blocked in the dnSNARE mouse. The data of this study supports that hippocampus-related behaviors are affected by a reduction in astrocytic coverage of synapses. Based on these set of evidence, one can believe that the astrocytic atrophy observed in our dnSNARE mice for the transgene-expressing cells, may account for a reduction of coverage and that this phenomenon could be also a consequence of the reduced synaptic plasticity (confirmed by others) and one cause of the cognitive deficits presented by our model. Nevertheless, despite of losing arbor complexity, the astrocyte density was not affected as confirmed for different

layers of both dHIP and dDG. This singularity was also observed in a study where chronic stress induced a structural atrophy, but not loss of astrocytes (Tynan et al., 2013). Based on these data, we can confirm that GFAP-structure (used in this work to measure the astrocyte main structure) can vary in a manner that is independent upon the viability of the cells. Moreover, these results also exclude the possibility of a putative compensatory mechanism, which could lead to a generalized increase in the number of astrocytes, which we did not observe.

We should still mention the fact, that the structural characterization of astrocytes was performed using the Simple Neurite Tracer software, and that this method excludes astrocytic morphological details that occur on a nanoscale level (Bushong et al., 2002; Rusakov et al., 2014). In order to access this level of detail, to address for instance the morphology of astrocytic micro-domains, a much more powerful reconstruction tool would be required, preferentially coupled with a higher level of image resolution. Nevertheless, this method was a powerful tool for the screening of the main structure of astrocytes at the microscale level across the CA1 hippocampal field.

Exogenous administration of D-serine effectively restored specifically theta synchronization in dnSNARE mice. However, in WT mice, no alterations were detected in terms of synchrony, while an increase of power followed by an increase in astrocytes complexity occurred for both genotypes (Figure 3.3). This suggests that exogenous D-serine may trigger neuronal activity, and in consequence, stimulates astrocyte to extend their processes, as reflected by the increase in the complexity of their main structure, similar to a response to an extraordinary activation of neuronal firing in all groups analyzed. Indeed, a study showed that the motility of synapse-associated astrocytic processes is enhanced after stimulating the hippocampus for the induction of synaptic LTP and astrocyte Ca^{2+} signaling. Both *in vitro* and *in vivo*, this was a rapid process occurring within 5 to 30 min, after stimulus (Perez-Alvarez et al., 2014). The authors demonstrated that the astrocytic structural remodeling is accompanied by functional changes in the ability of astrocytes to regulate synaptic transmission, and that this phenomenon depends mainly on presynaptic activity, mGluRs activation and astrocytic Ca^{2+} signaling. These structural changes might account for the observed changes in astrocytes main structure after supplementation with D-serine in our study, independently of genotypes. So, the increase in morphological complexity of dnSNARE mice astrocytes – in response to accentuated neuronal firing, and the rescue of theta synchrony in the dHIP-mPFC link, after supplementation with D-serine, can complementarily explain the cognitive performance improvement observed in dnSNARE mice (Figure 3.3).

3.2 Conclusion and future perspectives

Based in our observations on how interfering with astrocytic vesicular release affects the cognitive processing, the work developed during this PhD thesis showed that hippocampal-prefrontal theta synchrony supports the communication link between distant brain regions. Moreover, astrocyte-derived signaling appears to play an important role in the maintenance of the network and cognitive integrity in the adult brain, and D-serine is a good candidate to modulate these functions. Our results provide the first evidence of a mechanism by which astrocytic signaling is required for the entrainment of distant cortico-limbic circuits, being mandatory for cognitive performance. The presented results are of relevance since they open a novel window to the neuromodulatory function of astrocytes.

With this thesis we provided further insights on the role of gliotransmission in the cortico-limbic network (in particular the dHIP and mPFC), and on how this astrocyte-specific process is involved in the modulation of cognitive processing. Nevertheless, there are still open questions that arise from our data and that demand further exploration to achieve a better characterization of the influence of astrocytes, in cognitive function:

1) This work does not exclude the involvement of further astrocyte-secreted molecules which are known to be released by astrocytes and to participate in the regulation of memory processing, such as ATP/adenosine (Gibbs et al., 2011) and TNFα (Habbas et al., 2015), for instance. It is still unclear in which proportion each gliotransmitter might exactly be contributing to the electrophysiological, behavioral and morphological alterations observed in dnSNARE mice. Therefore, a more complete pharmacological screening should be performed to fully understand the implications of astrocytic signaling *in vivo*.

2) This study raised the need for a comprehensive understanding of the molecular mechanisms and signaling pathways involved in the functional alterations observed in dnSNARE mice. Since most of the phenotypes altered in our mouse model were either related or mainly dependent from hippocampal function, we believe that a complementary transcriptomic analysis, using macrodissected hippocampus, should be performed to

unravel the molecular regulation (e.g. glutamate/GABA receptor levels, calcium-dependent signaling, etc.) in the hippocampus of dnSNARE mice.

3) In our model, there is a brain widespread expression of the synaptobrevin II transgene that might lead to functional compromise of other brain regions leading to confounding behavior data. To overcome this issue, we suggest (i) the use of viral approaches to induce the expression of tetanus toxin that will specifically cleave synaptobrevin II in astrocytes, to block gliotransmission in specific brain regions such as the hippocampus, the prefrontal cortex or both; (ii) the use of viral-driven inhibition of specific NMDA receptors (e.g. NR1-containing), or (iii) conditional expression of D-serine racemase in astrocytes in full knock-outs of this enzyme. These approaches would exclude a possible influence from the disruption of other links in the brain, as a consequence of the whole brain expression of synaptobrevin II transgene in dnSNARE mice and, specify the brain region where D-serine signaling plays a central role in the support of theta synchronization.

4) For the functional rescue we intraperitoneally injected D-serine. To discard the influence of a systemic administration and to reach spatial specificity, we would suggest the local supply of D-serine, independently in the dHIP, vHIP and mPFC of dnSNARE mice. This way, we would be able to address which brain region is more responsive to this transmitter and by which pathway D-serine restores theta synchrony.

5) Finally, the repetition of electrophysiological and behavior experiments should be performed in recordings from freely moving and behaving mice. This experiment, could not only validate our results, but also it could give us new detail into memory and learning processes (e.g. by evaluating the several phases of the task) and about the influence exerted by astrocytic modulation on the acute modulation of neuronal oscillations.

Bibliography

Abel T, Lattal KM (2001) Molecular mechanisms of memory acquisition, consolidation and retrieval. Curr Opin Neurobiol 11:180–187.

Adhikari A, Topiwala MA, Gordon JA (2010) Synchronized Activity between the Ventral Hippocampus and the Medial Prefrontal Cortex during Anxiety. Neuron 65:257–269.

Agulhon C, Sun M-Y, Murphy T, Myers T, Lauderdale K, Fiacco TA (2012) Calcium Signaling and Gliotransmission in Normal vs. Reactive Astrocytes. Front Pharmacol 3:139.

Allaman I, Bélanger M, Magistretti PJ (2011) Astrocyte–neuron metabolic relationships: for better and for worse. Trends Neurosci 34:76–87.

Allen NJ (2014) Astrocyte Regulation of Synaptic Behavior. Annu Rev Cell Dev Biol 30:439–463.

Allen NJ, Barres BA (2009) Neuroscience: glia—more than just brain glue. Nature 457:675–677.

Anderson KL, Rajagovindan R, Ghacibeh GA, Meador KJ, Ding M (2010) Theta Oscillations Mediate Interaction between Prefrontal Cortex and Medial Temporal Lobe in Human Memory. Cereb Cortex 20:1604–1612.

Anderson MA, Ao Y, Sofroniew MV (2014) Heterogeneity of reactive astrocytes. Neurosci Lett 565:23–29.

Angulo MC, Kozlov AS, Charpak S, Audinat E (2004) Glutamate released from glial cells synchronizes neuronal activity in the hippocampus. J Neurosci Off J Soc Neurosci 24:6920–6927.

Araque A, Carmignoto G, Haydon PG, Oliet SHR, Robitaille R, Volterra A (2014) Gliotransmitters Travel in Time and Space. Neuron 81:728–739.

Araque A, Li N, Doyle RT, Haydon PG (2000) SNARE protein-dependent glutamate release from astrocytes. J Neurosci 20:666–673.

Araque A, Parpura V, Sanzgiri RP, Haydon PG, Araque A, Parpura V, Sanzgiri RP, Haydon PG (1999) Tripartite synapses: glia, the unacknowledged partner. Trends Neurosci 22:208–215.

Asada A, Ujita S, Nakayama R, Oba S, Ishii S, Matsuki N, Ikegaya Y (2015) Subtle modulation of ongoing calcium dynamics in astrocytic microdomains by sensory inputs. Physiol Rep 3:e12454.

Balu DT, Coyle JT (2015) The NMDA receptor "glycine modulatory site" in schizophrenia: d-serine, glycine, and beyond. Curr Opin Pharmacol 20:109–115.

Banasr M, Duman RS (2008) Glial Loss in the Prefrontal Cortex Is Sufficient to Induce Depressive-like Behaviors. Biol Psychiatry 64:863–870.

Bannerman D., Grubb M, Deacon RM., Yee B., Feldon J, Rawlins JN. (2003) Ventral hippocampal lesions affect anxiety but not spatial learning. Behav Brain Res 139:197–213.

Bardehle S, Krüger M, Buggenthin F, Schwausch J, Ninkovic J, Clevers H, Snippert HJ, Theis FJ, Meyer-Luehmann M, Bechmann I, Dimou L, Götz M (2013) Live imaging of astrocyte responses to acute injury reveals selective juxtavascular proliferation. Nat Neurosci 16:580–586.

Bayraktar OA, Fuentealba LC, Alvarez-Buylla A, Rowitch DH (2015) Astrocyte Development and Heterogeneity. Cold Spring Harb Perspect Biol 7:a020362.

Bechtholt-Gompf AJ, Walther HV, Adams MA, Carlezon WA, Öngür D, Cohen BM (2010) Blockade of astrocytic glutamate uptake in rats induces signs of anhedonia and impaired spatial memory. Neuropsychopharmacology 35:2049–2059.

Belzung C, Griebel G (2001) Measuring normal and pathological anxiety-like behaviour in mice: a review. Behav Brain Res 125:141–149.

Ben Achour S, Pascual O (2012) Astrocyte–Neuron Communication: Functional Consequences. Neurochem Res 37:2464–2473.

Benchenane K, Peyrache A, Khamassi M, Tierney PL, Gioanni Y, Battaglia FP, Wiener SI (2010) Coherent Theta Oscillations and Reorganization of Spike Timing in the Hippocampal-Prefrontal Network upon Learning. Neuron 66:921–936.

Benchenane K, Tiesinga PH, Battaglia FP (2011) Oscillations in the prefrontal cortex: a gateway to memory and attention. Curr Opin Neurobiol 21:475–485.

Bergersen LH, Morland C, Ormel L, Rinholm JE, Larsson M, Wold JFH, Røe AT, Stranna A, Santello M, Bouvier D, Ottersen OP, Volterra A, Gundersen V (2012) Immunogold detection of L-glutamate and D-serine in small synaptic-like microvesicles in adult hippocampal astrocytes. Cereb Cortex N Y N 1991 22:1690–1697.

Bernal GM, Peterson DA (2011) Phenotypic and Gene Expression Modification with Normal Brain Aging in GFAP-Positive Astrocytes and Neural Stem Cells. Aging Cell 10:466–482.

Bessa JM, Ferreira D, Melo I, Marques F, Cerqueira JJ, Palha JA, Almeida OFX, Sousa N (2008) The mood-improving actions of antidepressants do not depend on neurogenesis but are associated with neuronal remodeling. Mol Psychiatry 14:764–773.

Bevins RA, Besheer J (2006) Object recognition in rats and mice: a one-trial non-matching-to-sample learning task to study "recognition memory." Nat Protoc 1:1306–1311.

Bezzi P, Gundersen V, Galbete JL, Seifert G, Steinhäuser C, Pilati E, Volterra A (2004) Astrocytes contain a vesicular compartment that is competent for regulated exocytosis of glutamate. Nat Neurosci 7:613–620.

Bliss TVP, Collingridge GL (1993) A synaptic model of memory: long-term potentiation in the hippocampus. Nature 361:31–39.

Bott J-B, Muller M-A, Jackson J, Aubert J, Cassel J-C, Mathis C, Goutagny R (2015) Spatial Reference Memory is Associated with Modulation of Theta–Gamma Coupling in the Dentate Gyrus. Cereb Cortex:1–10.

Bourin M, Hascoët M (2003) The mouse light/dark box test. Eur J Pharmacol 463:55–65.

Bourin M, Petit-Demoulière B, Nic Dhonnchadha B, Hascöet M (2007) Animal models of anxiety in mice. Fundam Clin Pharmacol 21:567–574.

Bowser DN, Khakh BS (2007) Vesicular ATP Is the Predominant Cause of Intercellular Calcium Waves in Astrocytes. J Gen Physiol 129:485–491.

Buccafusco JJ ed. (2001) Methods of behavior analysis in neuroscience. Boca Raton, Fla.: CRC Press.

Burke JF, Zaghloul KA, Jacobs J, Williams RB, Sperling MR, Sharan AD, Kahana MJ (2013) Synchronous and Asynchronous Theta and Gamma Activity during Episodic Memory Formation. J Neurosci 33:292–304.

Bushong EA, Martone ME, Ellisman MH (2004) Maturation of astrocyte morphology and the establishment of astrocyte domains during postnatal hippocampal development. Int J Dev Neurosci 22:73–86.

Bushong EA, Martone ME, Jones YZ, Ellisman MH (2002) Protoplasmic astrocytes in CA1 stratum radiatum occupy separate anatomical domains. J Neurosci 22:183–192.

Butler JL, Paulsen O (2015) Hippocampal network oscillations — recent insights from in vitro experiments. Curr Opin Neurobiol 31:40–44.

Buzsáki G (2002) Theta oscillations in the hippocampus. Neuron 33:325–340.

Buzsáki G (2004) Large-scale recording of neuronal ensembles. Nat Neurosci 7:446–451.

Buzsáki G (2006) Rhythms of the brain. Oxford ; New York: Oxford University Press.

Buzsáki G, Draguhn A (2004) Neuronal Oscillations in Cortical Networks. Science 304:1926–1929.

Buzsáki G, Schomburg EW (2015) What does gamma coherence tell us about inter-regional neural communication? Nat Neurosci 18:484–489.

Cabezas R, Avila M, Gonzalez J, El-Bachá RS, Báez E, García-Segura LM, Jurado Coronel JC, Capani F, Cardona-Gomez GP, Barreto GE (2014) Astrocytic modulation of blood brain barrier: perspectives on Parkinson's disease. Front Cell Neurosci 8:211.

Cabral HO, Vinck M, Fouquet C, Pennartz CMA, Rondi-Reig L, Battaglia FP (2014) Oscillatory Dynamics and Place Field Maps Reflect Hippocampal Ensemble Processing of Sequence and Place Memory under NMDA Receptor Control. Neuron 81:402–415.

Cahoy JD, Emery B, Kaushal A, Foo LC, Zamanian JL, Christopherson KS, Xing Y, Lubischer JL, Krieg PA, Krupenko SA, Thompson WJ, Barres BA (2008) A Transcriptome Database for

Astrocytes, Neurons, and Oligodendrocytes: A New Resource for Understanding Brain Development and Function. J Neurosci 28:264–278.

Can A, Dao DT, Arad M, Terrillion CE, Piantadosi SC, Gould TD (2012a) The Mouse Forced Swim Test. JoVE J Vis Exp:e3638–e3638.

Can A, Dao DT, Terrillion CE, Piantadosi SC, Bhat S, Gould TD (2012b) The Tail Suspension Test. JoVE J Vis Exp:e3769–e3769.

Cannon J, McCarthy MM, Lee S, Lee J, Börgers C, Whittington MA, Kopell N (2014) Neurosystems: brain rhythms and cognitive processing. Eur J Neurosci 39:705–719.

Cao X, Li L-P, Wang Q, Wu Q, Hu H-H, Zhang M, Fang Y-Y, Zhang J, Li S-J, Xiong W-C, Yan H-C, Gao Y-B, Liu J-H, Li X-W, Sun L-R, Zeng Y-N, Zhu X-H, Gao T-M (2013) Astrocyte-derived ATP modulates depressive-like behaviors. Nat Med 19:773–777.

Cappaert NLM, Lopes da Silva FH, Wadman WJ (2009) Spatio-temporal dynamics of theta oscillations in hippocampal-entorhinal slices. Hippocampus 19:1065–1077.

Castagné V, Moser P, Roux S, Porsolt RD (2011) Rodent models of depression: forced swim and tail suspension behavioral despair tests in rats and mice. Curr Protoc Neurosci Chapter 8:Unit 8.10A.

Castilla-Ortega E, Sánchez-López J, Hoyo-Becerra C, Matas-Rico E, Zambrana-Infantes E, Chun J, De Fonseca FR, Pedraza C, Estivill-Torrús G, Santin LJ (2010) Exploratory, anxiety and spatial memory impairments are dissociated in mice lacking the LPA1 receptor. Neurobiol Learn Mem 94:73–82.

Catts VS, Wong J, Fillman SG, Fung SJ, Weickert CS (2014) Increased expression of astrocyte markers in schizophrenia: Association with neuroinflammation. Aust N Z J Psychiatry 48:722–734.

Cerqueira JJ, Mailliet F, Almeida OFX, Jay TM, Sousa N (2007) The Prefrontal Cortex as a Key Target of the Maladaptive Response to Stress. J Neurosci 27:2781–2787.

Chen H, Wang Y, Yang L, Sui J, Hu Z, Hu B (2016) Theta synchronization between medial prefrontal cortex and cerebellum is associated with adaptive performance of associative learning behavior. Sci Rep 6:20960.

Chen J, Tan Z, Zeng L, Zhang X, He Y, Gao W, Wu X, Li Y, Bu B, Wang W, Duan S (2013) Heterosynaptic long-term depression mediated by ATP released from astrocytes. Glia 61:178–191.

Chever O, Dossi E, Pannasch U, Derangeon M, Rouach N (2016) Astroglial networks promote neuronal coordination. Sci Signal 9:ra6-ra6.

Chun J, Brinkmann V (2011) A Mechanistically Novel, First Oral Therapy for Multiple Sclerosis: The Development of Fingolimod (FTY720, Gilenya). Discov Med 12:213–228.

Chung W-S, Welsh CA, Barres BA, Stevens B (2015) Do glia drive synaptic and cognitive impairment in disease? Nat Neurosci 18:1539–1545.

Ciocchi S, Passecker J, Malagon-Vina H, Mikus N, Klausberger T (2015) Selective information routing by ventral hippocampal CA1 projection neurons. Science 348:560–563.

Clark L, Cools R, Robbins TW (2004) The neuropsychology of ventral prefrontal cortex: Decision-making and reversal learning. Brain Cogn 55:41–53.

Clarke LE, Barres BA (2013) Emerging roles of astrocytes in neural circuit development. Nat Rev Neurosci 14:311–321.

Clasadonte J, Dong J, Hines DJ, Haydon PG (2013) Astrocyte control of synaptic NMDA receptors contributes to the progressive development of temporal lobe epilepsy. Proc Natl Acad Sci 110:17540–17545.

Colgin LL (2011) Oscillations and hippocampal–prefrontal synchrony. Curr Opin Neurobiol 21:467–474.

Colgin LL (2016) Rhythms of the hippocampal network. Nat Rev Neurosci 17:239–249.

Collingridge GL, Volianskis A, Bannister N, France G, Hanna L, Mercier M, Tidball P, Fang G, Irvine MW, Costa BM, Monaghan DT, Bortolotto ZA, Molnár E, Lodge D, Jane DE (2013) The NMDA receptor as a target for cognitive enhancement. Neuropharmacology 64:13–26.

Costa-Aze VDS, Quiedeville A, Boulouard M, Dauphin F (2012) 5-HT6 receptor blockade differentially affects scopolamine-induced deficits of working memory, recognition memory and aversive learning in mice. Psychopharmacology (Berl) 222:99–115.

Covelo A, Araque A (2016) Lateral regulation of synaptic transmission by astrocytes. Neuroscience 323:62–66.

Cryan JF, Mombereau C, Vassout A (2005) The tail suspension test as a model for assessing antidepressant activity: Review of pharmacological and genetic studies in mice. Neurosci Biobehav Rev 29:571–625.

De Bruin JP, Sànchez-Santed F, Heinsbroek RP, Donker A, Postmes P (1994) A behavioural analysis of rats with damage to the medial prefrontal cortex using the Morris water maze: evidence for behavioural flexibility, but not for impaired spatial navigation. Brain Res 652:323–333.

De Koning TJ, Snell K, Duran M, Berger R, Poll-The B-T, Surtees R (2003) L-serine in disease and development. Biochem J 371:653–661.

De Pittà M, Brunel N, Volterra A (2016) Astrocytes: Orchestrating synaptic plasticity? Neuroscience 323:43–61.

De Pittà M, Volman V, Berry H, Parpura V, Volterra A, Ben-Jacob E (2012) Computational quest for understanding the role of astrocyte signaling in synaptic transmission and plasticity. Front Comput Neurosci 6:98.

Deng Q, Terunuma M, Fellin T, Moss SJ, Haydon PG (2011) Astrocytic activation of A1 receptors regulates the surface expression of NMDA receptors through a Src kinase dependent pathway. Glia 59:1084–1093.

Devinsky O, Vezzani A, Najjar S, De Lanerolle NC, Rogawski MA (2013) Glia and epilepsy: excitability and inflammation. Trends Neurosci 36:174–184.

Di Castro MA, Chuquet J, Liaudet N, Bhaukaurally K, Santello M, Bouvier D, Tiret P, Volterra A (2011) Local Ca2+ detection and modulation of synaptic release by astrocytes. Nat Neurosci 14:1276–1284.

Dimou L, Gotz M (2014) Glial Cells as Progenitors and Stem Cells: New Roles in the Healthy and Diseased Brain. Physiol Rev 94:709–737.

Duan S, Anderson CM, Keung EC, Chen Y, Chen Y, Swanson RA (2003) P2X7 receptor-mediated release of excitatory amino acids from astrocytes. J Neurosci 23:1320–1328.

Dzamba D, Honsa P, Anderova M (2013) NMDA receptors in glial cells: pending questions. Curr Neuropharmacol 11:250–262.

Ehmsen JT, Ma TM, Sason H, Rosenberg D, Ogo T, Furuya S, Snyder SH, Wolosker H (2013) D-Serine in Glia and Neurons Derives from 3-Phosphoglycerate Dehydrogenase. J Neurosci 33:12464–12469.

Emsley JG, Macklis JD (2006) Astroglial heterogeneity closely reflects the neuronal-defined anatomy of the adult murine CNS. Neuron Glia Biol 2:175–186.

Ennaceur A (2010) One-trial object recognition in rats and mice: Methodological and theoretical issues. Behav Brain Res 215:244–254.

Fanselow MS, Dong H-W (2010) Are the Dorsal and Ventral Hippocampus Functionally Distinct Structures? Neuron 65:7–19.

Fell J, Axmacher N (2011) The role of phase synchronization in memory processes. Nat Rev Neurosci 12:105–118.

Fellin T, Halassa MM, Terunuma M, Succol F, Takano H, Frank M, Moss SJ, Haydon PG (2009) Endogenous nonneuronal modulators of synaptic transmission control cortical slow oscillations in vivo. Proc Natl Acad Sci 106:15037–15042.

Fellin T, Pascual O, Gobbo S, Pozzan T, Haydon PG, Carmignoto G (2004) Neuronal synchrony mediated by astrocytic glutamate through activation of extrasynaptic NMDA receptors. Neuron 43:729–743.

Fiacco TA, McCarthy KD (2004) Intracellular astrocyte calcium waves in situ increase the frequency of spontaneous AMPA receptor currents in CA1 pyramidal neurons. J Neurosci Off J Soc Neurosci 24:722–732.

Fields RD, Araque A, Johansen-Berg H, Lim S-S, Lynch G, Nave K-A, Nedergaard M, Perez R, Sejnowski T, Wake H (2014) Glial Biology in Learning and Cognition. The Neuroscientist 20:426–431.

Florian C, Vecsey CG, Halassa MM, Haydon PG, Abel T (2011) Astrocyte-Derived Adenosine and A1 Receptor Activity Contribute to Sleep Loss-Induced Deficits in Hippocampal Synaptic Plasticity and Memory in Mice. J Neurosci 31:6956–6962.

Foley JC, McIver SR, Haydon PG (2011) Gliotransmission modulates baseline mechanical nociception. Mol Pain 7:1.

Fossat P, Turpin FR, Sacchi S, Dulong J, Shi T, Rivet J-M, Sweedler JV, Pollegioni L, Millan MJ, Oliet SHR, Mothet J-P (2012) Glial D-Serine Gates NMDA Receptors at Excitatory Synapses in Prefrontal Cortex. Cereb Cortex 22:595–606.

Fujita T, Chen MJ, Li B, Smith NA, Peng W, Sun W, Toner MJ, Kress BT, Wang L, Benraiss A, Takano T, Wang S, Nedergaard M (2014) Neuronal Transgene Expression in Dominant-Negative SNARE Mice. J Neurosci 34:16594–16604.

Gao V, Suzuki A, Magistretti PJ, Lengacher S, Pollonini G, Steinman MQ, Alberini CM (2016) Astrocytic β_2-adrenergic receptors mediate hippocampal long-term memory consolidation. Proc Natl Acad Sci 113:8526–8531.

Giaume C, Koulakoff A, Roux L, Holcman D, Rouach N (2010) Astroglial networks: a step further in neuroglial and gliovascular interactions. Nat Rev Neurosci 11:87–99.

Gibbs ME, Hutchinson D, Hertz L (2008) Astrocytic involvement in learning and memory consolidation. Neurosci Biobehav Rev 32:927–944.

Gibbs ME, Shleper M, Mustafa T, Burnstock G, Bowser DN (2011) ATP derived from astrocytes modulates memory in the chick. Neuron Glia Biol 7:177–186.

Goldman SA, Nedergaard M, Windrem MS (2015) Modeling cognition and disease using human glial chimeric mice: Modeling Glial Disease. Glia 63:1483–1493.

Goldman-Rakic PS (1995) Architecture of the prefrontal cortex and the central executive. Ann N Y Acad Sci 769:71–84.

Gordon JA (2011) Oscillations and hippocampal–prefrontal synchrony. Curr Opin Neurobiol 21:486–491.

Goutagny R, Jackson J, Williams S (2009) Self-generated theta oscillations in the hippocampus. Nat Neurosci 12:1491–1493.

Graziano A, Petrosini L, Bartoletti A (2003) Automatic recognition of explorative strategies in the Morris water maze. J Neurosci Methods 130:33–44.

Guček A, Vardjan N, Zorec R (2012) Exocytosis in Astrocytes: Transmitter Release and Membrane Signal Regulation. Neurochem Res 37:2351–2363.

Guercio GD, Bevictori L, Vargas-Lopes C, Madeira C, Oliveira A, Carvalho VF, d'Avila JC, Panizzutti R (2014) d-serine prevents cognitive deficits induced by acute stress. Neuropharmacology 86:1–8.

Guillamon-Vivancos T, Gomez-Pinedo U, Matias-Guiu J (2015) Astrocytes in neurodegenerative diseases (I): Function and molecular description. Neurol Engl Ed 30:119–129.

Gundersen V, Storm-Mathisen J, Bergersen LH (2015) Neuroglial Transmission. Physiol Rev 95:695–726.

Habbas S, Santello M, Becker D, Stubbe H, Zappia G, Liaudet N, Klaus FR, Kollias G, Fontana A, Pryce CR, Suter T, Volterra A (2015) Neuroinflammatory TNFα Impairs Memory via Astrocyte Signaling. Cell 163:1730–1741.

Hahn J, Wang X, Margeta M (2015) Astrocytes increase the activity of synaptic GluN2B NMDA receptors. Front Cell Neurosci 9:117.

Haim LB, Rowitch DH (2017) Functional diversity of astrocytes in neural circuit regulation. Nat Rev Neurosci 18:31–41.

Halassa MM, Fellin T, Haydon PG (2007a) The tripartite synapse: roles for gliotransmission in health and disease. Trends Mol Med 13:54–63.

Halassa MM, Fellin T, Haydon PG (2009a) Tripartite synapses: Roles for astrocytic purines in the control of synaptic physiology and behavior. Neuropharmacology 57:343–346.

Halassa MM, Fellin T, Takano H, Dong J-H, Haydon PG (2007b) Synaptic Islands Defined by the Territory of a Single Astrocyte. J Neurosci 27:6473–6477.

Halassa MM, Florian C, Fellin T, Munoz JR, Lee S-Y, Abel T, Haydon PG, Frank MG (2009b) Astrocytic Modulation of Sleep Homeostasis and Cognitive Consequences of Sleep Loss. Neuron 61:213–219.

Hamilton NB, Attwell D (2010) Do astrocytes really exocytose neurotransmitters? Nat Rev Neurosci 11:227–238.

Han F, Xiao B, Wen L (2015a) Loss of Glial Cells of the Hippocampus in a Rat Model of Post-traumatic Stress Disorder. Neurochem Res 40:942–951.

Han H, Peng Y, Dong Z (2015b) d-Serine rescues the deficits of hippocampal long-term potentiation and learning and memory induced by sodium fluoroacetate. Pharmacol Biochem Behav 133:51–56.

Han J, Kesner P, Metna-Laurent M, Duan T, Xu L, Georges F, Koehl M, Abrous DN, Mendizabal-Zubiaga J, Grandes P, Liu Q, Bai G, Wang W, Xiong L, Ren W, Marsicano G, Zhang X (2012) Acute Cannabinoids Impair Working Memory through Astroglial CB1 Receptor Modulation of Hippocampal LTD. Cell 148:1039–1050.

Han X, Chen M, Wang F, Windrem M, Wang S, Shanz S, Xu Q, Oberheim NA, Bekar L, Betstadt S, Silva AJ, Takano T, Goldman SA, Nedergaard M (2013) Forebrain Engraftment by Human

Glial Progenitor Cells Enhances Synaptic Plasticity and Learning in Adult Mice. Cell Stem Cell 12:342–353.

Hangya B, Borhegyi Z, Szilágyi N, Freund TF, Varga V (2009) GABAergic neurons of the medial septum lead the hippocampal network during theta activity. J Neurosci Off J Soc Neurosci 29:8094–8102.

Harada K, Kamiya T, Tsuboi T (2015) Gliotransmitter Release from Astrocytes: Functional, Developmental, and Pathological Implications in the Brain. Front Neurosci 9:499.

Hashimoto A, Nishikawa T, Konno R, Niwa A, Yasumura Y, Oka T, Takahashi K (1993) Free D-serine, D-aspartate and D-alanine in central nervous system and serum in mutant mice lacking D-amino acid oxidase. Neurosci Lett 152:33–36.

Hassanpoor H, Fallah A, Raza M (2014) Mechanisms of hippocampal astrocytes mediation of spatial memory and theta rhythm by gliotransmitters and growth factors: Astrocytes, spatial memory and theta rhythm. Cell Biol Int 38:1355–1366.

Hasselmo ME, Stern CE (2014) Theta rhythm and the encoding and retrieval of space and time. NeuroImage 85:656–666.

Heller JP, Rusakov DA (2015) Morphological plasticity of astroglia: Understanding synaptic microenvironment. Glia 63:2133–2151.

Henneberger C, Papouin T, Oliet SHR, Rusakov DA (2010) Long-term potentiation depends on release of d-serine from astrocytes. Nature 463:232–236.

Hertz L (2004) The Astrocyte-Neuron Lactate Shuttle: A Challenge of a Challenge. J Cereb Blood Flow Metab 24:1241–1248.

Hertz L (2013) The Glutamate-Glutamine (GABA) Cycle: Importance of Late Postnatal Development and Potential Reciprocal Interactions between Biosynthesis and Degradation. Front Endocrinol 4:59.

Hines DJ, Haydon PG (2013) Inhibition of a SNARE-Sensitive Pathway in Astrocytes Attenuates Damage following Stroke. J Neurosci 33:4234–4240.

Hines DJ, Schmitt LI, Hines RM, Moss SJ, Haydon PG (2013) Antidepressant effects of sleep deprivation require astrocyte-dependent adenosine mediated signaling. Transl Psychiatry 3:e212.

Hoffmann LC, Cicchese JJ, Berry SD (2015) Harnessing the power of theta: natural manipulations of cognitive performance during hippocampal theta-contingent eyeblink conditioning. Front Syst Neurosci 9 Available at: http://www.ncbi.nlm.nih.gov/pmc/articles/PMC4394696/.

Hol EM, Pekny M (2015) Glial fibrillary acidic protein (GFAP) and the astrocyte intermediate filament system in diseases of the central nervous system. Curr Opin Cell Biol 32:121–130.

Horiike K, Tojo H, Arai R, Nozaki M, Maeda T (1994) d-Amino-acid oxidase is confined to the lower brain stem and cerebellum in rat brain: regional differentiation of astrocytes. Brain Res 652:297–303.

Hu X, Yuan Y, Wang D, Su Z (2016) Heterogeneous astrocytes: Active players in CNS. Brain Res Bull 125:1–18.

Huh CYL, Goutagny R, Williams S (2010) Glutamatergic neurons of the mouse medial septum and diagonal band of Broca synaptically drive hippocampal pyramidal cells: relevance for hippocampal theta rhythm. J Neurosci Off J Soc Neurosci 30:15951–15961.

Hyman JM, Hasselmo ME, Seamans JK (2011) What is the Functional Relevance of Prefrontal Cortex Entrainment to Hippocampal Theta Rhythms? Front Neurosci 5:24.

Igarashi KM (2015) Plasticity in oscillatory coupling between hippocampus and cortex. Curr Opin Neurobiol 35:163–168.

Ishiwata S, Umino A, Balu DT, Coyle JT, Nishikawa T (2015) Neuronal serine racemase regulates extracellular d-serine levels in the adult mouse hippocampus. J Neural Transm 122:1099–1103.

Jackson J, Amilhon B, Goutagny R, Bott J-B, Manseau F, Kortleven C, Bressler SL, Williams S (2014) Reversal of theta rhythm flow through intact hippocampal circuits. Nat Neurosci 17:1362–1370.

Jacobs J (2013) Hippocampal theta oscillations are slower in humans than in rodents: implications for models of spatial navigation and memory. Philos Trans R Soc B Biol Sci 369:20130304–20130304.

Jensen O, Colgin LL (2007) Cross-frequency coupling between neuronal oscillations. Trends Cogn Sci 11:267–269.

Jin J, Maren S (2015) Prefrontal-Hippocampal Interactions in Memory and Emotion. Front Syst Neurosci 9.

Jones MW, Wilson MA (2005) Theta Rhythms Coordinate Hippocampal–Prefrontal Interactions in a Spatial Memory Task Morris R, ed. PLoS Biol 3:e402.

Jones OD (2015) Astrocyte-mediated metaplasticity in the hippocampus: Help or hindrance? Neuroscience 309:113–124.

Jourdain P, Bergersen LH, Bhaukaurally K, Bezzi P, Santello M, Domercq M, Matute C, Tonello F, Gundersen V, Volterra A (2007) Glutamate exocytosis from astrocytes controls synaptic strength. Nat Neurosci 10:331–339.

Kafetzopoulos V, Kokras N, Sotiropoulos I, Oliveira JF, Leite-Almeida H, Vasalou A, Sardinha VM, Papadopoulou-Daifoti Z, Almeida OFX, Antoniou K, Sousa N, Dalla C (2017) The nucleus reuniens: a key node in the neurocircuitry of stress and depression. Mol Psychiatry.

Kandel E, Schwartz J, Jessell T, Siegelbaum S, Hudspeth AJ (2012) Principles of Neural Science, Fifth Edition. McGraw Hill Professional.

Kandel ER, Dudai Y, Mayford MR (2014) The Molecular and Systems Biology of Memory. Cell 157:163–186.

Kanemaru K, Sekiya H, Xu M, Satoh K, Kitajima N, Yoshida K, Okubo Y, Sasaki T, Moritoh S, Hasuwa H, Mimura M, Horikawa K, Matsui K, Nagai T, Iino M, Tanaka KF (2014) In Vivo Visualization of Subtle, Transient, and Local Activity of Astrocytes Using an Ultrasensitive Ca2+ Indicator. Cell Rep 8:311–318.

Kang J, Jiang L, Goldman SA, Nedergaard M (1998) Astrocyte-mediated potentiation of inhibitory synaptic transmission. Nat Neurosci 1:683–692.

Kang N, Peng H, Yu Y, Stanton PK, Guilarte TR, Kang J (2013) Astrocytes release d-serine by a large vesicle. Neuroscience 240:243–257.

Kazmierska P, Konopacki J (2013) Development of NMDA-induced theta rhythm in hippocampal formation slices. Brain Res Bull 98:93–101.

Kettenmann H, Verkhratsky A (2008) Neuroglia: the 150 years after. Trends Neurosci 31:653–659.

Khakh BS, Sofroniew MV (2015) Diversity of astrocyte functions and phenotypes in neural circuits. Nat Neurosci 18:942–952.

Kimelberg HK (2004) The problem of astrocyte identity. Neurochem Int 45:191–202.

Kimelberg HK, MacVicar BA, Sontheimer H (2006) Anion channels in astrocytes: Biophysics, pharmacology, and function. Glia 54:747–757.

Korotkova T, Fuchs EC, Ponomarenko A, von Engelhardt J, Monyer H (2010) NMDA Receptor Ablation on Parvalbumin-Positive Interneurons Impairs Hippocampal Synchrony, Spatial Representations, and Working Memory. Neuron 68:557–569.

Kowalczyk T, Bocian R, Caban B, Konopacki J (2014) Atropine-sensitive theta rhythm in the posterior hypothalamic area: In vivo and in vitro studies: Theta Rhythm in the Posterior Hypothalamic Area. Hippocampus 24:7–20.

Kowalczyk T, Konopacki J, Bocian R, Caban B (2013) Theta-related gating cells in hippocampal formation: In vivo and in vitro study. Hippocampus 23:30–39.

Kreft M, Jorgačevski J, Vardjan N, Zorec R (2016) Unproductive exocytosis. J Neurochem 137:880–889.

Kreft M, Potokar M, Stenovec M, Pangršič T, Zorec R (2009) Regulated Exocytosis and Vesicle Trafficking in Astrocytes. Ann N Y Acad Sci 1152:30–42.

Kreft M, Stenovec M, Rupnik M, Grilc S, Kržan M, Potokar M, Pangršič T, Haydon PG, Zorec R (2004) Properties of Ca2+-dependent exocytosis in cultured astrocytes. Glia 46:437–445.

Lalo U (2006) NMDA Receptors Mediate Neuron-to-Glia Signaling in Mouse Cortical Astrocytes. J Neurosci 26:2673–2683.

Lalo U, Palygin O, Rasooli-Nejad S, Andrew J, Haydon PG, Pankratov Y (2014a) Exocytosis of ATP From Astrocytes Modulates Phasic and Tonic Inhibition in the Neocortex Bacci A, ed. PLoS Biol 12:e1001747.

Lalo U, Rasooli-Nejad S, Pankratov Y (2014b) Exocytosis of gliotransmitters from cortical astrocytes: implications for synaptic plasticity and aging. Biochem Soc Trans 42:1275–1281.

Lamprecht R, LeDoux J (2004) Structural plasticity and memory. Nat Rev Neurosci 5:45–54.

Lazarewicz MT, Ehrlichman RS, Maxwell CR, Gandal MJ, Finkel LH, Siegel SJ (2010) Ketamine modulates theta and gamma oscillations. J Cogn Neurosci 22:1452–1464.

Le Bail M, Martineau M, Sacchi S, Yatsenko N, Radzishevsky I, Conrod S, Ait Ouares K, Wolosker H, Pollegioni L, Billard J-M, Mothet J-P (2015) Identity of the NMDA receptor coagonist is synapse specific and developmentally regulated in the hippocampus. Proc Natl Acad Sci U S A 112:E204-213.

Lee HS, Ghetti A, Pinto-Duarte A, Wang X, Dziewczapolski G, Galimi F, Huitron-Resendiz S, Pina-Crespo JC, Roberts AJ, Verma IM, Sejnowski TJ, Heinemann SF (2014) Astrocytes contribute to gamma oscillations and recognition memory. Proc Natl Acad Sci 111:E3343–E3352.

Lee HU, Yamazaki Y, Tanaka KF, Furuya K, Sokabe M, Hida H, Takao K, Miyakawa T, Fujii S, Ikenaka K (2013) Increased astrocytic ATP release results in enhanced excitability of the hippocampus. Glia 61:210–224.

Lee M-C, Ting KK, Adams S, Brew BJ, Chung R, Guillemin GJ (2010) Characterisation of the Expression of NMDA Receptors in Human Astrocytes White AR, ed. PLoS ONE 5:e14123.

Lega BC, Jacobs J, Kahana M (2012) Human hippocampal theta oscillations and the formation of episodic memories. Hippocampus 22:748–761.

Leger M, Quiedeville A, Bouet V, Haelewyn B, Boulouard M, Schumann-Bard P, Freret T (2013) Object recognition test in mice. Nat Protoc 8:2531–2537.

Lima A, Sardinha VM, Oliveira AF, Reis M, Mota C, Silva MA, Marques F, Cerqueira JJ, Pinto L, Sousa N, Oliveira JF (2014) Astrocyte pathology in the prefrontal cortex impairs the cognitive function of rats. Mol Psychiatry 19:834–841.

Lisman JE, Jensen O (2013) The Theta-Gamma Neural Code. Neuron 77:1002–1016.

Longair MH, Baker DA, Armstrong JD (2011) Simple Neurite Tracer: open source software for reconstruction, visualization and analysis of neuronal processes. Bioinformatics 27:2453–2454.

López-Hidalgo M, Schummers J (2014) Cortical maps: a role for astrocytes? Curr Opin Neurobiol 24:176–189.

Lubenov EV, Siapas AG (2009) Hippocampal theta oscillations are travelling waves. Nature 459:534–539.

Lushnikova I, Skibo G, Muller D, Nikonenko I (2009) Synaptic potentiation induces increased glial coverage of excitatory synapses in CA1 hippocampus. Hippocampus 19:753–762.

Malarkey EB, Parpura V (2008) Mechanisms of glutamate release from astrocytes. Neurochem Int 52:142–154.

Malarkey EB, Parpura V (2009) Mechanisms of transmitter release from astrocytes. In: Astrocytes in (Patho)Physiology of the Nervous System (Haydon PG, Parpura V, eds), pp 301–350. Boston, MA: Springer US.

Malenka RC, Bear MF (2004) LTP and LTD: An Embarrassment of Riches. Neuron 44:5–21.

Mariotti L, Losi G, Sessolo M, Marcon I, Carmignoto G (2016) The inhibitory neurotransmitter GABA evokes long-lasting Ca(2+) oscillations in cortical astrocytes. Glia 64:363–373.

Martín R, Bajo-Grañeras R, Moratalla R, Perea G, Araque A (2015) Circuit-specific signaling in astrocyte-neuron networks in basal ganglia pathways. Science 349:730–734.

Martineau M (2013) Gliotransmission: focus on exocytotic release of L-glutamate and D-serine from astrocytes. Biochem Soc Trans 41:1557–1561.

Martineau M, Parpura V, Mothet J-P (2014) Cell-type specific mechanisms of D-serine uptake and release in the brain. Front Synaptic Neurosci 6:12.

Martineau M, Shi T, Puyal J, Knolhoff AM, Dulong J, Gasnier B, Klingauf J, Sweedler JV, Jahn R, Mothet J-P (2013) Storage and Uptake of D-Serine into Astrocytic Synaptic-Like Vesicles Specify Gliotransmission. J Neurosci 33:3413–3423.

Mateus-Pinheiro A, Alves ND, Patrício P, Machado-Santos AR, Loureiro-Campos E, Silva JM, Sardinha VM, Reis J, Schorle H, Oliveira JF, Ninkovic J, Sousa N, Pinto L (2016) AP2γ controls adult hippocampal neurogenesis and modulates cognitive, but not anxiety or depressive-like behavior. Mol Psychiatry.

Matyash V, Kettenmann H (2010) Heterogeneity in astrocyte morphology and physiology. Brain Res Rev 63:2–10.

Maviel T (2004) Sites of Neocortical Reorganization Critical for Remote Spatial Memory. Science 305:96–99.

McDougle CJ, Landino SM, Vahabzadeh A, O'Rourke J, Zurcher NR, Finger BC, Palumbo ML, Helt J, Mullett JE, Hooker JM, Carlezon Jr. WA (2015) Toward an immune-mediated subtype of autism spectrum disorder. Brain Res 1617:72–92.

McIver SR, Faideau M, Haydon PG (2013) Astrocyte–Neuron Communications. In: Neural-Immune Interactions in Brain Function and Alcohol Related Disorders (Cui C, Grandison L, Noronha A, eds), pp 31–64. Boston, MA: Springer US.

Meunier CNJ, Dallérac G, Le Roux N, Sacchi S, Levasseur G, Amar M, Pollegioni L, Mothet J-P, Fossier P (2016) D-Serine and Glycine Differentially Control Neurotransmission during Visual Cortex Critical Period Tang S-J, ed. PLOS ONE 11:e0151233.

Miller SM, Piasecki CC, Lonstein JS (2011) Use of the light-dark box to compare the anxiety-related behavior of virgin and postpartum female rats. Pharmacol Biochem Behav 100:130–137.

Min R, Nevian T (2012) Astrocyte signaling controls spike timing–dependent depression at neocortical synapses. Nat Neurosci 15:746–753.

Mitra PP, Pesaran B (1999) Analysis of dynamic brain imaging data. Biophys J 76:691–708.

Mizuno K, Giese KP (2005) Hippocampus-dependent memory formation: do memory type-specific mechanisms exist? J Pharmacol Sci 98:191–197.

Molofsky AV, Kelley KW, Tsai H-H, Redmond SA, Chang SM, Madireddy L, Chan JR, Baranzini SE, Ullian EM, Rowitch DH (2014) Astrocyte-encoded positional cues maintain sensorimotor circuit integrity. Nature 509:189–194.

Montana V, Malarkey EB, Verderio C, Matteoli M, Parpura V (2006) Vesicular transmitter release from astrocytes. Glia 54:700–715.

Montana V, Verkhratsky A, Parpura V (2014) Pathological role for exocytotic glutamate release from astrocytes in hepatic encephalopathy. Curr Neuropharmacol 12:324–333.

Montero TD, Orellana JA (2015) Hemichannels: New pathways for gliotransmitter release. Neuroscience 286:45–59.

Morris R (1984) Developments of a water-maze procedure for studying spatial learning in the rat. J Neurosci Methods 11:47–60.

Mothet J-P, Le Bail M, Billard J-M (2015) Time and space profiling of NMDA receptor co-agonist functions. J Neurochem 135:210–225.

Mothet J-P, Parent AT, Wolosker H, Brady RO, Linden DJ, Ferris CD, Rogawski MA, Snyder SH (2000) D-serine is an endogenous ligand for the glycine site of the N-methyl-D-aspartate receptor. Proc Natl Acad Sci 97:4926–4931.

Mothet J-P, Pollegioni L, Ouanounou G, Martineau M, Fossier P, Baux G (2005) Glutamate receptor activation triggers a calcium-dependent and SNARE protein-dependent release of the gliotransmitter D-serine. Proc Natl Acad Sci U S A 102:5606–5611.

Mothet JP, Rouaud E, Sinet P-M, Potier B, Jouvenceau A, Dutar P, Videau C, Epelbaum J, Billard J-M (2006) A critical role for the glial-derived neuromodulator d-serine in the age-related deficits of cellular mechanisms of learning and memory. Aging Cell 5:267–274.

Nadjar A, Blutstein T, Aubert A, Laye S, Haydon PG (2013) Astrocyte-derived adenosine modulates increased sleep pressure during inflammatory response: Astrocytes Mediate Somnogenic Effects of LPS. Glia 61:724–731.

Nakashiba T, Young JZ, McHugh TJ, Buhl DL, Tonegawa S (2008) Transgenic Inhibition of Synaptic Transmission Reveals Role of CA3 Output in Hippocampal Learning. Science 319:1260–1264.

Navarrete M, Araque A (2010) Endocannabinoids Potentiate Synaptic Transmission through Stimulation of Astrocytes. Neuron 68:113–126.

Navarrete M, Araque A (2014) The Cajal school and the physiological role of astrocytes: a way of thinking. Front Neuroanat 8:33.

Navarrete M, Perea G, Maglio L, Pastor J, Garcia de Sola R, Araque A (2013) Astrocyte Calcium Signal and Gliotransmission in Human Brain Tissue. Cereb Cortex 23:1240–1246.

Newcomer JW, Krystal JH (2001) NMDA receptor regulation of memory and behavior in humans. Hippocampus 11:529–542.

Newman EA (2003) Glial Cell Inhibition of Neurons by Release of ATP. J Neurosci Off J Soc Neurosci 23:1659–1666.

Ni Y, Malarkey EB, Parpura V (2007) Vesicular release of glutamate mediates bidirectional signaling between astrocytes and neurons. J Neurochem 103:1273–1284.

Nishida H, Okabe S (2007) Direct astrocytic contacts regulate local maturation of dendritic spines. J Neurosci Off J Soc Neurosci 27:331–340.

Oberheim NA, Goldman SA, Nedergaard M (2012) Heterogeneity of astrocytic form and function. Methods Mol Biol Clifton NJ 814:23–45.

Oberheim NA, Takano T, Han X, He W, Lin JHC, Wang F, Xu Q, Wyatt JD, Pilcher W, Ojemann JG, Ransom BR, Goldman SA, Nedergaard M (2009) Uniquely Hominid Features of Adult Human Astrocytes. J Neurosci 29:3276–3287.

Oliveira JF, Dias NS, Jacinto LR, Cerqueira JJ, Sousa N (2013) Chronic stress disrupts neural coherence between cortico-limbic structures. Front Neural Circuits 7:10.

Oliveira JF, Sardinha VM, Guerra-Gomes S, Araque A, Sousa N (2015) Do stars govern our actions? Astrocyte involvement in rodent behavior. Trends Neurosci 38:535–549.

O'Neill P-K, Gordon JA, Sigurdsson T (2013) Theta Oscillations in the Medial Prefrontal Cortex Are Modulated by Spatial Working Memory and Synchronize with the Hippocampus through Its Ventral Subregion. J Neurosci 33:14211–14224.

Orr AG, Hsiao EC, Wang MM, Ho K, Kim DH, Wang X, Guo W, Kang J, Yu G-Q, Adame A, Devidze N, Dubal DB, Masliah E, Conklin BR, Mucke L (2015) Astrocytic adenosine receptor A2A and Gs-coupled signaling regulate memory. Nat Neurosci 18:423–434.

Orre M, Kamphuis W, Osborn LM, Jansen AHP, Kooijman L, Bossers K, Hol EM (2014) Isolation of glia from Alzheimer's mice reveals inflammation and dysfunction. Neurobiol Aging 35:2746–2760.

Osborn LM, Kamphuis W, Wadman WJ, Hol EM (2016) Astrogliosis: An integral player in the pathogenesis of Alzheimer's disease. Prog Neurobiol 144:121–141.

Pabst M, Braganza O, Dannenberg H, Hu W, Pothmann L, Rosen J, Mody I, van Loo K, Deisseroth K, Becker AJ, Schoch S, Beck H (2016) Astrocyte Intermediaries of Septal Cholinergic Modulation in the Hippocampus. Neuron 90:853–865.

Padilla-Coreano N, Bolkan SS, Pierce GM, Blackman DR, Hardin WD, Garcia-Garcia AL, Spellman TJ, Gordon JA (2016) Direct Ventral Hippocampal-Prefrontal Input Is Required for Anxiety-Related Neural Activity and Behavior. Neuron 89:857–866.

Panatier A, Theodosis DT, Mothet J-P, Touquet B, Pollegioni L, Poulain DA, Oliet SHR (2006) Glia-Derived d-Serine Controls NMDA Receptor Activity and Synaptic Memory. Cell 125:775–784.

Panatier A, Vallée J, Haber M, Murai KK, Lacaille J-C, Robitaille R (2011) Astrocytes Are Endogenous Regulators of Basal Transmission at Central Synapses. Cell 146:785–798.

Pankratov Y, Lalo U (2015) Role for astroglial α1-adrenoreceptors in gliotransmission and control of synaptic plasticity in the neocortex. Front Cell Neurosci 9:230.

Pannasch U, Rouach N (2013) Emerging role for astroglial networks in information processing: from synapse to behavior. Trends Neurosci 36:405–417.

Pannasch U, Vargova L, Reingruber J, Ezan P, Holcman D, Giaume C, Sykova E, Rouach N (2011) Astroglial networks scale synaptic activity and plasticity. Proc Natl Acad Sci 108:8467–8472.

Papouin T, Dunphy JM, Tolman M, Dineley KT, Haydon PG (2017a) Septal Cholinergic Neuromodulation Tunes the Astrocyte-Dependent Gating of Hippocampal NMDA Receptors to Wakefulness. Neuron 94:840–854.e7.

Papouin T, Henneberger C, Rusakov DA, Oliet SHR (2017b) Astroglial versus Neuronal D-Serine: Fact Checking. Trends Neurosci 0.

Papouin T, Ladépêche L, Ruel J, Sacchi S, Labasque M, Hanini M, Groc L, Pollegioni L, Mothet J-P, Oliet SHR (2012) Synaptic and Extrasynaptic NMDA Receptors Are Gated by Different Endogenous Coagonists. Cell 150:633–646.

Parent MA, Wang L, Su J, Netoff T, Yuan L-L (2010) Identification of the Hippocampal Input to Medial Prefrontal Cortex In Vitro. Cereb Cortex 20:393–403.

Park H, Han K-S, Oh S-J, Jo S, Woo J, Yoon B-E, Lee CJ (2013) High glutamate permeability and distal localization of Best1 channel in CA1 hippocampal astrocyte. Mol Brain 6:54.

Park HK (2006) Potential Role for Astroglial D-Amino Acid Oxidase in Extracellular D-Serine Metabolism and Cytotoxicity. J Biochem (Tokyo) 139:295–304.

Parpura V, Grubišić V, Verkhratsky A (2011) Ca2+ sources for the exocytotic release of glutamate from astrocytes. Biochim Biophys Acta BBA - Mol Cell Res 1813:984–991.

Parpura V, Haydon PG (2000) Physiological astrocytic calcium levels stimulate glutamate release to modulate adjacent neurons. Proc Natl Acad Sci 97:8629–8634.

Parpura V, Heneka MT, Montana V, Oliet SHR, Schousboe A, Haydon PG, Stout RF, Spray DC, Reichenbach A, Pannicke T, Pekny M, Pekna M, Zorec R, Verkhratsky A (2012) Glial cells in (patho)physiology: Glial cells in (patho)physiology. J Neurochem 121:4–27.

Parpura V, Zorec R (2010) Gliotransmission: Exocytotic release from astrocytes. Brain Res Rev 63:83–92.

Pascual O, Casper KB, Kubera C, Zhang J, Revilla-Sanchez R, Sul J-Y, Takano H, Moss SJ, McCarthy K, Haydon PG (2005) Astrocytic purinergic signaling coordinates synaptic networks. Science 310:113–116.

Paxinos G, Franklin KBJ (2004) The Mouse Brain in Stereotaxic Coordinates. Gulf Professional Publishing.

Pekny M, Pekna M, Messing A, Steinhäuser C, Lee J-M, Parpura V, Hol EM, Sofroniew MV, Verkhratsky A (2016) Astrocytes: a central element in neurological diseases. Acta Neuropathol (Berl) 131:323–345.

Pellerin L, Magistretti PJ (2012) Sweet Sixteen for ANLS. J Cereb Blood Flow Metab 32:1152–1166.

Pellizzari R, Rossetto O, Schiavo G, Montecucco C (1999) Tetanus and botulinum neurotoxins: mechanism of action and therapeutic uses. Philos Trans R Soc Lond B Biol Sci 354:259–268.

Peng L, Verkhratsky A, Gu L, Li B (2015) Targeting astrocytes in major depression. Expert Rev Neurother 15:1299–1306.

Perea G, Araque A (2007) Astrocytes potentiate transmitter release at single hippocampal synapses. Science 317:1083–1086.

Perea G, Gómez R, Mederos S, Covelo A, Ballesteros JJ, Schlosser L, Hernández-Vivanco A, Martín-Fernández M, Quintana R, Rayan A, Díez A, Fuenzalida M, Agarwal A, Bergles DE, Bettler B, Manahan-Vaughan D, Martín ED, Kirchhoff F, Araque A (2016) Activity-dependent switch of GABAergic inhibition into glutamatergic excitation in astrocyte-neuron networks. eLife 5.

Perea G, Navarrete M, Araque A (2009) Tripartite synapses: astrocytes process and control synaptic information. Trends Neurosci 32:421–431.

Perea G, Sur M, Araque A (2014) Neuron-glia networks: integral gear of brain function. Front Cell Neurosci 8:378.

Perez-Alvarez A, Navarrete M, Covelo A, Martin ED, Araque A (2014) Structural and functional plasticity of astrocyte processes and dendritic spine interactions. J Neurosci Off J Soc Neurosci 34:12738–12744.

Pernot P, Maucler C, Tholance Y, Vasylieva N, Debilly G, Pollegioni L, Cespuglio R, Marinesco S (2012) d-Serine diffusion through the blood–brain barrier: Effect on d-serine compartmentalization and storage. Neurochem Int 60:837–845.

Petit-Demouliere B, Chenu F, Bourin M (2004) Forced swimming test in mice: a review of antidepressant activity. Psychopharmacology (Berl) 177:245–255.

Petralia RS, Al-Hallaq RA, Wenthold RJ (2009) Trafficking and Targeting of NMDA Receptors. In: Biology of the NMDA Receptor (Van Dongen AM, ed) Frontiers in Neuroscience. Boca Raton (FL): CRC Press/Taylor & Francis.

Petrelli F, Bezzi P (2016) Novel insights into gliotransmitters. Curr Opin Pharmacol 26:138–145.

Pfrieger FW (2010) Role of glial cells in the formation and maintenance of synapses. Brain Res Rev 63:39–46.

Pfrieger FW, Slezak M (2012) Genetic approaches to study glial cells in the rodent brain. Glia 60:681–701.

Pilone MS (2000) D-Amino acid oxidase: new findings. Cell Mol Life Sci CMLS 57:1732–1747.

Poskanzer KE, Yuste R (2016) Astrocytes regulate cortical state switching in vivo. Proc Natl Acad Sci 113:E2675–E2684.

Potokar M, Kreft M, Li L, Daniel Andersson J, Pangršič T, Chowdhury HH, Pekny M, Zorec R (2007) Cytoskeleton and Vesicle Mobility in Astrocytes. Traffic 8:12–20.

Preston AR, Eichenbaum H (2013) Interplay of Hippocampus and Prefrontal Cortex in Memory. Curr Biol 23:R764–R773.

Prut L, Belzung C (2003) The open field as a paradigm to measure the effects of drugs on anxiety-like behaviors: a review. Eur J Pharmacol 463:3–33.

Purves D, Williams SM eds. (2004) Neuroscience, 3. ed. Sunderland, Mass: Sinauer.

Reichenbach A, Derouiche A, Kirchhoff F (2010) Morphology and dynamics of perisynaptic glia. Brain Res Rev 63:11–25.

Robinson J, Manseau F, Ducharme G, Amilhon B, Vigneault E, El Mestikawy S, Williams S (2016) Optogenetic Activation of Septal Glutamatergic Neurons Drive Hippocampal Theta Rhythms. J Neurosci Off J Soc Neurosci 36:3016–3023.

Ropert N, Jalil A, Li D (2016) Expression and cellular function of vSNARE proteins in brain astrocytes. Neuroscience 323:76–83.

Rosenberg D, Kartvelishvily E, Shleper M, Klinker CMC, Bowser MT, Wolosker H (2010) Neuronal release of D-serine: a physiological pathway controlling extracellular D-serine concentration. FASEB J 24:2951–2961.

Rowitch DH, Kriegstein AR (2010) Developmental genetics of vertebrate glial–cell specification. Nature 468:214–222.

Rusakov DA, Bard L, Stewart MG, Henneberger C (2014) Diversity of astroglial functions alludes to subcellular specialisation. Trends Neurosci 37:228–242.

Sahlender DA, Savtchouk I, Volterra A (2014) What do we know about gliotransmitter release from astrocytes? Philos Trans R Soc B Biol Sci 369:20130592–20130592.

Santello M, Bezzi P, Volterra A (2011) TNFα Controls Glutamatergic Gliotransmission in the Hippocampal Dentate Gyrus. Neuron 69:988–1001.

Sargin D, Botly LCP, Higgs G, Marsolais A, Frankland PW, Egan SE, Josselyn SA (2013) Disrupting Jagged1–Notch signaling impairs spatial memory formation in adult mice. Neurobiol Learn Mem 103:39–49.

Schmitt LI, Sims RE, Dale N, Haydon PG (2012) Wakefulness Affects Synaptic and Network Activity by Increasing Extracellular Astrocyte-Derived Adenosine. J Neurosci 32:4417–4425.

Schoch S (2001) SNARE Function Analyzed in Synaptobrevin/VAMP Knockout Mice. Science 294:1117–1122.

Schubert V, Bouvier D, Volterra A (2011) SNARE protein expression in synaptic terminals and astrocytes in the adult hippocampus: A comparative analysis. Glia 59:1472–1488.

Seibenhener ML, Wooten MC (2015) Use of the Open Field Maze to measure locomotor and anxiety-like behavior in mice. J Vis Exp JoVE:e52434.

Sharma S, Rakoczy S, Brown-Borg H (2010) Assessment of spatial memory in mice. Life Sci 87:521–536.

Shigetomi E, Jackson-Weaver O, Huckstepp RT, O'Dell TJ, Khakh BS (2013) TRPA1 Channels Are Regulators of Astrocyte Basal Calcium Levels and Long-Term Potentiation via Constitutive d-Serine Release. J Neurosci 33:10143–10153.

Siapas AG, Lubenov EV, Wilson MA (2005) Prefrontal Phase Locking to Hippocampal Theta Oscillations. Neuron 46:141–151.

Sibille J, Zapata J, Teillon J, Rouach N (2015) Astroglial calcium signaling displays short-term plasticity and adjusts synaptic efficacy. Front Cell Neurosci 9:189.

Sigurdsson T, Stark KL, Karayiorgou M, Gogos JA, Gordon JA (2010) Impaired hippocampal–prefrontal synchrony in a genetic mouse model of schizophrenia. Nature 464:763–767.

Singh P, Jorgačevski J, Kreft M, Grubišić V, Stout RF, Potokar M, Parpura V, Zorec R (2014) Single-vesicle architecture of synaptobrevin2 in astrocytes. Nat Commun 5:3780.

Sofroniew MV (2015) Astrogliosis. Cold Spring Harb Perspect Biol 7:a020420.

Sofroniew MV, Vinters HV (2010) Astrocytes: biology and pathology. Acta Neuropathol (Berl) 119:7–35.

Spellman T, Rigotti M, Ahmari SE, Fusi S, Gogos JA, Gordon JA (2015) Hippocampal–prefrontal input supports spatial encoding in working memory. Nature 522:309–314.

Srinivasan R, Huang BS, Venugopal S, Johnston AD, Chai H, Zeng H, Golshani P, Khakh BS (2015) Ca2+ signaling in astrocytes from Ip3r2−/− mice in brain slices and during startle responses in vivo. Nat Neurosci 18:708–717.

Stellwagen D, Malenka RC (2006) Synaptic scaling mediated by glial TNF-α. Nature 440:1054–1059.

Sultan S, Li L, Moss J, Petrelli F, Cassé F, Gebara E, Lopatar J, Pfrieger FW, Bezzi P, Bischofberger J, Toni N (2015) Synaptic Integration of Adult-Born Hippocampal Neurons Is Locally Controlled by Astrocytes. Neuron 88:957–972.

Sun W, McConnell E, Pare J-F, Xu Q, Chen M, Peng W, Lovatt D, Han X, Smith Y, Nedergaard M (2013) Glutamate-dependent neuroglial calcium signaling differs between young and adult brain. Science 339:197–200.

Suzuki A, Stern SA, Bozdagi O, Huntley GW, Walker RH, Magistretti PJ, Alberini CM (2011) Astrocyte-Neuron Lactate Transport Is Required for Long-Term Memory Formation. Cell 144:810–823.

Suzuki M, Sasabe J, Miyoshi Y, Kuwasako K, Muto Y, Hamase K, Matsuoka M, Imanishi N, Aiso S (2015) Glycolytic flux controls d-serine synthesis through glyceraldehyde-3-phosphate dehydrogenase in astrocytes. Proc Natl Acad Sci 112:E2217–E2224.

Takao K, Miyakawa T (2006) Light/dark transition test for mice. J Vis Exp JoVE:104.

Takata N, Mishima T, Hisatsune C, Nagai T, Ebisui E, Mikoshiba K, Hirase H (2011) Astrocyte Calcium Signaling Transforms Cholinergic Modulation to Cortical Plasticity In Vivo. J Neurosci 31:18155–18165.

Tanaka M, Shih P-Y, Gomi H, Yoshida T, Nakai J, Ando R, Furuichi T, Mikoshiba K, Semyanov A, Itohara S (2013) Astrocytic Ca 2+ signals are required for the functional integrity of tripartite synapses. Mol Brain 6:6.

Tang F, Lane S, Korsak A, Paton JFR, Gourine AV, Kasparov S, Teschemacher AG (2014) Lactate-mediated glia-neuronal signalling in the mammalian brain. Nat Commun 5:3284.

Tang W, Szokol K, Jensen V, Enger R, Trivedi CA, Hvalby O, Helm PJ, Looger LL, Sprengel R, Nagelhus EA (2015) Stimulation-Evoked Ca2+ Signals in Astrocytic Processes at Hippocampal CA3-CA1 Synapses of Adult Mice Are Modulated by Glutamate and ATP. J Neurosci 35:3016–3021.

Tatem KS, Quinn JL, Phadke A, Yu Q, Gordish-Dressman H, Nagaraju K (2014) Behavioral and locomotor measurements using an open field activity monitoring system for skeletal muscle diseases. J Vis Exp JoVE:51785.

Tavares G, Martins M, Correia JS, Sardinha VM, Guerra-Gomes S, das Neves SP, Marques F, Sousa N, Oliveira JF (2016) Employing an open-source tool to assess astrocyte tridimensional structure. Brain Struct Funct.

Terry AV (2009) Spatial Navigation (Water Maze) Tasks. In: Methods of Behavior Analysis in Neuroscience, 2nd ed. (Buccafusco JJ, ed) Frontiers in Neuroscience. Boca Raton (FL): CRC Press/Taylor & Francis.

Tewari SG, Parpura V (2015) Astrocytes Modulate Local Field Potential Rhythm. Front Integr Neurosci 9:69.

Theodosis DT, Poulain DA, Oliet SHR (2008) Activity-Dependent Structural and Functional Plasticity of Astrocyte-Neuron Interactions. Physiol Rev 88:983–1008.

Thorn P, Zorec R, Rettig J, Keating DJ (2016) Exocytosis in non-neuronal cells. J Neurochem 137:849–859.

Tierney PL, Degenetais E, Thierry A-M, Glowinski J, Gioanni Y (2004) Influence of the hippocampus on interneurons of the rat prefrontal cortex. Eur J Neurosci 20:514–524.

Trkov S, Stenovec M, Kreft M, Potokar M, Parpura V, Davletov B, Zorec R (2012) Fingolimod—A Sphingosine-Like Molecule Inhibits Vesicle Mobility and Secretion in Astrocytes. Glia 60:1406–1416.

Turner JR, Ecke LE, Briand LA, Haydon PG, Blendy JA (2013) Cocaine-related behaviors in mice with deficient gliotransmission. Psychopharmacology (Berl) 226:167–176.

Tynan RJ, Beynon SB, Hinwood M, Johnson SJ, Nilsson M, Woods JJ, Walker FR (2013) Chronic stress-induced disruption of the astrocyte network is driven by structural atrophy and not loss of astrocytes. Acta Neuropathol (Berl) 126:75–91.

Ujfalussy B, Kiss T (2006) How do glutamatergic and GABAergic cells contribute to synchronization in the medial septum? J Comput Neurosci 21:343–357.

Van Dijk BJ, Vergouwen MDI, Kelfkens MM, Rinkel GJE, Hol EM (2016) Glial cell response after aneurysmal subarachnoid hemorrhage — Functional consequences and clinical implications. Biochim Biophys Acta BBA - Mol Basis Dis 1862:492–505.

Van Horn MR, Sild M, Ruthazer ES (2013) D-serine as a gliotransmitter and its roles in brain development and disease. Front Cell Neurosci 7:39.

Vardjan N, Parpura V, Zorec R (2016) Loose excitation-secretion coupling in astrocytes. Glia 64:655–667.

Vardjan N, Verkhratsky A, Zorec R (2015) Pathologic Potential of Astrocytic Vesicle Traffic: New Targets to Treat Neurologic Diseases? Cell Transplant 24:599–612.

Verkhratsky A, Matteoli M, Parpura V, Mothet J-P, Zorec R (2016) Astrocytes as secretory cells of the central nervous system: idiosyncrasies of vesicular secretion. EMBO J 35:239–257.

Verkhratsky A, Nedergaard M, Hertz L (2015) Why are Astrocytes Important? Neurochem Res 40:389–401.

Verkhratsky A, Rodríguez JJ, Parpura V (2012) Neurotransmitters and Integration in Neuronal-Astroglial Networks. Neurochem Res 37:2326–2338.

Verrall L, Walker M, Rawlings N, Benzel I, Kew JNC, Harrison PJ, Burnet PWJ (2007) d-Amino acid oxidase and serine racemase in human brain: normal distribution and altered expression in schizophrenia: DAO and SRR in normal and schizophrenic brain. Eur J Neurosci 26:1657–1669.

Virginio C, MacKenzie A, Rassendren FA, North RA, Surprenant A (1999) Pore dilation of neuronal P2X receptor channels. Nat Neurosci 2:315–321.

Wagner B, Natarajan A, Grünaug S, Kroismayr R, Wagner EF, Sibilia M (2006) Neuronal survival depends on EGFR signaling in cortical but not midbrain astrocytes. EMBO J 25:752–762.

Wagner L, Pannicke T, Rupprecht V, Frommherz I, Volz C, Illes P, Hirrlinger J, Jägle H, Egger V, Haydon PG, Pfrieger FW, Grosche A (2017) Suppression of SNARE-dependent exocytosis in retinal glial cells and its effect on ischemia-induced neurodegeneration. Glia 65:1059–1071.

Walf AA, Frye CA (2007) The use of the elevated plus maze as an assay of anxiety-related behavior in rodents. Nat Protoc 2:322–328.

Wang DD, Bordey A (2008) The astrocyte odyssey. Prog Neurobiol 86:342–367.

Watrous AJ, Lee DJ, Izadi A, Gurkoff GG, Shahlaie K, Ekstrom AD (2013) A comparative study of human and rat hippocampal low frequency oscillations during spatial navigation. Hippocampus 23:656–661.

Watson C, Kirkcaldie M, Paxinos G (2010) The Brain: An Introduction to Functional Neuroanatomy. Academic Press.

Weber T, Zemelman BV, McNew JA, Westermann B, Gmachl M, Parlati F, Söllner TH, Rothman JE (1998) SNAREpins: minimal machinery for membrane fusion. Cell 92:759–772.

Winson J (1978) Loss of hippocampal theta rhythm results in spatial memory deficit in the rat. Science 201:160–163.

Wolosker H (2007) NMDA receptor regulation by D-serine: new findings and perspectives. Mol Neurobiol 36:152–164.

Wolosker H (2011) Serine racemase and the serine shuttle between neurons and astrocytes. Biochim Biophys Acta BBA - Proteins Proteomics 1814:1558–1566.

Wolosker H, Balu DT, Coyle JT (2016) The Rise and Fall of the d-Serine-Mediated Gliotransmission Hypothesis. Trends Neurosci 39:712–721.

Xu X, An L, Mi X, Zhang T (2013) Impairment of Cognitive Function and Synaptic Plasticity Associated with Alteration of Information Flow in Theta and Gamma Oscillations in Melamine-Treated Rats Boraud T, ed. PLoS ONE 8:e77796.

Yang J, Yang H, Liu Y, Li X, Qin L, Lou H, Duan S, Wang H (2016) Astrocytes contribute to synapse elimination via type 2 inositol 1, 4, 5-trisphosphate receptor-dependent release of ATP. eLife 5:e15043.

Yang Y, Ge W, Chen Y, Zhang Z, Shen W, Wu C, Poo M, Duan S (2003) Contribution of astrocytes to hippocampal long-term potentiation through release of D-serine. Proc Natl Acad Sci 100:15194–15199.

Ye Z-C, Wyeth MS, Baltan-Tekkok S, Ransom BR (2003) Functional Hemichannels in Astrocytes: A Novel Mechanism of Glutamate Release. J Neurosci 23:3588–3596.

Yoon B-E, Lee CJ (2014) GABA as a rising gliotransmitter. Front Neural Circuits 8:141.

Yoshikawa T, Watanabe A, Ishitsuka Y, Nakaya A, Nakatani N (2002) Identification of Multiple Genetic Loci Linked to the Propensity for "Behavioral Despair" in Mice. Genome Res 12:357–366.

Zhan Y (2015) Theta frequency prefrontal–hippocampal driving relationship during free exploration in mice. Neuroscience 300:554–565.

Zhang J, Wang H, Ye C, Ge W, Chen Y, Jiang Z, Wu C, Poo M, Duan S (2003) ATP Released by Astrocytes Mediates Glutamatergic Activity-Dependent Heterosynaptic Suppression. Neuron 40:971–982.

Zhang Q, Haydon PG (2005) Roles for gliotransmission in the nervous system. J Neural Transm 112:121–125.

Zhang Q, Pangrsic T, Kreft M, Krzan M, Li N, Sul J-Y, Halassa M, Van Bockstaele E, Zorec R, Haydon PG (2004) Fusion-related Release of Glutamate from Astrocytes. J Biol Chem 279:12724–12733.

Zhang Y, Barres BA (2010) Astrocyte heterogeneity: an underappreciated topic in neurobiology. Curr Opin Neurobiol 20:588–594.

Zhang Z, Gong N, Wang W, Xu L, Xu T-L (2008) Bell-Shaped D-Serine Actions on Hippocampal Long-Term Depression and Spatial Memory Retrieval. Cereb Cortex 18:2391–2401.

Zhou M, Xu G, Xie M, Zhang X, Schools GP, Ma L, Kimelberg HK, Chen H (2009) TWIK-1 and TREK-1 Are Potassium Channels Contributing Significantly to Astrocyte Passive Conductance in Rat Hippocampal Slices. J Neurosci 29:8551–8564.

Ziak D, Chvátal A, Syková E (1998) Glutamate-, kainate- and NMDA-evoked membrane currents in identified glial cells in rat spinal cord slice. Physiol Res Acad Sci Bohemoslov 47:365–375.

Zorec R, Araque A, Carmignoto G, Haydon PG, Verkhratsky A, Parpura V (2012) Astroglial excitability and gliotransmission: an appraisal of Ca2+ as a signalling route. ASN Neuro 4.

Zorec R, Verkhratsky A, Rodríguez JJ, Parpura V (2016) Astrocytic vesicles and gliotransmitters: Slowness of vesicular release and synaptobrevin2-laden vesicle nanoarchitecture. Neuroscience 323:67–75.

ANNEXES

GLIA WILEY

RESEARCH ARTICLE

Astrocytic signaling supports hippocampal–prefrontal theta synchronization and cognitive function

Vanessa Morais Sardinha[1,2] | Sónia Guerra-Gomes[1,2] | Inês Caetano[1,2] |

Gabriela Tavares[1,2] | Manuella Martins[1,2] | Joana Santos Reis[1,2] |

Joana Sofia Correia[1,2] | Andreia Teixeira-Castro[1,2] | Luísa Pinto[1,2] |

Nuno Sousa[1,2] | João Filipe Oliveira[1,2,3]

[1]Life and Health Sciences Research Institute (ICVS), School of Medicine, University of Minho, Campus Gualtar, Braga 4710-057, Portugal

[2]ICVS/3B's-PT Government Associate Laboratory, Braga/Guimarães, Portugal

[3]DIGARC, Polytechnic Institute of Cávado and Ave, Barcelos 4750-810, Portugal

Correspondence
João Filipe Pedreira de Oliveira, Life and Health Sciences Research Institute (ICVS), School of Medicine, University of Minho, Campus de Gualtar, 4710-057 Braga, Portugal. Email: joaooliveira@med.uminho.pt

Abstract

Astrocytes interact with neurons at the cellular level through modulation of synaptic formation, maturation, and function, but the impact of such interaction into behavior remains unclear. Here, we studied the dominant negative SNARE (dnSNARE) mouse model to dissect the role of astrocyte-derived signaling in corticolimbic circuits, with implications for cognitive processing. We found that the blockade of gliotransmitter release in astrocytes triggers a critical desynchronization of neural theta oscillations between dorsal hippocampus and prefrontal cortex. Moreover, we found a strong cognitive impairment in tasks depending on this network. Importantly, the supplementation with D-serine completely restores hippocampal–prefrontal theta synchronization and rescues the spatial memory and long-term memory of dnSNARE mice. We provide here novel evidence of long distance network modulation by astrocytes, with direct implications to cognitive function.

KEYWORDS

astrocyte, behavior, local field potential, neuronal morphology, oscillations

1 | INTRODUCTION

Brain networks display a high degree of complexity that supports behavior. This complexity relies on functional, morphological and molecular features of neurons and glial cells that integrate them. Among the glial cells, astrocytes maintain with neurons a dialogue that was shown to underlie the functional modulation of brain networks. In this dialogue, astrocytes are able to sense and process neuronal information and reply back to neurons, due to the close apposition at neuronal synapses of thin processes endowed with neurotransmitter receptors (Araque et al.,

2014; Clarke & Barres, 2013; Khakh & Sofroniew, 2015; Pannasch et al., 2014), to the development of complex calcium signaling in subcellular compartments (Haydon & Nedergaard, 2015; Perea, Sur, & Araque, 2014; Rusakov, 2015; Volterra, Liaudet, & Savtchouk, 2014), and to the controlled release of neuroactive substances (Araque et al., 2014; Perea et al., 2014; Petrelli & Bezzi, 2016). Particularly, the release of active molecules by astrocytes, a process named gliotransmission, has been critically appraised and extensively described (Araque et al., 2014; Petrelli & Bezzi, 2016; Verkhratsky, Matteoli, Parpura, Mothet, & Zorec, 2016). Gliotransmitters such as ATP, glutamate or D-serine were shown

to modulate the strength of neighboring synapses with functional consequences to the network output. In particular, D-serine, a potent NMDA-receptor co-agonist, was related to synaptic structure and function (Bail et al., 2015; Miller, 2004). This effect was described not only for neuron-derived (Balu & Coyle, 2012; Rosenberg et al., 2013), but also for astrocyte-derived D-serine. The latter is thought to represent the major source of D-serine (Kang et al., 2013; Martineau et al., 2013; Martineau, Galli, Baux, & Mothet, 2008; Oliet & Mothet, 2006; Papouin, Dunphy, Tolman, Dineley, & Haydon, 2017; Yang et al., 2003), and is critical for the maintenance of hippocampal synaptic plasticity (Fellin et al., 2009; Han, Peng, & Dong, 2015; Henneberger, Papouin, Oliet, & Rusakov, 2010; Martineau et al., 2013) and for dendritic maturation of newly-born neurons in the hippocampus (Sultan et al., 2015).

This neuron–astrocyte dialogue at the synaptic level should in turn be reflected in network outputs. In fact, a number of strategies have been employed to tackle the involvement of astrocytes on the computation of several behavioral dimensions, namely on cognition (Oliveira, Sardinha, Guerra-Gomes, Araque, & Sousa, 2015). However, the putative involvement of astrocytes in cognitive modulation remains unclear, mostly due to the current knowledge gap between cellular interactions and behavior levels. To address this issue, we have designed an approach to assess the role of astrocyte signaling in corticolimbic circuits involved in cognitive processing. For that we analyzed the hippocampus-prefrontal cortex electrophysiological synchrony and related cognitive computation in dominant negative SNARE (dnSNARE) mouse model of astrocyte-specific exocytosis impairment (Halassa et al., 2009; Pascual et al., 2005; Sultan et al., 2015). Within the hippocampus, cognitive functions rely primarily on the dorsal subregion (Fanselow & Dong, 2010). Despite its indirect connection to the prefrontal cortex (Preston & Eichenbaum, 2013), oscillations of the dorsal hippocampus highly synchronize with units and ensembles in the prefrontal cortex to support cognitive tasks, such as spatial learning and memory processing (Gordon, 2011; Jones & Wilson, 2005; O'Neill, Gordon, & Sigurdsson, 2013). Taking advantage of the specific dnSNARE transgene expression in astrocytes of the hippocampus and cortex (Pascual et al., 2005; Sultan et al., 2015), which causes a decrease of extracellular D-serine levels in those brain regions (Sultan et al., 2015), we analyzed electrophysiology fingerprints of the hippocampus–prefrontal cortex network, carried out a battery of cognitive tests and histological/molecular correlates to confirm the involvement of astrocytic signaling in cognitive function.

2 | MATERIALS AND METHODS

2.1 | Animals

All experimental procedures were conducted in accordance with the guidelines for welfare of laboratory animals, as described in the Directive 2010/63/EU, and were approved by the local ethical committee (SECVS 075/2015) and national authority for animal experimentation (DGAV). The generation of dominant-negative SNARE (dnSNARE) mice of gliotransmission impairment was performed as previously described (Pascual et al., 2005). The dnSNARE mice and respective wild-type littermates were obtained by crossing two transgenic mouse lines:

GFAP-tTA, in which the expression of tetracycline transactivator (tTA) is mediated by the astrocyte-specific human glial fibrillary acidic protein (hGFAP) promoter; tetO.dnSNARE, in which the dominant-negative domain of vesicular SNARE VAMP2/synaptobrevin II, as well as the reporter enhanced green fluorescence protein (EGFP) are coexpressed under the control of the tetO promoter. Developmental expression of dnSNARE was prevented by breeding the animals in the presence of doxycycline (Dox, Sigma-Aldrich) in the drinking water (100 μg/mL; water bottles covered with aluminum foil to avoid light exposure), which was removed 6 weeks before the beginning of the behavior experiments. The conditional expression of the dnSNARE transgenes caused interference with the SNARE complex formation and consecutive blockade of exocytosis specifically in astrocytes (astrocytes derived from dnSNARE mice displayed a 91% reduction in the number of fusion events) (Sultan et al., 2015), impairing the vesicular release of gliotransmitters. Founders of both mice lines were kindly supplied by Prof. Philip Haydon (Tufts University, USA), and were maintained in the C57Bl6/J genetic background. All mice had *ad libitum* access to food and water in their home cages (max 5 mice per cage) and lights were maintained on a 12 h light/dark cycle (lights on 8:00 A.M. to 8:00 P.M.). Male mice within ten to 12 weeks-old were used. Their genotype was confirmed by PCR: mice negative (wild-type) or positive for both transgenes (dnSNARE) were tested, while mice expressing single transgenes (GFAP-tTA or tetO.dnSNARE) were not included. Mice of both genotypes are visually indistinguishable and were kept in the housing cages mixed. Each mouse received a numbered tag which remained constant throughout the experiment and allowed to perform the complete behavior, electrophysiological, histological, and molecular analysis in a blind manner.

2.2 | *In vivo* electrophysiology

Surgical procedures, acquisition, and analysis of local field potential (LFP) signals from the medial prefrontal cortex (mPFC) and dorsal hippocampus (dHIP) were performed as previously described (Oliveira, Dias, Jacinto, Cerqueira, & Sousa, 2013).

Mice were anesthetized with sevofluorane (4%, SevoFlo, Abbott, USA) and the body temperature controlled and maintained at 37°C by a homoeothermic blanket (Stoelting, Ireland). When deeply anesthetized each animal was mounted on the stereotaxic apparatus (KOPF, USA). To avoid local pain during the surgery, Lidocaine (2%, B. Braun, Germany) was injected subcutaneously in the area of incision. The eyes were covered with an ophthalmic cream (Duratears Z, Alcon, USA) to avoid dehydration. Experimental procedures for electrode implantation were described previously (Oliveira et al., 2013). Briefly, concentric platinum/iridium recording electrodes (400 μm shaft diameter; Science Products, Germany) were placed in the prelimbic area (PL) of the mPFC (coordinates: 1.94 mm anterior to bregma, 0.4 mm lateral to the midline, 2.5 mm below bregma), and in CA1 of dHIP (coordinates: 1.94 mm posterior to bregma, 1.2 mm lateral to the midline, 1.5 mm below bregma), according to the mouse brain atlas (Paxinos & Franklin, 2001). A stainless-steel screw was placed above the contralateral hemisphere and used as reference electrode.

Local field potential (LFP) signals from the mPFC and dHIP were acquired and analyzed as previously described (Oliveira et al., 2013). These signals were simultaneously amplified, filtered (5000×; 0.1–300 Hz; LP511 Grass Amplifier, Natus, USA), acquired (Micro 1401mkII, CED, UK) and recorded on a personal computer running Signal Software (CED, UK). After surgery and a resting period of 20 min, 100 s of local field activity were recorded at the sampling rate of 1000 Hz. The power of PFC and dHIP regions, as well as the coherence assessment between both regions, were performed on LFP signals acquired for each mouse. Each measure was applied on 1 s long segments and the average of all segments was considered for statistical analysis. All LFP recordings were thoroughly inspected and those that presented significant noise corruption were excluded from further analyses. Power and coherence were calculated with custom-written MATLAB-based programs and scripts (MathWorks, USA), using the Chronux toolbox (http://www.chronux.org) (Mitra & Pesaran, 1999), for all frequencies from 4 to 40 Hz. For power quantification, the squared magnitude of Fourier data was evaluated, across the frequency domain for each brain region. Coherence analysis was based on multi-taper analysis of the signal magnitude for both regions. For group comparison, three frequency bands were analyzed based on previously described functional relevance: theta (4–12 Hz); beta (12–20 Hz); low gamma (20–40 Hz).

After the electrophysiological protocol, animals were euthanized with a lethal dose of sodium pentobarbital (150 mg/kg, i.p). A biphasic stimulus (5 s, 0.7 mA for mPFC, and 0.8 mA for dHIP) was delivered to both electrodes in order to mark the local of recording. Brains were carefully removed and the left hemisphere (electrodes location) was immersed in paraformaldehyde 4% (PFA) in PBS (0.1M, pH 7.4) for tissue fixation. One day after, it was sectioned in 50 μm slices using a vibratome (Leica Biosystems, Germany) and processed with cresyl violet staining to identify the electrolytic lesion at the recording sites. Whenever at least one of the electrodes was wrongly positioned in the targeted region, mice were discarded from the analysis (about 15% of the recordings). The right hemisphere was macrodissected and cryopreserved for molecular analysis.

2.3 | Behavior

Mice were tested during the light phase. Prior to experimentation, mice were handled daily for 5 min, throughout 1 week, and habituation to testing rooms was performed 1 h before the beginning of each test.

2.3.1 | Morris water maze

Morris water maze (MWM) was used to assess spatial reference memory, slightly modified from Lima et al. (2014). The test was conducted under dim light in a dark circular pool (106 cm diameter) filled with water at 23°C ± 1°C, with extrinsic visual cues (square, triangle, horizontal stripes, and cross). In order to increase the contrast to detect the mice, water was made opaque with the addition of nontoxic titanium dioxide (Sigma-Aldrich; 250 mg/L). A circular escape platform (10 cm diameter, 22 cm height) was placed in one of the four imaginary

quadrants of the pool submerged 1 cm below the water surface. The 4 days of protocol consisted in a hippocampal-dependent task whose goal was to assess the ability of mice to learn the position of the hidden platform kept always in the same position. Each day, mice performed four consecutive trials (maximum of 60 s, with a 30 s intertrial interval) being placed in the pool facing the maze wall and oriented to each of the extrinsic cues in random order. Whenever mice failed to reach the platform, they were manually guided to the platform for 30 s before being positioned at a new starting point. Escape latencies, distances swam and swim pattern were monitored and analyzed using a video camera and the EthoVision XT 11.5 software (Noldus, The Netherlands).

2.3.2 | Hole board

The hole board (HB) task was performed to assess spatial orientation, namely reference and working memory (Castilla-Ortega et al., 2010). Transgenic mice and WT littermates were food restricted for 4 days before the beginning of the test to achieve a body weight drop to 80–85% of their free-feeding weights and food deprivation lasted through the whole behavioral experiment. The behavioral test was performed in a hole board containing 16 equidistant holes (6 cm apart, 1.5 cm diameter, 2.5 cm depth; MedAssociates, USA). The hole board was placed inside a maze with Plexiglas walls with a different cue in each wall for orientation. All mice were submitted to 3 days of habituation (1 daily session of 10 min) and one food pellet was placed in each of the 16 holes to attract mice to explore holes and eat the pellets. In the following 4 days, only a fixed set of 4 holes was baited with a pellet in a pattern that remained constant (2 sessions per day with an intersession interval of 2 h, each session consisting in two trials with an intertrial interval of 45 s). Each trial had a maximum duration of 5 min, finishing whenever the animal found all four rewards. Mice were manually placed inside the HB arena at one of four random starting locations. Arenas were cleaned with 10% ethanol between trials. Tests were evaluated by tracking animals trail with an infrared detection system and a computer interface. The following measures were analyzed: RM ratio (number of visits to the baited set of holes over the number of visits to all holes—provides an index for the ability of animals to discriminate between baited and unbaited holes); and WM ratio (number of rewarded visits over the number of visits to the baited set of holes—reflects the ability of the animals to avoid re-visits to baited holes during a trial).

2.3.3 | Novel object recognition

The novel object recognition (NOR) task (Leger et al., 2013) was conducted under dim white-light illumination in a lusterless white box (30 × 30 × 30 cm). Habituation to the empty box was performed in three consecutive days for 20 min. In the fourth day of the task animals were submitted to a training phase consisting in the exploration of two equal objects (glass bottles) for 10 min. In the fifth day, for the novel object recognition phase, one of the familiar objects was replaced by a novel (Lego® brick) and mice were placed in the arena and allowed to explore both for 10 min. This trial assesses the ability to recognize a novel object 24 h after the first exposition, evaluating long-term recognition memory. After an interval of 1 h in their home cages, the novel object was displaced to the opposite side of the box and mice were allowed to

explore this new configuration. This trial allowed the assessment of the spatial recognition memory of the subjects. Boxes were cleaned between trials and subjects with 10% ethanol. Behavior was video-recorded and analyzed using EthoVision XT 11.5 software (Noldus, The Netherlands). Exploration time of the novel or displaced objects over the total exploration time was used as measure of object preference.

2.3.4 | Two-trial place recognition

The two-trial place recognition (2TPR) task is based on the innate predisposition of rodents to explore novel environments. The 2TPR is a test performed in the Y-Maze arena to assess spatial recognition memory, a form of episodic-like memory in rodents (Costa-Aze, Quiedeville, Boulouard, & Dauphin, 2012). It does not require learning of a rule being useful in particular for the study of genetic influences on the response to spatial novelty. The Y-maze consisted in an apparatus made of white Plexiglas with three identical arms (33.2 L × 7 W × 15 cm H) which were randomly designated start (S), familiar (F), and novel (N) arms. Visual cues were placed at the end of each arm of the maze. In the first trial, mice were placed in the start arm and allowed to explore only two arms (S and F) for 5 min. Mice were replaced in their home cages for a period of 30 s, and then they were placed in the start arm of the maze and allowed to explore the three arms for 2 min for memory retrieval. The maze was cleaned with 10% ethanol between trials and subjects, and the test was performed in a dim light room. Mice trail was video-recorded and analyzed using EthoVision XT 11.5 software (Noldus, Netherlands). The percentage of time spent in the distal third of the novel arm was considered a measure of spatial recognition memory.

2.4 | Molecular analysis

2.4.1 | Macrodissection, RNA isolation, cDNA synthesis, and real-time PCR analysis

In order to assess the transcription levels of the dnSNARE and EGFP transgenes, relative mRNA levels of both genes were quantified by RT-PCR. Animals were first anesthetized with a mixture of ketamine (75 mg/kg, i.p.; Imalgene 1000, Merial, EUA) and medetomidine (1 mg/kg, i.p.; Dorbene Vet, Pfizer, EUA) and transcardially perfused with 0.9% saline. Brains were carefully removed and macrodissected, and tissue samples were stored at −80°C until further analysis. To avoid experimenter-dependent bias, all brains were macrodissected by a single investigator.

Total RNA was isolated from macrodissected tissue of the prefrontal cortex of dnSNARE mice ($n = 15$), using the Direct-zol RNA mini-Prep kit (Zymo Research, USA), according to manufacturer's instructions. Briefly, tissue was mechanically homogenized with a syringe and 20G needle using the NZYol reagent (NZYTech, Portugal).

Total RNA (500 ng) was reverse-transcribed using qScript™ cDNA SuperMix (Quanta Biosciences, USA). The following primers were designed using PRIMER-BLAST (NCBI, http://www.ncbi.nlm.nih.gov/tools/primer-blast/) and used for expression quantification: EGFP (F 5′-CCCGACAACCACTACCTGAG-3′; R 5′-ACTTTGACCATCAGAGGA-CATT-3′); dnSNARE (F 5′-TACCAGTAACAGGAGACTGC-3′; R 5′-

ACTTTGACCATCAGAGGACATT-3′). Quantifications were performed using the Fast Real-Time PCR System (Applied Biosystems, USA) and 5× HOT FIREPol® EvaGreen® qPCR Mix Plus, ROX (Solis Biodyne, Estonia). Target gene expression levels were normalized against the housekeeping gene 18S rRNA and the relative expression was calculated using the ΔΔCt method.

2.4.2 | Western blot analysis

In order to screen the transgenic protein levels in the brain regions analyzed in the behavior and electrophysiology experiments, relative EGFP levels were quantified by western-blot. Brain samples containing the hippocampus were lysed in cold HEPES-buffered sucrose (0.32M sucrose, 4 mM HEPES, pH 7.4) with 1% Nonidet-P40, 0.5% SDS, and a mixture of protease inhibitors (cOmplete, EDTA-free, Roche, Switzerland). Then, samples were sonicated for 10 s and centrifuged at 10,000 rpm during 25 min at 4°C. The supernatant was collected and protein concentrations were determined using the Bradford protein assay (Bio-Rad, USA). Total lysates were denatured in 2× Laemmli buffer (Bio-Rad, USA) by heating for 5 min at 100°C. Each sample was centrifuged during 10 s before loading. Equal protein amounts (50 μg) were loaded into SDS-PAGE (10%) gels and then transferred to a nitrocellulose membrane (Trans-blot Turbo Kit, Bio-Rad, USA). Membranes were blocked in 5% dry milk/TBS (1 h) before incubation overnight at 4°C with the primary antibodies: mouse anti-α-tubulin (1:500, DSHB, USA); goat anti-GFP (RRID: AB_305643; 1:2000, Abcam, UK). After washing with TBS-T, membranes were incubated with secondary antibodies: anti-mouse HRP (RRID: AB_11125547; 1:15,000; Bio-Rad, USA) and antigoat HRP (1:5000, Bio-Rad, USA), respectively. Detection of the chemiluminescent signal was performed with the Clarity Western ECL substrate kit (Bio-Rad, USA) using a gel blot imaging system (Chemidoc, Bio-Rad, USA). Band quantification was assessed using the Image Lab software (Bio-Rad, USA), and all the samples were normalized according to the loading control (α-tubulin). Given the difficulty of quantifying dnSNARE protein levels in brain tissue (available antibodies detect similarly both the truncated and endogenous forms of synaptobrevin 2), and the fact that the EGFP levels observed are highly correlated with the EGFP mRNA levels, which in turn directly correlate with the dnSNARE levels, the quantification of GFP by western blot was used throughout to screen the transgene expression levels in all mice tested. To confirm the induction of expression of dnSNARE transgenes after Dox removal from the diet, groups of 2 dnSNARE mice were sacrificed at different timepoints (on Dox, 1, 2, 3, 4, and 8 weeks after Dox removal). Additionally, 2 wild-type littermates were sacrificed for negative control. Protein extracts were obtained from whole-brain lysates. To quantify the relative levels of GFP across brain regions and across animals, the brains of 13 dnSNARE mice were macrodissected 6 weeks after Dox removal, and each brain region was processed independently by western blot as described above.

2.4.3 | Immunofluorescence analysis

Brain tissue of the tested animals was stained by immunofluorescence to visualize the expression of transgene reporters, to study the co-expression with astrocytic and neuronal markers, to allow the

3D reconstruction of astrocytes and assessment of astrocytic densities. Mice were deeply anaesthetized with the ketamine and medetomidine mix, and readily perfused transcardially with 4% PFA. Brains were carefully removed and immersed during 48 h in 4% PFA. After impregnation with 30% sucrose PBS solution (at 4°C, until sinking), brains were frozen by immersion in isopentane, cooled with liquid nitrogen in Neg-50 medium (ThermoFisher Scientific, USA) and stored at −20°C. The immunofluorescence procedures were performed in coronal brain sections (20 μm thick) obtained by means of a cryostat (Leica, Germany). The double staining protocol started with three washes with PBS followed by a permeabilization with 0.3% v/v Triton X-100 in PBS. Sections were washed over again and submitted to an antigen retrieval step, with citrate buffer (10 mM, pH 6.0, Sigma-Aldrich) during 20 min at 100W microwave potency. Once cooled, slices were rinsed in PBS and incubated with 10% fetal bovine serum (FBS) in PBS blocking solution for 30 min at room temperature (RT), followed by the overnight incubation, at 4°C, with combinations of the primary antibody goat polyclonal anti-GFP (RRID: AB_305643; 1:300, Abcam, UK) and one of the following: rabbit polyclonal anti-GFAP (RRID: AB_10013482; 1:200, DakoCytomation, Denmark), or rabbit polyclonal anti-S100β (1:200, DakoCytomation, Denmark) for staining of astrocytes; or mouse polyclonal anti-NeuN (RRID: AB_10807945; 1:100, Millipore, Germany) for staining of mature neurons; all prepared in PBS with 0.3% Triton X-100 and 4% fetal bovine serum (FBS). On the next morning tissue sections were rinsed in PBS and then incubated with the respective species-specific secondary antibodies: Alexa Fluor® 488 donkey antigoat, Alexa Fluor® 594 donkey antirabbit and Alexa Fluor® 594 donkey antimouse (1:1000, ThermoFisher Scientific, USA) in PBS with 4% FBS, during 2 h at room temperature. After rinsing the brain slices with PBS, the nucleic acids were indiscriminately labeled by 10 min incubation with DAPI (RRID: AB_ 2307445; 1:1000, Invitrogen, USA) in the dark. After a final series of rinses in PBS, slides were mounted using Immu-mount (ThermoFisher Scientific, USA) mounting media and evaluated through confocal microscopy imaging (FV1000, Olympus, Japan) and FIJI open source software (http://fiji.sc/Fiji).

2.5 | 3D-reconstruction of neurons

All procedures employed to assess the morphology of neurons were previously described (Lima et al., 2014). In order to assess dendritic morphology of hippocampal neurons a set of animals ($n = 5$ WT and $n = 5$ dnSNARE) were perfused with 0.9% saline under deep anesthesia (ketamine and medetomidine mix) and were processed for Golgi–Cox staining. Briefly, brains were removed and immersed in Golgi–Cox solution (1:1 solution of 5% potassium dichromate and 5% mercuric chloride diluted 4:10 with 5% potassium chromate) for 14 days; transferred to a 30% sucrose solution (minimum 3 days) and sectioned by means of a vibratome. Coronal sections (200 μm thick) were collected in 6% sucrose and blotted dry onto gelatin-coated microscope slides and subsequently alkalinized in 18.7% ammonia, developed in Dektol (Kodak, USA), fixed in Kodak Rapid Fix, dehydrated and xylene cleared, mounted, and coverslipped. All incubation steps were performed in a dark room.

Three-dimensional (3D) reconstruction of Golgi–Cox impregnated neurons was performed in the CA1 subregion of the dorsal hippocampus following the mouse brain atlas (Paxinos & Franklin 2001). CA1 pyramidal neurons were readily identified by their characteristic triangular soma-shape, apical dendrites extending toward the stratum radiatum. Neurons were selected for reconstruction following these criteria: (i) identification of soma within the pyramidal layer of CA1 (ii) full impregnation along the entire length of the dendritic tree; (iii) no morphological changes attributable to incomplete dendritic impregnation of Golgi–Cox staining or truncated branches. To avoid selection bias, brain slices containing the region of interest were randomly searched and the first six neurons from each animal were reconstructed from at least three brain slices (containing both hemispheres). The dendritic reconstruction was performed by using a motorized microscope controlled by the Neurolucida software (MBF Bioscience, USA) under 100× magnification. The analyzed dendritic features were: total length, number of endings and nodes and Sholl analysis (number of dendrite intersections at radial intervals of 20 μm). Dendritic spine densities were also assessed in randomly selected 30 μm segments of three proximal and three distal dendritic branches per neuron, and were categorized in four types (thin, mushroom, wide, and ramified). The features of both reconstructed neurons and spines were quantified using NeuroExplorer software (MBF Bioscience, USA).

2.6 | D-Serine administrations

In order to rescue the functional impairments displayed by dnSNARE mice, D-serine was administered to mice of both genotypes during electrophysiology and behavior experiments (Sigma-Aldrich, USA; 1 g/kg of body weight, 10 mL/kg of body weight in saline, i.p.). This administration was described to increase the intracerebral levels of D-serine and rescue functional deficits in different contexts and independent laboratories (Guercio et al., 2014; Han et al., 2015; Takata et al., 2011). Details are provided as Supporting Information.

For the electrophysiological experiments, surgical procedures and electrode placement were performed as described above. After the surgery and resting period, 15 periods of 100 s of local field activity were recorded each 5 min. D-Serine was administered i.p. after the third recording, and the effect of D-serine was observed during the next 12 recordings (60 min). The first three recordings represent the basal activity, while the 12 following recordings represent the longitudinal effect of D-serine administration. The electrode positions were verified as described above.

For the behavior experiments, either D-serine or saline were administered to an independent set of mice 20 min before the first trial on each day in the MWM task, or 20 min before the training session in the NOR task. Despite the i.p. injection, mice behaved normally and no signs of distress or potential drug side effects were observed, therefore no animal was excluded for those reasons.

2.7 | Statistical analysis

Results are presented throughout as mean ± SEM (standard error of the mean) and the statistical significance of the comparisons for

each statistical test was set with a confidence interval of at least 95%. All data sets passed the normality tests for Gaussian distributions (D'Agostino and Pearson for $n > 7$; Kolmogorov–Smirnov for $n = 5$–6), therefore parametric tests were applied. Two-way analysis of variance repeated measures (ANOVA) and Sidak *post hoc* tests were used to analyze the performance in the MWM, HB (factors: genotype and test day); and Sholl analysis data for neuronal 3D reconstructions (factors: genotype and radial distance from soma). Two-way ANOVA and Fisher's LSD test were applied to analyze the 2TPR, spines distribution and effects of D-serine. One-way ANOVA was used to compare data between three groups (WT, dnSNARE, and IGFP). Pearson coefficients were calculated to assess correlations between: mRNA relative levels of dnSNARE and EGFP transgenes; between behavior performance and GFP levels or electrophysiological activity. In the remaining experiments, unpaired two-sided *t* tests were applied to compare data between the two groups: WT and dnSNARE. Statistical analysis was performed using the GraphPad Prism 6 (GraphPad Software, USA).

3 | RESULTS

3.1 | dnSNARE transgenes are highly expressed in the hippocampus and prefrontal cortex and display intersubject variability

We employed the dnSNARE mouse model (Pascual et al., 2005) to study the role of gliotransmission in complex cognitive processing, which allowed the inducible blockade of the vesicular release by exocytosis selectively from astrocytes (Fellin et al., 2009; Sultan et al., 2015), preventing developmental effects that could mask potential behavior implications. This strategy selectively perturbs exocytosis-dependent gliotransmission (Sultan et al., 2015; Zhang et al., 2004), thus allowing to dissect its implications for the neuron–astrocyte network and behavior. Independent studies showed that dnSNARE expression in astrocytes is accompanied by reduction of available gliotransmitters in cell culture (glutamate) (Zhang et al., 2004), in brain slices of hippocampus (ATP) (Cao et al., 2013) or cortex (D-serine and ATP) (Cao et al., 2013; Pankratov & Lalo, 2015), or *in vivo* in the hippocampus (D-serine) (Sultan et al., 2015). In spite of being used in different labs in the past decade (Oliveira et al., 2015), the validity of this mouse model was challenged (Fujita et al., 2014). Nevertheless, we and others have recently validated this model for the study of signaling dependent on astrocyte exocytosis (Pankratov & Lalo, 2015; Papouin, et al. 2017; Sultan et al., 2015; Wagner et al., 2017). In our lab, we firstly performed complementary sets of experiments to validate the co-expression of dnSNARE and reporter transgenes, the inducible control, the astrocyte specificity and the level of transgene expression among brain regions and subjects.

Since the dnSNARE transgene corresponds to the cytosolic portion of endogenous synaptobrevin II, the available antibodies target both proteins indiscriminately. Therefore, we assessed the co-expression of dnSNARE and enhanced green fluorescent protein (EGFP) reporter

transgenes in order to use the EGFP as a reporter to screen the expression levels in all mice tested. The quantification of the relative expression of dnSNARE and EGFP mRNA by RT-PCR in one set of dnSNARE mice showed a direct correlation between the amount of transcripts of both mRNAs (Figure 1a, top), meaning that the transcription of both transgenes should follow similar regulatory mechanisms, which matches with the described elevated rate of co-localization (Halassa et al., 2009). Additionally, the relative quantification of GFP levels by western blot (using anti-GFP antibody) in the same mice showed that the relative levels of protein and mRNA follow a direct correlation (Figure 1a, bottom). Altogether, this set of data indicates that mice that express higher levels of dnSNARE, also express higher levels of EGFP mRNA, which in turn translates into increased EGFP levels in those mice. Thus, from this moment on, GFP staining or relative levels, will be used as a correlate of dnSNARE expression.

The removal of doxycycline from the mice diet triggers the expression of dnSNARE transgenes, as measured by the GFP levels of animals sacrificed at different timepoints, reaching a maximum at weeks 3–4, that remains stable in time, and is completely absent in wild-type littermates (Figure 1b); these results are in accordance with previous observations using doxycycline-controlled systems (Halassa et al., 2009; Nakashiba, Young, McHugh, Buhl, & Tonegawa, 2008). The expression of transgenes occurred throughout the brain, displaying a typical mosaic-like distribution (Figure 1d–i) (Florian, Vecsey, Halassa, Haydon, & Abel, 2011; Sultan et al., 2015). We consistently verified the astrocyte specificity of transgene expression, by performing immunofluorescence staining of brain slices containing the hippocampus and prefrontal cortex (regions of critical interest for this study (Gordon, 2011; Hoffmann, Cicchese, & Berry, 2015; Lima et al., 2014; Oliveira et al., 2013; O'Neill et al., 2013)), using specific antibodies to target GFP and astrocytic or neuronal markers. GFP-labeling revealed only structures with the characteristic bushy astrocytic morphology (Florian et al., 2011; Khakh & Sofroniew, 2015; Pascual et al., 2005). These structures were regularly positive for the astrocyte-specific marker glial fibrillary acidic protein (GFAP) (Khakh & Sofroniew, 2015) both in the CA1 region of the dorsal hippocampus (dHIP) and in the medial prefrontal cortex (mPFC), in line with previous reports (Florian et al., 2011; Halassa et al., 2009) (Figure 1d–e). GFP was also co-localized with the astrocyte cytosolic marker S100β (Khakh & Sofroniew, 2015) in both brain regions (Figure 1f–g). Together, the typical GFP-arborization and the double immunostainings indicate that the transgenes were expressed by astrocytes of both populations. Moreover, the numbers of 59.9 ± 4.8% of GFAP-immunostained astrocytes co-expressed GFP in the dorsal hippocampus ($n = 4$ mice), as previously described (Sultan et al., 2015). Additionally, to support astrocyte specificity and to exclude neuronal expression of dnSNARE transgenes, we performed double immunostainings against GFP and NeuN (neuron specific) in the same brain regions. The detailed observation of images of each confocal section excluded staining overlap between GFP and NeuN both at the dHIP and mPFC (Figure 1h–i). Furthermore, we performed double-stainings including EGFP and two additional neuronal markers: βIII tubulin that stains neurites, and calbindin that is found in the cytosol (Supporting Information Figure S1). One clearly observes that neurites
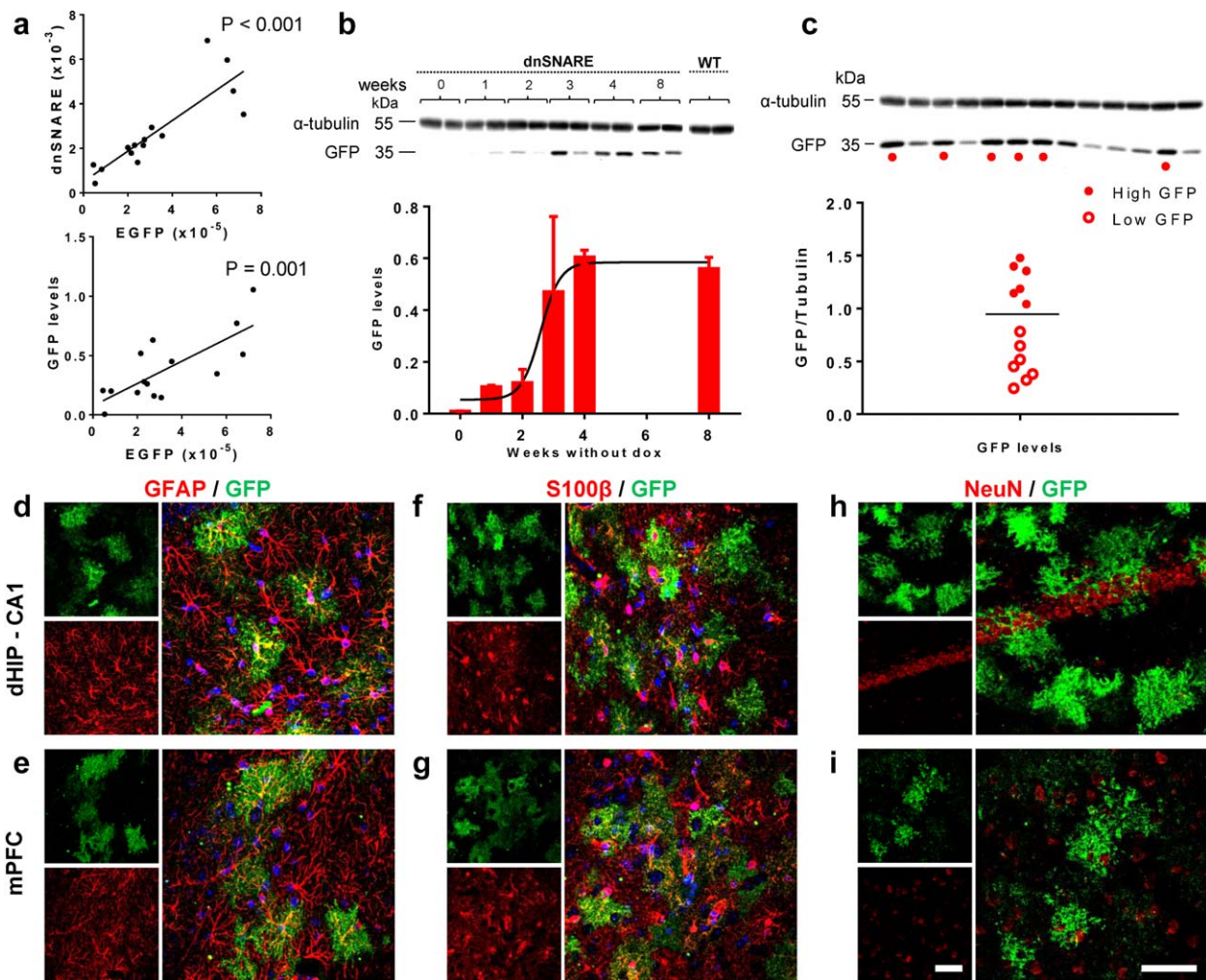
FIGURE 1 GFP reporter is a good readout of dnSNARE transgene expression and intersubject variability. (a) Pearson's correlations between relative expression levels of EGFP mRNA and dnSNARE mRNA (top), or GFP protein levels (bottom), measured in the same set of dnSNARE mice ($n = 15$); (b) doxycycline (dox) removal from the mice diet triggers transgene expression specifically in dnSNARE mice, as assessed by the quantification of GFP (35 kDa) expression on the hippocampus of dnSNARE mice by western blot analysis at 0, 1, 2, 3, 4, and 8 weeks after dox removal from drinking water. Tubulin (55 kDa) was used as control ($n = 2$/timepoint); wild-type (WT) mice were used as negative controls; data plotted as mean $\pm$ SEM. (c) Quantification of the transgene reporter GFP from the hippocampus of dnSNARE mice ($n = 13$) was performed by western blot analysis (35 kDa), relatively to tubulin (55 kDa) for each set of animals after behavioral and electrophysiological assessment (the mean value of GFP expression, black dash, was used as criteria to separate two clusters of animals in each set: the high and low "expressors" of the transgenes; (d–e) Confocal micrographs illustrating co-expression of GFP reporter transgenes (green) with GFAP (red) in the CA1 of the dorsal hippocampus (D, dHIP, stratum radiatum) and medial prefrontal cortex (E, mPFC, layers III–V) of dnSNARE mice; (f–g) Confocal micrographs illustrating co-expression of GFP reporter transgenes (green) with S100β (red) in the dorsal CA1 (f, stratum radiatum) and mPFC (G, layers III–V) of dnSNARE mice; (h–i) confocal micrographs illustrating double staining of GFP reporter transgenes (green) and NeuN (red) in the dorsal CA1 (h, oriens, pyramidal and radiatum layers), and mPFC (i, layer V) of dnSNARE mice. DAPI staining, blue. Scale bars = 50 μm [Color figure can be viewed at wileyonlinelibrary.com]

that originate in the pyramidal layer and spread across the radiatum layer are devoid of EGFP staining, which remains restricted to the bushy-like astrocyte structure. In the detail of a single confocal plane presented, three neurites clearly cross the astrocyte territory independently (Supporting Information Figure S1a,b). Regarding the calbindin double staining, we also failed to find co-localization of staining in the same cellular structures (Supporting Information Figure S1c,d). Since EGFP is also found in the cytosol, by using this combination, we definitely excluded the expression of transgenes in neurons. Absence of co-staining in microglia, NG2-positive cells and oligondendrocytes, also

ruled out co-expression in these cells (Fellin et al., 2009; Sultan et al., 2015). It is noteworthy, that our observations were extremely consistent across brain areas, and across experimental sets ($n = 5$ mice screened per group), confirming the specific expression of dnSNARE transgenes in astrocytes.

In order to characterize the regional distribution of dnSNARE transgenes, we quantified the relative GFP levels across several brain regions, macrodissected from dnSNARE mice ($n = 13$; Supporting Information Figure S2). Interestingly, we observed a variable expression of transgenes across animals, which was maintained between brain
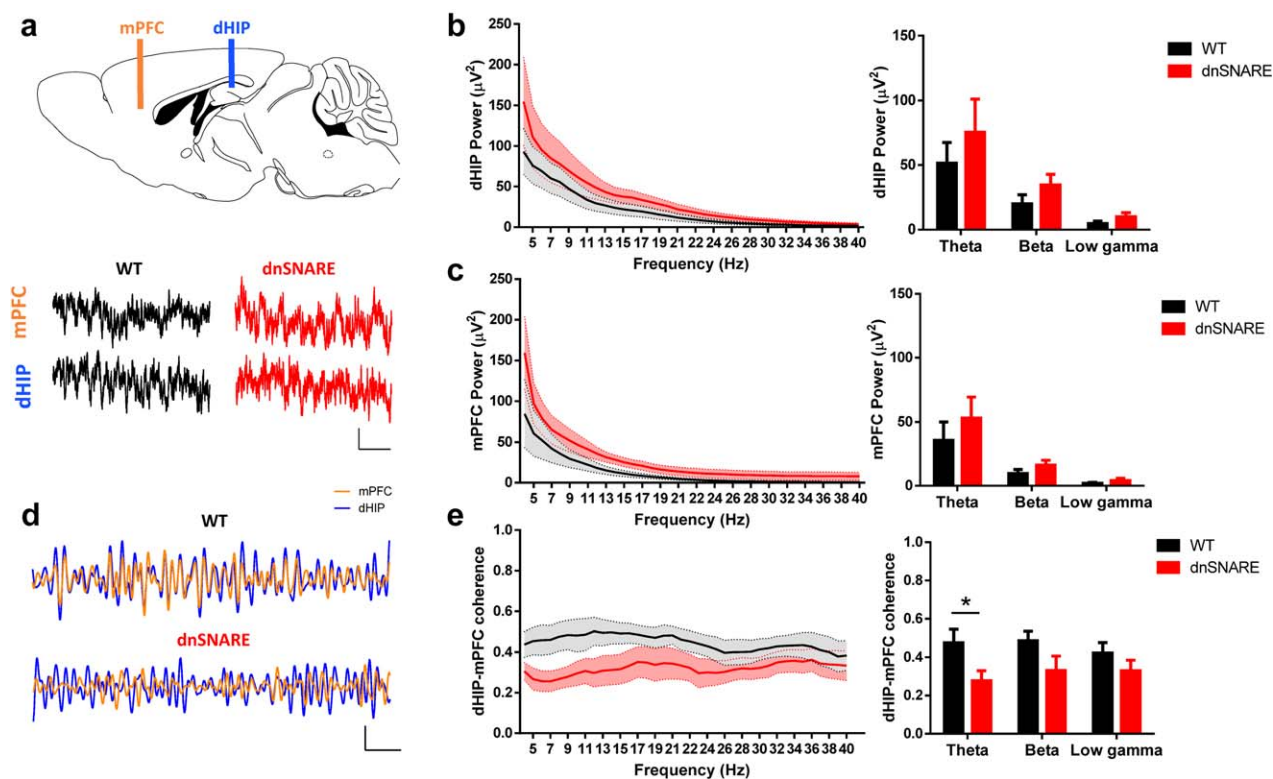
FIGURE 2 Gliotransmission impairment compromises theta coherence in the hippocampal–prefrontal network in dnSNARE mice. (a) Scheme depicting the electrode position for recording of local field potentials (LFP) in the medial prefrontal cortex (mPFC, orange) and CA1 region of dorsal hippocampus (dHIP, blue; top); representative LFP traces recorded from the mPFC and dHIP of WT and dnSNARE mice (bottom; scale bars: 100 μV, 1 s); (b–c) LFP power analysis between WT and dnSNARE; left, power spectra for dHIP (b) and mPFC (c); right, power analysis by frequency bands (theta: 4–12 Hz; beta: 12–20 Hz; low gamma: 20–40 Hz); (d) Overlap of representative theta filtered LFP traces of mPFC and dHIP, recorded from WT and dnSNARE mice (scale bars: 50 μV, 500 ms); (e) analysis of synchrony between dHIP and mPFC with dHIP–mPFC coherence spectra (left) and measured by frequency bands (right). WT mice are represented in black and dnSNARE mice in red lines and bars. Data plotted as mean ± SEM. Two-way ANOVA, Fisher's LSD tests, *$p < .05$ ($n = 8$–9 per group) [Color figure can be viewed at wileyonlinelibrary.com]

regions, meaning that mice that presented high levels of expression in the hippocampus also displayed high expression in other brain regions, while the opposite was also true. The distinct levels of transgene expression observed among different animals may be due to the regulation of gene expression upstream and/or coupled with transcription. Epigenetic regulation may vary among different animals determining chromatin availability (e.g., DNA methylation, histone acetylation), which may impact directly in transgene expression both at the mRNA and protein levels. Since the expression of truncated synaptobrevin II (dnSNARE) rules the level of exocytosis blockade, one shall expect that only mice displaying high levels of dnSNARE would present an effective impairment in functions dependent on exocytotic release from astrocytes. Therefore, we divided mice into two groups, based on the relative expression of GFP: low and high transgene "expressors" (Figure 1c). Since we were interested in hippocampal-dependent behaviors, we quantified the relative GFP levels in the hippocampus of every mouse that carried both tTA and tetO transgenes (double-transgenic). This quantification was repeated for each animal set, and only those mice who expressed higher levels of GFP transgenes than the group mean were included in the dnSNARE group, being compared to their wild-type (WT) littermates throughout. Since this analysis was

performed after the sacrifice, the experimenters were blind both to the animal genotype and to its relative level of transgene expression. The data including the low GFP "expressors" will be plotted as Supporting Information Figures for the verification of transgene level-dependent loss of function.

3.2 | Astrocyte signaling is crucial for hippocampal–prefrontal theta synchronization

Knowing that the release of gliotransmitters from astrocytes was previously shown to modulate synaptic communication in the dHIP and PFC (Araque et al., 2014; Perea et al., 2014; Petrelli & Bezzi, 2016), one might expect that this cellular modulation might impact the function of these circuits. To address this idea, we characterized the electrophysiological fingerprints of this network *in vivo*, by analyzing local field potentials (LFPs; oscillations that result from coordinated rhythmic activity of neuronal populations) recorded simultaneously from the dHIP and mPFC of a set of dnSNARE mice and wild-type (WT) littermates (Figure 2a and Supporting Information Figure S3). The individual analysis of the LFP power on the frequency domain gives an estimate of the amplitude of network activity for a given frequency in the basal

condition. The LFP power measured in WT and dnSNARE mice was similar both in the dHIP and mPFC at theta, beta and low gamma frequencies (Figure 2b,c). Moreover, the total power recorded was similar between genotypes (Supporting Information Figure S4a). The analysis of the distribution of power across frequency bands revealed that theta oscillations represent most the activity recorded in the dHIP and mPFC, however dnSNARE mice display similar levels of relative power for the different frequency bands (Supporting Information Figure S4b). These results, indicate equivalent energy of the neuronal oscillations at the given frequencies within each region, which is in line with previous observations of electroencephalogram data (Fellin et al., 2009). The analysis by specific frequency bands, defined by their functional relevance (Gordon, 2011; Oliveira et al., 2013), confirmed the power similarities between both genotypes. Next, we addressed the coherence between the LFPs recorded from the dHIP and mPFC, as a measure of phase and amplitude synchronization between these regions. Interestingly, dnSNARE mice displayed decreased levels of dHIP–mPFC coherence in the lower frequencies, visible by the superposition of theta-filtered LFP traces (Figure 2d), which were significantly different form their WT counterparts for the theta frequency band (Figure 2e). The level of decrease of dHIP–mPFC theta coherence found in dnSNARE mice is in line with previous reports from us and others linking this synchrony measure to comparable cognitive deficits (Benchenane et al., 2010; Oliveira et al., 2013; Sigurdsson, Stark, Karayiorgou, Gogos, & Gordon, 2010). Next, we took advantage of the variable transgene expression levels observed between subjects to verify whether the neuronal activity was modulated by the level of transgene expression. Indeed, double-transgenic mice that display low levels of expression display similar electrophysiological activity to controls, being significantly different from strongly expressing-dnSNARE mice (Supporting Information Figure S5a,b). It is noteworthy that the levels of expression in double-transgenic mice strongly correlate with dHIP–mPFC theta, but not beta nor low gamma coherence (Supporting Information Figure S5c–e). Together, these results suggest that astrocyte signaling is required for maintenance of a basal theta synchronization between hippocampus and prefrontal cortex, which might be important for cognitive performance.

3.3 | dnSNARE mice display impaired cognitive function

Based on the available evidence linking dHIP–mPFC correct dialogue and cognitive processing (Anderson, Rajagovindan, Ghacibeh, Meador, & Ding, 2009; Benchenane et al., 2010; Hoffmann et al., 2015; Jones & Wilson, 2005; Oliveira et al., 2013; O'Neill et al., 2013; Siapas, Lubenov, & Wilson, 2005; Zhan, 2015), we hypothesized that the observed loss of dHIP–mPFC synchronization might underlie a cognitive loss in mice lacking astrocyte signaling. To address this idea, independent sets of mice were submitted to tasks that assess spatial learning and long-term memory consolidation (highly dependent on the interaction between the dHIP and mPFC), using different motivations (e.g., exploratory drive, or hunger) and different environments (e.g., water-free arenas) (Figure 3).

The Morris water maze (MWM) task was performed to assess reference memory (RM) (Figure 3a–c) (Lima et al., 2014). In this task, WT animals learnt to follow the external cues to reach the platform as confirmed by the decreasing latencies and distances swam during the trials, while dnSNARE mice needed to swim longer to reach the same platform, especially in the last days of the task (Figure 3a). In accordance, dnSNARE mice failed more often to reach the platform within the 60 s of each trial, and whenever they reached it, they employed rather random searching and scanning strategies (Graziano, Petrosini, & Bartoletti, 2003) indicating a poor spatial orientation (Figure 3b,c). To confirm these results, RM was additionally tested in the hole board (HB) task (Castilla-Ortega et al., 2010), which is performed in a different environment, using food deprivation as motivation to learn the location of hidden food pellets with the help of spatial cues. In this task, WT mice learnt to perform the task, as indicated by the increasing RM ratio measured along the days (Figure 3d). Also in this case, dnSNARE mice with impaired gliotransmission faced difficulties to discriminate between baited and unbaited holes, supporting an impairment in RM. Curiously, the calculation of working memory ratios (more dependent on the function of the prefrontal cortex) (Castilla-Ortega et al., 2010; Lima et al., 2014) also pointed out an impairment of the function in the dnSNARE mice, namely in the first test days. Furthermore, the novel object recognition (NOR) test was used to assess long-term memory and spatial recognition memory driven by novelty exploration (Leger et al., 2013), processes critically dependent on hippocampal and cortical networks. In this test, WT mice dedicated higher percentages of time exploring the novel object, which was not the case of the dnSNARE mice (Figure 3e). Regarding the time spent exploring the object displaced after a short period (1 h), although WT mice spent more time in the displaced object than dnSNARE mice, this difference was not statistically significant. These observations support a specific impairment of long-term recognition memory that matches with the hippocampal deficits observed in the previous tasks. Finally, we examined the spatial recognition memory of WT and dnSNARE mice using the two-trial place recognition task, in which animals were expected to preferentially explore a novel arm marked by spatial cues, after a short delay. This configuration allowed the assessment of both dHIP and mPFC functions (Costa-Aze et al., 2012). The analysis of percentage of time spent in the distal quadrants showed that, as expected, WT mice explore significantly more the novel arm, which was not the case of their dnSNARE littermates (Figure 3f), which reveals deficits on place recognition memory in the latter. Together, these results indicate a striking cognitive deficit, namely on functions that rely on the dHIP and its interaction with the mPFC. Double-transgenic mice that display low levels of expression perform in the different tasks similarly to controls, being significantly different from strongly expressing-dnSNARE mice in the four tasks (Supporting Information Figure S6a–d, left panels). It is noteworthy that the levels of expression in double-transgenic mice strongly correlate with a worse performance in the tests that rely on the dHIP–mPFC link (Supporting Information Figure S6a–d right panels), supporting the use of dnSNARE mice for *in vivo* testing. This means that, the higher the expression of truncated synaptobrevin II by astrocytes *in vivo*, the stronger the cognitive impairment.
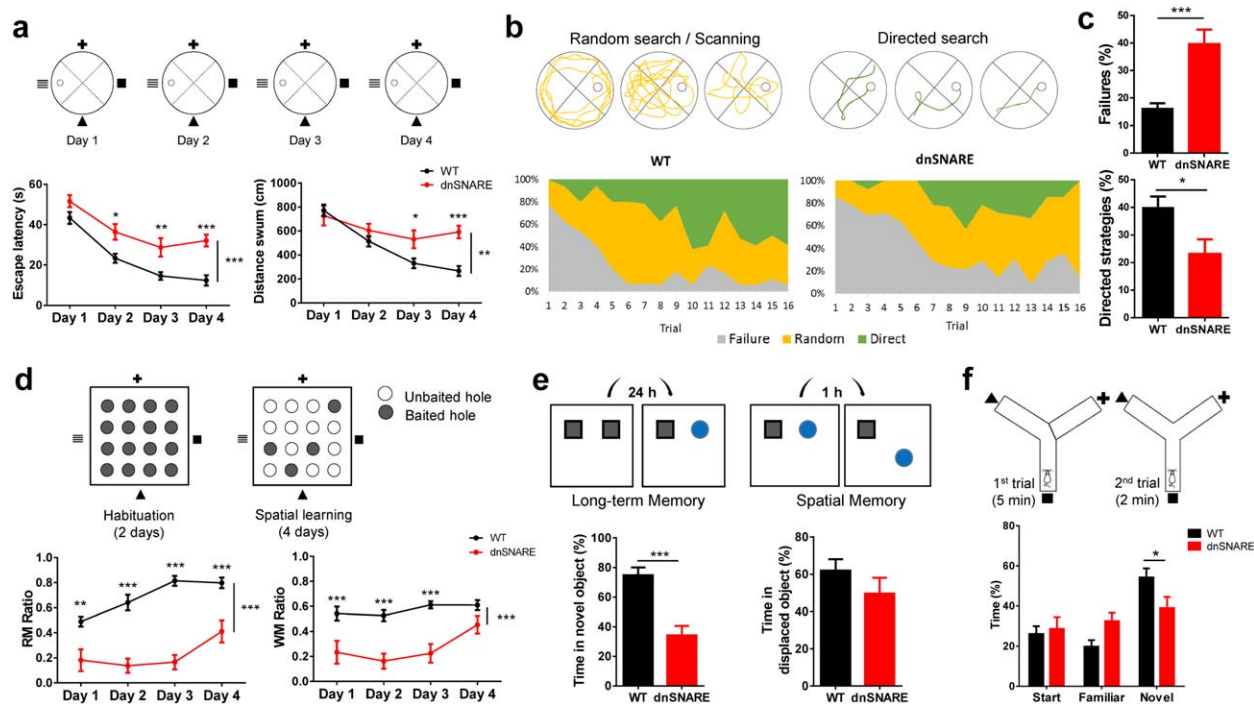
FIGURE 3 Gliotransmission impairment compromises spatial learning and reference memory in dnSNARE mice. (a–c) Morris Water Maze test (n = 14–15 per group); (a) reference memory task scheme (RM, top) and learning curves (bottom, two-way ANOVA repeated measures, Sidak *post hoc* tests) showing escape latencies and distances swam; (b) representative swim tracks used to reach the hidden platform (top), of random search/scanning (yellow) and directed search strategies (green); stacked area charts (bottom) displaying the percentage of failures (gray) and strategies used to reach platform over the 16 trials of RM for wild-type (WT, left) and dnSNARE mice (right); (c) percentage of failures (top) and cue-based/directed strategies to reach the platform in RM (bottom, *t* tests); (d) hole board task scheme (top; baited holes, gray; unbaited holes, white); RM and working memory (WM) ratios for WT and dnSNARE mice (bottom; n = 9–14 per group, two-way ANOVA repeated measures, Sidak *post hoc* tests); RM ratio: number of visits to the baited holes/total number of visits; WM ratio: number of rewarded visits/number of visits to the baited holes; (e) novel object recognition task schemes (top) for assessment of long-term (left) and spatial (right) recognition memories; percentages of exploration time of novel (bottom left) and displaced objects (bottom right; n = 7–9 per group, *t* test); (f) Two-trial place recognition task scheme (top); percentage of time spent in the distal third of start, familiar or novel arms in the retrieval trial (bottom; n = 9–12 per group, two-way ANOVA, Fisher's LSD tests). WT mice represented in black and dnSNARE mice in red lines and bars. Data plotted as mean ± SEM *p < .05, **p < .01, ***p < .001 [Color figure can be viewed at wileyonlinelibrary.com]

Until now, our results suggest a link between hippocampal–prefrontal synchronization impairment and poor performance in cognitive tasks that rely on those areas. To confirm this idea, we measured dHIP–mPFC synchrony in mice that performed the MWM task, and we correlated the levels of dHIP–mPFC synchronization with behavior measures. Data show that the lower levels of theta coherence directly correlate with the poor performance after the third day of the RM task (longer latencies and distances swam), with the use of directed strategies and with the success to reach the platform (Figure 4a–c). Moreover, this effect was quite specific, since the dHIP–mPFC coherence in the beta band only seems to be significantly correlated with the distance swam in day 1 or the success to reach the platform (Figure 4d–f), and low gamma coherence fails to correlate with any of the parameters measured (Figure 4g–i). We and others showed previously that the HIP-PFC theta coherence is crucial for reference memory processing (Benchenane et al., 2010; Jones & Wilson, 2005; Oliveira et al., 2013; Siapas et al., 2005). Now, we specify that by releasing signaling molecules, astrocytes are required to support hippocampal–prefrontal synchronization that underlies cognitive performance.

3.4 | Neuronal structures in the dorsal hippocampus and prefrontal cortex of dnSNARE mice are intact

The results observed hitherto prompted us to seek for structural alterations in neuronal networks that, together with the lack of astrocytic signaling, could justify the loss of theta synchronization and cognitive function observed. Therefore, we characterized dendritic morphology and spine distribution of hippocampal neurons (Lima et al., 2014) since these features may condition the operation of hippocampal networks. Tridimensional reconstruction of pyramidal neurons in the dorsal CA1 (dCA1) subregion showed that WT neurons are very similar to dnSNARE neurons (Figure 5a) for all parameters analyzed (total dendritic length, number of nodes and endings and complexity given by the number of intersections at increasing radial distances from the soma; Figure 5b). Furthermore, the proximal and distal spine densities, as well as its distribution according to maturity criteria remained constant in mice of both genotypes (Figure 5c). Additional analysis of the dentate gyrus (DG) subregion of the dorsal hippocampus (Supporting Information Figure S7a–c) and the prelimbic region of the prefrontal cortex (Supporting Information Figure S7d–f) showed that neuronal
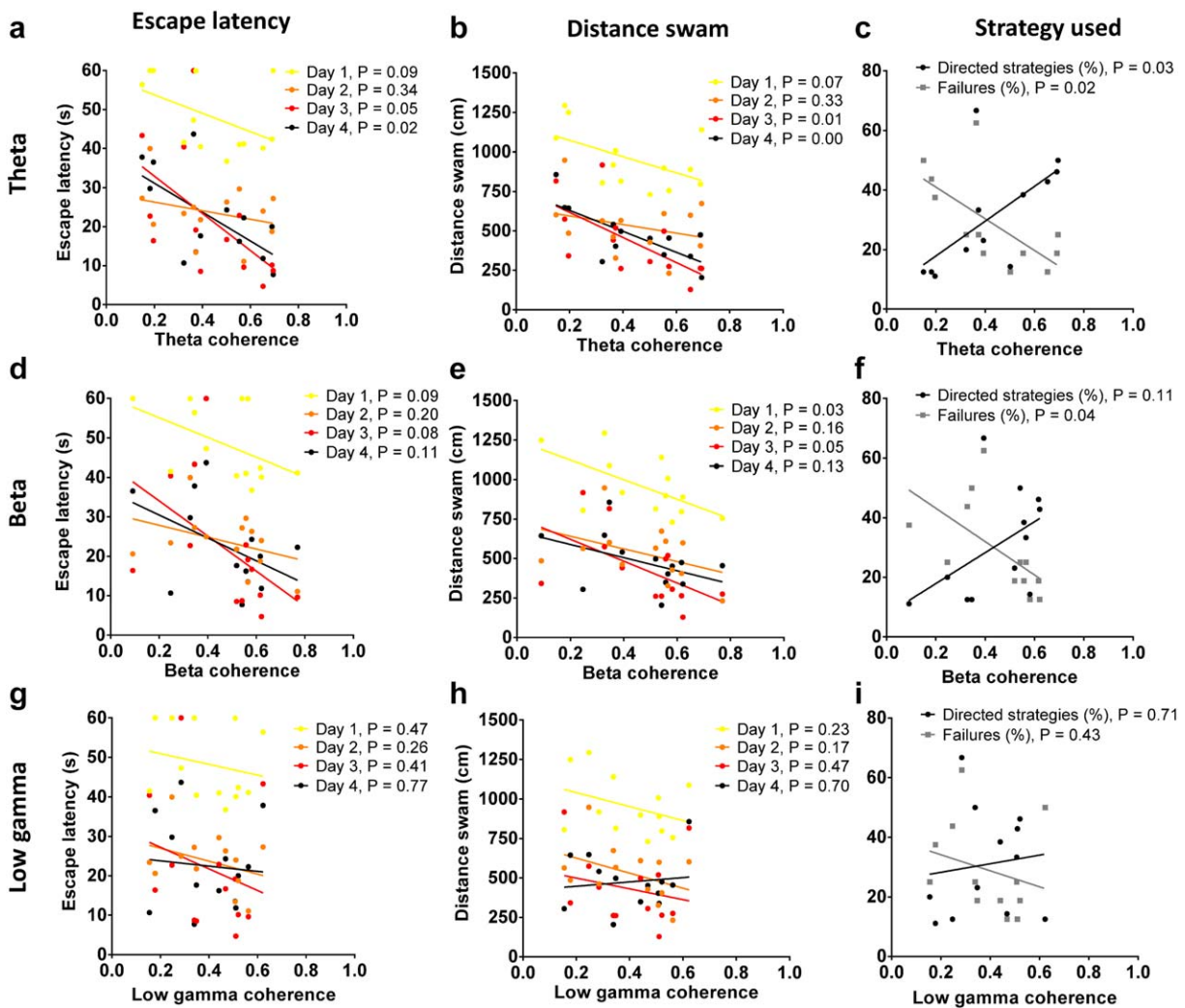
FIGURE 4 Theta dHIP–mPFC coherence correlates with the consolidation of reference memory. Pearson's correlation plots between behavior parameters analyzed for the reference memory MWM task (escape latency, distance swam, directed strategies, and failures to reach the platform) and levels of dHIP–mPFC coherence measured in the same mice (one dot per each WT and dnSNARE mouse) (a–c) theta; (d–f) beta and (g–i) low gamma frequency bands, and the respective *p* values of each Pearson correlation. Performance of day 1 in yellow, day 2 in orange, day 3 in red, day 4 in black. The percentage of use of directed strategies is plotted in black and percentage of failures to reach platform is plotted in gray [Color figure can be viewed at wileyonlinelibrary.com]

morphologies are also intact in dnSNARE mice. It is noteworthy that our analysis covers the complete structure of the neurons, regardless of their maturity and location within the territory of transgene-expressing astrocytes. Previously, Sultan and colleagues elegantly described changes in the morphological properties of the subset of adult-born granule neurons in the DG of dnSNARE mice, which does not collide with our data. Notably, they also showed that the existing large population of granule cells is intact. Although we cannot exclude that the sub-set of novel cells in the DG might account for the performance of the behavior tasks, the outputs of the hippocampus are produced by the majority of intact neuronal populations. Moreover, our LFP recordings are obtained by electrodes implanted in the pyramidal/radiatum layers of the CA1, where no neurogenesis occurs. Therefore, these results support the general integrity of the neuronal structures notwithstanding the lack of surrounding gliotransmitters.

3.5 | D-serine administration rescues the hippocampal–prefrontal theta coherence and the cognitive deficits in dnSNARE mice

We next sought for the molecular mechanism of the alterations so far reported. Recent literature showed that the release of gliotransmitters is significantly decreased in the dnSNARE mice (Cao et al., 2013; Pankratov & Lalo, 2015; Sultan et al., 2015). Amongst the different transmitters, the NMDA-receptor co-agonist D-serine arises as a good candidate, since astrocytes derived from dnSNARE mice release significantly less D-serine (Sultan et al., 2015), and D-serine is involved in synaptic modulation in the hippocampus and cortex (Fossat et al., 2012; Henneberger et al., 2010; Takata et al., 2011; Yang et al., 2003). To test whether D-serine was implicated in the dnSNARE loss of dHIP–mPFC theta synchrony, and consequent cognitive deficits, we repeated these experiments including two sets of WT and dnSNARE mice
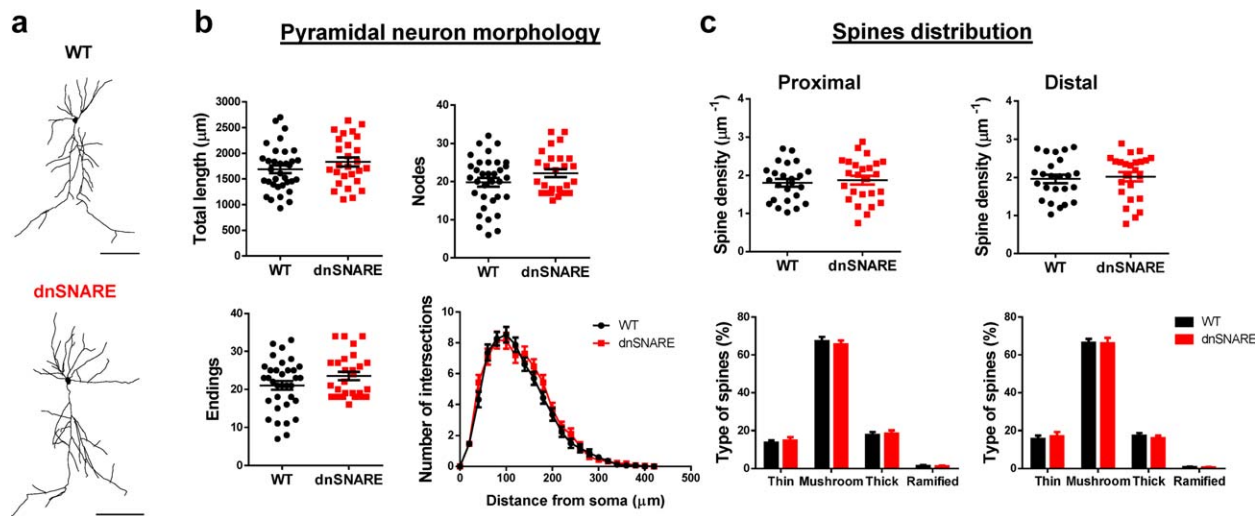
FIGURE 5 Structural characterization of neurons in the dorsal hippocampus CA1 of the WT and dnSNARE mice. (a) Representative 3D reconstructions of dorsal CA1 pyramidal neurons of WT (top) and dnSNARE mice (bottom); scale bars = 100 μm; (b) characterization of the 3D structure of apical dendrites by analysis of total dendritic length, number of nodes and endings (t test), and Sholl intersections (n = 27–34 neurons; 5 mice per group; two-way ANOVA repeated measures, Sidak post hoc tests); (c) density of spines (top) and distribution of spine types (bottom) at proximal and distal portions of the apical dendrites (n = 19–25 neurons; 5 mice per group; t test and two-way ANOVA, Fisher's LSD tests). Data plotted as mean ± SEM [Color figure can be viewed at wileyonlinelibrary.com]

supplemented with either saline or D-serine intraperitoneally (an approach described to increase the intracerebral levels of D-serine (Guercio et al., 2014; Han et al., 2015; Takata et al., 2011)).

First, we performed the simultaneous recording of LFPs from the dHIP and mPFC of WT and dnSNARE mice, and measured the levels of coherence between both regions longitudinally, after the administration of D-serine (Figure 6a). D-serine administration triggered a sustained increase of dHIP–mPFC theta coherence after 20–30 min to levels similar to those recorded from of WT mice in the same conditions, and significantly larger than at baseline (Figure 6a–c). Regarding beta coherence, no differences were observed between genotypes. Low gamma coherence decreased in WT mice during the protocol, however dnSNARE mice displayed levels of coherence similar to WT before and after D-serine administration. In sum, D-serine administration restored specifically the theta coherence (Figure 6d–e). Spectral power increases in the three frequency bands analyzed after the administration of D-serine regardless of the mouse genotype (Supporting Information Figure S8). Despite these results, the specific rescue of dHIP–mPFC coherence in the theta frequency band only in the dnSNARE mice (while WT mice display stable levels of coherence after D-serine administration; Figure 6), confirms the strength of spectral coherence as a robust readout of inter-regional synchrony, independently of the amplitude of neuronal oscillations recorded.

Next, the question was if the rescue of the dHIP–mPFC theta synchronization by D-serine supplementation would also revert the cognitive impairments observed in dnSNARE mice. Indeed, D-serine administration rescued this phenotype in the MWM test in dnSNARE mice (Figure 7a), without affecting the performance of WT mice. This is supported by the shorter latencies and distances swam, the low percentage of failures and use of directed strategies to reach the hidden

platform of D-serine-treated dnSNARE mice (Figure 7b,c). In accordance, D-serine administration restored long-term recognition memory in NOR test for the dnSNARE mice to levels of WT (Figure 7d,e). It is noteworthy that both low and high transgene "expressors" preformed at levels of WT mice in the two tasks, as confirmed by the lack of correlation between GFP levels in the hippocampi of these mice and their respective behavior performance (Supporting Information Figure S9). This suggests that exogenous D-serine fulfilled the network signaling needs, despite the variable extracellular levels due to the different levels of exocytosis blockade.

Together, these results show that astrocyte-derived signaling is required for hippocampal–prefrontal theta coherence, which in turn seems to support spatial learning and reference memory. Additionally, they suggest that D-serine might be the gliotransmitter involved in the astrocyte–neuron signaling.

4 | DISCUSSION

The use of complementary electrophysiological and behavior analysis of the dnSNARE mice to assess the involvement of astrocyte-derived gliotransmitters on cognition, suggests that the D-serine mediated signaling is critical for the synchronization of theta oscillations between the hippocampus and the prefrontal cortex, which underlies performance in spatial learning and memory tasks.

Astrocyte signaling appears to be important for the modulation of the cortical oscillations (Deng, Terunuma, Fellin, Moss, & Haydon, 2011; Fellin et al., 2009; Lee et al., 2014; Poskanzer & Yuste, 2016). However, the modulation of neuronal oscillations that allow the entrainment of deep brain areas required for cognitive computation remains elusive. The involvement of D-serine mediated astrocytic
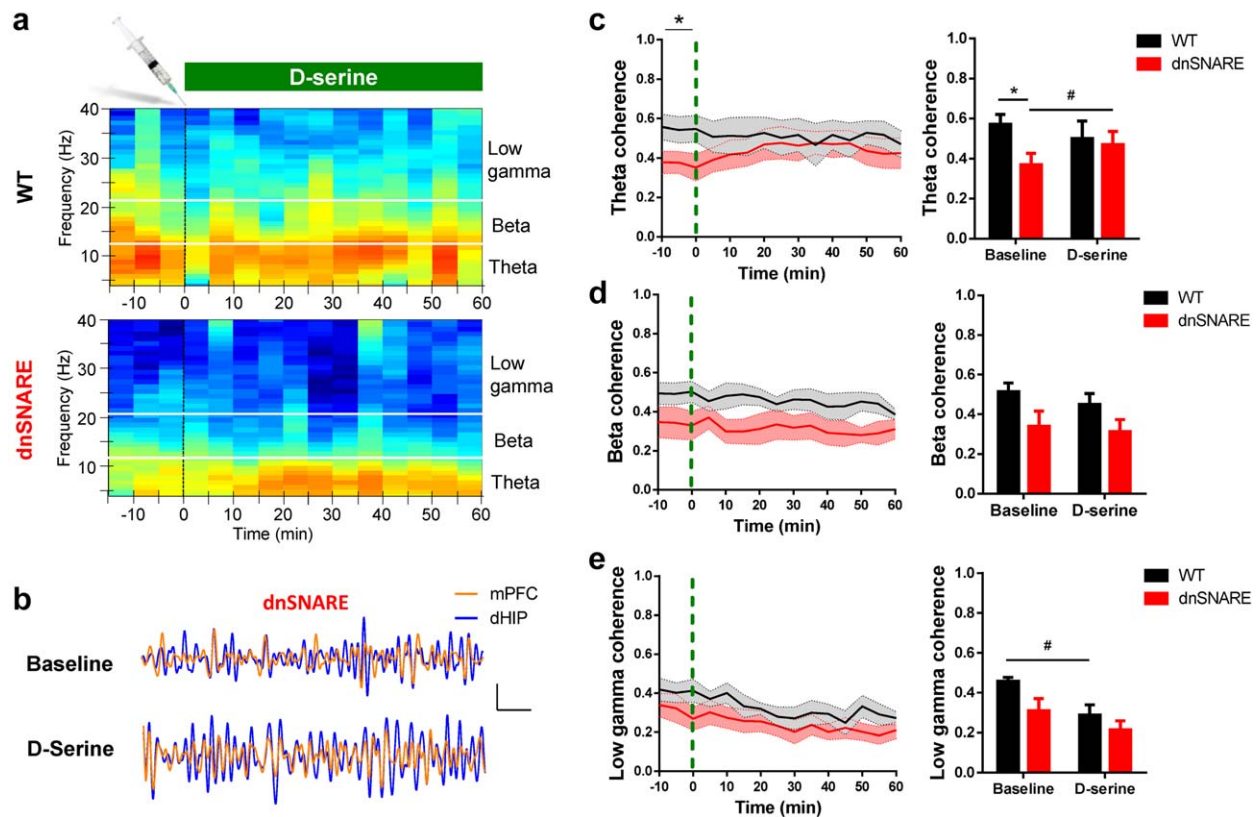
FIGURE 6 D-serine supplementation restores dorsal hippocampus-prefrontal theta synchronization in dnSNARE mice. (a) Representative heatmaps of dorsal hippocampus-prefrontal (dHIP–mPFC) spectral coherence for WT (top) and dnSNARE mice (bottom) over time; dashed line indicates the moment of D-serine administration; each spectrogram represents the dHIP–mPFC coherence calculated in intervals of 5 min for 4–40 Hz (theta, 4–12 Hz; beta, 12–20 Hz; low gamma, 20–40 Hz); color range: 0, dark blue; 1, red; (b) Representative theta filtered LFP traces of mPFC (orange) and dHIP (blue), recorded from dnSNARE mice at baseline or after D-serine administration (scale bars: 50 μV, 500 ms); (c–e) evolution of dHIP–mPFC coherence for theta (c), beta (d), and low gamma (e) frequencies in WT and dnSNARE mice over time (left; dashed line: administration of D-serine); values of dHIP–mPFC coherence at baseline (average of three recordings before injection) and after D-serine administration (average of three recordings, 30 min after injection) (right). WT mice are represented in black and dnSNARE mice in red lines and bars. Data plotted as mean ± SEM. Two-way ANOVA, Fisher's LSD tests, *$p < .05$ from WT; #$p < .05$ from baseline ($n = 6$–7 per group) [Color figure can be viewed at wileyonlinelibrary.com]

signaling in theta HIP-PFC synchronization is supported by several pieces of correlational evidence. Theta desynchronization was observed in dnSNARE mice that display blocked exocytosis specifically in astrocytes. The expression of dnSNARE transgenes that interfere with the SNARE-complex (Bohmbach, Schwarz, Schoch, & Henneberger, n.d.; Schubert, Bouvier, and Volterra, 2011) is restricted to astrocytes, as confirmed by: the bushy morphology of all GFP-labeled structures; the double immunostainings of the GFP reporter and cellular markers performed repeatedly by us and others (Fellin et al., 2009; Sultan et al., 2015); and the similarity between electrophysiological power (4–40 Hz) measured in the dHIP and mPFC of WT and dnSNARE mice discarding a neuronal compromise. Moreover, this expression of dnSNARE transgenes drastically reduced the number of fusion events and release of D-serine in astrocytes derived from dnSNARE mice (Sultan et al., 2015), leading to decreased levels of extracellular D-serine in the hippocampus and cortex of dnSNARE mice (Pankratov & Lalo, 2015; Sultan et al., 2015). Finally, it is now well documented that astrocytic D-serine is critical for the function of individual synapses of the hippocampus and

cortex, namely by supporting synaptic plasticity (Fossat et al., 2012; Henneberger et al., 2010; Takata et al., 2011; Yang et al., 2003).

The role of astrocytes in the modulation of neuronal ensembles is still poorly understood. The activity produced by synchronized cell ensembles generates oscillations that may vary in a wide range of frequencies. Neural oscillations are critical for information processing, and provide the nervous system with a mechanism that allow dynamic coupling within and between brain regions (Buzsáki, 2004). Theta oscillations play a pivotal role in the function of the hippocampus and in its association to cortical regions. They are a result of a concerted work of both rhythm generators and oscillators in different locations (Buzsáki, 2002). Cholinergic and GABAergic, as well as the recently described glutamatergic (Huh, Goutagny, & Williams, 2010) afferents originating from the medial septum-diagonal band of Broca, provide the main extrinsic rhythm inputs to support theta oscillations, by modulation of interneurons, and CA1 and CA3 pyramidal neurons. Input originating from CA3 and entorhinal cortex add up to the establishment of the CA1 theta rhythm (Buzsáki, 2002). In spite of being classically accepted
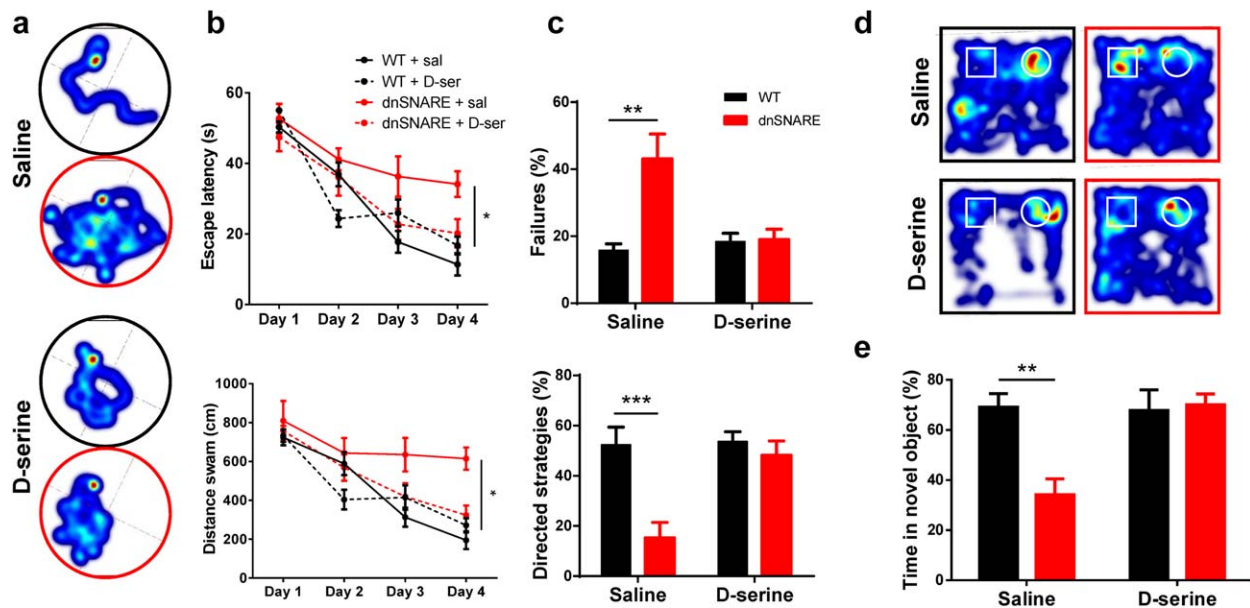
FIGURE 7 D-serine supplementation rescues the cognitive deficits observed in dnSNARE mice. (a–c) Reference memory rescue in the MWM (*n* = 6–9 per group); (a) Representative heatmaps of cumulative trajectories at day 4 of WT (black pool) and dnSNARE mice (red pool) under saline (top) and D-serine administration (bottom); (b) escape latencies (top) and distances swam (bottom) to reach the hidden platform after administration of saline (line) or D-serine (dashed line; two-way ANOVA repeated measures, Sidak *post hoc* tests); (c) failures to reach the platform (top) and the percentage of directed strategies used to find the platform (bottom), after administration of saline or D-serine (two-way ANOVA, Fisher's LSD tests); (d–e) Long-term memory rescue in NOR (*n* = 6–8 per group); (d) representative heatmaps of cumulative exploration of a familiar (square) and novel (circle) objects in the long-term memory task, for WT (black arenas) and dnSNARE mice (red arenas), after saline (top) or D-serine administration (bottom); (e) percentages of exploration time of novel object by WT and dnSNARE, after saline or D-serine administration (two-way ANOVA, Fisher's LSD tests). WT mice are represented in black and dnSNARE mice in red lines and bars. Data plotted as mean ± SEM. *p < .05, **p < .01, ***p < .001 [Color figure can be viewed at wileyonlinelibrary.com]

as oscillators, CA1 pyramidal neurons are also included in an intrinsic loop circuit, which is able to self-generate theta rhythm (Goutagny, Jackson, & Williams, 2009). In these septal–entorhinal–hippocampal circuits, glutamatergic modulation via NMDA receptors appears to mediate theta oscillations, at least partially. Glutamatergic neurons play a role in hippocampal theta generation through local modulation of septal neurons (Robinson et al., 2016). Moreover, the pharmacological inhibition of NMDA receptors significantly impairs hippocampal theta oscillations *in vivo* (Lazarewicz et al., 2009), while the paired activation of NMDA and GABA receptors are able to generate theta oscillations *in vitro* (Kazmierska & Konopacki, 2013). More importantly, the genetic deletion of NMDA receptors in parvalbumin-positive interneurons interfered with theta oscillations, decreasing theta-gamma phase locking, with impact in spatial memory (Korotkova, Fuchs, Ponomarenko, von Engelhardt, & Monyer, 2010). Finally, a transgenic mouse line lacking the NR1 NMDAR subunit fails to reshape hippocampal theta rhythms after the switch between place and sequence representations in a spatial navigation task (Cabral et al., 2014). These studies denote the importance of NMDA-mediated theta oscillations for behavior performance. Due to their ubiquitous distribution and close apposition of processes endowed with machinery to send and interpret physiological signals resulting in modulation of hippocampal NMDA receptors (for review, Araque et al., 2014; Henneberger et al., 2010), astrocytes are in a good position to modulate theta oscillations. Despite the lack of literature in this sub-field, recent suggest that the physiological activation

of astrocytes leads to the release of signals that may add up to hippocampal theta. The deletion of GABA B receptors specifically in astrocytes leads to a decrease in hippocampal theta oscillations (Perea et al., 2016). Moreover, septohippocampal cholinergic input to hilar astrocytes leads to hilar interneuron activation and consecutive dentate gyrus inhibition (Pabst et al., 2016), while cholinergic input to CA1 astrocytes leads to release of D-serine and modulation of CA1 pyramidal neuron activation (Papouin et al., 2017).

While the literature provides substantial amount of information on the generation of hippocampal theta oscillations, the same is not true for the understanding of synchronization of theta between the hippocampus and other brain regions, such as the cortex (Lisman & Jensen, 2013). In our study, dnSNARE mice exhibit lower levels of dHIP–mPFC theta synchronization, whereas the two regions produce similar amounts of theta oscillations of WT controls. Since coherence measures the synchrony of both phase and amplitude of the signals, one might speculate that astrocyte modulation of NMDA receptors might have a role on the phase component of the theta produced, which could be synchronized by supplementing D-serine. Further experiments are needed to specifically address this issue. Together, these correlational evidences support the hypothesis that D-serine released by astrocytes modulates specifically basal theta synchronization, that may entrain unit or ensemble firing in anatomically connected cortical areas (Anderson et al., 2009; Benchenane et al., 2010; Hoffmann et al., 2015; Jones & Wilson, 2005; O'Neill et al., 2013; Siapas et al., 2005; Yang

et al., 2003). Nevertheless, due to the lack of literature and causal observations that support this hypothesis, further work is needed to address these open questions: (1) Does astrocyte signaling modulate simultaneously several ensembles of the septal–entorhinal–hippocampal circuit, i.e., is there a spatial modulation of the theta generation or its phase? (2) Since the administration of D-serine reaches virtually both hippocampus and prefrontal cortex indiscriminately, does HIP–PFC synchrony require simultaneous modulation in the two regions? or Does this modulation occurs in the hippocampus and from there it entrains the prefrontal cortex? (3) Since this basal HIP–PFC theta synchrony is continuously present in WT mice, does this astrocytic modulation result from a tonic release of signals that maintain it over time? How tight is the relationship between surrounding activity and exocytotic release of signals (Vardjan, Parpura, & Zorec, 2016)?

The cognitive deficits observed in dnSNARE mice are likely a consequence of the loss of HIP–PFC synchrony, as D-serine supplementation also restored behavioral function in dnSNARE mice. However, and despite the specificity of basal desynchronization for theta frequency range in this link, we should not exclude the possibility that the hippocampus may be desynchronized with other brain regions, which could help to explain the cognitive deficits observed. Nevertheless, the basal hippocampus–prefrontal desynchronization shall be responsible for a large extent of this effect. The dorsal hippocampus is connected to prefrontal cortex indirectly. The loop closes by a multi-synaptic circuit, being the prefrontal cortex connected to the hippocampus also indirectly (Preston & Eichenbaum, 2013). Within this circuit, the dorsal hippocampus performs primarily cognitive functions, while the ventral relates to emotional behavior (Fanselow & Dong, 2010). Moreover, synchrony between oscillations of hippocampal dorsal or ventral subregions, and PFC has been related respectively to cognitive (O'Neill et al., 2013) and emotional behavior (Adhikari, Topiwala, & Gordon, 2010; Kafetzopoulos et al., 2017; Mateus-Pinheiro et al., 2016; Oliveira et al., 2013). Specifically, and despite the indirect connections, O'Neill and colleagues demonstrated that dHIP theta oscillations are synchronized with theta oscillations in the mPFC, and that theta synchrony is critical for a spatial memory task. Interestingly, both single units and ensembles in the prefrontal cortex appear to entrain with the theta rhythm from the dorsal hippocampus. On the one hand, this type of memory task was previously shown to be dependent on the synchronization of theta oscillations between the hippocampus and prefrontal cortex (Benchenane et al., 2010; Jones & Wilson, 2005; Siapas et al., 2005). Our data shows now that the poor consolidation of reference memory directly correlates with lower levels of basal theta coherence presented by a given dnSNARE mouse, which is in accordance with previous reports showing that the pathological decrease of theta coherence triggered this cognitive deficit (Gordon, 2011; Oliveira et al., 2013). On the other hand, the higher expression of dnSNARE transgenes in the hippocampus strongly correlates with a worse cognitive performance in double-transgenic mice, suggesting that those impairments are due to the lack of astrocyte-derived exocytosis. It is noteworthy, that this variability of genetic modulation may explain negative results in studies in which mice displaying variable levels of transgene expression or genomic recombination were analyzed as a single group (Oliveira et al., 2015).

In conclusion, our results provide the first evidence of a mechanism by which D-serine mediated astrocytic signaling is required for entrainment of distant corticolimbic circuits, being mandatory for cognitive performance.

CONFLICTS OF INTEREST

The authors declare no competing financial interests.

ORCID

João Filipe Oliveira (iD) http://orcid.org/0000-0002-1005-2328

REFERENCES

Adhikari, A., Topiwala, M. A., & Gordon, J. A. (2010). Synchronized activity between the ventral hippocampus and the medial prefrontal cortex during anxiety. *Neuron*, *65*, 257–269.

Anderson, K. L., Rajagovindan, R., Ghacibeh, G. A., Meador, K. J., & Ding, M. (2009). Theta oscillations mediate interaction between prefrontal cortex and medial temporal lobe in human memory. *Cerebral Cortex*, *20*, 1604–1612.

Araque, A., Carmignoto, G., Haydon, P. G., Oliet, S. H. R., Robitaille, R., & Volterra, A. (2014). Gliotransmitters travel in time and space. *Neuron*, *81*, 728–739.

Bail, M. L., Martineau, M., Sacchi, S., Yatsenko, N., Radzishevsky, I., Conrod, S., . . . Mothet, J.-P. (2015). Identity of the NMDA receptor coagonist is synapse specific and developmentally regulated in the hippocampus. *Proceedings of the National Academy of Sciences*, *112*, E204–E213.

Balu, D. T., & Coyle, J. T. (2012). Neuronal d-serine regulates dendritic architecture in the somatosensory cortex. *Neuroscience Letters*, *517*, 77–81.

Benchenane, K., Peyrache, A., Khamassi, M., Tierney, P. L., Gioanni, Y., Battaglia, F. P., & Wiener, S. I. (2010). Coherent theta oscillations and reorganization of spike timing in the hippocampal–prefrontal network upon learning. *Neuron*, *66*, 921–936.

Bohmbach, K., Schwarz, M. K., Schoch, S., & Henneberger, C. (2017). The structural and functional evidence for vesicular release from astrocytes *in situ*. *Brain Research Bulletin*. doi:10.1016/j. brainresbull.2017.01.015

Buzsáki, G. (2002). Theta oscillations in the hippocampus. *Neuron, 33*, 325–340.

Buzsáki, G. (2004). Large-scale recording of neuronal ensembles. *Nature Neurosciences, 7*, 446–451.

Cabral, H. O., Vinck, M., Fouquet, C., Pennartz, C. M. A., Rondi-Reig, L., & Battaglia, F. P. (2014). Oscillatory dynamics and place field maps reflect hippocampal ensemble processing of sequence and place memory under NMDA receptor control. *Neuron, 81*, 402–415.

Cao, X., Li, L.-P., Wang, Q., Wu, Q., Hu, H.-H., Zhang, M., . . . Gao, T.-M. (2013). Astrocyte-derived ATP modulates depressive-like behaviors. *Nature Medicine, 19*, 773–777.

Castilla-Ortega, E., Sánchez-López, J., Hoyo-Becerra, C., Matas-Rico, E., Zambrana-Infantes, E., Chun, J., . . . Santin, L. J. (2010). Exploratory, anxiety and spatial memory impairments are dissociated in mice lacking the LPA1 receptor. *Neurobiology of Learning & Memory, 94*, 73–82.

Clarke, L. E., & Barres, B. A. (2013). Emerging roles of astrocytes in neural circuit development. *Nature Reviews: Neuroscience, 14*, 311–321.

Costa-Aze, V. D. S., Quiedeville, A., Boulouard, M., & Dauphin, F. (2012). 5-HT6 receptor blockade differentially affects scopolamine-induced deficits of working memory, recognition memory and aversive learning in mice. *Psychopharmacology, 222*, 99–115.

Deng, Q., Terunuma, M., Fellin, T., Moss, S. J., & Haydon, P. G. (2011). Astrocytic activation of A1 receptors regulates the surface expression of NMDA receptors through a Src kinase dependent pathway. *Glia, 59*, 1084–1093.

Fanselow, M. S., & Dong, H.-W. (2010). Are the dorsal and ventral hippocampus functionally distinct structures? *Neuron, 65*, 7–19.

Fellin, T., Halassa, M. M., Terunuma, M., Succol, F., Takano, H., Frank, M., . . . Haydon, P. G. (2009). Endogenous nonneuronal modulators of synaptic transmission control cortical slow oscillations *in vivo*. *Proceedings of the National Academy of Sciences of the United States of America, 106*, 15037–15042.

Florian, C., Vecsey, C. G., Halassa, M. M., Haydon, P. G., & Abel, T. (2011). Astrocyte-derived adenosine and A1 receptor activity contribute to sleep loss-induced deficits in hippocampal synaptic plasticity and memory in mice. *The Journal of Neuroscience, 31*, 6956–6962.

Fossat, P., Turpin, F. R., Sacchi, S., Dulong, J., Shi, T., Rivet, J.-M., . . . Mothet, J.-P. (2012). Glial d-serine gates NMDA receptors at excitatory synapses in prefrontal cortex. *Cerebral Cortex, 22*, 595–606.

Fujita, T., Chen, M. J., Li, B., Smith, N. A., Peng, W., Sun, W., . . . Nedergaard, M. (2014). Neuronal transgene expression in dominant-negative SNARE mice. *Journal of Neuroscience, 34*, 16594–16604.

Gordon, J. A. (2011). Oscillations and hippocampal–prefrontal synchrony. *Current Opinion in Neurobiology, 21*, 486–491.

Goutagny, R., Jackson, J., & Williams, S. (2009). Self-generated theta oscillations in the hippocampus. *Nature Neuroscience, 12*, 1491–1493.

Graziano, A., Petrosini, L., & Bartoletti, A. (2003). Automatic recognition of explorative strategies in the Morris water maze. *Journal of Neuroscience Methods, 130*, 33–44.

Guercio, G. D., Bevictori, L., Vargas-Lopes, C., Madeira, C., Oliveira, A., Carvalho, V. F., . . . Panizzutti, R. (2014). d-Serine prevents cognitive deficits induced by acute stress. *Neuropharmacology, 86*, 1–8.

Halassa, M. M., Florian, C., Fellin, T., Munoz, J. R., Lee, S.-Y., Abel, T., . . . Frank, M. G. (2009). Astrocytic modulation of sleep homeostasis and cognitive consequences of sleep loss. *Neuron, 61*, 213–219.

Han, H., Peng, Y., & Dong, Z. (2015). d-Serine rescues the deficits of hippocampal long-term potentiation and learning and memory induced by sodium fluoroacetate. *Pharmacology Biochemistry & Behavior, 133*, 51–56.

Haydon, P. G., & Nedergaard, M. (2015). How do astrocytes participate in neural plasticity? *Cold Spring Harbor Perspectives in Biology, 7*, a020438.

Henneberger, C., Papouin, T., Oliet, S. H. R., & Rusakov, D. A. (2010). Long-term potentiation depends on release of d-serine from astrocytes. *Nature, 463*, 232–236.

Hoffmann, L. C., Cicchese, J. J., & Berry, S. D. (2015). Harnessing the power of theta: Natural manipulations of cognitive performance during hippocampal theta-contingent eyeblink conditioning. *Frontiers in Systems Neuroscience, 9*. doi:10.3389/fnsys.2015.00050

Huh, C. Y. L., Goutagny, R., & Williams, S. (2010). Glutamatergic neurons of the mouse medial septum and diagonal band of Broca synaptically drive hippocampal pyramidal cells: Relevance for hippocampal theta rhythm. *Journal of Neuroscience, 30*, 15951–15961.

Jones, M. W., & Wilson, M. A. (2005). Theta rhythms coordinate hippocampal–prefrontal interactions in a spatial memory task. *PLoS Biology, 3*, e402.

Kafetzopoulos, V., Kokras, N., Sotiropoulos, I., Oliveira, J. F., Leite-Almeida, H., Vasalou, A., . . . Dalla, C. (2017). The nucleus reuniens: A key node in the neurocircuitry of stress and depression. *Molecular Psychiatry*. https://doi.org/10.1038/mp.2017.55

Kang, N., Peng, H., Yu, Y., Stanton, P. K., Guilarte, T. R., & Kang, J. (2013). Astrocytes release d-serine by a large vesicle. *Neuroscience, 240*, 243–257.

Kazmierska, P., & Konopacki, J. (2013). Development of NMDA-induced theta rhythm in hippocampal formation slices. *Brain Research Bulletin, 98*, 93–101.

Khakh, B. S., & Sofroniew, M. V. (2015). Diversity of astrocyte functions and phenotypes in neural circuits. *Nature Neuroscience, 18*, 942–952.

Korotkova, T., Fuchs, E. C., Ponomarenko, A., von Engelhardt, J., & Monyer, H. (2010). NMDa receptor ablation on parvalbumin-positive interneurons impairs hippocampal synchrony, spatial representations, and working memory. *Neuron, 68*, 557–569.

Lazarewicz, M. T., Ehrlichman, R. S., Maxwell, C. R., Gandal, M. J., Finkel, L. H., & Siegel, S. J. (2009). Ketamine modulates theta and gamma oscillations. *Journal of Cognitive Neuroscience, 22*, 1452–1464.

Lee, H. S., Ghetti, A., Pinto-Duarte, A., Wang, X., Dziewczapolski, G., Galimi, F., . . . Heinemann, S. F. (2014). Astrocytes contribute to gamma oscillations and recognition memory. *Proceedings of the National Academy of Sciences, 111*, E3343–E3352.

Leger, M., Quiedeville, A., Bouet, V., Haelewyn, B., Boulouard, M., Schumann-Bard, P., & Freret, T. (2013). Object recognition test in mice. *Nature Protocols, 8*, 2531–2537.

Lima, A., Sardinha, V. M., Oliveira, A. F., Reis, M., Mota, C., Silva, M. A., . . . Oliveira, J. F. (2014). Astrocyte pathology in the prefrontal cortex impairs the cognitive function of rats. *Molecular Psychiatry, 19*, 834–841.

Lisman, J. E., & Jensen, O. (2013). The theta-gamma neural code. *Neuron, 77*, 1002–1016.

Martineau, M., Galli, T., Baux, G., & Mothet, J.-P. (2008). Confocal imaging and tracking of the exocytotic routes for d-serine-mediated gliotransmission. *Glia, 56*, 1271–1284.

Martineau, M., Shi, T., Puyal, J., Knolhoff, A. M., Dulong, J., Gasnier, B., . . . Mothet, J.-P. (2013). Storage and uptake of d-serine into astrocytic synaptic-like vesicles specify gliotransmission. *The Journal of Neuroscience, 33*, 3413–3423.

Mateus-Pinheiro, A., Alves, N. D., Patrício, P., Machado-Santos, A. R., Loureiro-Campos, E., Silva, J. M., . . . Pinto, L. (2016). AP2γ controls

adult hippocampal neurogenesis and modulates cognitive, but not anxiety or depressive-like behavior. *Molecular Psychiatry*. https://doi.org/10.1038/mp.2016.169

Miller, R. F. (2004). d-serine as a glial modulator of nerve cells. *Glia*, *47*, 275–283.

Mitra, P. P., & Pesaran, B. (1999). Analysis of dynamic brain imaging data. *Biophysical Journal*, *76*, 691–708.

Nakashiba, T., Young, J. Z., McHugh, T. J., Buhl, D. L., & Tonegawa, S. (2008). Transgenic inhibition of synaptic transmission reveals role of CA3 output in hippocampal learning. *Science (New York, NY)*, *319*, 1260–1264.

Oliet, S. H. R., & Mothet, J.-P. (2006). Molecular determinants of d-serine-mediated gliotransmission: From release to function. *Glia*, *54*, 726–737.

Oliveira, J. F., Dias, N. S., Jacinto, L. R., Cerqueira, J. J., & Sousa, N. (2013). Chronic stress disrupts neural coherence between cortico-limbic structures. *Frontiers in Neural Circuits*, *7*, 10.

Oliveira, J. F., Sardinha, V. M., Guerra-Gomes, S., Araque, A., & Sousa, N. (2015). Do stars govern our actions? Astrocyte involvement in rodent behavior. *Trends in Neurosciences*, *38*, 535–549.

O'Neill, P.-K., Gordon, J. A., & Sigurdsson, T. (2013). Theta oscillations in the medial prefrontal cortex are modulated by spatial working memory and synchronize with the hippocampus through its ventral subregion. *Journal of Neuroscience*, *33*, 14211–14224.

Pabst, M., Braganza, O., Dannenberg, H., Hu, W., Pothmann, L., Rosen, J., ... Beck, H. (2016). Astrocyte intermediaries of septal cholinergic modulation in the hippocampus. *Neuron*, *90*, 853–865.

Pankratov, Y., & Lalo, U. (2015). Role for astroglial α1-adrenoreceptors in gliotransmission and control of synaptic plasticity in the neocortex. *Frontiers in Cellular Neuroscience*, *9*. https://doi.org/10.3389/fncel.2015.00230

Pannasch, U., Freche, D., Dallérac, G., Ghézali, G., Escartin, C., Ezan, P., ... Rouach, N. (2014). Connexin 30 sets synaptic strength by controlling astroglial synapse invasion. *Nature Neuroscience*, *17*, 549–558.

Papouin, T., Dunphy, J. M., Tolman, M., Dineley, K. T., & Haydon, P. G. (2017). Septal cholinergic neuromodulation tunes the astrocyte-dependent gating of hippocampal NMDA receptors to wakefulness. *Neuron*, *94*, 840–854.e7.

Papouin, T., Henneberger, C., Rusakov, D. A., & Oliet, S. H. R. (2017). Astroglial versus neuronal d-serine: Fact checking. *Trends in Neurosciences*. https://doi.org/10.1016/j.tins.2017.05.007[]

Pascual, O., Casper, K. B., Kubera, C., Zhang, J., Revilla-Sanchez, R., Sul, J.-Y., ... Haydon, P. G. (2005). Astrocytic purinergic signaling coordinates synaptic networks. *Science (New York, NY)*, *310*, 113–116.

Paxinos, G., & Franklin, K. B. J. (2001). *The mouse brain in stereotaxic coordinates* (2nd ed.). San Diego: Academic Press.

Perea, G., Gómez, R., Mederos, S., Covelo, A., Ballesteros, J. J., Schlosser, L., ... Araque, A. (2016). Activity-dependent switch of GABAergic inhibition into glutamatergic excitation in astrocyte–neuron networks. *ELife*, *5*, e20362.

Perea, G., Sur, M., & Araque, A. (2014). Neuron–glia networks: Integral gear of brain function. *Frontiers in Cellular Neuroscience*, *8*, 378.

Petrelli, F., & Bezzi, P. (2016). Novel insights into gliotransmitters. *Current Opinion in Pharmacology*, *26*, 138–145.

Poskanzer, K. E., & Yuste, R. (2016). Astrocytes regulate cortical state switching *in vivo*. *Proceedings of the National Academy of Sciences*, *113*, E2675–E2684.

Preston, A. R., & Eichenbaum, H. (2013). Interplay of hippocampus and prefrontal cortex in memory. *Current Biology*, *23*, R764–R773.

Robinson, J., Manseau, F., Ducharme, G., Amilhon, B., Vigneault, E., Mestikawy, S. E., & Williams, S. (2016). Optogenetic activation of septal glutamatergic neurons drive hippocampal theta rhythms. *Journal of Neuroscience*, *36*, 3016–3023.

Rosenberg, D., Artoul, S., Segal, A. C., Kolodney, G., Radzishevsky, I., Dikopoltsev, E., ... Wolosker, H. (2013). Neuronal d-serine and glycine release via the Asc-1 transporter regulates NMDA receptor-dependent synaptic activity. *Journal of Neuroscience*, *33*, 3533–3544.

Rusakov, D. A. (2015). Disentangling calcium-driven astrocyte physiology. *Nature Reviews Neuroscience*, *16*, 226–233.

Schubert, V., Bouvier, D., & Volterra, A. (2011). SNARE protein expression in synaptic terminals and astrocytes in the adult hippocampus: A comparative analysis. *Glia*, *59*, 1472–1488.

Siapas, A. G., Lubenov, E. V., & Wilson, M. A. (2005). Prefrontal phase locking to hippocampal theta oscillations. *Neuron*, *46*, 141–151.

Sigurdsson, T., Stark, K. L., Karayiorgou, M., Gogos, J. A., & Gordon, J. A. (2010). Impaired hippocampal–prefrontal synchrony in a genetic mouse model of schizophrenia. *Nature*, *464*, 763–767.

Sultan, S., Li, L., Moss, J., Petrelli, F., Cassé, F., Gebara, E., ... Toni, N. (2015). Synaptic integration of adult-born hippocampal neurons is locally controlled by astrocytes. *Neuron*, *88*, 957–972.

Takata, N., Mishima, T., Hisatsune, C., Nagai, T., Ebisui, E., Mikoshiba, K., & Hirase, H. (2011). Astrocyte calcium signaling transforms cholinergic modulation to cortical plasticity *in vivo*. *The Journal of Neuroscience*, *31*, 18155–18165.

Vardjan, N., Parpura, V., & Zorec, R. (2016). Loose excitation–secretion coupling in astrocytes. *Glia*, *64*, 655–667.

Verkhratsky, A., Matteoli, M., Parpura, V., Mothet, J.-P., & Zorec, R. (2016). Astrocytes as secretory cells of the central nervous system: Idiosyncrasies of vesicular secretion. *The EMBO Journal*. *35*, 239–257.

Volterra, A., Liaudet, N., & Savtchouk, I. (2014). Astrocyte Ca^{2+} signalling: An unexpected complexity. *Nature Reviews Neuroscience*, *15*, 327–335.

Wagner, L., Pannicke, T., Rupprecht, V., Frommherz, I., Volz, C., Illes, P., ... Grosche, A. (2017). Suppression of SNARE-dependent exocytosis in retinal glial cells and its effect on ischemia-induced neurodegeneration. *Glia*, *65*, 1059–1071.

Yang, Y., Ge, W., Chen, Y., Zhang, Z., Shen, W., Wu, C., ... Duan, S. (2003). Contribution of astrocytes to hippocampal long-term potentiation through release of d-serine. *Proceedings of the National Academy of Sciences*, *100*, 15194–15199.

Zhan, Y. (2015). Theta frequency prefrontal–hippocampal driving relationship during free exploration in mice. *Neuroscience*, *300*, 554–565.

Zhang, Q., Pangršič, T., Kreft, M., Kržan, M., Li, N., Sul, J.-Y., ... Haydon, P. G. (2004). Fusion-related release of glutamate from astrocytes. *Journal of Biological Chemistry*, *279*, 12724–12733.

SUPPORTING INFORMATION

Additional Supporting Information may be found online in the supporting information tab for this article.